MONITORING OF THE PISTON RING-PACK AND CYLINDER LINER INTERFACE IN DIESEL ENGINES THROUGH ACOUSTIC EMISSION MEASUREMENTS

Ryan McAllister Douglas

Submitted for the degree of Doctor of Philosophy on completion of research
in the Department of Mechanical Engineering, School of Engineering
and Physical Sciences, Heriot-Watt University

July 2007

Abstract

Investigation of novel condition monitoring systems for diesel engines has received much recent attention due to the increasing demands placed upon engine components and the limitations of conventional techniques. This thesis documents experimental research conducted to assess the monitoring capabilities of Acoustic Emission (AE) analysis. In particular it focuses on the possibility of monitoring the piston ring-pack and cylinder liner interface, a critical engine sub-system for which there are currently few practical monitoring options.

A series of experiments were performed on large, two-stroke and small, four-stroke diesel engines. Tests under normal operating conditions developed a detailed understanding of typical AE generation in terms of both the source mechanisms and the characteristics of the resulting activity. This was supplemented by specific tests to investigate possible AE generation at the ring-pack/liner interface. For instance, for the small engines measures were taken to remove known AE sources in order to accentuate any activity originating at the interface whilst for the large engines the interfacial conditions were purposely deteriorated through the removal of the lubricating oil supply to one cylinder.

Interpretation of the results was based mainly upon comparisons with published work encompassing both the expected ring-pack behaviour and AE generation from tribological processes. This provided a strong indication that the source of the ring-pack/liner AE activity was the boundary frictional losses. The ability to monitor this process may be of significant benefit to engine operators as it enhances the diagnostic information currently available and may be incorporated into predictive maintenance strategies. A further diagnostic technique considered was the possibility of using AE parameters combined with information of crankshaft speed fluctuations to evaluate engine balance and identify underperforming cylinders.

Acknowledgements

I would first of all like to thank my supervisors Prof. J. Steel and Prof. R. Reuben for their guidance, support and encouragement throughout the duration of this project, and indeed throughout my time at Heriot-Watt University.

Next, I would like to thank the mechanical and electronics technicians, in particular Mr. R. Kinsella and Mr. A. Haston, for their help and assistance in building test-rigs and equipment. I am also indebted to colleagues, past and present, at Heriot-Watt University who have provided assistance and helpful discussions. I am especially grateful to Dr. P. Nivesrangsan for developing data acquisition software and for help getting started with Matlab and also to Mr. A. Robertson, Mr. E. Brown and Mr. J. Gill.

Thanks are also due to the collaborators within the AE-WATT project who have facilitated and supported this research, particularly Dr. T. Fog for providing valuable data and technical advice, and also staff at MAN B&W Diesel, the Technical University of Denmark, Public Power Corporation and Envirocoustics. I would also like to express my appreciation to staff at Cummins Recon, Cumbernauld for kindly providing work experience and allowing access to engines for testing, and also to Mr. D. Ritchie for technical support and help in sourcing equipment.

Finally, I would like to thank the European Commission for their financial assistance provided under the EU Competitive and Sustainable Growth Programme, Project no: GRD2-2001-50014, which made this research possible.

ACADEMIC REGISTRY
Research Thesis Submission

Name*:*	Ryan McAllister Douglas		
School/PGI:	EPS/Mechanical Engineering		
Version: *(i.e. First, Resubmission, Final)*	Final	Degree Sought:	Ph.D.

Declaration

In accordance with the appropriate regulations I hereby submit my thesis and I declare that:

1) the thesis embodies the results of my own work and has been composed by myself
2) where appropriate, I have made acknowledgement of the work of others and have made reference to work carried out in collaboration with other persons
3) the thesis is the correct version of the thesis for submission*.
4) my thesis for the award referred to, deposited in the Heriot-Watt University Library, should be made available for loan or photocopying, subject to such conditions as the Librarian may require
5) I understand that as a student of the University I am required to abide by the Regulations of the University and to conform to its discipline.

* *Please note that it is the responsibility of the candidate to ensure that the correct version of the thesis is submitted.*

Signature of Candidate*:*		Date:	

Submission

Submitted By *(name in capitals):*	
Signature of Individual Submitting:	
Date Submitted:	

For Completion in Academic Registry

Received in the Academic Registry by *(name in capitals):*			
Method of Submission *(Handed in to Academic Registry; posted through internal/external mail):*			
Signature:		Date:	

Table of Contents

List of Tables

List of Figures

List of Abbreviations

AE	Acoustic Emission
BDC	Bottom Dead Centre
DAQ	Data Acquisition Card
FFT	Fast Fourier Transform
HSDI	High Speed Direct Injection
ICA	Independent Component Analysis
ICAV	Instantaneous Crankshaft Angular Velocity
IMEP	Indicated Mean Effective Pressure
LIF	Laser-Induced Fluorescence
MCR	Maximum Continuous Rating
NDT	Non Destructive Testing
NI	National Instruments
PAC	Physical Acoustics Corporation
PCA	Principal Component Analysis
PSD	Power Spectral Density
RMS	Root Mean Square
RPM	Revolutions Per Minute
SCU	Signal Conditioning Unit
STFT	Short Time Fourier Transform
TAN	Total Acid Number
TBN	Total Base Number
TDC	Top Dead Centre
TEU	Twenty-foot Equivalent Unit

List of Publications from this Thesis

Douglas, R. M., Hymers, D. A., Steel, J. A. and Reuben, R. L. Source identification of piston ring and cylinder liner interaction using acoustic emission. *Proc. 17th Intl. Conference on Condition Monitoring and Diagnostic Engineering Management, COMADEM*, Cambridge, UK, 23-25 August 2004, pp. 305-314.

Douglas, R. M., Nivesrangsan, P., Robertson, A. I. F, Brown, E. R., Steel, J. A., Reuben, R. L and Fog, T. L. Acoustic emission as a tool to reveal diesel injector performance. *Proc. 17th Intl. Conference on Condition Monitoring and Diagnostic Engineering Management, COMADEM*, Cambridge, UK, 23-25 August 2004, pp. 315-324.

Douglas, R. M., Steel, J. A. and Reuben, R. L. A study of the tribological behaviour of piston ring/cylinder liner interaction in diesel engines using acoustic emission. *Tribology International*, 2006, 39(12), pp. 1634-1642.

Douglas, R. M. An emerging technology – performance and condition monitoring of diesel engines and gas turbines via acoustic emissions measurements. *The Power Engineer – Journal of the Institution of Diesel and Gas Turbine Engineers,* February 2006.

Douglas, R. M., Steel, J. A, Reuben, R. L. and Fog, T. L. On-line power estimation of large diesel engines using acoustic emission and instantaneous crankshaft angular velocity. *International Journal of Engine Research*, 2006, 7(5), pp. 399-410.

Pontoppidan, N. K. and Douglas, R. Event alignment, warping between running speeds. *Proc. 17th Intl. Conference on Condition Monitoring and Diagnostic Engineering Management, COMADEM*, Cambridge, UK, 23-25 August 2004, pp. 624-628.

Robertson, A. I. F., Douglas, R. M., Nivesrangsan, P., Brown, E. R., Steel, J. A. and Reuben, R. L. Source identification using acoustic emission on large bore cylinder liners. *Proc. of 26th Conference on Acoustic Emission Testing, EWGAE*, Berlin, Germany, 15-17 September 2004, pp. 773-781.

Chapter 1

Introduction

1.1 Condition monitoring

Demand for condition monitoring of machinery has advanced at a rapid pace in recent years. This has been driven primarily by the requirement within industry to improve the effectiveness of assets, that is the necessity to extract maximum profits from minimum investment in plant and equipment [1]. This translates into a need to attain high levels of asset availability, reliability and performance whilst minimising unplanned downtime and the cost of maintenance.

The need to make more cost effective maintenance actions has seen a shift in practise from corrective and preventative strategies to predictive strategies. Corrective maintenance, also referred to as breakdown or run-to-failure maintenance, involves operating machinery till failure or till an obvious fault has developed before any maintenance action is considered. Whilst this may be the least expensive strategy in the initial term it is generally considered bad practice and for process critical machinery the losses incurred due to breakdowns can be considerable. Preventative maintenance, also known as planned or calendar based maintenance, aims to avoid the deterioration of components to the point of failure through scheduled maintenance activities and the replacement of parts at conservative fixed intervals based upon failure statistics. However, the nature of this strategy implies a degree of wastage as in many cases components are replaced whilst still perfectly serviceable. This approach can also fail to protect against early failure of components and the maintenance actions may serve only to introduce further potential fault sources.

Predictive maintenance is a more flexible strategy in which maintenance actions are performed based only upon need. This requires the use of condition monitoring techniques to asses the condition of components and to detect fault sources well in advance of failure. The benefits of this approach are that the maintenance and operational strategies can then be based around the prognosis of remaining serviceable life. In this way failures can be avoided, downtime can be minimised through improved

planning opportunities, and if required, component life can be taken to the fullest. Furthermore, since this strategy is based upon an on-line, or near to on-line, measure of condition then it can also be used pro-actively to optimise operation by avoiding where possible the conditions that severely reduce component life.

Clearly, the success of this approach lies with the assessment of component condition. The complexity of this task varies depending upon factors such as the difficulty in acquiring the measurements, the difficulty in extracting the relevant diagnostic information from the measurements and the required accuracy of the prediction. Systems for diagnosis of faults or condition typically comprise some form of knowledge base and the application of rule-, case- or model- based reasoning [2]. Further, to ascertain the remaining component serviceable life requires the development of prognostic techniques, these can range from simple historical failure rates to complex physical models.

The ability of current monitoring techniques to monitor and diagnose all known faults and conditions is limited, particularly for processes which have traditionally been considered difficult to monitor. The demand for improved diagnostic information, combined with advances in sensor technology, signal processing and computational power, and lower costs, mean that it is now possible to consider new techniques which may offer greater diagnostic capabilities. The potential of one of these, Acoustic Emission (AE) monitoring, to reveal information about critical processes in diesel engines is investigated in this thesis.

1.2 Engine lubrication optimisation and incipient fault detection

A specific example of a process where a condition monitoring system is required is the piston ring-pack and cylinder liner interface in large, two-stroke, diesel engines. This interface is prone to excessive abnormal wear conditions [3], due ultimately to the lack of a sufficient lubricating film. As engines have developed to generate more power per unit capacity the demands placed upon the interface and the lubricating oil have increased and consequently this has led to an increased likelihood of severe wear.

These engines are distinctive in a number of ways; one is that the amount of lubricant supplied to the ring-pack/liner interface can be adjusted to suit operational requirements. The consequences of under-lubrication can be severe. Abnormal wear can quickly be initiated and if not detected and rectified then irreversible damage can occur, possibly resulting in a costly overhaul and unplanned downtime. Due to the extreme conditions in which the interface operates and the limited margins for out-of-the-normal operation it is also possible that severe wear can occur during periods of normal lubrication [3].

Whilst over-lubrication may alleviate this problem it comes at a cost, not only through significant economic wastage, but also through increased exhaust emissions and the introduction of further potential fault sources. Excessive amounts of lubricating oil can result in carbon deposition in the ring-pack area which can instigate excessive wear in addition to causing sticking piston rings and choked ports [4]. There are also safety implications as an accumulation of this material can lead to potentially fatal fires and explosions. Hence, although many ship operators make it common practise to over-lubricate the engine cylinders, with the perceived benefit of lengthening component service life, their actions can often be counterproductive, resulting in possible harmful operation of the engine and expensive lubricant wastage.

Therefore, there is an optimal lubricant dosage which can allow for reduced operating costs, carbon build-up and exhaust emissions whilst ensuring that a sufficient oil film is maintained to avoid severe wear conditions. To achieve this optimisation, and to provide incipient detection of fault sources, a condition monitoring system is required that can offer information as regards the running conditions at the ring-pack/liner interface. The work in this thesis specifically aims to examine the capability of AE monitoring to address this requirement.

1.3 Acoustic emission monitoring

AE is the expression given to transient, high-frequency elastic waves in the range 0.1 to 1 MHz which occur as the result of a rapid release of strain energy within or on the surface of a material [5]. In machinery operation, a number of source mechanisms are known to generate AE such as mechanical impacts, fluid flows, sliding contact and wear. The resulting AE signals can be measured at the surfaces of machinery via an

appropriate transducer and can be analysed in a variety of ways to suit the type of information desired, the most fundamental of which is the characterisation of signals with regards to behaviour of the machine under observation [5]. Since AE sensors can be located externally the technique is inherently non-intrusive, furthermore, the AE signals are associated with the actual operating and degradative processes, whereas other monitoring techniques typically measure symptoms of degradation and are often intrusive [6]. Such are the benefits of AE monitoring that research into various applications has accelerated in recent years and commercial AE based monitoring systems have become established in a number of engineering disciplines [7].

1.4 Research objectives

In this work, AE measurements acquired from external surfaces of diesel engines are investigated under the premise that these measurements can reveal information about the operation of critical processes within the engines. The type of engine of primary interest is large, two-stroke diesels, as utilised for marine propulsion and power generation. This is because the capital investment and life cycle costs of such machinery are significant and the applications are critical, in terms of safety as well as business profitability and operational reliability. However, this work is not constrained to just these engines as it also encompasses small, four-stroke diesels as found in a wide range of road transport applications.

The first objective is to investigate what information can be extracted from AE measurements regarding engine operation. This necessitates an evaluation of AE signals acquired from various sensor arrays with the aim of correlating features in the AE signals to the actual processes occurring within the engines.

The second objective is to study specifically AE arising from the piston ring-pack and cylinder liner interface. This interface is one of the key elements of engine operation, the condition of which impacts upon engine performance, emissions and reliability, and importantly, it is a process which lacks a suitable monitoring tool even though a number of techniques have been considered in the past. The influence of engine parameters such as engine speed, load, temperature and lubrication condition will be investigated in

order to develop understanding of the source mechanisms responsible for AE generation, and thereby of the aspects of interfacial behaviour which can be monitored.

A third objective is, using the same sensors and sensor positions, to explore the possibility of combining information obtained from AE measurements relating to the fuel injection process (i.e. engine input) with a more established monitoring technique based upon variations in the instantaneous speed of the crankshaft (i.e. engine output). The intention being to examine whether the amalgamation of these two techniques can be used to indicate engine performance, aid engine balancing and identify variations in individual cylinder performance.

1.5 Thesis outline

This thesis is structured in nine Chapters, the content and function of which are summarised below:

Chapter 1: Introduction

This Chapter introduces the general background of condition monitoring of machinery, the industrial context of the work in terms of the problem it attempts to address and some fundamentals of AE monitoring. The objectives of the research and the claimed contribution to knowledge are also identified.

Chapter 2: Diesel engines, condition monitoring techniques and the piston ring-pack and cylinder liner interface

This first part of this Chapter presents an overview of the types of diesel engine that the work in this thesis relates to. Published literature on various methods of monitoring engine condition is then reviewed in detail. The remainder of the Chapter provides background knowledge and reviews literature concerning a number of aspects of the operation and monitoring of the ring-pack/liner interface.

Chapter 3: Acoustic emission monitoring

This Chapter provides understanding of the principles of AE and methods for analysis of AE signals for the purposes of condition monitoring. Thorough reviews of published literature in the areas of AE monitoring of reciprocating engines and of sliding contact

are provided in order to understand what has been achieved to date. These lay the foundations for the work in this thesis.

Chapter 4: Experimental apparatus, procedures and signal processing

This Chapter provides details of the engines investigated, the AE measurement apparatus and the individual tests performed on each engine. It further describes the processing steps consistently applied to the acquired AE signals in order to make them suitable for comparative analysis.

Chapter 5: Four-stroke, trunk-piston, diesel engines

This Chapter presents the results and findings from tests performed mainly on four-stroke, diesel engines at Heriot-Watt University with the specific aim of investigating AE generation from the ring-pack/liner interface. The findings are compared to published literature concerning typical ring-pack tribological behaviour and AE monitoring of sliding contact in order to identify the likely source mechanisms of the AE activity.

Chapter 6: Two-stroke, crosshead, diesel engines: survey of AE generation

This Chapter surveys the characteristics of AE generation within the upper cylinder areas of large, two-stroke, diesel engines located at MAN B&W Diesels, Copenhagen, and at Public Power Corporation, Kos Island, Greece. It details the process of identifying sources for the numerous AE events generated during an engine cycle through the use of event mapping, knowledge of engine operation and information from multi-sensor AE arrays.

Chapter 7: Two-stroke, crosshead, diesel engines: monitoring of sliding contact at the piston ring-pack and cylinder liner interface

This Chapter presents and discusses the results from tests conducted to investigate AE generation from the ring-pack/liner interface in large, two-stroke engines. It considers tests over the engine operating range with both normal running conditions and attempts made to degrade ring-pack lubrication. The results are discussed and compared to findings from work on the smaller engines.

Chapter 8: Two-stroke, crosshead, diesel engines: monitoring of cylinder performance via measurements of AE and instantaneous crankshaft angular velocity

This Chapter considers the possibility of using measurements of AE activity during the fuel injection/combustion period combined with information about the fluctuations in rotational speed of the crankshaft to provide monitoring of engine balance over varying loads and diagnostic information regarding individual cylinder performance.

Chapter 9: Conclusions and recommendations for future work

This Chapter summarises the work as a whole, presenting the main results and achievements, and provides recommendations for future studies that could complement and extend the findings of this thesis.

1.6 Original contribution

The overall outcome of improved monitoring capabilities of engine processes based upon analysis of AE signals is the specific area in which a contribution to knowledge is claimed. As far as the author is aware there are very few published studies which have considered the possibility of monitoring running conditions at the ring-pack/liner interface in diesel engines through analysis of non-intrusive AE measurements. Those that are available [8, 9] have been conducted to an extent in parallel with this work, although with a different set of objectives. The work presented in this thesis considers a greater array of tests conducted over a wider range of engines and provides far more detailed interpretation of the signals. This has developed new understanding and has demonstrated that analysis of AE signals provides the ability to monitor aspects of the tribological behaviour at the ring-pack/liner interface, which, to the author's knowledge, is a significant contribution. Furthermore, the use of AE and crankshaft speed fluctuation parameters together to monitor engine performance is a new concept.

Chapter 2

Diesel engines, condition monitoring techniques and the piston ring-pack and cylinder liner interface

2.1 Introduction

This Chapter aims to provide background knowledge and understanding in three areas; characteristics of diesel engines, techniques for condition monitoring of engines and operation of the piston ring-pack and cylinder liner interface.

It commences with a brief overview of the types of diesel engine that the work in this thesis relates to, covering the principles by which they operate and their distinguishing features. Published literature regarding techniques available for condition monitoring of engines is then reviewed, though this is an ongoing research topic. The remainder of the Chapter is concerned with issues relevant to the operation of the ring-pack/liner interface. This includes discussion of the basic functions of piston rings, their tribological characteristics, and of specific issues and problems affecting large marine engines. Current piston ring monitoring techniques are evaluated in addition to a review of typical ring-pack behaviour as ascertained through experimental work and theoretical analyses. Understanding of ring-pack/liner interaction is identified as one of the key areas of research where this work can make a contribution to knowledge.

2.2 Diesel engines: types, basic principles and characteristics

Compression ignition engines, or diesel engines as they are commonly known after their inventor Dr. Rudolph Diesel, convert chemical energy stored in fuel into mechanical work at the crankshaft. Whilst these engines come in a variety of different forms and vastly different sizes they are all reliant upon the principle that fuel is ignited by heat generated during compression in the cylinder. Furthermore, their operation is generally based upon either the two- or four- stroke engine cycles, which refers to the number of piston strokes occurring during any one cycle of events.

Diesel engines can be further sub-divided into three categories; slow, medium and high speed. Engines which operate below 300 Revolutions Per Minute (RPM) are classified as slow speed and are found in large vessels and power plants. Medium speed engines cover the range 300 to 900 RPM and are typically used in smaller vessels and for power generation. High speed engines, above 900 RPM, are the most common, finding widespread use in road transport amongst many other applications.

The work in this thesis, although potentially applicable to all forms of reciprocating machinery, concerns experimental work conducted on slow-speed, two-stroke and high-speed, four-stroke diesel engines. This section details the characteristics of these engines and the principles by which they operate.

2.2.1 Two-stroke, crosshead, diesel engines

These are slow-speed, large-bore, diesel engines which are used to propel large, deep-water vessels and also for power generation. An annotated cross-section of a cylinder with piston at Top Dead Centre (TDC), the uppermost point of piston travel, is shown in Figure 2.1. This type of engine is the most powerful of all reciprocating engines with the largest generating over 90 MW from up to 14 cylinders using bore sizes upwards of 1000 mm and stroke lengths up to 2660 mm. They are also the most fuel efficient prime mover in the range 10 to 50 MW, offering thermal efficiencies that can exceed 50 %, whilst burning a variety of cheaper fuels such as heavy and intermediate fuel oils. Aside from their large size there are several important features which distinguish these engines.

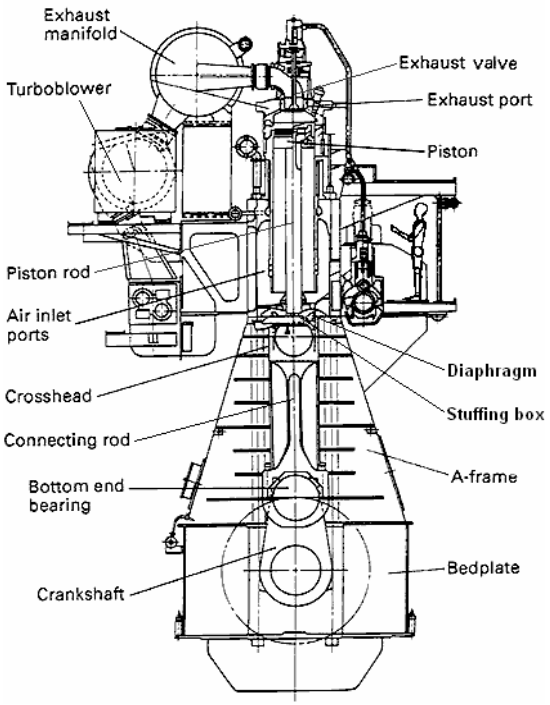

Figure 2.1: Annotated cross-section of a two-stroke engine with piston at TDC.

A major feature is that they employ a crosshead. This serves two functions; firstly, in combination with a diaphragm and stuffing box it effectively separates the combustion and scavenging (air inlet) spaces from the crankcase. This stops crankcase oil being transferred to the scavenge space and scavenge air from entering the crankcase, thereby reducing fouling and associated fire and safety risks. Secondly, the crosshead bearing surfaces take up the lateral thrust generated by the connecting rod, which significantly reduces the lateral forces acting at the ring-pack/liner interface.

Since this interface is separated from the crankcase the piston rings require a separate means of lubrication. This is achieved through a total-loss lubricating system in which high-alkalinity oil is metered and injected into the cylinder through a number of quills located circumferentially around the bore at the same time as the ring-pack passes the injection points. The piston rings largely facilitate the axial spread of the oil, with additional effects from the high-pressure gas, whilst circumferential spreading is aided by internal liner features such as a machined groove connecting the oil injection points and the wave-cut surface profile. The oil is consumed during the normal process of engine operation, either through combustion or scraped down the liner. In addition to ring-pack lubrication the oil is also required to counter the possibility of acidic corrosive attack which arises due to the burning of low-grade fuels that typically contain high sulphur levels.

These engines operate principally in two modes, either on the propeller curve for marine applications or the generator curve for power generation purposes. The term, propeller curve, refers to engine propulsion usage with a fixed pitch propeller (where torque $\sim n^2$ and power $\sim n^3$) hence both engine speed and torque output vary in order to meet the applied load. In generator mode a constant overall engine speed is required, irrespective of engine load, in order to generate electricity at constant frequency. Therefore, to meet an increase in engine load an increased amount of torque is generated.

A further point to note concerns the governing and control mechanisms of these engines. This is achieved either through the traditional cam-driven arrangements or the recently introduced electronic method [10]. The latter negates the use of a camshaft and instead uses electrohydraulic systems to actuate the exhaust valves and fuel injectors. This permits a greater degree of operational flexibility which is advantageous as it

enables operation to be optimised for various requirements such as improved fuel economy or reduced emissions.

2.2.2 Two-stroke, diesel engine cycle

Since these engines operate on the two-stroke principle an engine cycle consists of one crankshaft revolution and two piston strokes. Contained within these two strokes are the processes of scavenging (gas exhaust and air intake), compression, fuel injection, combustion and expansion. A diagrammatic example of this cycle showing the sequence and timing of the major processes is given in Figure 2.2.

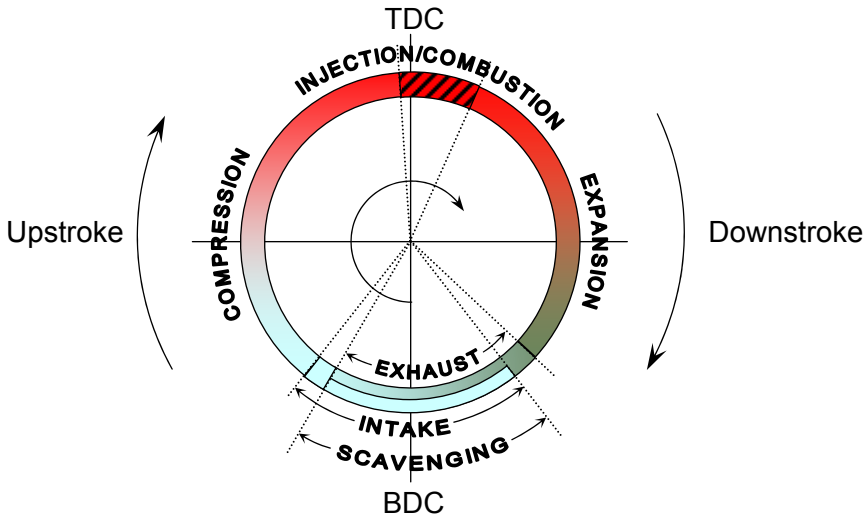

Figure 2.2: Schematic of a typical two-stroke diesel engine cycle.

At Bottom Dead Centre (BDC) the piston is momentarily at rest at its lowermost point, and the scavenging process is in progress, i.e. the removal of spent gases from the previous cycle and the admission of fresh charge. To permit this the exhaust valve is open and, as a result of the piston position, the scavenging ports (air inlet ports in Figure 2.1) at the lower end of the liner are uncovered. Air is blown under pressure into the cylinder through the scavenging ports and swirls upwards displacing the spent gases out of the cylinder via the exhaust valve. From BDC the piston ascends with the scavenging process continuing until the exhaust valve is closed. The cylinder is then supercharged for a short period until the ring-pack passes and closes the scavenging ports; this also marks the beginning of the compression phase.

The piston continues upwards and at around TDC fuel oil is injected into the combustion chamber as a spray of finely atomised droplets. At this point the

temperature of the compressed charge is sufficient to ignite the fuel and the combustion process begins. The gases then expand rapidly, and this coinciding with the piston passing through TDC results in the piston being forced down the liner, hence providing the power, or expansion, phase of the cycle. This continues until the exhaust valve is opened and the pressure in the cylinder is equalised. The ring-pack then descends past the scavenging ports, allowing fresh air to enter the cylinder and expel the spent gas. Scavenging occurs, the piston reaches BDC and the cycle begins again.

2.2.3 Four-stroke, trunk-piston, diesel engines

This form of engine is probably the most common, with engines available in numerous configurations covering the range 2 kW to 25 MW. The widespread use of these engines is due to their performance, reliability, compactness, versatility and relatively low cost. Road transport accounts for the largest market, although they are used in many other applications such as marine propulsion and power generating sets.

An annotated cross-section of a typical small, High Speed Direct Injection (HSDI), diesel engine is shown in Figure 2.3. These engines burn a light distillate fuel, generally known as diesel, which is more expensive than heavy fuel oil (although some larger variants do permit operation on the heavier fuel). In four-stroke engines the crankcase and the ring-pack/liner interface are not separated and therefore the same oil is required to lubricate all components. Oil is circulated continually throughout the engine via a number of passageways with the ring-pack lubricated by means of splash lubrication, spray bars and oil mists. The term trunk-piston refers to the piston skirt or trunk. Since these engines do not employ a crosshead, the piston skirt takes up lateral forces caused by the crank/connecting rod angularity and transmits it to the liner wall. It also allows these engines to be more compact than their two-stroke counterparts.

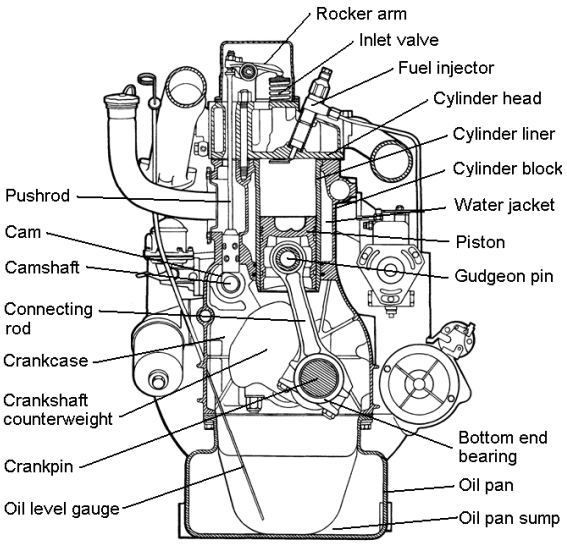

Figure 2.3: Annotated cross-section of a typical high-speed, four-stroke diesel.

2.2.4 Four-stroke, diesel engine cycle

As the name suggests for each engine cycle there are four strokes of the piston, hence two crankshaft revolutions, with combustion of fuel occurring every second revolution. For this operating cycle there is a process associated with each piston stroke. The cycle begins with the induction stroke. The inlet valve is open and the piston travels towards the crankshaft on its downstroke causing a charge of air to be drawn into the cylinder due to the partial vacuum created (natural aspiration) or to be forced in by means of turbo- or super- charging. The compression stroke follows, both valves are closed and the piston travels towards TDC, compressing the air and raising the temperature. Near the end of the compression stroke fuel is injected and ignited. The piston moves through TDC and the increased pressure caused by the expanding gases act on the piston to force it down the liner, i.e. the expansion stroke. In order for the engine cycle to be continuous, the expanded gases must be removed. This is accomplished on the exhaust stroke where the exhaust valve is open and the piston travels from BDC to TDC ejecting the majority of the spent charge.

2.3 Condition monitoring of engines

This section reviews the principles of engine condition monitoring and outlines a number of existing techniques. These mainly involve monitoring the performance of the combustion process and the resulting in-cylinder pressure, as this is often considered the heart of the engine, but also includes other engine sub-systems such as the valve train. Monitoring of the piston ring-pack and cylinder liner interface is considered later.

2.3.1 Motivation

Condition and performance monitoring of engines is important for technical, economic and safety reasons. This is particularly true for large, two-stroke diesels since they represent significant capital investments and efficient reliable operation is essential. A fundamental aspect of this is the engine maintenance strategy, with the ideal scenario being the adoption of condition-based maintenance practices that utilise monitoring

techniques to provide early indication of faults and progressive information regarding fault severity. The benefits of this approach are:

- Reduced potential for engine breakdown and subsequent unplanned downtime and repair.
- Maintenance actions, including the supply of parts and equipment, can be scheduled to best suit operational requirements.
- Inspections can be focussed on specific components suspected of deterioration.

Perhaps the most important objective is to reduce the risk of main engine failure. This is a problem faced by ship operators as the losses incurred due to engine failure can be severe, both financially, through repair costs, loss of hire and late delivery penalties, and more importantly through the considerable safety risk which, depending upon mode of failure or consequences of an adrift vessel, can in the worst cases lead to the loss of vessels, severe injury or death. A survey of marine accident statistics confirms that engine failure is a problem, for instance over the twelve year period, 1994 to 2005, machinery failure was reported to be responsible for 24 % of marine accidents involving UK merchant vessels over 100 gross tonnage [11]. More specifically, a survey of marine accidents involving oil tankers in Japanese waters in 2003 found that 8 % were attributable to insufficient maintenance, inspection or handling of the main engine [12].

Therefore, there is a strong case for ship-owners to consider installing condition monitoring systems in order to protect their assets and guard against failures. Whilst condition monitoring of smaller engines may not be as important, due to lower capital values and less critical usage, the application and improvement of monitoring techniques can still be of value, for instance to gain a greater insight into aspects of engine performance during engine developmental work.

2.3.2 Signal analysis

The initial condition monitoring techniques applied to diesel engines involved fault detection through use of the human senses; sound, smell, touch and sight. It is not too difficult to imagine that reliance on human perception alone is often uncertain and imprecise. This, combined with the increasing complexity of engines, has necessitated

the investigation of other means to monitor engine operation. The result is that a wide range of measurement and analytical techniques have been developed to measure and process data into a form where it can be interpreted with regards to engine condition. These range from systems which trend basic operational parameters to sophisticated techniques that require a high level of human expertise to fully automated, on-line, monitoring systems which fuse together data from dozens of separate engine measurements [13]. Most importantly, due to the continual demand for better-quality diagnostic information, developments in measurement and monitoring techniques are ongoing, with a number of new techniques, such as AE monitoring, actively being pursued.

Regardless of the sophistication of a condition monitoring system they are fundamentally similar in that they rely upon the measurement of parameters that vary either directly with the physical deterioration of a component, or indirectly from the effects of deterioration. Such measurands include variables such as pressures, temperatures and exhaust emissions, together with other signals that result from these variables, for example, engine surface vibrations, crankshaft speed fluctuations and manifold noise levels. In many cases the measured signal fluctuates continuously during an engine cycle and is therefore analysed on the basis of a cyclic signature.

Analysis of observed signatures generally aims to detect deviations from the norm. This can present major challenges. Signal changes relating to component or process deterioration have to be detected from the background of normal signal variation that arises from operation over the engine range, i.e. varying speeds, torques, ambient conditions, etc. The requirement for incipient fault detection further adds complexity as this may involve discrimination between subtle features in signals. However, early detection is an essential criterion of an ideal condition monitoring system as advanced stage faults, although easier to detect due to larger deviations from the norm, may require immediate attention. Additionally, accurate root cause diagnosis of faults in an advanced state can be difficult due to the cause-and-effect nature of fault propagation. A further aspect of the condition monitoring process is to construe a physical explanation for identified signal changes and in doing so, determine whether a fault is present and if so, the nature and severity of that fault.

2.3.3 Combustion investigation and cylinder power balancing

The most important element of engine operation is the combustion process as this ultimately determines such factors as the power generated, the stresses placed on various components and the emissions produced. For multi-cylinder engines, disparity between each cylinder's performance can lead to an unbalanced power delivery; this has been defined as when the average firing pressures for each cylinder are greater than 5 % of the engine average peak firing pressure [14]. In such circumstances the cylinders generating more power experience greater pressures and temperatures which can lead to increased stress levels, reduced lubricant effectiveness, increased susceptibility to improper fuel detonation, increased emissions and generally an overall increased likelihood of premature failure.

For these reasons, a great deal of work has focussed on developing methods to gauge combustion performance in each cylinder. Direct measurement of in-cylinder pressure is most desirable; however, for many cases this can prove impractical [15, 16, 17]. A fairly standard approach is to monitor the effects of combustion via the logging of pressure and/or temperature of the various fluid streams, i.e. exhaust gas, inlet (scavenge) air, lubricant, coolant, crankcase and fuel supply, as well as component temperatures and exhaust emissions. These measurements allow aspects of engine thermodynamic behaviour to be determined which can be an effective way to highlight performance trends. However, used alone they are often insufficient to determine component condition, and generally not with the sensitivity required for incipient fault detection.

Therefore, a number of alternative approaches have been proposed. These are based upon the monitoring of parameters directly related to the processes occurring in the cylinders such as:

- Crankshaft angular velocity and torque fluctuations [15-30]
- Vibration signatures [14, 31-42]
- Acoustic signatures [43-48]
- Structural strains in the engine [10, 18, 49]
- Exhaust gas pressure and temperature transients [50, 51]

2.3.4 In-cylinder pressure

Measurement of in-cylinder pressure is the fundamental approach for evaluating performance of large marine diesels on a cylinder by cylinder basis. The development of the in-cylinder pressure during an engine cycle is represented either with respect to the crank-angle position, as shown in Figure 2.4, or to the related cylinder volume. A number of measurement parameters can then be extracted including; maximum compression pressure, peak firing pressure, Indicated Mean Effective Pressure (IMEP), maximum rate of pressure change, as well as associated crank-angle timings. These values can be compared to the predetermined ideal condition or trended over time to identify gradual changes in performance. Furthermore, the nature of any faults can usually be diagnosed, for instance, a reduction in the maximum compression pressure may indicate a problem with the sealing effectiveness of the piston ring-pack.

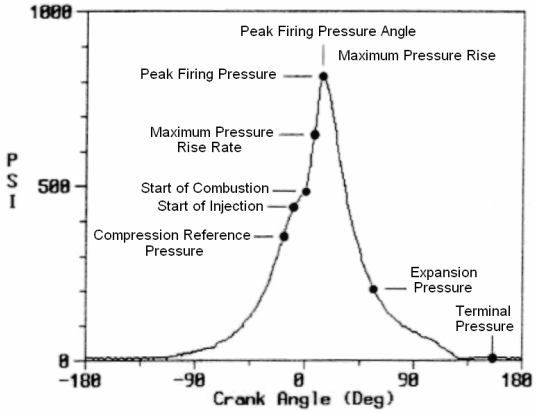

Figure 2.4: In-cylinder pressure measurement parameters, from Long and Boutin [14].

Hountalas and Kouremenos [52] showed how analysis of in-cylinder pressure measurements could inform as to the operating condition of large, two-stroke, diesel engines. A system was developed which evaluated performance against a thermodynamic model formed from shop trial reference tests and additional gas-stream pressure measurements. This allowed the condition of a number of engine sub-systems to be determined such as; cylinder compression quality, power output per cylinder, injection quality and fuel consumption. The system was tested on an engine suffering from poor performance and it revealed a series of faults that could not be detected from indications provided by conventional process measurements.

Instrumentation for measurement of in-cylinder pressure has been subject to a great deal of development. The traditional method involves the use of indicator valves built into each cylinder and mechanisms which graphically represent the in-cylinder pressure on paper. Improvements were made through the use of pressure transducers installed in the

indicator valve. Warkman [53] described a performance monitoring system for cylinder balancing based upon measurements acquired from air-cooled piezo-electric transducers. Accuracy of the transducers was noted as being of paramount importance. Takai and Tsukahara [54] also demonstrated that meaningful measurements could be made from transducers installed in indicator valves. Data were acquired continuously over a 2½ hour voyage of a high-speed ferry in order to investigate combustion performance. In this case a fibre-optic pressure sensor and a custom fixing mechanism were used to reduce the detrimental thermal effects of the combustion gases. This technique still has problems relating to reliable long-term monitoring as there is a tendency for the indicator bore to foul and clog up [10].

Pressure transducers have been developed that can be located directly in the combustion chamber thereby giving the ideal measurement of in-cylinder pressure. There are numerous examples where such instrumentation has been used for engine research and developmental work [15, 16, 41, 49], however, although reliability of these devices has improved in recent years there are still concerns for long-term application due to continual exposure to the harsh combustion environment [16]. Other problems relate to space limitations in the cylinder head area, particularly for smaller engines, and prohibitive instrumentation costs. Therefore, alternative techniques have been investigated whereby variables affected by the in-cylinder pressure are used to assess condition.

2.3.5 Instantaneous crankshaft angular velocity

One parameter that has been used extensively is measurement of the Instantaneous Crankshaft Angular Velocity (ICAV). The crankshaft experiences small accelerations and decelerations about the mean engine speed due to the rapid changes of in-cylinder pressure that occur during the compression and expansion phases. Generally, as a cylinder fires the resulting force on the crankshaft generates a torque greater than the load torque, which causes it to accelerate. As the next cylinder to fire goes through the compression phase, energy is extracted and the overall torque output drops below the load torque causing the crankshaft to decelerate. This process is repeated and the outcome is a fluctuating ICAV waveform which is directly related to the individual

cylinder-by-cylinder torque contribution, and thereby to the in-cylinder pressure and combustion performance within each cylinder.

Both measurement of instantaneous crankshaft torque and ICAV can be used to investigate the original in-cylinder pressure information. However, torque can be a difficult parameter to measure directly. Methods do exist, as outlined by Fleming [18], but to achieve this with sufficient precision in an industrial environment can require a complex custom solution and substantial modifications. In contrast, measurement of crankshaft speed is relatively simple and non-intrusive, with the only requisite being time-based measurements of crankshaft position. A number of methods to achieve this are reviewed by Li *et al* [19]; typical systems are an induction sensor to measure each gear tooth profile on the flywheel starting ring or an optical shaft encoder.

Many researchers have proposed systems that reconstruct the in-cylinder pressure trace, or its significant features, from ICAV measurements [16, 17, 22-24]. This conventionally has depended upon a model of the engine which is an attractive approach as it exploits engineering knowledge of the engine and provides insight into the physical mechanisms responsible for the ICAV fluctuations, an overview shall therefore be presented.

2.3.5.1 Instantaneous crankshaft angular velocity: theory

Modelling of ICAV fluctuations depends upon satisfying an angular momentum balance of the crankshaft system, described in Equation 2.1, through the engine cycle. This relies upon the assumptions that the crankshaft is rigid and that the engine is operating under steady-state conditions.

$$I_o \frac{d^2\theta}{dt^2} = T_n = T_o - T_l \tag{2.1}$$

where I_o is the inertia of the system, θ is the angular position of the crankshaft, t is time and T_n is the instantaneous net torque generated by the engine, which can be considered as the difference between the engine output torque, T_o, and the load torque, T_l.

The engine output torque is itself the sum of several components:

$$T_o = T_i + T_r - T_f \tag{2.2}$$

where T_i is the torque generated by the in-cylinder pressure, and is referred to as the indicated torque, T_r is the inertial torque due to the effective reciprocating mass and piston motion, and T_f is the sum of the frictional losses incurred, for instance, the sliding piston assembly/cylinder liner interfaces and the pumping losses.

For investigations based upon ICAV measurements the component of interest is usually the indicated torque. This is related to the in-cylinder pressure purely through the geometry of the reciprocating assembly [20]:

$$T_i = A_p r \sum_{k=1}^{N} P_k(\theta) f_k(\theta) \tag{2.3}$$

where A_p is the piston area, r is the crank radius, N is the number of cylinders, $P_k(\theta)$ is the in-cylinder pressure for the k^{th} cylinder, and $f_k(\theta)$ is a function of the engine geometry [20]:

$$f_k(\theta) = \sin(\theta + \phi_k) + \frac{\lambda \sin(2(\theta + \phi_k))}{2\sqrt{1 - \lambda^2 \sin^2(\theta + \phi_k)}} \tag{2.4}$$

where ϕ_k is the firing phase for the k^{th} cylinder and $\lambda = r/l$, i.e. the ratio of crank throw to connecting rod lengths.

A second component of engine torque output is the torque due to the inertial forces of the reciprocating assemblies. This is dependent upon engine geometry and speed, and although it does not contribute net energy to the system it can be responsible for significant fluctuations in the torque output during a cycle [15]:

$$T_r = \frac{1}{2} m r^2 \omega^2 \sum_{k=1}^{N} \left(-\frac{\lambda}{2} \sin(\theta + \phi_k) + \sin 2(\theta + \phi_k) + \frac{3\lambda}{2} \sin 3(\theta + \phi_k) \right) \tag{2.5}$$

where m is the reciprocating inertial mass and ω is the mean angular speed.

Depending upon the construction of the engine Equation 2.5 can be simplified. For instance, for a four-cylinder, four-stroke engine the inertial torque reduces to $T_r = -2m\omega^2 \sin 2\theta$ [15].

The friction incurred due to piston assembly/cylinder liner interfaces and gas pumping represents a loss component to be overcome. These can be considered separately but have traditionally been grouped together due to the difficulty in separating the effects of one from the other. The piston assembly friction is particularly difficult to determine, although it can be expected to vary with engine operating conditions, and will also vary during an engine cycle. Some researchers have attempted to estimate the frictional loss component based upon empirical observations of the torque required to motor an engine, for instance Rizzoni and Ribbens [21]. The topic of piston assembly friction shall be covered in greater detail in a later section of this Chapter.

Figure 2.5 shows modelling of torque behaviour during an engine cycle based upon measured in-cylinder pressure data [15]. Both a single- and a four-cylinder engine are considered, Figures 2.5a and 2.5b respectively, with the total torque and relative contributions from indicated and inertial torques shown, friction and external loading components have been omitted. For the four-cylinder case the engine is assumed to be operating uniformly, i.e. the in-cylinder pressure traces for each cylinder are identical when the phase shift due to the firing order is taken into account.

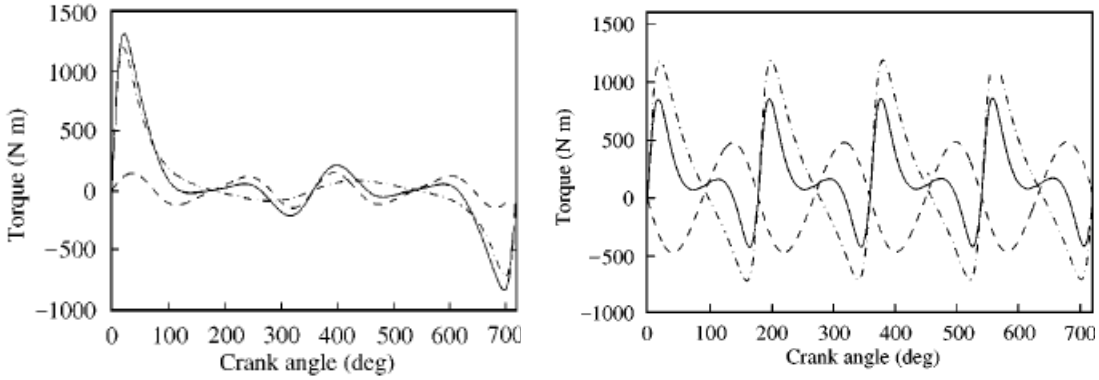

(a) *(b)*

Figure 2.5: Modelled torque behaviour, (a) single-cylinder, four-stroke engine, (b) four-cylinder, four-stroke engine, both at 1000 RPM and no load, where —— torque output, T_o, - · - · indicated torque due to in-cylinder pressure, T_i, and - - - - - inertial torque, T_r, from Yang et al [15].

2.3.5.2 Instantaneous crankshaft angular velocity: applications

Citron *et al* [22] demonstrated reconstruction of in-cylinder pressure traces during the compression/expansion phases using an elastic modelling approach for a four-cylinder engine. They assumed that the indicated torque at any moment in the cycle results from only the cylinder entering the power stroke and found that the in-cylinder pressure could be predicted with good accuracy in the vicinity of the peak pressure. It was shown that this method could be used to detect faulty cylinders as per traditional pressure trace diagnosis. One cylinder was underfuelled to simulate partial misfire conditions and the reconstructed pressure trace exhibited the expected reduction in peak pressure.

Lida *et al* [23] used a similar modelling approach to estimate IMEP on a cylinder-by-cylinder basis. Again, this method was dependant upon identifying angular intervals in which the net torque was dominated by the effects of one cylinder. Azzoni *et al* [20] described work where the indicated torque over a range of operating conditions was reconstructed to a precision sufficient for engine control applications. Yang *et al* [15] compared measurements of ICAV to that modelled from in-cylinder pressure data and reported a strong resemblance, particularly at lower engine speeds.

A significant problem with the use of engine models is that errors can be introduced due to the simplifying assumptions upon which the models are based. This is especially true for the notion that the crankshaft system is rigid. It is of course, an elastic structure and therefore subject to torsional vibrations. This can confuse matters, particularly for large engines [24], and is complicated further when interaction between engine and loading mechanism is considered. In fact, the torsional dynamics of the crankshaft are such that the monitoring of torsion angles has been shown to be of diagnostic value. Both Mauer and Watts [25] and Shimuza [26] describe systems which measure the phase difference from two shaft encoders located at either end of the crankshaft. This allows instantaneous torque to be inferred, from which abnormalities such as induced compression faults [25] and blocked injector orifices [26] have been detected.

In addition to torsional vibrations, a further problem is that the inertial torque component increases in proportion with the square of engine speed and therefore at high engine speeds it can effectively mask the torque contribution from individual cylinder

pressures [23, 25]. For engines consisting of a large number of cylinders the identification of an individual cylinder's contribution is further complicated due to overlap of power strokes.

Because of these deficiencies the use of pattern recognition techniques to relate ICAV fluctuations to in-cylinder pressures has been investigated. For instance, Brown and Neill [24] have applied pattern recognition to estimate peak cylinder pressures using a knowledge base of ICAV waveforms corresponding to known normal and underfuelled cylinder conditions. Observed ICAV waveforms were then compared to the database and linear interpolation used to estimate cylinder peak pressures. This method was reported more successful for higher cylinder pressures and a value for the overall standard deviation of prediction errors was given as 5.8%.

Gu *et al* [16, 17] expanded upon this to reconstruct the entire in-cylinder pressure trace using a Radial Basis Function neural network. The reconstructed trace was found consistent with the measured pressure over all stages of the compression/expansion phase and therefore diagnostic parameters such as peak pressure, rate of pressure rise and IMEP could be extracted. An example of application towards fault diagnosis was given. The combustion chamber was effectively enlarged through the drilling and plugging of a small hole into the chamber and the subsequent reconstructed in-cylinder pressure trace showed a reduction in pressure consistent with this fault.

A further approach towards analysis of ICAV fluctuations has been to directly assess engine non-uniformity or detect abnormalities without first reconstructing in-cylinder pressure or torque waveforms [15, 21, 27-30]. These investigations have typically involved diagnostic parameters based upon the relative amount of ICAV fluctuation resulting from each cylinder's compression and expansion strokes.

Yang *et al* [15] investigated whether underfuelling in one cylinder of a four-cylinder engine could be detected, the effect of which was an approximate 10% reduction in peak in-cylinder pressure. Waveforms corresponding to normal and underfuelled operation for two different speeds and no load are shown in Figure 2.6. From these the ICAV increase due to combustion in the affected cylinder and the amount of this increase as a percentage of the total ICAV range were identified as diagnostic parameters. For the underfuelled case these both showed a significant reduction from

the normal values. Other researchers have performed fault diagnosis in a similar manner, for instance, Tinaut *et al* [27] used the same parameters to identify a compression fault in one cylinder of a 5.8 MW, eight-cylinder, diesel engine.

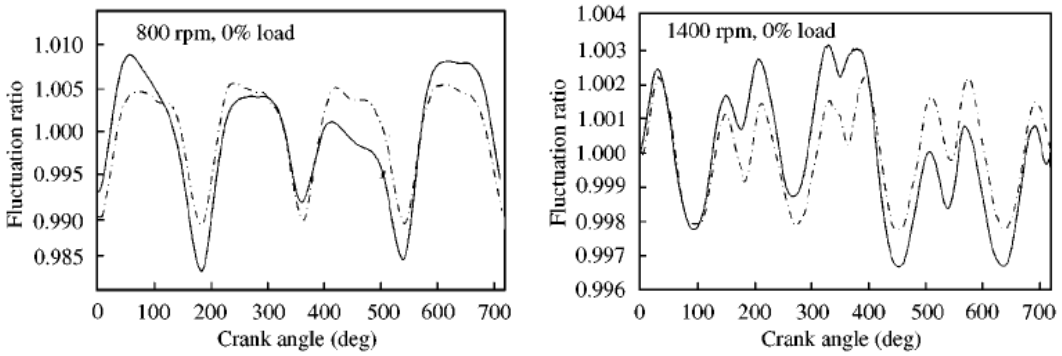

Figure 2.6: Measured ICAV waveforms at 800 and 1400 RPM, where - · - normal condition, — one cylinder underfuelled and fluctuation ratio = ICAV / mean engine speed, from Yang et al [15].

Rizzoni and Ribbens [21] defined a parameter, again based upon local ICAV maxima and minima resulting from each cylinder's compression and expansion phases, which returned a zero value for uniform operation and increased monotonically with engine non-uniformity. It was shown that this parameter could be used to easily detect continual misfire conditions induced in one cylinder through disabling of a spark plug or a complete fuel injector. Over a range of engine speeds and for two different six-cylinder engines the overall non-uniformity parameter was consistently significantly greater for the misfire conditions than for normal operation.

Similar findings were described by Mihelc and Citron [28]. In this case, engine performance was assessed through a roughness index based upon the difference in ICAV at successive TDCs. It was shown that this parameter was proportional to the mean cylinder-to-cylinder torque variation and that this would decrease with increased engine speeds, as demonstrated in Figure 2.7. When one cylinder was disabled the roughness index increased significantly. Further tests over varying air to fuel ratios showed that for lean mixtures the index increased and for rich mixtures it was slightly less than the normal. Work by Takats *et al* [29] found that a simplistic measure of ICAV fluctuation variance, the standard deviation calculated over half a crankshaft revolution, was a sensitive diagnostic indicator through which lean running conditions and occasional misfire could be detected.

Other researchers have investigated frequency analysis of the ICAV waveform to good effect; Taraza *et al* [30] showed that the harmonic structure contained information useful for misfire detection. For uniform engine operation the frequency spectrum for both a four- and a six-cylinder engine consisted of mainly their major harmonic orders with insignificant contributions from other orders. However, when misfire conditions were simulated in one cylinder the spectral contribution from the major orders reduced and the lower non-major orders increased. Further, the authors went on to show that for the six-cylinder engine the amplitude of the lowest major harmonic, at 3 times the running speed, was linearly correlated to the average IMEP of the engine and they described how this observation could be used to determine engine loading and the scale of cylinder unbalance.

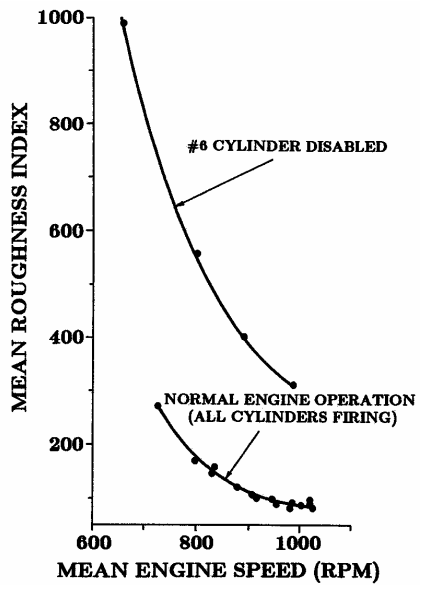

Figure 2.7: Mean roughness index as a function of engine speed, from Mihelc and Citron [28].

2.3.6 Vibration monitoring

Monitoring of surface vibration via accelerometers has proven to be an effective technique for condition monitoring. This is particularly true for rotating machinery, where fault detection usually consists of identifying rotational speed frequencies or their harmonics [31]. Application towards reciprocating machinery is not quite as straightforward although it has been suggested, Autar [32], that when compared to more classical monitoring techniques vibration signature analysis provides by far the most information about engine internal condition.

Engine surface vibration results from excitation forces associated with operational events such as mechanical impacts, fluid flows and friction [14]. The simplest form of analysis is to compare an observed signature against a reference indicative of normal operation. Deviations of amplitude or timing of expected events, or the appearance of unexpected events, combined with knowledge of engine operation, can be used to

diagnose performance or condition. Other process variables such as temperatures and pressures are often used to aid and strengthen this process. Analysis of vibration signatures has allowed diagnostic information to be obtained about processes such as fuel injection [14, 34, 36], combustion and diesel knock [34, 37, 38], valve operation [14, 34, 35] and tribological failure of crosshead bearings [39]. Further fault detection capabilities have been demonstrated through the reconstruction of the in-cylinder pressure trace [40-42]. It has also been applied towards monitoring the ring-pack/liner interface in large diesel engines [35]; this shall be discussed in a later section.

Long and Boutin [14] described a number of case studies where vibration and ultrasound signature analysis were used to diagnose a variety of faults including valve bouncing, damaged exhaust valve lifter, improper tappet setting, valve seating problems and faulty fuel injection. Similar work was reported by Haller and Kelleher [33]. In both cases fault diagnosis was achieved through comparison to reference normal signals. However, there were ambiguities as to the instrumentation used, particularly regarding the location of sensors and the acquisition of the ultrasonic signals. Nevertheless, the advantages and increased diagnosis potential over conventional monitoring techniques were clear. Chandroth *et al* [34] further showed through the use of an artificial neural network that a variety of commonly occurring valve and injector faults in a small, twin-cylinder engine could be identified through analysis of vibration signals.

Sasaki [35] used an array of accelerometers to survey surface vibration characteristics of a large, two-stroke diesel and again found that the origins of most activity were injector/combustion or valve related. Using additional TDC, shaft encoding and in-cylinder pressure signals the events in the vibration signals were mapped to their respective mechanical and fluid sources. This process was aided through approximate source location using array characteristics, for instance, vibration events resulting from exhaust valve activity were more prominent in signals acquired from the upper cylinder liner and exhaust valve housing components.

A common topic in engine vibration diagnostics is monitoring of injector operation. A non-intrusive solution is particularly attractive since other techniques such as needle lift and fuel-line monitoring are intrusive, can detrimentally affect injector performance and are also potentially hazardous. Gu and Ball [36] reported that needle impacts and high-

pressure fluid flows are the principle vibration sources during injector operation. It was also noted that the measured vibration response was influenced by the dynamic properties of the injector body and less so by other potential noise sources such as combustion and piston slap. They proceeded to show that the timing of injector events could be extracted from the vibration signal and that these were similar to those obtained from simultaneous needle lift measurements.

Molinaro and Canstanié [37] described a method for improved knock detection in spark ignition engines using vibration signals and pattern recognition, the aim being to improve upon techniques whereby knock is deemed to occur if abnormally high-energy vibration is observed in a windowed period. The disadvantage to an energy-based approach is that the knock-induced vibration has to be detected against a background of other sources and this can result in a very poor signal to noise ratio, especially at high engine speeds. A further method for knock detection through extraction of both time- and frequency- domain parameters was outlined by Ghasemloonia and Behzad [38].

Kitahara *et al* [39] investigated vibration monitoring of tribological failure on a rig which simulated operation of a crosshead bearing in a large, two-stroke, diesel engine. Lubrication condition and the applied load were varied to assess if lubricant film failure and the beginning of severe metal-to-metal contact could be detected prior to complete seizure. They found that vibration events were generated when the reciprocating speed between the bearing surfaces was momentarily zero and oil film thickness was at a minimum. When the oil supply was stopped the level of vibration at these points increased progressively in amplitude. Similar observations were made when loading was progressively increased under normal lubricating conditions. These abnormal vibration spikes were attributed to severe metal-to-metal contact that is precursor to complete seizure. It was noted that this could be used to provide early warning of problems so to allow remedial measures to be taken.

Vibration signals have also been used to reconstruct the in-cylinder pressure trace. This has been accomplished successfully for both single-, Randall and co-workers [40, 41], and multi-cylinder engines, Zurita *et al* [42], operating under steady-state conditions. This technique is based on the presumption that transient vibrations are generated by the pressure waveform during the combustion phase. Therefore, if the transfer function relating the forcing pressure wave to the surface acceleration response can be identified

then the inverse of this function can be used to reconstruct the pressure trace. However, not all attempts have been successful. Azzoni *et al* [20] commented that pressure reconstruction based upon vibration measurements was unsatisfactory; finding instead that similar analysis using ICAV measurements produced better results. Gu *et al* [16] further questioned the ability of vibration-based reconstruction methods to estimate the compression phase and also whether a transfer function is constant during the service life of an engine.

Vibration monitoring in general does have other problems, mainly regarding event isolation and the resulting signal to noise ratio. With regards to engines some events generated during the cycle of one cylinder can have marginal separation and when events originating from other cylinders are considered then the levels of event overlap can make focused analysis difficult. Autar [32] noted that this was common for small, multi-cylinder engines. Means by which events could be separated were elucidated to, with the example given of signal isolation through careful filtering. It was also observed that much random noise is present in vibration signals [32]. Albarbar *et al* [43] concurred that the diagnostic information is dominated by both background and interference noise and proposed methods such as coherent filtering techniques and adaptive noise cancelling to improve this situation.

2.3.7 Air-borne acoustics

In a similar manner to vibration monitoring analysis of air-borne acoustics has been used to assess engine condition. Gu and co-workers have performed a thorough investigation [43-46], particularly of injector operation and combustion [44, 45]. They found that better-quality diagnostic information was contained in the higher frequency band, 10 to 50 kHz, than at frequencies below 10 kHz. In the upper band they identified a source of the acoustic signal to be combustion; hence it was suggested that this could be used to evaluate aspects of combustion uniformity and power balance. A significant drawback with acoustic monitoring of engines is that the various sources overlap greatly making it difficult to study each source in detail. Recent works have attempted to address this problem by decomposing the signal into individual sources [43, 46]; however, other problems remain such as accounting for the influence of room acoustics on measured signals.

Kimura *et a*l [47] analysed sound generated in the range 0.1 to 20 kHz from a medium-speed, six-cylinder, diesel engine. Frequency spectra were used in conjunction with a neural network in order to classify signals. Two faults were artificially induced; leaking exhaust gas through loosening of an exhaust manifold bolt and misfire through removal of the fuel supply to one cylinder. Both were reported to be detectable with reasonable success. Autar [32] reported that valve leakage was detectable through analysis of inlet manifold sound levels and Kawai *et al* [48] proposed a method whereby valve clearance could be estimated to an accuracy of 0.1 mm from wavelet analysis of engine acoustics.

Koike *et al* [55] described the use of an ultrasonic microphone for non-contact detection of abnormal engine bearing wear due to oil-film deterioration. For this work a microphone with a centre frequency of 80 kHz was used with any low-frequency signal suppressed through high-pass filtering at 50 kHz. The oil supply to one of the main bearings was stopped in order to purposely raise interfacial temperatures and induce scuffing conditions. This was accompanied at the initial stage by an increase in ultrasonic activity as is shown in Figure 2.8. The amount of this activity progressively increased as lubrication condition deteriorated and eventually irreversible scuffing occurred.

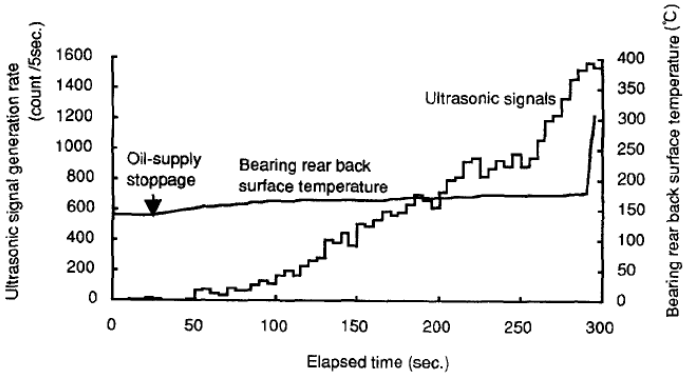

Figure 2.8: Increase in ultrasonic activity due to removal of oil supply to engine bearing, from Koike et al [55].

2.3.8 Structural strains

Measurements of strains imparted on engine components have been used to monitor engine operation. Pederson and Grøne [10] described the use of strain gauges installed on the cylinder cover studs of a large, two-stroke diesel to provide a

measurement representative of in-cylinder pressure. Although this system provided stable measurements over a period of more than 10,000 operating hours it was found to be susceptible to electrical noise. Fog *et al* [49] used similar strain gauge measurements to predict in-cylinder pressures using a neural network approach. As shown in Figure 2.9 these measurements contained a considerable amount of information regarding the in-cylinder pressure.

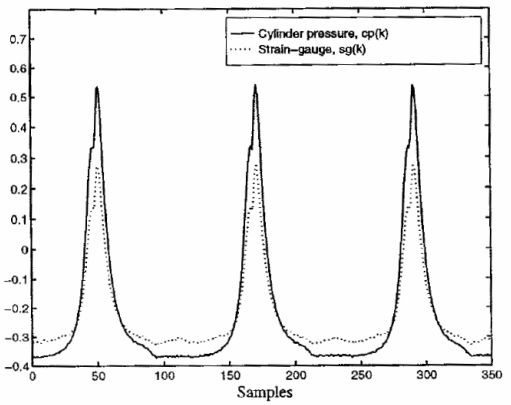

Figure 2.9: Strain gauge and in-cylinder pressure measurements, from Fog et al [49].

A further system which provides indirect measurements of in-cylinder pressure makes use of strain-pin type pressure transducers located close to the chamber surface [10]. These devices are again for use on large, two-stroke diesels and they operate by measuring the cylinder cover distortion caused by the cylinder pressure. This system is reported as being stable and reliable, and has been found acceptable as a normal engine monitoring and balancing tool by the crew of a merchant vessel [10]. However, although this system is non-intrusive in terms of the combustion chamber it does require modification to the cylinder cover, and furthermore, it may not be feasible for smaller engines where space around the cylinder head area is limited. Further structural strain monitoring techniques exist; some make use of piezoelectric washer sensors mounted beneath spark plug seats or cylinder head bolts [18].

2.3.9 Exhaust gas temperature and pressure

Measurement of exhaust gas temperatures is a standard technique through which fuel system malfunctions can be identified such as incorrect timing, incorrect fuel/air mixture ratios and inferior fuel quality. Exhaust gas temperatures are also often used towards cylinder power balancing through equalising the temperature for each cylinder. Unfortunately, as pointed out by Haller and Kelleher [33], this can prove ineffective due to erroneous measurements caused by carbon build-up on exhaust gas thermocouples and the varying influence of manifold gas dynamics. A further form of exhaust gas temperature monitoring, applicable to engines with a common exhaust manifold, is to

analyse temperature fluctuations caused by the discharge of gases from each cylinder through the use of a fast response thermocouple [32]. This can, to some extent, indicate relative cylinder performance, although it is again susceptible to instrumentation problems.

Similarly, analysis of instantaneous exhaust gas pressures has been used to assess combustion performance in individual cylinders. Chiavola [50] presented examples of the exhaust manifold pressure signal resulting from normal operation and with misfire simulated in one cylinder of a four-cylinder, spark ignition engine. The example given in Figure 2.10 clearly shows the individual contribution of each cylinder and the effects of a misfire induced at approximately 1000 degrees. The variation of the pressure pulses during normal operation are due to the individual cylinder performance, the exhaust system configuration and the relative transducer location. Similar to other signal analysis techniques, time- and frequency- domain processing methods were proposed in order to extract information regarding cylinder specific combustion quality.

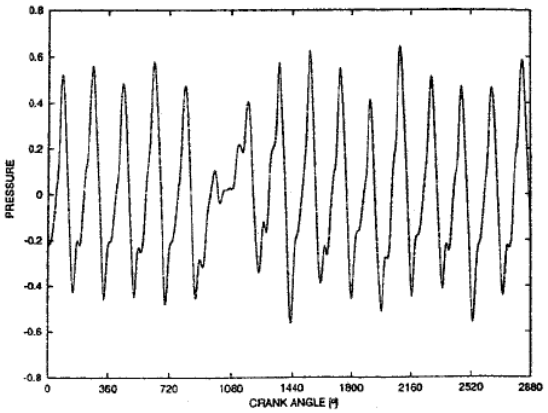

Figure 2.10: Exhaust pressure signal from a four-cylinder, petrol engine with misfire induced at approximately 1000 degrees, from Chiavola [50].

Gennish *et al* [51] further investigated analysis of exhaust manifold pressure fluctuations for fault detection. In their work the exhaust valve clearance was adjusted in one cylinder resulting in valve leakage and poor combustion conditions. The pressure signal exhibited a corresponding effect in the locality of the adjusted cylinder's firing and valve opening phases, with the irregularity increasing with valve clearance. The authors noted that the transducer location and sensitivity are very important if this technique is to be applied successfully.

2.3.10 Further engine monitoring parameters

A number of other parameters have been considered for monitoring of engine operation. The use of magnetorestrictive sensors has shown potential [56]. This technique is based upon the inverse magnetorestrictive effect, a phenomenon whereby physical deformations and strains produce a change in the magnetisation of ferromagnetic materials [57]. Monitoring of these changes is a passive technique through which stress waves can be detected up to the region of several hundred kHz, i.e. comparable to AE monitoring. Furthermore, magnetorestrictive monitoring is at an advantage over piezo-electric based techniques in some regards, for instance, it requires no direct physical contact and no use of couplant.

To the author's best knowledge investigation of magnetorestrictive monitoring for engine diagnostics has been limited to one study in which the combustion characteristics within a small, petrol engine were evaluated [56]. This reported that induced detonation was easily detectable through spectral analysis of the high frequency stress waves generated during combustion. Further work on detection of engine irregularities caused by mechanical faults led the investigators to state that "the number of faults detectable with magnetostrictive sensors is almost limitless. It provides the potential for engine diagnostics at a level we did not believe possible". This bodes well for the capabilities of AE monitoring since this is based upon measurement of the same high frequency waves. One noted problem was the identification and interpretation of signal characteristics, and specifically the separation of significant signals from the insignificant noise.

For spark ignition engines, measurement of the ionic current flowing through the spark plug has been used to monitor combustion performance and permit fault detection [58, 59]. A further technique which has shown promise is thermography, a tool which has developed through extensive use for monitoring of electrical equipment. This allows infrared radiation emitted by an engine or ancillary equipment to be interpreted graphically and is particularly useful for situations where thermal deviations are indicative of deteriorations in performance.

2.4 Piston ring-pack and cylinder liner interface

Since the main objective of this thesis is to investigate a novel technique for monitoring piston ring-pack and cylinder liner interfacial behaviour it is necessary to review a number of issues concerning this deceptively simple interface. This includes the basic types of piston rings, their functions and tribological characteristics. Specific issues and problems affecting large, two-stroke diesels will be reviewed in detail as this provides motivation for improving upon current monitoring capabilities. Issues relevant to ring-pack operation in four-stroke engines will also be outlined, including a review of experimental monitoring techniques and of typical ring-pack behaviour.

2.4.1 Piston ring fundamentals

The piston seal is an essential component in the operation of diesel engines [60]. Its primary role is to separate the hostile environment of the combustion chamber from the scavenge air space in marine two-stroke engines and the crankcase in four-stroke engines. The piston ring-pack generally consists of a number of split metal rings which sit loosely in circumferential grooves cut into the piston body to form a labyrinth seal. This is demonstrated by the schematics in Figure 2.11 which show the location of the ring-pack in the piston assembly and the typical ring-pack arrangement for a four-stroke, diesel engine.

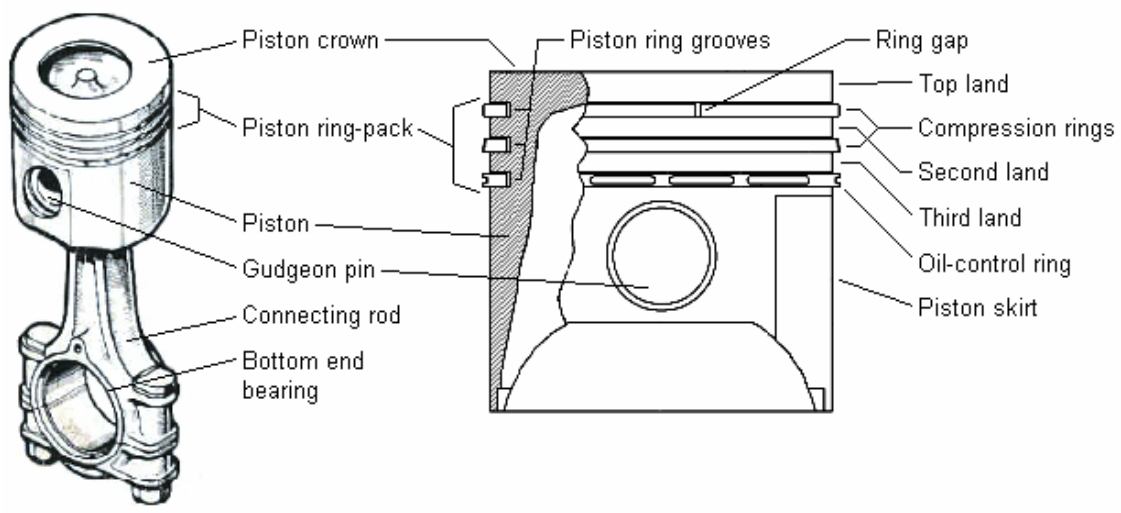

Figure 2.11: Schematics illustrating piston and connecting rod assemblies, and typical piston ring-pack arrangement for a four-stroke, diesel engine.

Undeformed piston rings have a diameter greater than the cylinder bore so that when compressed in the bore their elasticity provides a modest sealing action. This is enhanced by the radial force developed in the groove behind each ring by the high combustion chamber pressure, which the mechanism is designed to seal. This sealing force varies with the in-cylinder pressure and therefore the ring-pack forms an effective self-adjusting sealing mechanism. Secondary roles for the piston rings are to transfer heat from the piston into the cylinder wall, and thence into the coolant, to stabilise the piston, and additionally for four-stroke engines, to limit the amount of oil that is transported from the crankcase to the combustion chamber [61].

For optimal operation the objectives are to maintain a good sealing quality whilst controlling oil consumption and exhaust emissions, minimising frictional losses and maintaining low wear rates. The frictional losses are not insignificant. Richardson [62] reviewed cylinder friction for four-stroke engines and estimated that the piston assembly (including connecting rods) accounted for between 40 to 55 % of the total mechanical friction within an engine. Priest and Taylor [63] identified that even a modest reduction in friction would represent a significant efficiency improvement, stating that a 10 % reduction in mechanical losses would lead to a 1.5 % reduction in fuel consumption. Low wear rates are essential to ensure engine durability and extend the service life of components. One of the key factors in achieving these objectives is the performance of the lubricant which separates the interacting surfaces.

Piston rings are perhaps the most complicated tribological components in internal combustion engines [63]. This is reflected by the number of factors which may bear influence; piston motion (both primary and secondary), gas pressures, oil viscosities, ring twist motions, ring end gap effects, elastic and thermal deformations, component wear, and lubricant formulation, condition and availability, etc. The ring interfaces are subjected to severe and rapid variations of the aforementioned variables, particularly sliding speed, applied load, temperature and lubricant availability, and the result is that in a single piston stroke it may experience boundary, mixed and full film lubrication regimes. The characteristics of these are briefly explained in Table 2.1 and are represented by means of the modified Stribeck diagram in Figure 2.12 which relates film thickness ratio to the resulting friction coefficient. Film thickness ratio is the ratio of lubricant film thickness, itself a function of geometry, speed, load and oil viscosity, to the composite surface roughness.

Regime of lubrication	Characteristics
Hydrodynamic	Full fluid lubrication in which the surfaces are completely separated. The dynamic viscosity of the lubricant is its most important property.
Elastohydrodynamic	Nominally also full film lubrication with surface separation, but a more concentrated mechanism where elastic deformation of the surfaces and the effect of pressure on viscosity are important.
Mixed	There is surface asperity interaction to some degree and the characteristics of both Elastohydrodynamic and Boundary Lubrication are influential.
Boundary	The surfaces are in normal contact with behaviour characterised by the chemical (and physical) actions of thin films of molecular proportions.

Table 2.1: Summary of lubrication regimes, from Priest and Taylor [63].

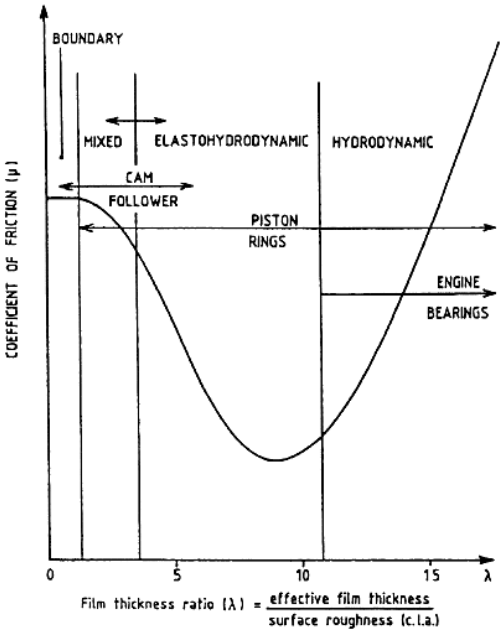

Figure 2.12: Lubrication regimes as identified via the modified Stribeck diagram, from Priest and Taylor [63].

Investigation of piston ring tribology has been a sustained research theme over several decades, as indicated by the numerous articles published on various aspects of this topic. Methods for this research have included theoretical modelling, miniaturised experimental work and full-scale engine testing. This Section reviews significant findings from this work in order to provide an appreciation of the typical behaviour of piston rings and of methods for monitoring their operation. For a more comprehensive review of understanding to date regarding piston ring tribology the reader is referred to Andersson *et al* [64].

2.4.2 Types of piston rings and ring-pack compositions

Piston rings form a ring-pack, typically consisting of 2-5 rings, with the number of rings dependant upon engine type and specification, although usually comprising 2-4 compression rings, which provide the sealing capability, and 0-3 oil-control rings [64]. The function of each ring and the force distribution at the ring/liner interface is largely determined by the profile of the ring face in contact with the liner. Figure 2.13 shows a number of commonly used face profiles. For compression rings these include plain rectangular, barrel- and taper-faced profiles, with each designed to provide gas sealing and in some cases perform additional tasks such as oil scraping and shortening of the running-in time. Oil-control rings have different profiles, generally consisting of two lands and an inserted ring expander or coil spring to bolster ring pre-tension. These rings offer little in the way of sealing ability and instead are designed to distribute oil evenly on the cylinder liner and scrape off surplus oil to be returned to the crankcase. The additional forces acting on these rings mean that although they control the oil film they experience the harshest lubricating conditions of the ring-pack as they operate on average with thinner oil films than compression rings [64].

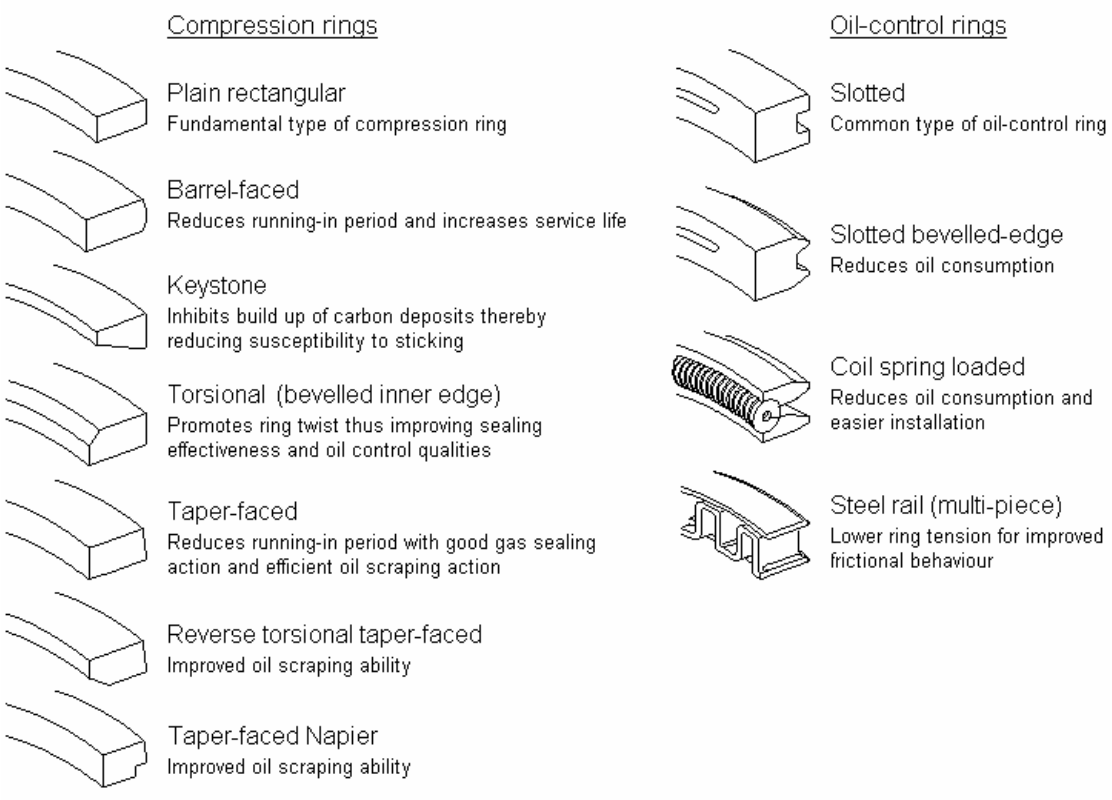

Figure 2.13: Typical face profiles of compression and oil-control rings.

The need for an oil-control ring depends upon the engine type and the method of lubrication. For four-stroke, trunk-piston engines, where the ring-pack is lubricated by splash lubrication, oil mists or pressurised supply, an oil–control ring is necessary to distribute oil evenly. However, for two-stroke, crosshead diesels the total-loss ring-pack lubrication system means that an oil-control ring is not required. For this type of engine the ring-pack consists of several compression rings.

2.4.3 Piston and piston ring kinematics

Fundamental aspects of piston ring operation are the piston and piston ring dynamics, which comprise the primary and secondary piston motions, radial and axial ring motions and ring twist. These motions influence all facets of ring operation; the formation of oil films, the resulting friction between ring and liner, wear of the components and blow-by across the ring pack.

The primary motion of the piston rings is equal to that of the piston. This can be determined as a function of the crank angle when the geometry of the crank-slider mechanism is known; a schematic of this assembly for a trunk-piston engine is shown in Figure 2.14a. Thus, expressions can be derived for piston displacement, velocity and acceleration, and these are given in Equations 2.6, 2.7 and 2.8 respectively.

$$s = r\left[\left(1-\cos\theta\right)+n(1-\cos\alpha)\right] \tag{2.6}$$

$$v = \omega r(\sin\theta + \frac{\sin 2\theta}{2n}) \tag{2.7}$$

$$a = \omega^2 r(\cos\theta + \frac{\cos 2\theta}{n}) \tag{2.8}$$

where s is piston displacement from TDC, r is the crank radius, θ is the crank angular displacement from TDC, n is the ratio of connecting rod length to crank radius (i.e. l/r), α is the connecting rod angle to the line of stroke, v is piston velocity, ω is the mean angular speed of the crankshaft and a is piston acceleration.

Examples of piston displacement, velocity and acceleration during a four-stroke engine cycle, with a connecting rod/crank radius ratio, n, of 2.6, are shown in Figure 2.14b.

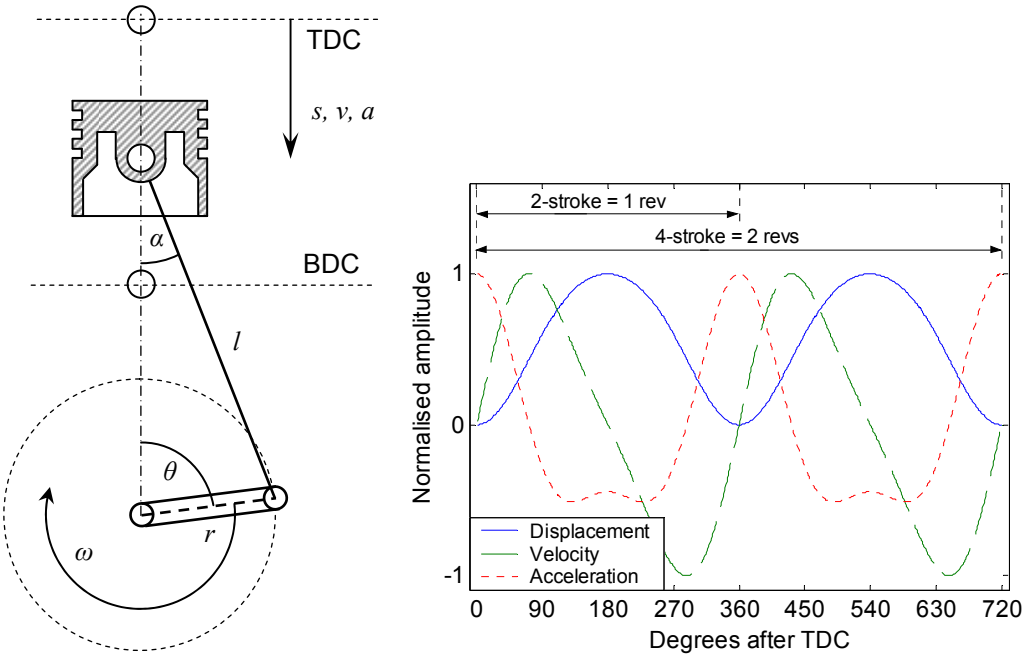

(a) *(b)*

Figure 2.14: (a) Schematic of crank-slider mechanism, (b) piston primary motion assuming n = 2.6.

Piston secondary motion also affects ring operation. This is caused by clearance between the piston and liner which allows lateral movement and rotation of the piston about the piston pin according to the forces and moments acting upon it. Piston rings also exhibit secondary motions; again including lateral movement and ring rotations, and additionally, ring lift and ring twist. These arise from the various forces acting on the rings, a summary of which is presented in Figure 2.15. These include; inertial forces from piston acceleration and deceleration, forces owing to the pressure difference across the ring, oil film damping forces, and friction forces from shearing of the lubricating film and contact pressure at the ring/liner interface.

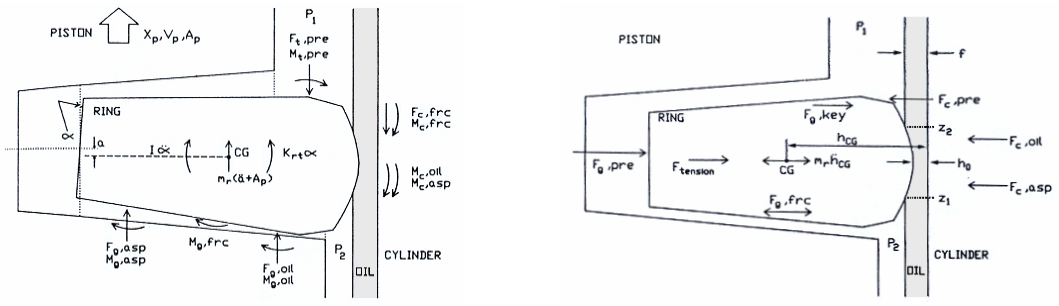

(a) *(b)*

Figure 2.15: Forces acting on a cross-section of a top compression ring, (a) Axial forces and moment balance, (b) radial forces, from Keribar et al [65].

2.4.4 Two-stroke, crosshead, diesel engines

2.4.4.1 Wear at the piston ring-pack and cylinder liner interface

For two-stroke, marine diesels the ring-pack/liner interface has been recognised as one of the principal causes of engine failure. This is supported by Figure 2.16 which shows the distribution of over 400 failure cases by engine sub-system [66] and identifies the liner and its lubrication as responsible for the greatest proportion of these failures. Faults encountered included cracked liners and abnormal, excessive wear caused by poor lubricating conditions.

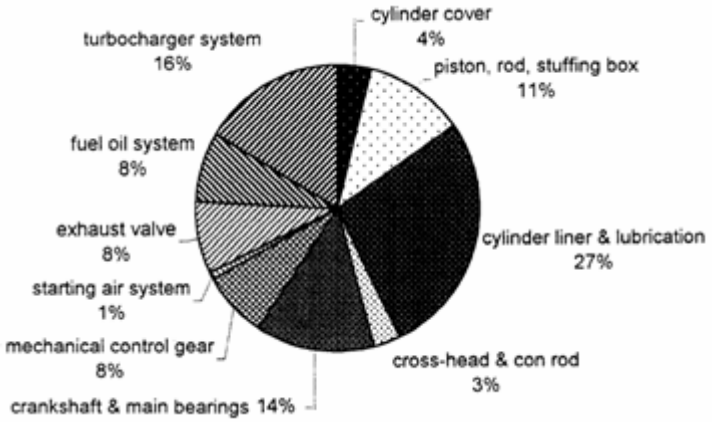

Figure 2.16: Failure distribution of two-stroke engines, from Wilson et al [66].

The familiar pattern of normal liner wear is that maximum wear occurs at or just below the top of ring travel, with the lowest wear being around the middle of the liner, and a small increase occurring again at the bottom of ring travel [67]. For two-stroke engines increased wear is also observed just above the scavenging ports. This wear pattern is a direct result of the various lubricating regimes that exist along the length of the piston stroke. At the top of ring travel the demands placed upon the oil film due to low sliding speeds, high gas loading (particularly the top ring), and high temperatures (hence low oil film viscosity) can cause breakdown of the oil film resulting in mixed and boundary lubricating conditions, i.e. metal-to-metal contact and subsequent wear. At the middle of the stroke pressure and temperature conditions are less arduous and piston speed is such that hydrodynamic lubrication can be achieved. At the bottom of the stroke wear rates increase again partly due to the reduced piston speeds and partly due to the scouring effect of the incoming scavenge air.

For large, two-stroke diesels liner wear rates of up to 0.1 mm per 1,000 hours are normally considered acceptable [67] with liners replaced when wear approaches 0.8 to 1 % of the original diameter. This gives an approximate liner life of seven years meaning that they have to be changed twice if the life of the ship is 20 years, although it is not unknown for ships to be retired with original liners in place. However, although acceptable wear rates apply to the majority of engines, instances of much heavier wear do occur that can result in costly overhauls and premature renewal of liners, pistons and rings. Abnormally high wear rates are generally attributed to corrosive, severe adhesive and abrasive wear mechanisms brought on by conditions such as poor lubrication, excessive blow-by and particle contamination.

Historically, until the 1990's the principal reason for abnormal wear was corrosive wear caused by the formation of sulphuric acid within the cylinder due to the high sulphur level of heavy fuel oil [68]. The introduction of high Total Base Number (TBN) lubricating oils countered this problem with further protection afforded through changes in engine design that saw the use of higher liner temperatures so to maintain sulphuric acid above its dew point.

However, higher liner temperatures, combined with other factors such as greater in-cylinder pressures, have increased susceptibility to a severe adhesive wear condition known as scuffing. This results in accelerated wear well in excess of the typical low adhesive wear rates associated with normal running conditions. Scuffing wear can quickly result in massive damage and it therefore represents a significant problem for reliable operation of large, marine diesels [3].

2.4.4.2 Scuffing wear

2.4.4.2.1 Definition

Scuffing, also referred to as microseizure, has been defined by the IMechE as "gross damage characterised by the formation of local welds between sliding surfaces" [69].

During normal operation the piston rings slide over the liner surface under boundary, mixed or full-film lubricating conditions. However, if there is breakdown of the oil film

then the resulting asperity contact can trigger a degenerative cycle of events which may eventually lead to scuffing. Initially, the asperity contact generates a localised increase in surface temperature which causes material expansion in the form of a small thermal bump. This increases the contact pressure at the ring/liner interface which, in turn, leads to more severe contact, greater temperatures and expansion. If the wear rate is sufficient to remove the thermal bump as soon as it develops then the condition remains stationary, otherwise, the contact severity will continue to increase [3]. At high temperatures this is aggravated through lubricant degradation in the surrounding areas, in terms of reduced oil viscosity, oil vaporisation, carbon deposition and additive stripping [70]. Ultimately, if lubrication is not re-established the condition escalates till the point where local flash temperatures exceeding 400 °C can occur [4], resulting in the local welding of asperities. The problem is then spread by movement of the piston through tearing or dragging of the surfaces.

It is presumed that scuffing is initiated on ring surfaces rather than liners [71]. This is because ring surface conditions are more severe since friction is experienced continuously as opposed to an area on a liner which experiences friction only intermittently. Neale [72] surveyed scuffing in a wide range of engines finding that in the majority of cases it occurred initially at the top ring as it tended to carry the highest gas loading, experience the highest temperatures and operate furthest from the usual oil supply. Wilson [3] reported that some engine operators have observed scuffing to initiate at the ring ends, presumably due to blow-by burning off the oil film.

2.4.4.2.2 Consequences

The extent and severity of scuffing determines the consequences. For minor instances normal stable operation can usually be recovered. Wilson [3] comments that increasing the lubricating oil supply may not necessarily accomplish this and instead suggested that the oil film may be re-established by lowering the liner cooling water temperature so to permit greater heat transfer away from the surface. For major occurrences of scuffing over a broad area then there may be no action available other than to replace the liner.

A potentially catastrophic consequence of scuffing is a crankcase fire or explosion. This can result in injury or loss of life and occurs when an oil mist in the scavenge air space accumulates to a concentration whereby it can be ignited via hot-spots such as those encountered during scuffing.

2.4.4.2.3 Factors behind emergence of scuffing as a problem

Incidences of scuffing have increased over the last few decades due to the continued development of large-bore, two-stroke engines. As shown in Figure 2.17 during this time the IMEP for engines from one manufacturer has increased from 13 to 19.5 bar with peak firing pressures similarly rising from 90 to 150 bar [73]. Nakano [74] compared engine operating parameters for 1980 and 1990 and found that in this period the likelihood of scuffing had increased by a factor of 2.2 when taking into account maximum cylinder pressure, mean piston speed and oil film temperature. Wilson [3] provided a number of examples, collated from users of two-stroke engines, where scuffing had led to cylinder overhaul, and further suggested that newly designed engines operate on a knife edge with little or no apparent reserve for out-of-the-normal operation.

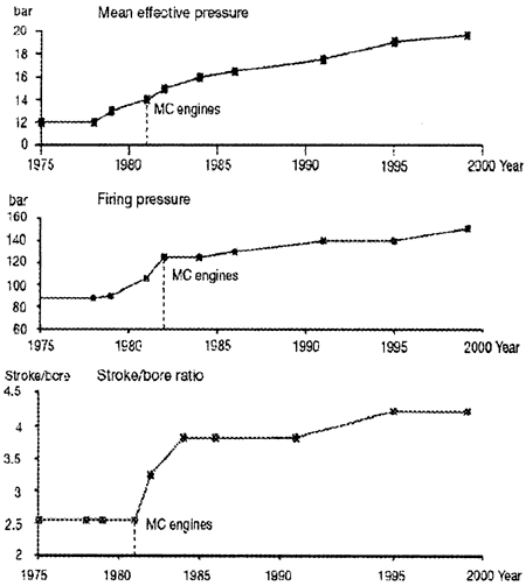

Figure 2.17: Development of key MAN B&W engine parameters, from Schenk et al [73].

Although the occurrence of scuffing is generally associated with extreme conditions of temperature or pressure there are a number of other possible causes, as summarised by Wilson [3] in his 'fish-bone' diagram shown in Figure 2.18. Others have identified specific causes from operational experience, for instance, the presence of water in the scavenge air [73] or carbon deposits on piston crown lands [4] may displace or scrape away the oil film from the liner. Carbon deposits in ring grooves can initiate scuffing through restriction of ring movement leading to greater contact pressures [4]. Fuel injection patterns and combustion characteristics are a further possible source as a slow

burning fuel may burn away the oil film [73]. Figure 2.18 also demonstrates that there is not yet a full understanding of all possible circumstances that lead to scuffing.

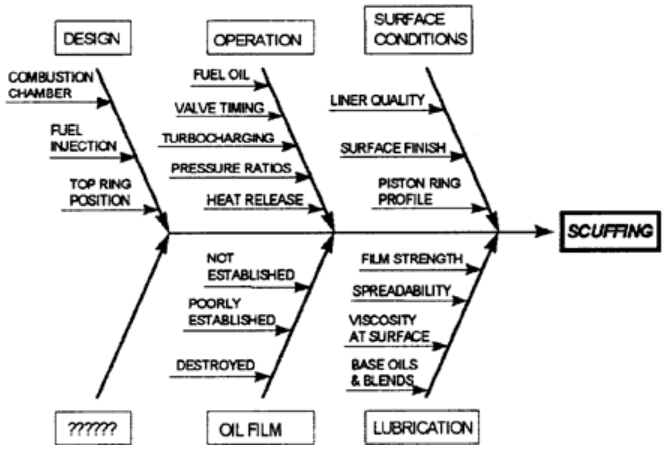

Figure 2.18: Overview of possible causes of scuffing, from Wilson [3].

2.4.4.2.4 A restriction to future engine development

The current rate of engine development is predicted to continue, driven by demand from ship operators for more powerful engines without large increases in the physical engine space required. Allan and Yura [4] reported a requirement for vessels of 12,000 TEU to be propelled at 27 knots, which would require an engine output of over 100 MW. To begin to achieve these power outputs further increases in in-cylinder pressure, liner surface temperatures and surface area are likely, all of which coalesce to increase the likelihood of scuffing.

A further factor is the engine running costs. Engine developments have been reflected by the generally upward trend in the amount of oil required to provide adequate lubrication. This now represents a not insignificant engine operating cost; Lauritsen *et al* [75] conservatively estimated that cylinder lubricating oil accounts for 73% of the total lifetime cost of keeping a cylinder unit in service. Motivation with engine designers therefore is to find ways of reducing lubricating oil consumption, with a reduction in oil film thickness the likely outcome. Developments of this manner are envisaged to further increase susceptibility to scuffing.

2.4.4.2.5 Prevention of scuffing

There are several operational measures which can be taken to lessen the risk of scuffing, such as lowering the cylinder jacket cooling water temperature and increasing the lubricant feed rate. However, these can also have a detrimental impact upon ring-pack operation through increased possibility of corrosive wear and lubricant deposition/sludge formation.

There have also been developments in engine design aimed at reducing susceptibility to scuffing. These have included the introduction of carbon control, or anti-polish rings, that prevent the formation of deposits on piston crown lands [4]. The lubricant delivery system has also been improved through development of high speed [76, 77] and swirl spray [75] optimised timing injection systems which improve upon the inefficiencies of previous designs and control oil dosage in proportion to fuel sulphur content [77]. This has been aided by investigations to enhance understanding of oil distribution and retention on different liner surface profiles [78]. Surface coatings have also received attention with plasma coated rings and liner surfaces shown to give improved sliding wear performance [70, 79, 80]. Efforts have also been made to improve lubricant formulation to offer greater scuffing resistance [68, 81].

An important aspect of scuffing prevention is the development of monitoring systems that can detect abnormal wear at an early stage in order that countermeasures can be taken. Of further appeal is a system which possesses the ability to monitor the precursor stages to scuffing regarding the interfacial frictional behaviour. The mechanisms associated with scuffing and friction are also recognised as potential sources of AE and it is this which has provided the motivation to explore the capabilities of AE monitoring in this thesis. However, to be successful in this endeavour an understanding of AE generation from all the mechanical and fluid processes within an engine is needed as well.

2.4.4.3 Blow-by and ring collapse

There are other faults which affect the operation of piston rings. Excessive blow-by is a condition where a reduction in sealing effectiveness allows excessive amounts of combustion gases to escape past the ring-pack to the scavenge air or crankcase area. In

addition to loss of performance this can lead to severe damage to the piston, rings and liner through hot gas erosion and overheating. Furthermore, excessive blow-by also increases the possibility of fire in the scavenge air chamber as sparks may ignite any oil mist accumulation or deposits. Fog [82] states that the main reason for excessive blow-by is unsatisfactory ring conditions, i.e. worn, sticking, collapsed or broken rings.

Deposits in the piston ring groove areas, caused by excessive lubricant, a poor combustion process or a poor fuel/lubricant combination, can cause the rings to stick in their grooves which may lead to ring collapse, as illustrated in Figure 2.19, through the prevention of gas pressure building up behind the ring. The ensuing blow-by then effectively hammers the ring into the bottom of the ring groove, with the extreme temperatures and pressures aggravating the situation. Ring collapse may be permanent or periodic but in any case the resulting loss of ring tension will eventually lead to breakage [82].

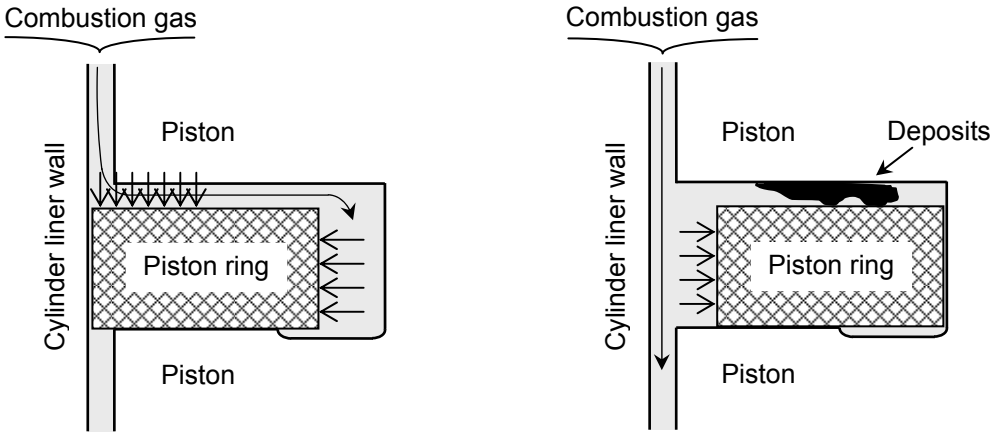

Figure 2.19: (a) Piston ring in normal running condition with perfect sealing, (b) piston ring collapse caused by carbon deposits which hinder pressure build-up behind the ring, from Fog [82].

2.4.4.4 Cylinder oil feed rate optimisation

In addition to the detection of abnormal wear conditions a further reason to pursue development of a ring-pack/liner monitoring system is so that the information can be used towards the optimisation of cylinder oil feed rates in order to achieve savings in running costs.

Evidence suggests that if abnormal wear conditions are avoided then there is a rough relationship between the consumption of cylinder oil and the wear rate of the liner [67, 83]. Hence, there then exists an optimal balance between the cost of ring-pack lubrication and the cost of liner replacement. Ship operators have considered this, one Greek operator has estimated liner maintenance and lubricating costs over varying oil feed rates for a very large crude carrier tanker operating over a 15 year period [84], a breakdown of these costs is given in Table 2.2 and is shown graphically in Figure 2.20.

			Specific lube consumption [gr/hp/hr]		Total lube consumption [ltrs]		Total lube cost [$]	Expected liner lifetime [Years]		Yearly cost of liner maintenance [$]	
Power [NCR]		Time span [Years]		Lubricant cost [$/ltr]		Yearly cost of lube [$]			Cost of liner maintenance [$]		Total cost [$]
36	0.80	15	3,308,936	0.75	2,481,702	165,447	5	1,260,000	84,000	3,741,702	
36	0.85	15	3,515,745	0.75	2,636,809	175,787	7	900,000	60,000	3,536,809	
36	0.90	15	3,722,553	0.75	2,791,915	186,128	9	700,000	46,667	3,491,915	
36	0.95	15	3,929,362	0.75	2,947,021	196,468	10	630,000	42,000	3,577,021	
36	1.00	15	4,136,170	0.75	3,102,128	206,809	12	525,000	35,000	3,627,128	
36	1.05	15	4,342,979	0.75	3,257.234	217,149	14	450,000	30,000	3,707,234	

Table 2.2: Breakdown of lubricating costs versus liner maintenance costs, from Hatzigrigoris [84].

However, as Saddler [85] advises, optimisation is not a straightforward, single event as Figure 2.20 would indicate, but rather a dynamic ever-changing process. It requires thorough knowledge, or a model of, liner wear rates with consideration of the influence of multiple variables such as; different engine types and bore sizes, different fuel sulphur levels, various loading profiles, cylinder parameters such as surface profile, operation in various climates and of course oil feed rates. A further approach to optimisation is to identify a measurable parameter indicative of condition and correlate this with the condition of liner and rings and the oil consumption.

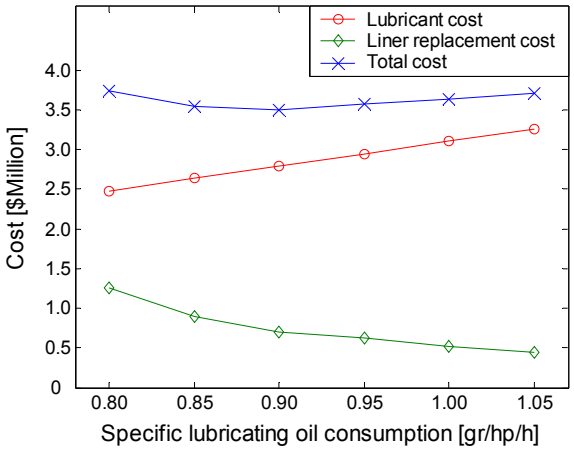

Figure 2.20: Oil feed rate optimisation, from Hatzigrigoris [84].

Evidence from Daniolos [86] suggests that a satisfactory model or a reliable condition indicator has yet to be developed or identified. It was stated that different theories of best practise exist, with Japanese operators preferring to consume cylinder oil at maximum rates (up to 1.5 gr/bhp/h) in order to save on maintenance and component costs whilst North European operators prefer to set minimum cylinder oil feed rates (0.7 gr/bhp/h) related to maximum piston overhaul times at the expense of cylinder liner wear.

2.4.4.5 Condition monitoring of the ring-pack/liner interface

Traditionally, evaluation of liner and ring-pack condition is carried out by an experienced engineer through visual inspections from the scavenge ports or the exhaust valve opening with the engine stopped [82]. This can reveal evidence of blow-by and scuffing. Liner gauging is also carried out if the unit is opened up for any reason. This involves measurement of liner diameter at fixed points down the liner length, thereby allowing wear rate to be determined and a prognosis given as to the remaining service life.

Some ship owners set their own guidelines for evaluation of cylinder condition, for instance, inspection intervals of once a month or preferably every fortnight have been recommended [82]. Although this is a reliable approach to evaluating condition, it can cause unwarranted engine downtime, plus an unexpected event is unlikely to be noticed until the damage is done or there is a serious deterioration. A variety of other methods have been developed, predominantly involving oil analysis, but also including monitoring through intrusive measurements and analysis of surface vibration and air-borne acoustics.

2.4.4.5.1 Oil analysis

A method commonly used to assess running condition is analysis of used lubricating oil. This can become degraded in a number of ways such as in terms of viscosity, oxidisation or additive depletion. Solid or liquid contaminants may also become mixed or dissolved in the oil; either ingressed, for example, sand or water in the air intake, or generated internally through combustion products, wear or fatigue. The vast majority of

oil degradation occurs within the ring-pack due to the high operating temperatures and interaction with combustion gases which pass through the ring-pack. A variety of means exist to identify oil degradation including ferrography, spectrometry, kinematic viscosity and TBN tests. The results can then be used to determine condition; for instance, increased concentrations of particular metals can indicate deterioration of specific components.

For two-stroke diesels samples are usually obtained from the oil scraped down by the ring-pack to the drain in the scavenge area [84, 85, 87]. Hashimoto *et al* [87] sampled oil intermittently over a long time scale and analysed it using ferrography. It was observed that both the quantity of iron particles and the characteristics, or grading, of the particles were approximately related to the total wear rate of ring-pack and liner. This led the authors to specify a particulate content level considered indicative of acceptable conditions. Similar observations are used commercially to provide information for condition monitoring and oil feed rate optimisation [83, 85], parameters monitored typically include the amount of iron, vanadium, phosphorus, zinc, calcium, soot insolubles and water in the oil in addition to oil TBN, dispersancy and viscosity. Although analysis of drain oil can be valuable others have noted limitations, particularly regarding the influence of the scavenge drain condition [88] and unexplained scatter in scrapedown analysis results [85].

Sampling directly from the liner surface has also been considered by Mitsutake *et al* [89]. They investigated oil distribution and deterioration through sampling oil from a number of positions on the liner surface. The quantity of sampled oil was measured in addition to ferrography analysis and pH, Total Acid Number (TAN) and TBN values. Oil deterioration, principally due to the fuel sulphur content, was signified by a low pH number and high TAN. As expected, a lower quantity of oil and higher level of deterioration were observed when oil feed rates were low, and also from samples obtained between oil feed points when compared to that sampled in line with feed points. Further deterioration and lesser oil quantities were observed from samples obtained closer to TDC. In addition to evaluating oil distribution and anti-corrosive wear properties the authors also specified that mechanical wear mechanisms could be identified via a high iron particle content.

A problem with oil analysis is that considerable time and expense is required to examine samples remotely in laboratories. Therefore, this does not lend itself well to continuous monitoring onboard vessels and instead oil analysis is usually conducted intermittently or when faults are suspected.

2.4.4.5.2 Intrusive measurements

There are several intrusive monitoring techniques which utilise transducers mounted flush with the cylinder liner wall. These include proximity, inductive and flash temperature monitoring.

Proximity sensors measure the distance between each ring and the liner surface. This can be used to determine whether a ring is working satisfactorily, if it is sticking in its groove or has collapsed, or if it has broken or is missing [90]. Martens [13] noted that the use of proximity sensors requires a magnetic material, therefore rings coated with an antimagnetic material such as plasma sprayed will not produce a signal until the coating is worn down. Furthermore, since proximity is measured at only one point on the piston stroke rings which are only periodically sticking or collapsed might go unnoticed.

Commercial ring monitoring systems, described by Fog [82], have been developed which are based upon inductive monitoring of the top ring. These require installation of a special top ring whose construction contains either a non-magnetic band or a separate wear groove. These systems can be used to monitor ring wear, ring rotation and the occurrence of sticking or collapsed rings. However, these techniques are limited in that only the top ring operation is monitored and measurements are again taken at only one point on the piston stroke. A derivative of this method is a transducer based upon wear-down resistive elements which is fitted flush with the liner wall in such a manner that the elements are worn down with the liner. A measure of the element resistance generates a signal proportional to the amount of wear [13, 91].

Since scuffing is accompanied by very high flash temperatures the monitoring of these flashes can be a sensitive indicator. To achieve this thermocouples with an extremely fast response time are mounted flush with the liner surface in the upper part of the cylinder. Martens [13] described the use of the rate of measured flashes as a parameter

to indicate scuffing. However, since scuffing develops quickly continual monitoring and immediate reaction is required. A simpler but less sensitive indication of thermal overload can be obtained from the use of thermocouples embedded within the liner but away from the inner surface [13].

2.4.4.5.3 Vibration and acoustic monitoring

Running condition at the ring-pack/liner interface has been assessed using non-intrusive measurements of surface vibration, ultrasound, and to a lesser extent, airborne acoustics. Recent work has also considered AE monitoring and this shall be discussed in detail in the following Chapter.

Long and Boutin [14] demonstrated that measurements of vibration and ultrasound could be used to identify faults including piston slap, scuffing and blow-by. The signal characteristics of normal operation were first established, as shown in Figure 2.21a. Changes in the signals were then attributed to the development of faults, for instance, strong vibration spikes occurring coincident with either maximum cylinder pressure or maximum lateral piston force were deemed indicative of piston slap. Vibration events occurring symmetrically about TDC, shown in Figure 2.21b by events marked A and B, were believed to indicate liner scuffing or scoring and in the author's opinion should prompt a boroscope inspection and/or oil analysis. High vibration and ultrasonic energy coinciding with high cylinder pressures, as shown in Figure 2.21c, was considered symptomatic of excessive blow-by.

Haller and Kelleher [33] used similar techniques to inspect running condition before and after maintenance actions. Through inspection of overhauled components and differences in signatures it was claimed that ring damage, excessive blow-by and scuffing could all be identified. In one case study, contrary to [14], blow-by was thought indicated by unexpected vibration events occurring around the piston mid-stroke areas whilst in another case liner scuffing and blow-by occurring together were believed represented by the signal changes shown in Figure 2.22.

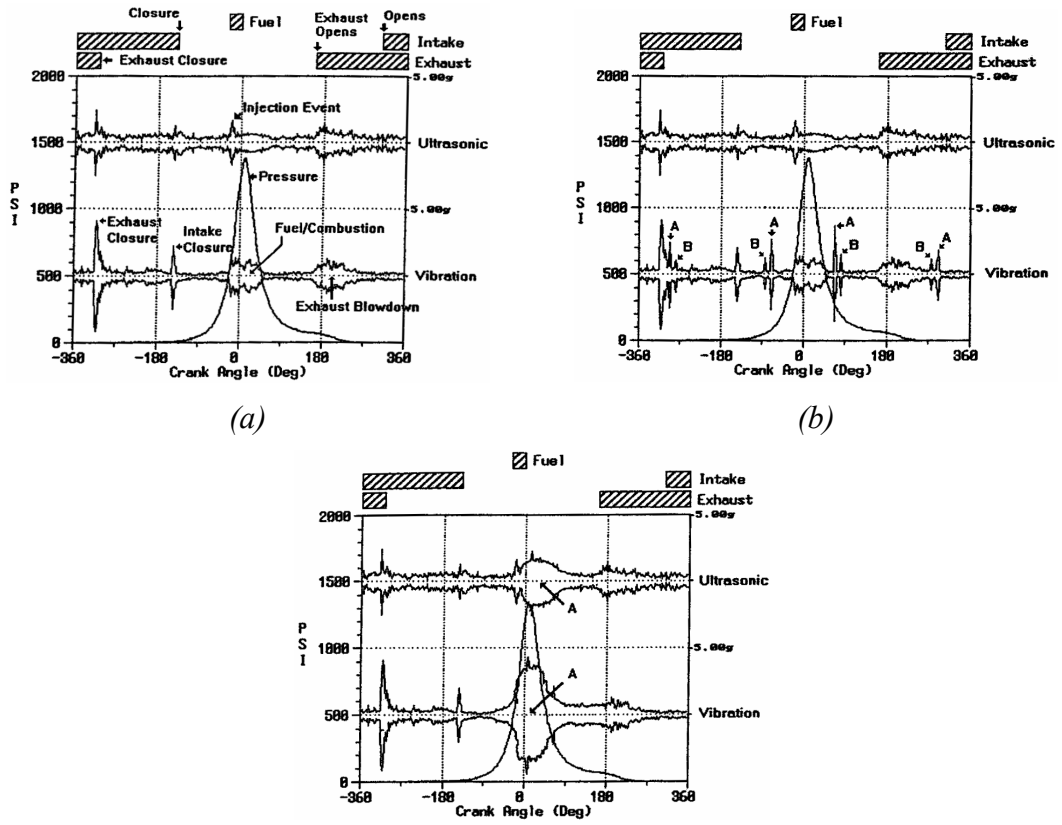

Figure 2.21: Vibration and ultrasonic signals corresponding to (a) normal running, (b) scuffing, as signified by events occurring symmetrically about TDC, (c) blow-by, from Long and Boutin [14].

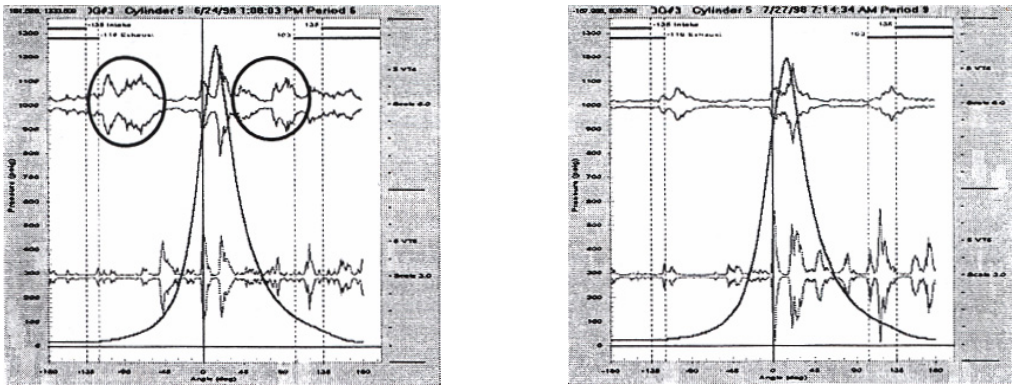

Figure 2.22: Presence of scuffing signals in vibration signature, (a) with fault, (b) after liner replacement, from Haller and Kelleher [33].

Kimura [92] investigated diagnosis of ring-pack running condition through spectral analysis of surface vibration and air-borne acoustic measurements. Data were acquired periodically from engine manufacture until a year and a half of service (7800 hours) with vibration measured on the cylinder water jacket and radiant sound 5 cm from the

surface. Short Time Fourier Transform (STFT) analysis of the cyclic vibration data revealed several bow-shaped features as shown in Figure 2.23a. Each of these features was attributed to a single piston stroke, and more specifically the sliding of the piston assembly against the liner wall, from two cylinders in the sensor vicinity. The variation of frequency was thought related to the mid-liner location of the accelerometer and the approaching and passing of the piston. Testing over time showed that these features reduced in size and clarity. After 10 hours operation the vibration level reduced by 10 dB with further reductions apparent till the end of testing at 7800 hours. These changes were attributed to the changing nature of the ring-pack/liner interaction and led the author to believe that an understanding of the running conditions could be achieved from vibration measurements. Similar analysis of the radiant sound was found to be far less revealing with regards to features thought to relate to piston movement.

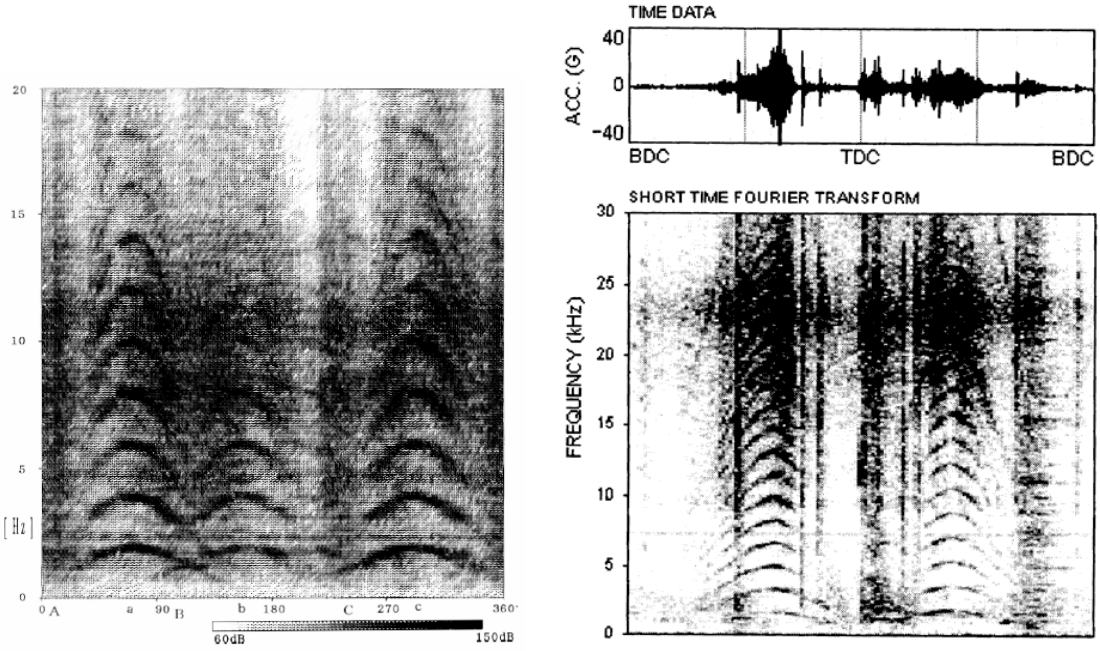

(a) *(b)*

Figure 2.23: STFT analysis of vibration measurements, (a) from Kimura [92], (b) top panel - time-series, bottom panel - STFT analysis, from Sasaki [35].

Sasaki [35] conducted similar analysis of liner vibration measurements during the running-in process. Sources for the various vibration events such as those shown in the upper panel of Figure 2.23b were determined. Asides from impulses relating to injector and valve operation both continuous and non-continuous contact at the ring-pack/liner interface were identified as sources. Non-continuous contact occurring between the piston rings and the oil groove and scavenging ports was found to generate impulsive vibrations, particularly contact between the top ring and oil groove on both compression

and expansion strokes. Vibration resulting from contact between rings and scavenging ports was noted as occurring intermittently, possibly due to the relative positioning of the ring ends and the scavenging ports.

Similarly to Kimura [92] continuous sliding contact and friction occurring at the ring-pack/liner interface was identified as a source. This was noted to be predominant in areas of maximum piston speed, i.e. around mid-strokes, and STFT analysis, Figure 2.23b, again showed the bow-shaped curves initially identified in [92]. Sasaki [35] found that the fundamental frequency of these curves was proportional to piston speed and suggested that the signals were due to contact between the ring-pack and the crests of the wave-cut liner surface. Furthermore, since these measurements were taken during the running-in period this contact would be more severe. A comparison of spectra of signals acquired during the running-in process and after 20 hours of operation, shown in Figures 2.24a and 2.24b respectively, revealed a decrease of energy at higher frequencies that was believed to represent the changes in ring-pack/liner interaction. The author also highlighted the possibility for abnormal wear detection although it was noted that investigation of maximum wear conditions around TDC would require developments in signal processing to separate the ring-pack/liner contact source from the combustion related vibration.

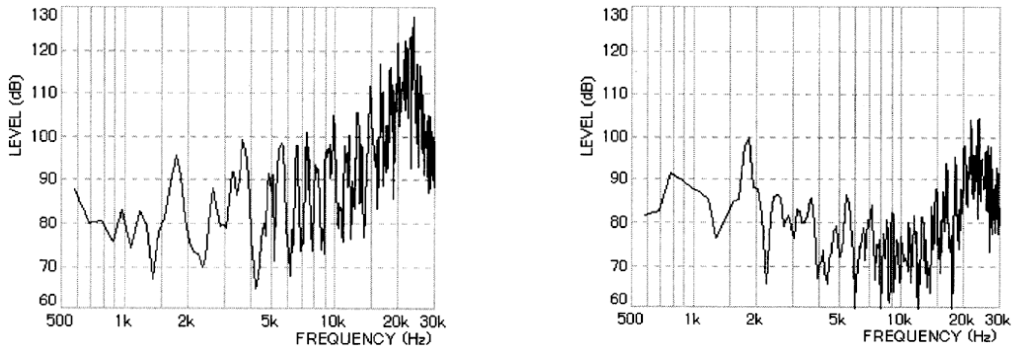

(a) *(b)*

Figure 2.24: Spectrum of cylinder liner vibration at 50 % load, (a) during running-in process, (b) after 20 hours operation, from Sasaki [35].

2.4.5 Four-stroke, trunk-piston, diesel engines

The ring-pack/liner interface in four-stroke engines may not give rise to such a large percentage of engine failures as per the large, two-stroke engines but there are similar

pressures to improve upon ring-pack operation. The onus of improvements is on efficiency, durability and emissions; it is desired that:

- Oil offer increased protection from wear and corrosion for increasingly longer periods of time between drain intervals.
- Engine performance, fuel economy and efficiency be improved through a reduction in ring-pack frictional losses.
- Ever more stringent environmental legislation requires that harmful exhaust emissions be reduced. Since the burning of oil during the combustion process is a principal contributor to these emissions then oil transportation through the ring-pack should be reduced.

However, these aims are not necessarily achieved together. For instance, it is anticipated that to limit oil transport reduced oil-film thicknesses will be necessary. As indicated by the Stribeck diagram shown in Figure 2.12 this may reduce hydrodynamic frictional losses but at the same time incur greater amounts of boundary friction, leading to an increase in overall frictional losses and also impacting upon wear rates and durability.

Regardless of the changes required to meet the aforementioned objectives there are a number of other factors which have increased the severity of the ring-pack/liner operating environment in recent years:

- Higher engine power outputs, achieved using smaller displacements and smaller sumps, and with greater pressures and temperatures.
- Increased stop/start operation, both through typical driving behaviour and engine developments such as engine hybrids and deactivated cylinders.
- Developments such as exhaust gas recirculation, this represents a significant problem as it increases soot levels which can lead to abrasive wear and bore polishing.
- Constraints on lubricant formulation; limits on lubricant sulphur, phosphorus and sulphated ash levels, i.e. tried and tested additives are being forced out of lubricant formulations.
- Introduction of new materials, surface topographies and fuels which require different optimum lubricant formulations.

Despite these obstacles improvements in ring-pack performance are thought possible. Priest *et al* [93] comment that although manufacturers can produce rings that possess excellent life expectancies, these components may be far from optimum from a lubrication and friction standpoint. To improve performance a greater understanding is required of the complex mechanisms involved in ring-pack operation. This has encouraged numerous experimental and theoretical investigations.

2.4.5.1 Experimental ring-pack monitoring techniques

A great deal of understanding regarding piston ring behaviour has been developed through experimental investigations. The results are also increasingly used to verify theoretical models of ring-pack operation. However, there are difficulties and limitations with experimental monitoring techniques and it is considered worthwhile to provide a review in order to illustrate this.

2.4.5.1.1 Oil analysis

Similar to the large engines, oil sampling has been used extensively as a means of monitoring the tribological conditions under which the ring-pack operates. Typically oil is sampled from the sump or from an oil passageway. An extension to this is to examine the small quantity of oil entrapped in the ring-pack region; this is far more contaminated than the bulk oil due to the presence of fuel, water vapour and other combustion products. Some researchers have devised methods of extracting oil from this region, for instance Lee *et al* [94] used a tapping in the rear of the top ring and a tubing arrangement in a gasoline engine. Upon analysis this oil was found to have such distinctly different traction and friction properties than sump oil that the authors considered analysis of the latter to be an unsuitable method from which to infer tribological behaviour at the ring-pack/liner interface.

2.4.5.1.2 Measurement of oil film thickness

A common approach for investigating ring-pack operation is to measure the oil film thickness supporting the rings on the liner surface. Methods developed for this comprise of mainly electrical and optical techniques which are discussed below.

2.4.5.1.2.1 Electrical techniques

Similar to the condition monitoring techniques available for large engines these are based on intrusive resistance, inductance and capacitance measurements.

Resistance measurements aim to measure the electrical resistance of the oil film. However, due to frequent short-circuiting caused by ring/liner contact this method is unsuitable for continuous measurements over the whole piston stroke. Instead, the number of short circuits has been used to identify different lubrication regimes as they reflect the degree of lubricant breakdown.

Inductance techniques measure the inductance change of a coil as a metallic object, i.e. the piston ring, passes in front. Transducers can be mounted in a variety of ways, such as flush with the liner wall or in the end face of the ring gap, so to provide single point or continuous measurements over the piston stroke [95]. Transducers can also be fitted within the piston to investigate characteristics including oil film thickness, piston secondary motion and ring motion [96]. It has been noted however, that some measurements can be unreliable due to the highly temperature-sensitive nature of the transducers [95].

Capacitance transducers have been widely used to measure oil film thickness. This technique, initially developed by Hamilton and Moore [97], is considered to provide the most quantifiable results [98]. They work by measuring the capacitance formed between the piston ring and a probe mounted in the cylinder liner, or vice-versa, with oil serving as the dielectric material. One of the main problems with this technique is that it relies upon the assumption that the region between the ring, or liner, and the probe is flooded with oil. If however, there are gaseous inclusions, such as may be introduced through cavitation, then the oil dielectric is changed causing errors in the film thickness measurement [95].

2.4.5.1.2.2 Optical techniques

Oil-film thickness has also been measured using optical methods. These typically rely on Laser-Induced Fluorescence (LIF) of the oil, i.e. the use of doped lubricant films by die particles, although other methods such as interference pattern and infra-red spectra analysis have also been used. All these techniques require the use of transparent cylinder apparatus or the insertion of optical fibres into the liner. However, mechanical limitations of transparent materials restrict application to motored engines [95], although the use of fibre optics presents no such limitations [96]. Further difficulties with optical techniques have been noted; illumination from the combustion process can cause interference [95], limitations set by the die particle size can be a problem, and accurate calibration of LIF techniques is difficult due to the dependence of the fluorescent components on temperature [98].

2.4.5.1.3 Measurement of cylinder friction

A further approach to investigate piston ring behaviour is to measure or determine the cylinder friction. This is a difficult task and requires an accurate measurement technique if realistic values are to be obtained. A further problem is in isolating the friction incurred by each component, i.e. separating piston assembly friction from the total friction, and identifying friction for each ring.

2.4.5.1.3.1 Engine performance measurements

Monitoring of engine performance data such as in-cylinder pressure and fuel consumption measurements can be used to infer differences in frictional behaviour. However, these techniques suffer in that absolute friction cannot be determined. Furthermore, changes due to cylinder friction are likely to be low when compared to the overall engine power output and they can therefore be effectively masked by slight variations in engine parameters such as manifold pressures and temperatures [62].

2.4.5.1.3.2 Motoring teardown tests

This is a commonly used method that can provide values for the frictional losses incurred by each component. It involves measuring the torque required to motor an engine at a specific speed. The cylinder head, piston rings and piston are then sequentially removed with the difference in motoring torque attributed to the frictional contribution of each component. However, the results may not represent the actual conditions in a firing engine due to the lower cylinder pressures and temperatures of a motored engine. There have been attempts to simulate both these parameters in order to make the test more realistic but true representation of ring operation in a fired engine can still not be achieved since the functioning of the piston rings are heavily interrelated. This has been proven experimentally by Furuhama *et al* [99] who observed that friction incurred by the ring-pack as a unit was 70 % greater than the total of the friction for each ring operated individually. Other indirect techniques applicable to firing engines have been proposed. These include the Willans line, free deceleration and morse tests, however, these techniques, at best, can provide only a rough estimate of overall cylinder friction.

2.4.5.1.3.3 Direct measurement

Richardson [62] outlined several methods for direct measurement of cylinder friction under firing conditions, these are summarised in Table 2.3. These techniques can give good insight into ring-pack operating characteristics and can be used with the full ring-pack or in conjunction with teardown tests. Unfortunately they can also be complex and generally require major modifications to the engine.

Technique		Comments
Moveable or floating liner	- Cylinder is mounted elastically with friction determined by measuring the forces acting on the liner as the piston reciprocates.	Friction measured directly and accurately. Requires extensive and costly modifications.
Fixed sleeve	- A derivative of the above. A thin liner is mounted inside a modified original liner with friction forces measured by strain gauges. Gas forces needs to be subtracted from the measured force.	Requires custom components therefore not possible to test production hardware. Requires measurement of cylinder pressure.
Reciprocating liner	- Mount piston elastically and reciprocate the liner. Friction measured in the piston.	Not possible to fire engine.
Instantaneous IMEP	- Forces measured on connecting rod through strain gauges. Pressure and inertial contributions are subtracted to obtain the friction contribution.	Dependant upon accurate pressure measurements and requires detailed calculations of inertial forces.
Angular velocity	- Measure instantaneous changes in crankshaft angular velocity caused by cylinder kit friction variations.	Requires very little engine modification but may require significant computation to obtain results.

Table 2.3: Methods for direct measurement of cylinder friction, from Richardson [62].

2.4.5.2 Observations from experimental work

Taylor and Evans [96] measured the instantaneous frictional force acting on the ring-pack of a single-cylinder diesel engine using a floating-liner technique. Figure 2.25 shows the results obtained for three oils of different viscosity at constant engine speed and liner temperature. The friction force incurred at mid-stroke was found to increase with oil viscosity whilst the peak frictional force occurring just after TDC firing reduced. A measure of frictional loss was obtained through summation of the area under the friction curve. With increasing engine speed the frictional loss increased, Figure 2.26a, and the value of peak friction decreased, Figure 2.26b, this was observed to be consistent for all three oil viscosities.

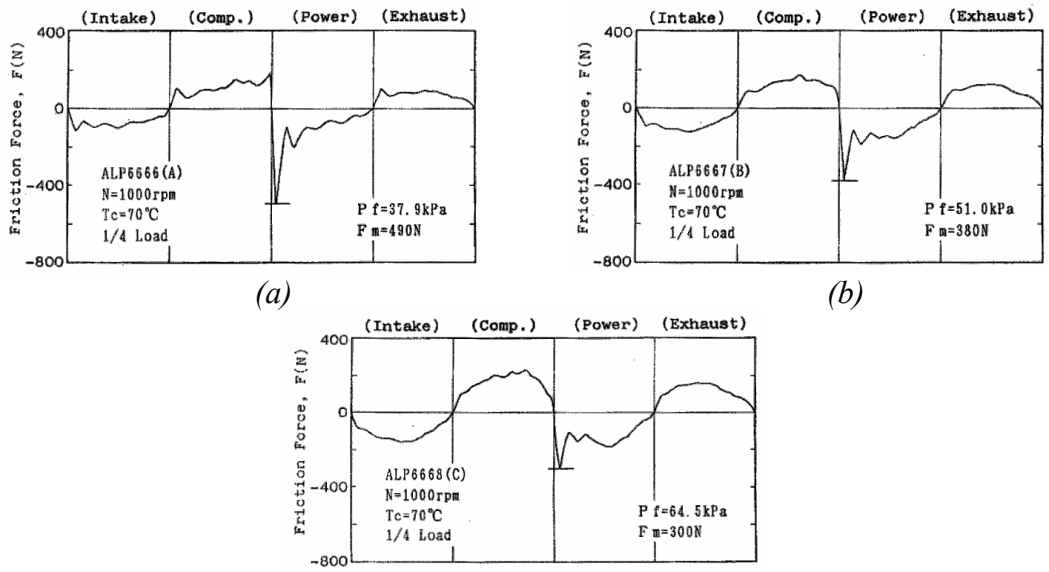

Figure 2.25: Measured piston assembly friction for three different lubricants, (a) SAE-10W, (b) SAE-20, (c) SAE-50, from Taylor and Evans [96].

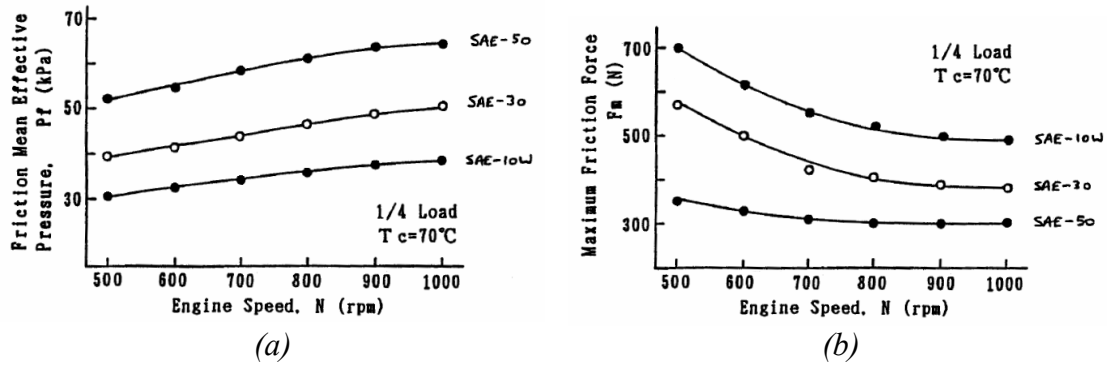

Figure 2.26: Variation of friction characteristics with engine speed, (a) overall frictional loss, (b) peak friction force, adapted from Taylor et al [100].

Further work [96] attempted to quantify boundary lubrication in the ring-pack. Friction force was measured with and without friction modifiers added to the oil. It was clear that the addition of the modifiers reduced the peak boundary frictional force although there was little change at around the mid-stroke regions. The effect of this on frictional losses was less pronounced since power loss is equal to the product of friction force and piston speed, and the significant friction reduction occurs close to TDC where piston speed is low. Even so, a reduction in peak friction is important as it can benefit wear rates.

Cho *et al* [101] further investigated ring-pack frictional forces using a floating liner technique. Although the effects of cylinder pressure, oil starvation and piston

secondary motion were excluded they found that the frictional patterns could be classified into five modes dependant upon the combination of predominant lubrication regimes at mid-stroke and dead centres, these modes are summarised in Figure 2.27.

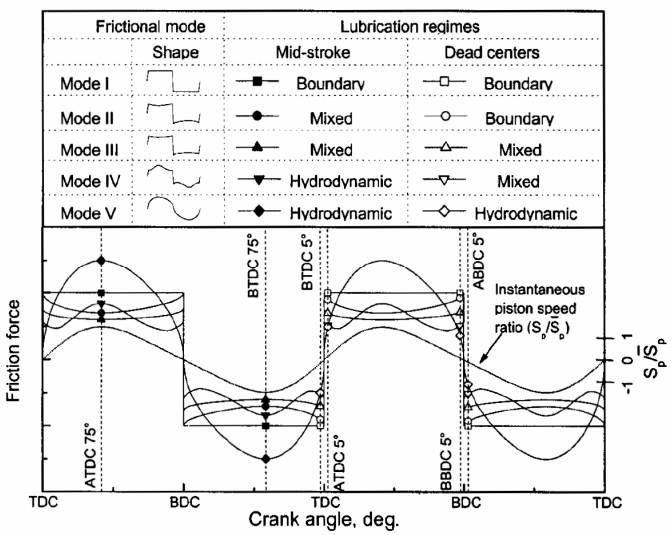

Figure 2.27: Piston ring frictional modes, from Cho et al [101].

2.4.5.3 Theoretical modelling of ring-pack operation

Theoretical analyses of ring-pack operation have become increasingly important in understanding piston ring behaviour. A large body of literature exists which describes models that claim to predict with reasonable accuracy; ring dynamics, oil film development, blow-by, oil consumption, wear characteristics and other facets of ring-pack performance. Predictions are also used to substantiate experimental work, or vice-versa, and are finding increasing use in the design process. Models of ring operation mathematically define features encountered in real ring-packs; however, due to the great many inter-related factors the analysis can quickly become very complex. Hence, some factors are excluded, considered either unimportant or beyond modelling capabilities, and are instead replaced by simplifying assumptions.

Early analyses of ring lubrication were based upon a balance of radial forces, viscous shear considerations and application of Reynolds equation to a single ring, e.g. Furuhama [102] and Dowson *et al* [103]. Reynolds equation takes into account parameters of geometry, viscosity, pressure and surface velocities, and can be solved for pressure distribution, load capacity, friction force and oil flow. Subsequent analyses offered a more realistic calculation of ring friction through the inclusion of asperity interaction and mixed lubrication models [104]. A significant improvement was made

through consideration of the effects of the ring-pack as a whole and the interaction between rings in terms of oil availability, i.e. the leading ring will lay down an oil film which supplies the following rings. This led to the belief that compression rings may operate under 'starved lubrication' conditions, where the inlet region of the ring profile is starved of a full supply of lubricant [93, 105], as opposed to the unrealistic assumption of an unlimited supply of lubricant available at each ring throughout the engine cycle, termed 'fully flooded lubrication'.

Further developments have resulted in models that are increasingly sophisticated and which rely on fewer limiting assumptions. Some focus on particular features of ring-pack operation although most generally make predictions of oil-film thickness and friction; recent attention has also shifted to include predictions of oil transport and consumption. Specific examples of sub-systems investigated and their impact upon ring-pack operating characteristics include; changes in ring profile over time caused by wear [93], consideration of bore distortion and ring conformability with an improved oil availability model [105], and oil-film cavitation [106]. Others attempt to further enhance interaction between sub-systems in order to reflect the highly interrelated nature of ring-pack operation [65].

Many models are based on two-dimensional, axisymmetric analysis. Unfortunately, this introduces a major simplification in that the lubrication condition is assumed uniform around the ring circumference. In reality, due to the combined effects of piston secondary motion, ring end gap effects and ring/bore non-conformability, this is not the case. As a result it has been noted that, at a fixed crank angle, a ring can experience boundary, mixed and hydrodynamic lubrication simultaneously around its circumference [107].

2.4.5.4 Observations from ring-pack theoretical analyses

A review of ring-pack modelling work reveals that whilst there are general similarities in predicted behaviour there is no definitive answer as to how rings behave, and consequently there are conflicting views on some aspects. This is not surprising considering; the number of factors which influence ring-pack operation, the number of

modelling attempts of varying degrees of sophistication, and because model predictions vary depending upon what the model author(s) consider to be significant.

The most general agreement concerns the behaviour of the compression rings. As a brief summary, the lubrication regime in the vicinity of the dead centres is a combination of boundary or mixed lubrication with an additional lubricant film squeeze effect, whilst during the piston mid-stroke regions hydrodynamic lubrication is prevalent. This has been established from both modelling [65, 93, 107] and experimental work [97, 100, 101, 108]. Determining the behaviour of the oil-control ring seems rather more problematic, as is reflected by the differing predictions that have been made. However, understanding the behaviour of this ring is important as it has a dominant effect on the performance of the whole ring-pack [93, 107-109].

Figure 2.28a shows a typical modelled prediction of oil-film thicknesses for a three ring ring-pack operating under assumed fully-flooded conditions [107]; similar predictions have been reported by other researchers [65, 108]. The top compression ring, ring 1, operates with small film thicknesses at dead centres, particularly TDC firing, where cylinder pressure and liner temperature are at their greatest and piston speed is low. Oil-film thickness increases during the stroke as a result of increased piston speeds, lower loading and reduced temperatures. The second ring exhibits behaviour typical of a scraper ring with much smaller film thicknesses during the piston downstroke due to the assumed ring profile.

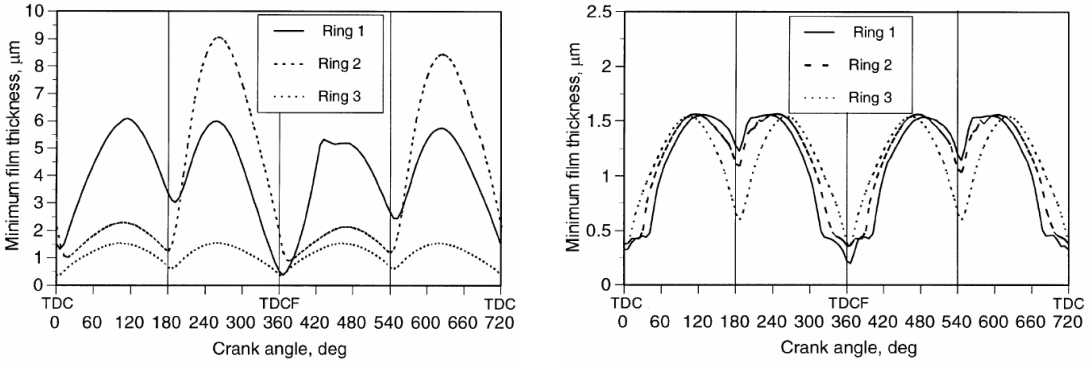

Figure 2.28: Effect of oil availability on predicted oil-film thicknesses, (a) fully-flooded conditions (b) starved lubrication (note different scales), from Ma et al [107].

However, these predicted film thicknesses are based on the assumption of a copious supply of oil to each ring at all times. When the effects of oil availability and possible

oil-starvation are taken into account then the predictions change dramatically. Figure 2.28b shows the same model as Figure 2.28a but with the inclusion of a flow-continuity model to better represent oil availability. The effect is that the film thicknesses for both compression rings are significantly reduced.

An experimental investigation by Seki *et al* [108] would seem to confirm some of the modelled characteristics of top ring behaviour. Oil-film thickness was measured at several points on the liner using a LIF optical technique, thus allowing the variation of film thickness during the cycle to be established, Figure 2.29. A prediction of oil-film thickness based upon a dynamic lubrication theory proposed by Furuhama [102] assuming fully-flooded operation is also shown. The top compression ring showed a reasonable correlation to the predicted behaviour although smaller thicknesses were observed at TDC firing due to oil starvation. The second, or scraper, ring would appear to suffer from the effects of oil starvation due to the influence of the oil-control ring as the measured thicknesses are markedly different to the predicted behaviour. Operation over the engine range was investigated. Both a reduction in engine speed and engine load did not significantly affect oil-film thicknesses although oil starvation of the top compression ring at TDC was relieved by the latter. Other experimental work [107] corroborates the view that the surfaces of the compression rings are not covered with oil and hence starved lubrication conditions exist.

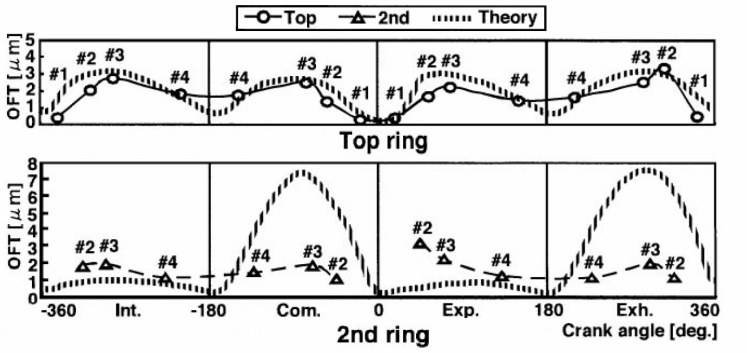

Figure 2.29: Oil-film thickness measurements compared to theory, from Seki et al [108].

One modelling investigation, undertaken by Keribar *et al* [65], is of interest due to parametric studies conducted over the operating range of the engine. In this case predictions were made for oil-film thickness, friction force (combined boundary and hydrodynamic) and frictional power loss for each ring, assuming fully-flooded

conditions. These are shown for full load conditions at 1900 RPM in Figures 2.30a, 2.30b and 2.30c respectively.

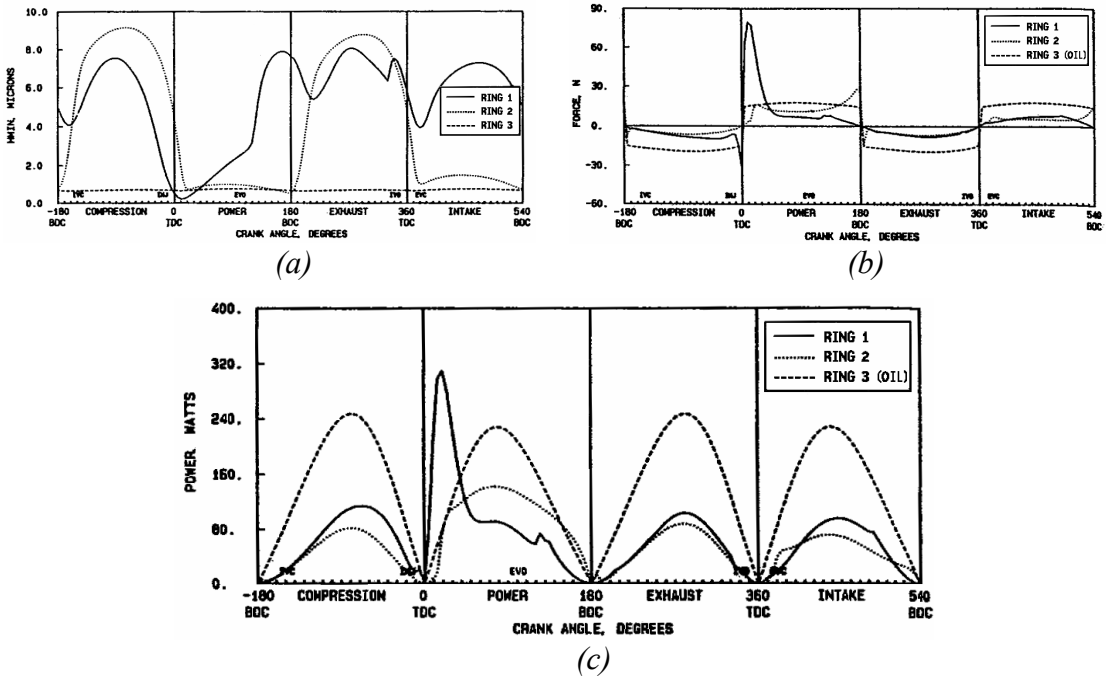

Figure 2.30: Predicted cyclic history (a) minimum oil-film thickness, (b) instantaneous ring friction force, (c) instantaneous ring frictional power loss; ring 1 = barrelled compression ring, ring 2 = tapered (scraper) ring, ring 3 = oil-control ring, from Keribar et al [65].

Figure 2.30a shows the conventional oil-film behaviour for both a top ring and scraper ring as described previously. The operation of the oil-control ring is different, the authors state that it maintains an almost constant and small film thickness since its narrow rails cannot generate a hydrodynamic load carrying capacity, and its load (mostly tension) is therefore supported almost entirely by asperity contact. The friction forces acting on each ring during the engine cycle, shown in Figure 2.30b, are consistent with the variation of oil-film thickness. Therefore, the compression rings experience hydrodynamic friction during the majority of the cycle and periods of boundary friction near the dead-centres. For the oil-control ring boundary friction is continuous and is augmented with a small hydrodynamic friction component in the middle of each stroke. Instantaneous power losses attributed to the frictional forces are shown in Figure 2.30c and these indicate that the oil-control ring is responsible for the highest mean frictional power loss.

Predictions of friction were made over the engine operating range, for varying engine speed at full load, and for varying load at a fixed speed of 1900 RPM, with the results shown in Figures 2.31a and 2.31b respectively. For the former it was observed that the frictional power loss for each ring generally increased with speed, with the oil-control ring responsible for the greatest amount, as already implied by Figure 2.30c. The only exception is the second ring which increases in friction below 750 RPM due to boundary friction becoming dominant. For the varying load, constant speed test, Figure 2.31b, the frictional losses from both compression rings increased slightly with load due to greater ring loading. The oil-control ring, however, is vented to the crankcase and is unaffected by in-cylinder pressure and therefore it displayed no change in frictional power losses.

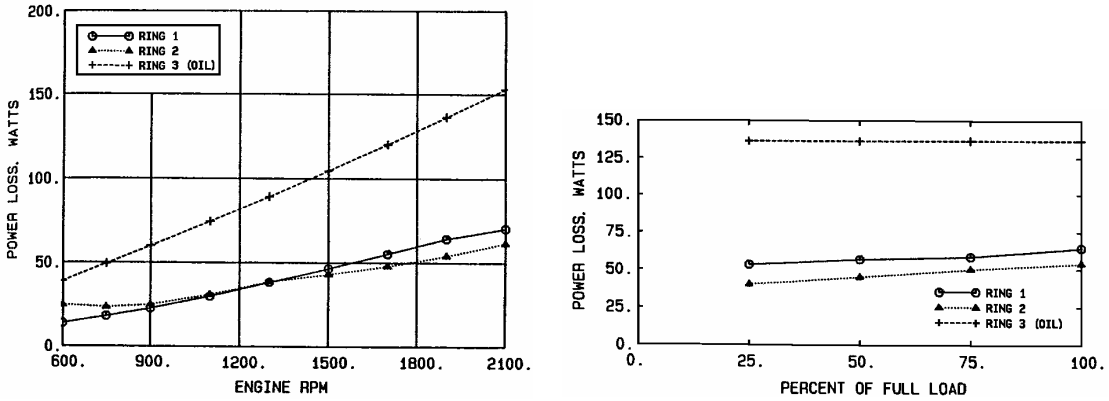

(a) *(b)*

Figure 2.31: Frictional power loss, (a) effect of engine speed, (b) effect of load, from Keribar et al [65].

As recognised by the authors their model failed to fully account for the possibility of starved lubrication conditions. However, it did allow an oil availability thickness to be defined, and when this was reduced the boundary frictional losses for both compression rings increased considerably. The oil-control ring, since it was already predicted to operate under mixed lubrication conditions, was not significantly affected.

Richardson [62] corroborates the view that the oil-control ring is responsible for the greatest amount of ring-pack friction, estimating it to account for between 50 to 75 % of the total ring friction. Again, the reason identified was that the oil-control ring is incapable of generating a sufficient hydrodynamic oil film. Cho *et al* [101] also agreed that the oil-control ring operates with mixed lubricating conditions dominant throughout the entire stroke.

Other researchers display a difference of opinion regarding operation of the oil-control ring, and the proportion of ring-pack friction attributable to it. Predictions by Taylor *et al* [100] suggest that it operates under hydrodynamic conditions. A breakdown of predicted boundary and hydrodynamic frictional losses incurred by each ring for different viscosity oils was provided, as shown in Table 2.4. From this it appears that there are no boundary frictional losses for the oil-control ring which implies it operates under hydrodynamic conditions throughout. The predicted losses were typically less than the actual measured values, shown previously in Figure 2.26, although this was explained by the absence of a piston skirt frictional component in the modelled prediction. The comparison in this case suggested that the ring-pack contributed 60 % to the piston assembly friction and the piston skirt the remaining 40 %.

	Average power loss [W]							
	Oil-control ring		Second ring		Top ring		Total	
Oil	H	B	H	B	H	B	H	B
SAE-10W	35.39	0.05	53.01	0	61.07	8.37	149.47	8.42
SAE-30	58.53	0.01	82.64	0	97.26	1.81	238.42	1.82
SAE-50	92.45	0	126.42	0	149.02	0.40	367.89	0.40

Table 2.4: Breakdown of predicted frictional losses, H = hydrodynamic, B = boundary, adapted from Taylor et al [100].

Ma *et al* [107] predicted that the oil-control ring film thickness during a cycle is similar to that of the compression rings operating under starved lubrication conditions, i.e. it experiences boundary, mixed and hydrodynamic lubrication. They also found that the amount of oil-control ring boundary friction was sensitive to the ring specification, it increased significantly with ring tension and also when land height was reduced.

Priest *et al* [93] predicted film thicknesses for the oil-control ring during the running-in process using measured ring profiles. Their work again suggested that the ring can operate under boundary, mixed or hydrodynamic conditions. They also predicted that the frictional losses are lower than any of the compression rings if they are assumed to operate under starved lubrication conditions. Predicted oil-control ring film thicknesses after 0, 120 and 628 hours of operation are shown in Figures 2.32a, 2.32b and 2.32c respectively, included in each figure is a dotted line which represents the transition from mixed to full-film lubrication calculated on the basis of the composite surface roughness. At 0 hours the ring is predicted to generate full-film lubrication on the upstroke but to operate under mixed conditions on the downstroke. After 120 hours the

initial wear has resulted in modest hydrodynamic film action on all strokes but full film lubrication achieved only on the downstroke. After 628 hours, Figure 2.32c, further wear has resulted in full film lubrication on the downstroke and boundary lubrication on the upstroke. However, the authors state that their predictions may be too severe as they led to a degree of oil starvation and oil-film thicknesses at the compression rings that would seem to be unrealistic in practise. Comparison to experimentally found film thicknesses substantiated this view.

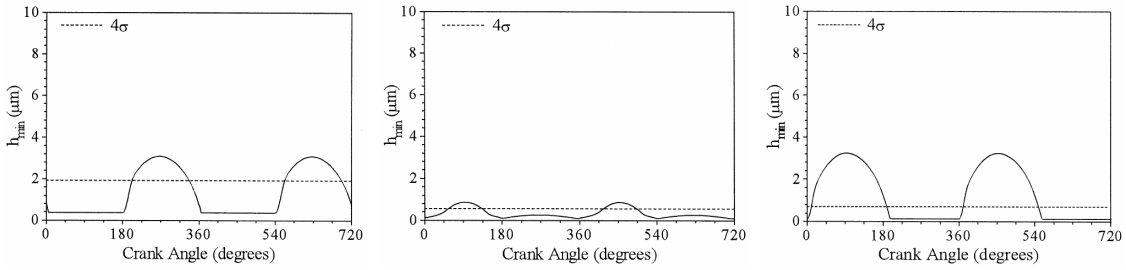

(a) *(b)* *(c)*

Figure 2.32: Predicted oil film thickness using measured ring profiles at (a) 0 hours, (b) 120 hours, (c) 628 hours, dotted line represents transition from mixed to full-film conditions, from Priest et al [93].

Ruddy *et al* [109] analysed oil-control ring operation by considering radial and torsional ring equilibrium, and assuming fully-flooded conditions. They again predicted that it can operate under any lubricating regime, depending upon the land profiles, the attitude of the ring and the surface roughness of the ring and liner. For relatively smooth surfaces, σ = 0.1 μm, hydrodynamic conditions would prevail throughout, whilst for rough surfaces, σ = 3 μm, there would be negligible hydrodynamic action on the piston downstroke and the ring load would be supported by asperity contact. Furthermore, it was predicted that oil-film thicknesses left on the liner by the oil-control ring during the downstroke, even with smooth surfaces, would be such that the lowest compression ring would be considerably starved of lubricant. This effect would be greater for the case of rough surfaces, in which case the entire ring-pack would operate with a large amount of asperity contact. Although not included in their model it was also recognised that the oil-control ring may itself be starved of oil by the compression rings on the upstroke.

Experimental work by Seki *et al* [108]] suggested that the oil-control ring may operate rather differently to predicted behaviour. Figure 2.33 shows measured oil-film thicknesses compared to a theoretical analysis. The measured values were found to be

significantly greater in the early part of the downstroke and oil supply mechanisms related to the piston motion (primary/secondary/slap) were identified as the likely cause.

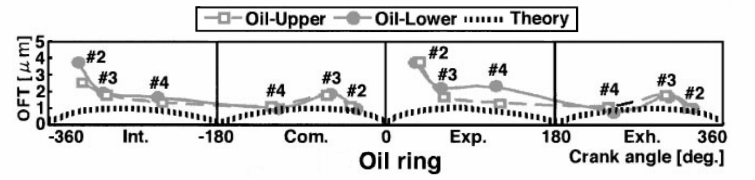

Figure 2.33: Oil-film thickness measurements compared to theory, from Seki et al [108].

2.5 Summary

The shift to predictive maintenance strategies and erosion of operational safety margins has created a requirement for more revealing diagnostic information than that currently available. Two aspects of engine operation that this applies to and which are considered within the scope of this thesis are monitoring of the ring-pack/liner interface, particularly for large, marine diesels, and to a lesser extent, identification of underperforming cylinders.

As regards the former, a wide range of novel monitoring techniques have been investigated, with some proving more successful than others. Of these, analysis of vibration signals appears the most promising due to the non-intrusive nature of the measurements, the rich information content of the signals and recent advances in signal processing techniques. Furthermore, it appears that more diagnostic information is contained in the higher-frequency emission range and therefore monitoring based upon significantly higher-frequency AE measurements is anticipated to offer even greater capabilities. Previous work in this area shall be reviewed in the following Chapter.

A review of ring-pack/liner tribological behaviour in four-stroke engines reveals that although there is general agreement on some aspects there are also some conflicting views, particularly regarding the oil-control ring. It also demonstrates that establishing ring behaviour using experimental techniques is a difficult process that typically requires substantial engine modifications; and again this highlights that there is a clear opportunity for further techniques that can offer new insight into ring-pack operation.

Chapter 3

Acoustic emission monitoring

3.1 Introduction

This Chapter aims to provide understanding in three areas of AE monitoring that are central to the research work presented in this thesis. Firstly, the principles of AE are outlined, which includes discussion of AE sources, data acquisition, signal processing techniques and recognised AE analysis parameters, and a brief review of the growing range of applications. Secondly, developments to date concerning AE monitoring of diesel engines and other reciprocating machinery are reviewed. Finally, previous work on AE monitoring of sliding contact is examined in detail for a variety of applications including; laboratory wear tests, hard disk drive operation and the meshing of gears. This provides the opportunity to examine relationships between variables that govern sliding contact and any resulting AE activity, similar to that which may occur at the ring-pack/liner interface.

3.2 Acoustic emission principles, processing and applications

The purpose of this section is to provide understanding as to the foundations of AE monitoring; how AE is generated, how AE can be measured, methods to process AE signals in order to provide information for condition monitoring and how AE monitoring fares when evaluated against comparable techniques.

3.2.1 Fundamental principles

Acoustic Emission (AE) is the expression given to transient, elastic waves of surface displacement that occur within the approximate frequency range 100 kHz to 1 MHz due to changes in the microstructure of materials. Such phenomena which cause these impulsive releases of energy and which conform to the classical definition of an AE source, i.e. they occur due to mechanical deformation of a stressed material, include crack growth, movement and creation of dislocations, and slip, twinning and grain

boundary sliding in metals. In essence, any form of atomic level material dislocations can generate AE and it has been claimed that displacements as small as $1/1000^{th}$ of an atomic radius can produce well-distinguished AE signals [7]. There are a number of other mechanisms that either give rise to the fundamental sources or occur in the absence of any deformation process, these are known as pseudo- or secondary sources, and in terms of machinery operation include mechanical impacts, sliding contact, turbulent fluid flows and fluid cavitation.

Once generated AE waves radiate in all directions, propagating throughout the material in a variety of forms; namely compression, shear and Lamb waves, and ultimately manifesting themselves as Rayleigh surface waves. As the waves propagate they suffer a loss of amplitude with distance. Pollock [110] identified four reasons for this attenuation; geometric spreading of the wavefront, internal friction, dissipation of energy into adjacent media and velocity dispersion.

Geometric spreading of the wave from a point source inevitably results in attenuation since the wave has a fixed amount of energy which must be distributed over an ever larger wavefront. The wave amplitude will decrease inversely with distance in three-dimensional solids and inversely as the square root of the distance in two-dimensional structures such as plates and shells. This form of attenuation has been noted as being dominant close to the source, i.e. in the near field [110]. Internal friction involves the conversion of elastic wave energy into thermal energy through various damping mechanisms. This results in exponential attenuation with distance that becomes dominant at greater distances from the source, i.e. the far field.

Further signal distortion occurs when material boundaries are encountered as wave reflection, refraction, transmission and mode conversions can all occur. Therefore, for complicated structures that feature, for instance, intricate geometries, cavities and contained fluids, wave propagation will be considerably more complex than for simple plates and strips. These effects generally cause a reduction in wave amplitude with distance although local constructive or deconstructive interference effects may also exist. Wave dispersion is a further form of attenuation which causes different frequency components of a signal to propagate through a material at different velocities. The outcome is that a signal of initially short duration spreads out as it travels and loses amplitude accordingly.

In effect this means that by the time measurement of the signal is possible at the material surface the waveform will merely be a representation of the original source excitation. Nevertheless, significant information is still available, and it is typically the variation of the measured signal, either with time or distance, which is of interest. The benefit of AE propagation is that, given a source is of sufficient energy, external remote investigation of material behaviour can be achieved. This is a significant advantage when the area of interest is at an inaccessible location or is one which prohibits the use of other monitoring techniques.

AE monitoring, also referred to as stress wave monitoring, is the practise of characterising and evaluating AE signals in order to investigate material or component behaviour. It is inherently a passive Non Destructive Testing (NDT) technique that relies on energy being released from a material. This is distinctly unlike conventional ultrasonic NDT inspection techniques, where the effects of introducing external, artificial waves of a known type are monitored.

3.2.2 Measurement of AE

There are several methods of measuring absolute surface displacement which involve capacitive, electromagnetic and laser-optical measurement techniques. However, practical difficulties in applying these methods in an industrial environment has meant that the vast majority of AE monitoring has used resonant transducers based on piezoelectric elements. These sensors have proven to be suitably sensitive and robust to the extent that they become accepted as the norm. The material used for the active element is most usually lead zirconate titanate (PZT), a piezoceramic, although it has been shown that other piezo-active materials such as polyvinylidene diflouride (PVDF) are equally feasible [111]. The work reviewed in this Chapter features almost exclusively AE measurements made with piezoelectric element sensors, exceptions to this shall be made clear.

The construction of a piezoelectric AE sensor is shown schematically in Figure 3.1. These sensors rely on the fact that a voltage is generated in proportion to the compression of the piezoelectric element; hence nanometre surface displacements are

converted into an electrical signal. However, the output of most piezoelectric sensors is not an accurate description of the surface movement under inspection. Rather, the AE signal, i.e. the sensor output, is the sensor's response to the forcing transient waves. This is influenced by the sensor construction and consequent frequency response, the amplitude sensitivity and associated self-resonance (ringing after initial excitation), and also by whatever means the sensor is coupled to the material.

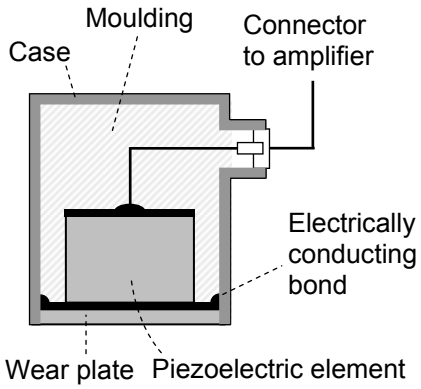

Figure 3.1: Schematic of an AE sensor, from Vallen [7].

The sensor response characteristics are determined by the geometry of the piezoelectric element, these can be manufactured in a variety of forms so as to offer a range of resonance frequencies and sensor sizes for various applications, although for sensor selection there is usually a compromise between bandwidth and sensitivity. If prior information is known about the source frequency characteristics then narrowband sensors can be selected to provide high sensitivity, conversely, if source characteristics are unknown then broadband sensors with lower sensitivity are available. With regards to monitoring of machinery the AE sources of interest have typically broad and varied frequency contents and therefore broadband sensors are generally required if all mechanical and fluid processes are to be considered. Moreover, since most of these sources are of reasonably high amplitude the loss of sensor sensitivity is less important than the broadness of frequency response. A further factor in sensor selection is the anticipated source to sensor transmission distance. Given that higher frequencies suffer from greater attenuation they inherently possess a lesser detection distance and therefore the spatial range of a sensor is indirectly determined by its resonance frequency.

The use of resonant sensors incurs further distortion of the original source AE, but this is tolerable, and somewhat unavoidable, since these transducers represent the most practical means of measuring emissions in the upper frequency range. Although the impact of this may be minimal for comparative work when a consistent set-up is used, it can be a problem when absolute measurements are required. Furthermore, the lack of a universally accepted, and applied, method of signal calibration means that quantitative

comparison of test results obtained from different detection systems is highly questionable.

Attempts have been made to overcome this problem through signal normalisation and characterisation of AE sensor response to reproducible broadband sources such as pencil-lead breaks [112] (also referred to as the Hsu-Nielsen source), glass capillary breaks [112, 113] and helium gas jets [113]. However, there are problems with this approach, particularly since the generated waveforms are reproducible only at a single point on a given structure and even then although the structure can generally be well-defined the amplitude is dependant upon the source energy. As a result these methods are not universally employed in practise and instead are typically used as a check to ensure the functionality of the AE detection system and to confirm the quality of sensor coupling. A further use for these reproducible sources is to investigate AE propagation in structures, in which case the acquired signals require to be normalised as a function of the source energy.

There are several other essential components in an AE measurement system. Signal amplification is necessary and is provided either integral to the sensor or externally via a pre-amplifier. Filtering of the signal is necessary to eliminate unwanted frequency components and background noise, the range of this filtering can typically be varied to suit the application although a prerequisite is the removal of any low-frequency energy and this lower limit varies from 20 to 100 kHz. A relatively recent development has been the advent of Analogue to Digital converters of sufficient capabilities to continuously digitise raw AE signals at full bandwidth, i.e. at sampling rates up to 10 MHz, and store this data for future analysis. Prior to this digitised acquisition of raw AE was limited to small batches that for many applications would be insufficient to permit a full investigation. Other means have also been used to acquire AE signals, such as analogue recording of signals via videotape.

Analogue Root Mean Square (RMS) averaging of the raw signal is a further method commonly used in the acquisition of AE data. This significantly reduces the required sampling rate thus allowing the use of less sophisticated data acquisition equipment. However, this is at the expense of information loss, both of the fine detail of the raw AE waveform and of the associated spectral content. Further methods have been used, for instance, some researchers have used specific circuitry which does not acquire and store

data for future analysis but instead analyses the signal in real-time through the extraction of waveform features. Analysis of the frequency content via conventional spectrum analysers, rather than time-series data, has also been used.

3.2.3 AE analysis and signal processing techniques

There are two basic types of AE signal. The first is burst-type emission, where the signal consists of clearly defined 'events' as shown in Figure 3.2a. These events are characterised by an amplitude significantly larger than the background level, distinct sharp signal rises and close to exponential decays, and individual pulses are usually well-separated in the time-domain. The second type is continuous emission; this occurs when burst generation is so rapid that the signal appears continuous and resolution of individual events is not possible. Typically, signals acquired from machinery will be a combination of both to varying degrees, for example, Figure 3.2b shows a raw AE signal measured from the surface of a running engine in which a number of overlapping burst- and continuous- type events of varying amplitude are evident.

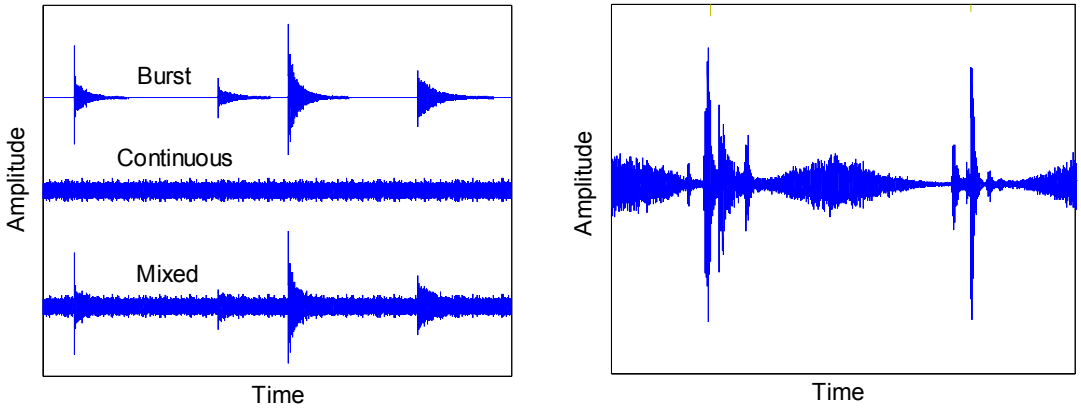

(a) *(b)*

Figure 3.2: (a) Examples of AE emission types, (b) typical AE signal acquired from a running engine.

3.2.3.1 Time-domain analysis

There are various means by which AE signals can be processed and evaluated in order to extract information useful for condition monitoring, the most fundamental being the characterisation of signals with regards to the behaviour of the object under observation. The most common method for achieving this is time-domain characterisation of burst-

type events through extraction of waveform parameters. This typically involves monitoring the sensor output continuously for activity that exceeds a predefined threshold level. When this occurs an event is registered and the signal is then processed to extract parameters such as those identified in Figure 3.3, these include; peak amplitude, event rise time, event decay time, signal duration, AE event count and AE count rate.

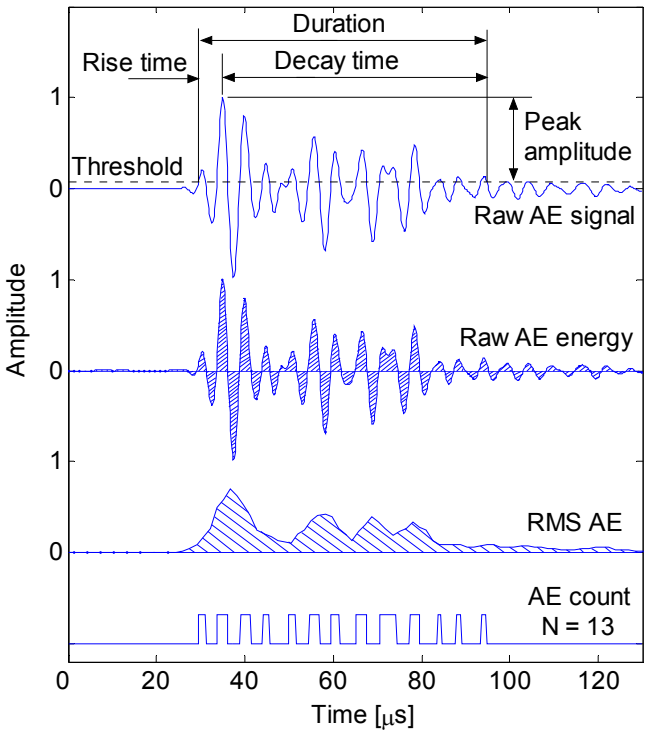

Figure 3.3: Typical time-domain parameters extracted from AE signals.

Of all the waveform descriptors, the measure of threshold crossing counts has probably been the most widely used, likely due to the simplicity of measurement system required and the applicability towards both burst and continuous type emissions. However, there are disadvantages associated with the sole use of count parameters to describe AE signals. These were outlined by Beattie and Jaramillo [114] who stated that firstly, AE count rate considers the amplitude of a signal only indirectly in that a large amplitude signal will usually persist for a longer time than a low amplitude signal, thus producing more counts. Secondly, for two signals of equal amplitude and duration, the one with the higher frequency content will register most counts. They suggested that a more quantitative measure is desirable, with the most obvious being the amount of AE energy emitted.

A further problem with applying threshold-based analysis to machinery monitoring is that burst type activity is often accompanied by a high level of continuous signal. If the burst activity is generated from a fault-related source, such as the early signs of wear, then this may effectively be buried in the continuous signal, which can make identification via threshold-analysis difficult. Therefore, to fully preserve the possibility of incipient fault detection and to better understand AE generation from machinery continuous and mixed AE should be analysed through other means.

AE energy is a measurement parameter used extensively in AE monitoring. However, the calculation of energy is open to interpretation. For the work in this thesis, energy is taken as the area under the absolute of the signal, as defined in Equation 3.1; this is in contrast to a number of researchers who define AE energy as the area under the square of the signal.

$$E = \int_0^t |v(t)| dt \tag{3.1}$$

where $|v(t)|$ is the absolute amplitude of the AE signal in volts, although in this work amplitude is given in arbitrary units due to the sensors being resonant, t is time in seconds and E is the AE energy in V.s, although given in this work as arbitrary units.

A point to note regarding Equation 3.1 is that although it is presented in relation to time this does not preclude the use of other bases. For instance, for AE acquired from rotating equipment the AE signal is often transformed from a time-domain waveform to one which is a function of angular displacement. The resulting AE energy is then also an angular-domain parameter and the integration limits may be angular positions, as defined in Equation 3.2.

$$E_\theta = \int_a^b |v(\theta)| d\theta \tag{3.2}$$

where $|v(\theta)|$ is the absolute amplitude of the angular-domain AE signal, again given in arbitrary units, θ is angular position in degrees, E_θ is the angular-domain AE energy, and *a* and *b* are angular positions.

A further parameter widely used to indicate energy is the Root Mean Square (RMS) value of the raw AE signal, calculated using Equation 3.3.

$$RMS = \sqrt{\frac{1}{N}\sum_{i=1}^{N} x_i^2} \tag{3.3}$$

where x is the data value at a discrete point in time and N is the total number of data samples in the selected time period.

This can be applied as post-acquisition processing in which the RMS value for each successive time window is calculated, as shown in Figure 3.3 for a burst-type event. Otherwise, a signal averaging circuit can be in-built into the acquisition equipment which continually calculates the RMS value over a sliding time period. This allows data acquisition at a lower, more conventional rate thereby bringing about a significant reduction in data size. This can be beneficial when analysis of many hundreds or thousands of lengthy acquisitions is considered as analysis of raw waveforms can be extremely computationally intensive.

Further simple statistical parameters are commonly used to describe signals such as the mean, $\bar{x}$, standard deviation, σ, and variance, σ^2, as defined in Equations 3.4, 3.5 and 3.6 respectively. These can be applied to a whole signal, to sections, or windows, of a signal, or to determine variation between sets of signals.

$$\bar{x} = \frac{1}{N}\sum_{i=1}^{N} x_i \tag{3.4}$$

$$\sigma = \sqrt{\frac{1}{N-1}\sum_{i=1}^{N}\left[x_i - \bar{x}\right]^2} \tag{3.5}$$

$$\sigma^2 = \frac{1}{N-1}\sum_{i=1}^{N}\left[x_i - \bar{x}\right]^2 \tag{3.6}$$

Other statistical indicators often used are the skewness and kurtosis parameters [115] as well as crest, impulse, clearance and shape factors.

3.2.3.2 Frequency-domain analysis

Frequency domain analysis offers further options for investigation of AE signals, and is a proven technique for machinery diagnostics. This has been established through a long association with vibration monitoring where spectral analysis is considered one of the principal analytical tools and is used in many commercial monitoring packages.

Moreover, since AE is regarded by some as an extension of vibration monitoring, in that both are measurements of surface motion as a function of time, then the transference of many diagnostic principles from the latter to the former has been investigated.

In general, frequency analysis involves the decomposition of time-series data into the frequency domain, this is typically achieved as an estimate through an algorithm known as the Fast Fourier Transform (FFT). For many applications this method alone is sufficient to describe the signal. However, other algorithms have been developed which implement the FFT in order to estimate the distribution of the signal energy in the frequency domain, the principal methods for this are known as the Power Spectral Density (PSD) and Welch's PSD estimate [116].

Regarding condition monitoring, analysis of frequency spectra can be similar to time-domain analysis, in that deviations from the expected normal condition may be indicative of faults. Some frequency parameters are directly associated with aspects of normal machine operation such as running speed or resonance, however, the development of faults may result in the emergence of discrete frequencies which can be related to the physical behaviour of the machine. A further feature of AE spectral analysis is that it has been suggested that the content can be used to distinguish between different types of source mechanism. This may be of benefit for investigation of events of unknown origin. A further approach commonly used is to filter the signal to separate it into its constituent parts. If the filter is carefully constructed then this can then allow increased focus on specific events through enhanced signal-to-noise ratios.

Irrespective of which method is used to estimate spectral content a singular usage cannot satisfactorily describe how non-stationary signals, such as AE, vary with time. Therefore, to overcome this, techniques which combine time and frequency analysis are widely-used, with the simplest being the Short Time Fourier Transform (STFT). This implements the FFT algorithm at time increments through the signal using a sliding window approach. Other methods for time-frequency analysis include wavelet decomposition [117, 118], a spectral decomposition technique which returns scaled, variable resolution in both time and frequency axes.

The aforementioned spectral analysis tools are generic techniques, which for AE analysis are most usually applied towards the raw AE signal. However, for machinery

monitoring, and particularly for rotating and reciprocating machinery, there is merit in applying these techniques towards the RMS AE signal. In this case, the features of interest would be any superfluous lower-frequency modulation that may be introduced to the carrier AE signal through the presence of faults. These modulations are typically found at the rotational speed of the machinery, for instance in the case of blade rubbing in turbine monitoring [119], or at multiples of the running speed, the identification of which can determine the nature and location of faults in rolling element bearings [115].

3.2.3.3 Feature extraction and pattern recognition

A number of other approaches exist for AE signal processing which do not involve applying a threshold, are applicable for burst and continuous type emissions, and for both time- and frequency- domain information. Although the work in this thesis does not apply these techniques it is considered worthwhile to provide a brief review.

Many of these methods are considered attractive to condition monitoring as they introduce some form of automation to the analysis process and therefore lend themselves well to real-time monitoring. Also, they can be adapted to quickly handle large amounts of data and to identify changes in signals, or signal features which do not conform to the expected case. A further point is that many of these processes are purely statistical in nature, and require minimal interpretation of the complex AE signals with regards to the material or component behaviour. Hence, they are generic and transferable over applications as is borne out in the wide range of data processing problems to which they have been applied, such as speech recognition, machine vision, medical diagnostics and financial market analysis.

One technique used for isolating significant features from large and often complex datasets is Principal Component Analysis (PCA). This is a form of higher-level statistical analysis whereby variance is analysed and a simplified description of the data is returned which preserves as much statistically relevant information as possible. The removal of redundant features is deemed desirable, especially for the large datasets which AE monitoring usually generates, as it permits the application of further statistical classification and diagnostic aids.

Independent Component Analysis (ICA) is a further signal isolation technique, and is considered an extension of PCA. It assumes that the measured signal is a composite of separate signals which can be resolved using ICA algorithms based upon the assumption that the source signals are statistically independent. The outcome is the source signals and also a measure of their separation effectiveness, i.e. how strongly they appear in the measured signal. This technique is especially useful for extracting low-level, or hidden signals, which may otherwise be obscured by dominant sources.

Pattern recognition techniques are extensively used in condition monitoring applications, either using simple time-domain parameters, or in combination with feature extraction or other analytical processes. The overall aim with pattern recognition is to ascertain condition through comparison of measured signal parameters against a reference bank in which signals over varying conditions are mathematically and statistically well-defined. A best-match is identified and the acquired signal is then classified as representative of that particular condition. One drawback with this process is that in order to minimise misclassifications prior knowledge is required of all conditions that may be encountered. This may be impractical due to the many different operating conditions and fault scenarios; hence the pattern recognition process may be limited to differentiating between normal and abnormal conditions.

Neural networks have regularly been used to recognise and classify complex fault patterns without requiring a great deal of prior knowledge about the process, the signals, or the specific fault patterns. Neural networks are structured in layers of interconnecting processing elements (neurons), with the behaviour of the network determined by the weights associated with each connection. These weights can be adaptively trained using example signals to associate a particular input pattern to an output classification. Hence, if something similar to that pattern is presented again then the network will recognise it and return the appropriate output. Many output possibilities can be programmed in this manner and it is not unusual to have several processing layers in order to achieve an output classification. Neural networks are adept at handling large amounts of data in a short period of time and are therefore useful for real-time analysis and for data fusion, i.e. the amalgamation of information obtained from a variety of sensory inputs.

Further generic signal processing tools include fuzzy logic and expert systems. Fuzzy logic is a technique used when fault threshold values for conventional time-domain and frequency-content analysis are felt too rigid to suit the complex nature of mechanical condition monitoring. Expert systems is a term used to describe the application of knowledge-based procedures and programs that are the equivalent to the knowledge, or reasoning processes, that would be expected from human experts in a particular field.

3.2.4 Relative merits of AE, vibration and air-borne acoustic monitoring

The source mechanisms that produce AE are generally also responsible for vibration and audible air-borne acoustic waves. All can be exploited as non-intrusive condition monitoring techniques, although it has been widely recognised that AE has significant advantages over both.

The principal benefit is that far greater signal to noise ratios can be achieved for signals relating to the most important mechanisms and processes. Because of the very high frequency content and relatively high damping of AE the lower-frequency background noise, which can be troublesome for vibration monitoring, has little bearing on the AE signal. Accelerometers offer monitoring of surface motion up to approximately 50 kHz using current instrumentation. However, operational noise and machine resonances are also prevalent in this region and because this background vibration is often orders of magnitude greater than any fault-induced vibration then early, accurate detection of faults can be difficult. Consequently, when abnormalities in the vibration signal are detected the machine or component is usually close to failure or it has already occurred. AE monitoring on the other hand is of such sensitivity that it can be used to detect the degradative processes that lead to failure rather than the consequences. A further benefit of high-frequency AE is that the temporal and spatial resolutions are significantly greater than for vibration monitoring. Again, this is because higher frequency waves attenuate quicker with regards to both time and distance. The monitoring of air-borne acoustics via instrumentation located away from the material surface is a further step down in diagnostic capabilities where further acoustical environmental effects also have to be considered.

Numerous investigations have directly compared AE and vibration monitoring, and to a lesser extent air-borne acoustics for machinery diagnosis. This has included experimentation on rolling element bearings [115, 120, 121], reciprocating engines and compressors [82, 122-124], centrifugal pumps [125] and the meshing of gears [126-128]. In each of these cases AE monitoring has shown to be the more effective for fault detection and performance monitoring. One aspect where AE monitoring shows a particular improvement on vibration monitoring is an increased sensitivity to fluid flows, both for normal and faulty operation [82, 123, 124].

The improvement offered through AE monitoring is emphasised in Figure 3.4, which shows simultaneous in-cylinder pressure, RMS AE and accelerometer measurements acquired from the cylinder head of a running gas-fuelled engine [122]. It is evident that the vibration signal lacks clear correlation with the timing of the valve activity (denoted in Figure 3.4 as IVO and IVC for inlet valve opening and closing, and EVO and EVC for exhaust valve opening and closing) whereas the AE signal displays more information with transient AE events generated at each valve action. In this case the accelerometer measurements appear to show a particular lack of information as other researchers have reported that valve impacts within engines are identifiable from vibration signals [14, 32, 35].

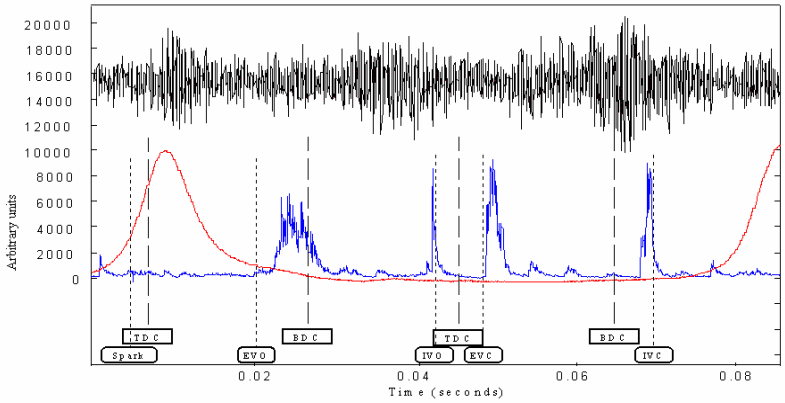

Figure 3.4: Simultaneous in-cylinder pressure ——, RMS AE —— and acceleration —— measurements from a gas-fuelled engine, from El-Ghamry et al [122].

Vibration monitoring does possess some advantages when compared to AE monitoring. Accelerometers can be mounted so to measure the vector components of acceleration thereby providing a 3-dimensional account of whole-body surface movement. This is in contrast to the 1-dimensional measurements available through AE measurements. Absolute measurements of acceleration can be obtained; hence data can be compared on

a quantitative basis. This has resulted in vibration monitoring being widely-used, well-understood and industrially accepted. Currently, AE monitoring is not as widely-understood or as accepted although it is quickly gaining in recognition as a condition monitoring technique.

3.2.5 Applications of AE monitoring

Such are the benefits of AE monitoring it has become an established technique in a number of engineering disciplines with a number of bespoke AE-based commercial monitoring systems available for specific applications. This is particularly true in the field of pressure vessel proof testing where the non-destructive nature and high sensitivity to cracks and fluid flow through confined spaces make it a valuable tool for structural assessment and defect location [7, 129]. A particular problem that AE analysis has proven to be well suited to is the monitoring of crack initiation and propagation [130]. This has been ascertained through applications as varied as the monitoring of cables in suspension bridges [131] and of the structural integrity of historical statues [132].

On a smaller scale, laboratory materials research is a further successful application. The generation of AE from microscopic material disturbances has allowed materials properties, damage mechanisms and resulting material behaviour to be investigated in detail using insight that may not be available through other means. Condition monitoring of machinery via AE measurements is an expanding area of active research. Of all mechanical components, AE monitoring of bearings is perhaps the most advanced, likely as a result of the regularity of bearing faults occurring in industry and the ease of investigation. Other components investigated include gearboxes, turbines and reciprocating engines. Progress to date in monitoring of reciprocating engines shall be detailed in the following section.

Recent developments in computational and data acquisition capabilities have permitted further investigation into these established research themes as well as opening up additional research possibilities. These have been in fields as diverse as orthopaedic diagnostics, where friction during bending of human knees has been detected [133], and botany, where phenomena such as flora cavitation have been studied [134].

3.3 AE monitoring of reciprocating machinery

The purpose of this section is to provide a review of achievements to date regarding AE monitoring of reciprocating machinery; this primarily involves diesel engines, both large and small, but also includes work on reciprocating compressors. The use of non-intrusive AE analysis in engine diagnostics is a relatively recent development that has centred primarily on research institutions, although the progression into commercial use has of late been observed, with at least one AE-based engine diagnostic system currently available.

This monitoring method is based on the premise that the mechanical and fluid events and processes occurring within engines, e.g. valve activity, injector operation, piston motion, fuel combustion and exhaust, generate AE which can then be measured with suitably placed external sensors. Therefore with appropriate analysis and signal understanding there is the possibility to monitor these aspects of machine operation and inherent faults thereof. Details shall be given as to what has been investigated and also the analytical techniques that have been employed. A thorough review of this topic is also provided by Steel and Reuben [6].

3.3.1 Initial identification

To the author's best knowledge the first published work concerning AE acquisition from engines was reported by West *et al* [135, 136]. However, these works made no attempt to understand the AE generated during engine operation, rather, they were largely exercises in signal-processing with the aim being to extract a digitally embedded burst-type AE signal, relating to a microcrack, from background AE acquired from a lawnmower engine. Nevertheless, it was recognised that certain aspects of engine operation could result in AE generation [135]:

> *"We are looking at scenarios where the AE signal is buried in strong interference (which could be periodic) due to a mechanical motion, like the movement of a piston in an engine"*

Much of the AE was in this case regarded as noise, as opposed to signal, and was noted to be dominated by frequencies below 30 kHz. This is below the typical AE frequency band lower limit, although it is not clear what, if any, pre-processing filtering steps were taken. Hence this observation may simply be a consequence of un-filtered AE acquisition.

Gill *et al* [137] first reported on the possibility of engine diagnostics via AE measurements. This study focused in particular on the combustion process, with RMS data acquired from sensors located close to the combustion chambers of small, four-stroke HSDI diesel engines. Information about the timing and sequence of mechanical operation within the engine was used to map the events in AE signals acquired during normal operation to their respective origins. This showed that events were generated from combustion, or combustion-related, processes as well as from valve activity for all four cylinders. The presence of these events was found dependant upon sensor location with signals from other positions on the engine noted as being more complex with contributions from other engine driven components.

Two induced fault conditions were investigated; fuel starvation through disconnection of the fuel-feed pipe to a cylinder, and reduced injection discharge pressure. Under fuel starvation conditions a simple comparison revealed that the events purported to relate to the combustion process in normal operation were absent. To characterise a progressive reduction in injector discharge pressure the authors used a simple technique whereby the energy in a time-windowed section of the signal was calculated and compared as conditions varied. It was also found practical to use the average signal of 10 cycles, presumably to gain a better overall representation of the AE signature at a particular running condition. The energy in a window corresponding to the combustion process was found to increase with a reduction in discharge pressure. It was reasoned that this was due to an increase in combustion harshness as a result of poorer fuel atomisation. Analysis of event timing was also found to be useful for fault detection, the initial event, postulated to be combustion-related, and occurred earlier in the cycle with decreasing injection pressure. This was consistent with the premise that the event was injection related since the lower delivery pressures would be achieved by the fuel pump earlier in the cycle.

3.3.2 Monitoring of injection, combustion and combustion-related processes

Gill *et al* [138] expanded upon their earlier work [137] to investigate more detailed raw AE signals acquired from a the fuel injector body of a small, HSDI diesel engine operating under reduced injection discharge pressures. To provide a thorough evaluation of injector operation the AE data were supplemented by measurements of injection pressure, needle lift and in-cylinder pressure. As in the previous study, the relatively small size of the engine meant that AE originating from all four cylinders of the engine propagated to the sensor location with the most prominent events found to relate to fuel injection and combustion in the cylinder closest to the sensor.

The level of temporal resolution offered through AE monitoring permitted the injection AE signature to be separated further into its constituent events. The authors suggested that the initial AE burst was due to the sudden increase in fuel pressure whilst the main AE burst was generated due to the injector needle attaining the fully open position and subsequently impacting with the injector body. Importantly, these observations were validated through comparison with the needle lift measurements.

Again, similar to [137], the timing of injection events was observed to advance for a reduction in injection discharge pressure. This was found consistent both cyclically and also over all considered engine speeds and loads. The authors also report that for the lowest pressure the duration of the whole injection/combustion AE event was prolonged by a period of low amplitude AE when referenced to the normal condition. This was thought related to coarse fuel atomisation which would require a longer combustion period. Validation of this theory was not provided, and indeed would prove difficult to achieve, but it does illustrate that examination of AE activity may reveal further insight than needle lift and fuel pressure monitoring.

Several other research groups have investigated AE relating to injection and combustion processes [122, 139-145]. Berjger [139] confirmed that operation of a fuel injector without combustion was indeed a source of AE. Fuel was injected into a combustion chamber of a four-stroke engine filled with inert gas thereby inhibiting fuel ignition and combustion and leaving only the injection events, namely the pressure increase in the injector body, the resulting needle movements and high-pressure fuel flow, as possible AE sources. Analysis presented in this work was limited but AE events were noted and

attributed to injector operation, with the amount of activity dependant on both the quantity and diameter of the nozzle orifices. The proposed use of such knowledge was for injector nozzle diagnostics in ship injection systems. Recently, Bialkowski *et al* [140] performed similar tests on a common-rail diesel injection system again finding that significant AE activity was generated for injector operation in the absence of combustion. In this case, AE activity was found to increase with both injection pressure and fuel pre-heating.

Godinez *et al* [141] reported that injector cavitation and detonation could be diagnosed from analysis of time-domain AE characteristics. These claims were corroborated through simultaneous acquisition of other engine data, in this case load measurements from the rocker. Time-domain analysis of windowed injection/combustion events was also found to be a suitable method for identification of operating conditions over varying load by Frances *et al* [142]. Eleven statistical features were extracted from a window corresponding to the combustion AE events for a 3.8 MW, medium speed, four-stroke engine, namely; signal energy, mean, standard deviation, variance, skewness, kurtosis, maximum amplitude, peak start location, peak ignition location, peak end location and power spectral density ratio. PCA was used to identify and eliminate redundant features and a neural network was then applied to differentiate between operating conditions. The results of this process showed that engine loading condition could be reasonably identifiable, although not with complete confidence. Further frequency-domain analysis showed that engine loading could not be determined through analysis of frequency content but could be distinguished through wavelet analysis.

Chandroth *et al* [143] described a data acquisition system which acquired AE measurements alongside vibration and in-cylinder pressure data for the detection of combustion-related faults in a small, four-stroke diesel engine. This was expanded upon by Sharkey *et al* [144] who applied neural networks to survey the value of each measurement technique for the detection of these faults. Selective pre-processing methods were employed, in the case of AE data this consisted of frequency-domain analysis. The authors reported that the best performance in terms of generalisation, i.e. when one dataset is tested against validation data, with a value of 97.7 %, was from the AE measurements. This compared with 94.0 % and 88.7 % for the vibration and in-

cylinder pressure data respectively, providing further evidence of the usefulness of AE measurements towards engine diagnostics.

Other combustion-related features have been investigated. The possibility of using AE measurements to infer fuel-to-air ratios in an 8-cylinder, 430 kW, four-stroke gas engine was investigated by El-Ghamry *et al* [122]. For this work a window of raw AE data corresponding to the combustion period in the cylinder closest to the transducer was extracted from the rest of the signal. Simple features were then calculated such as the mean, peak, peak to mean ratio, standard deviation and variance over 10 individual cycles acquired at various running conditions. The amount of AE activity was observed to increase for both lean and rich running conditions compared to the reference normal condition, with variance noted as the most distinct parameter. The changes in fuel supply were also evident, although to a lesser degree, from inspection of in-cylinder pressure data.

El-Ghamry *et al* [145] further outlined a technique whereby the in-cylinder pressure trace could be reconstructed from the AE signal over the compression/expansion period. This would be to the same effect as others who have attempted similar reconstructions using vibration [40-42] and ICAV measurements [16, 17, 22-26] with the next step being to diagnose combustion deficiencies from the in-cylinder pressure trace. Although this work centred on the combustion period, data were presented, see Figure 3.5, which showed a number of other events, both large and small in relation to the prominent injection/combustion events, and these appear regularly during the cycle and are cyclically consistent.

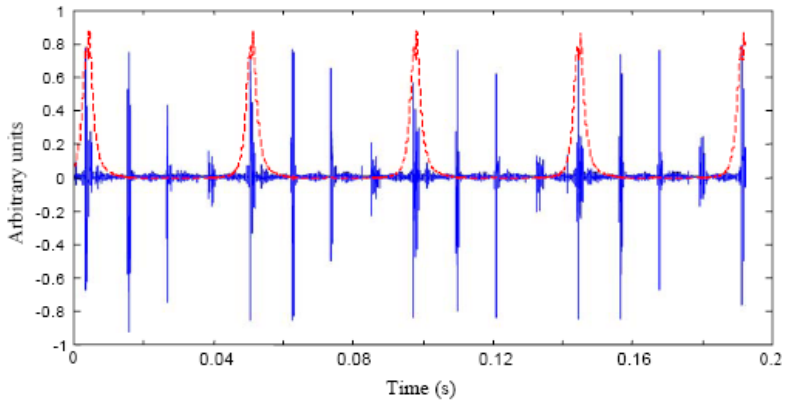

Figure 3.5: Raw AE acquired from a small, four-stroke engine showing injection/ combustion events at areas of maximum pressure, other smaller events appear regularly, AE (—) and in-cylinder pressure (----), from El-Ghamry et al [145].

3.3.3 Monitoring of exhaust valve and gasket leakage

Much use has been made of the sensitivity of AE to gas flow excitation to investigate the monitoring of fluid flows within engines, including normal processes and leakages from both exhaust valves and gaskets.

El-Ghamry *et al* [122] reported that AE was generated at coincident times as valve movements for a 0.5 MW gas engine; the specific example given was of exhaust valve opening, which was observed to be accompanied by a broad, high-amplitude AE event. It was reasoned that the AE generated during valve opening may be indicative of the gas flow properties through the exhaust port, and thus this activity would be affected by such factors as in-cylinder pressure, valve leakage and deposition. The authors also noted that the AE signals were much more defined and responsive to these valve actions than simultaneously acquired vibration measurements.

Fog *et al* [82, 123, 146] have detected exhaust valve leakage in a large, two-stroke diesel using AE measurements, again finding this more effective than acceleration, in-cylinder pressure and temperature measurements. For this work the exhaust valve was degraded by cutting a groove in the valve face, with two leakage areas, 4 and 20 mm^2, considered in addition to the normal case. It was found that due to the large size of this engine the cylinder-by-cylinder analysis was simpler than for small engines because the propagation distances and signal attenuation were such that cross-cylinder interference was minimal. This allowed for easier isolation of events, and using knowledge of the engine cycle the AE events were then related to mechanical actions within the engine, Figure 3.6 shows such events labelled as XVO, XVC, IJS and IJE which relate to exhaust valve opening and closing and the start and end of the injection process. A further pre-processing step was the resampling of the data, which effectively related one AE sample to one pulse of the shaft encoder signal thereby overcoming signal non-stationarity over varying operating conditions. Furthermore, it greatly reduced the amount of data per cycle which permitted the application of higher statistical analysis techniques.

RMS AE signals acquired from the exhaust valve housing of the engine operating under normal conditions and with a large exhaust valve leak are given in Figures 3.6a and 3.6b respectively. It is clear that with the leak induced there is a significant increase in AE

activity. As might be expected, this occurs during the compression and expansion phases and increases in amplitude with in-cylinder pressure. This leakage activity was also observed to increase in proportion to leakage area.

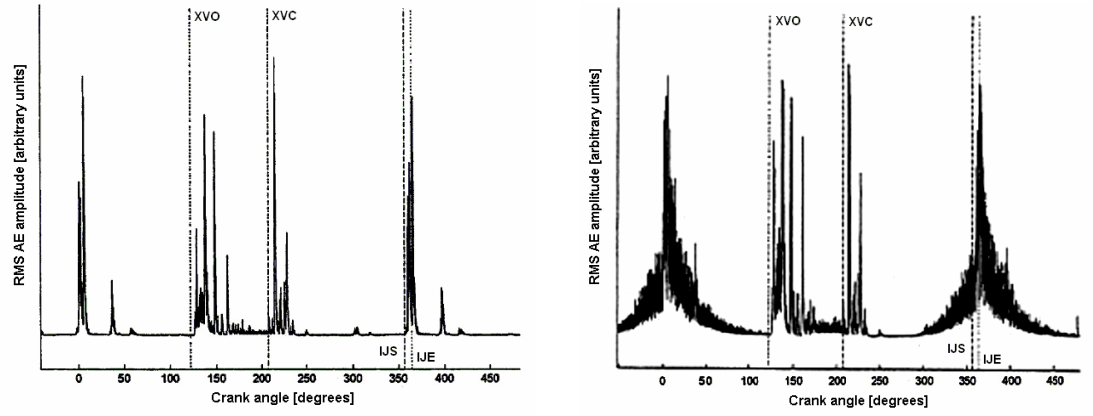

(a) *(b)*

Figure 3.6: RMS AE signals acquired from a large, two-stroke diesel, (a) normal condition, (b) large exhaust valve leak, from Fog et al [82].

Friis-Hansen and Fog [147] investigated the same dataset and found that a simple calculation of the mean value in a windowed region relating to the compression stroke, 300 to 350 degrees after TDC, was sufficient to distinguish between leakage sizes with only a small percentage of misclassifications. This window was chosen carefully to avoid signals relating to injector and valve sources. The possibility of monitoring injector misfire was also investigated, not through analysis of AE generated during the injection process but through the consequences of combustion, i.e. the in-cylinder pressure and related leakage levels. Detection was proposed through comparison of AE energy during windows of the AE signal before and after TDC. Ratios above and below unity were found to be suitable for distinguishing between normal operating and complete misfire conditions. However, it was not clear whether this method would work under no leakage conditions.

Monitoring of head gasket leakage in a small, four-stroke diesel engine was investigated by El-Ghamry *et al* [148]. As with others who have considered AE generation from small engines a high level of cylinder cross-talk was observed, hence sensor positioning was important in order to target specific engine areas. When gasket leakage was induced AE activity during the compression/expansion phase increased significantly, in a similar manner to that observed previously by Fog [82, 123, 146] for exhaust valve leakage. An algorithm based upon signal thresholding and statistical quantifiers was

developed to automatically identify this gasket leakage feature. Frances *et al* [149] also reported that the energy content of a windowed section of the signal varied when a fault was introduced to the exhaust manifold gasket of a small, four-stroke engine. However, although a change was generally observed between fault and no fault conditions the difference was not systematic over varying engine speeds and loads.

Variability of AE signals over several cylinders of a medium-speed, four-stroke diesel operating under normal conditions was evaluated by Frances *et al* [150]. For each cylinder statistical parameters were calculated over a number of cycles for a windowed area of the signal containing the compression and expansion phases. In each case the AE energy content was found to be cyclically consistent; however, substantial variation was observed between cylinders. One cylinder displayed a significant increase from the normal variance, and tests over varying loads indicated that the additional AE activity was related to the in-cylinder pressure. Frequency analysis showed that it contained energies at higher frequencies and although this was not investigated further this led the authors to suggest that the additional AE activity was indicative of leakage.

AE measurements have also been successfully used to monitor normal and faulty valve processes and associated leakages in reciprocating compressors, Gill *et al* [124, 151]. AE signals acquired from the cylinder head of a small, two-cylinder compressor during normal operation showed all mechanical activities of inlet and exhaust valves [151]. In this case, the valves were of the plate variety and their operation was therefore dictated by the pressure differential between the cylinder and exhaust manifold. Several faults were induced. For both a grooved discharge valve seat and an unseated discharge valve additional AE features relating to gas leakage were evident in addition to changes in event timing brought about by variations in pressure balance. Analysis of event timing also permitted the detection of a weakened valve spring.

Testing on a large scale, industrial, ethylene compressor [124] further showed the sensitivity of AE monitoring to valve actions and fluid flows. Valve opening and closing events were readily identifiable. A further source was identified as fluid flow in and out of the cylinder; in addition to being active at valve opening this also generated a low-amplitude feature at around mid-stroke positions. Data acquired immediately prior to an overhaul, with ‘real’ faults in place, showed that significant AE activity resulted

from leakage past the valves and also from leakage through the stuffing box to the sump.

3.3.4 Event mapping and source location

The task of relating AE events to their respective mechanical and fluid-mechanical sources within an engine, termed 'event mapping', has been described in a number of works. This is effectively the source location of a sequence of AE events aided by knowledge of the processes that constitute an engine cycle and which may be anticipated to give rise to AE. Acquisition of other engine signals can also be useful, engine timing signals are particularly valuable as they provide calibrated timing references; also, needle lift measurements have proved effective in understanding AE generation during fuel injector operation [138]. Even when further engine information is unavailable the processes of varying engine operating conditions and inducing faults will generally bring about changes to the cyclic AE signature which can then be used to understand the original source mechanisms.

It has been demonstrated that the temporal resolution of AE signals acquired from engines is of an extremely high order, due to burst-type events usually being of a relatively short duration. Therefore, this allows the events to be separated and mapped in the time, or angular, domain to a precise level. This is particularly true for large, low-speed engines where interference between events is often minimal.

Nivesrangsan *et al* [152-155] conducted a thorough investigation into the mapping of AE events generated within the cylinder head of a small HSDI diesel engine. In doing so they introduced techniques for the spatial reconstitution [154] and source location [155] of events using multi-sensor arrays. The motivation for developing such techniques was to provide focussed monitoring of specific components and/or processes and thereby improve the diagnostic capabilities of AE. This is particularly relevant for small, multi-cylinder engines as the small propagation distances and material attenuation properties results in AE from all cylinders contributing to the AE measured at a single point. This is exemplified in Figure 3.7a which shows raw AE data acquired from sensors located on the cylinder head adjacent to cylinders 1, 2 and 4 [153]. The windowed firing period for each cylinder is also indicated and immediately it is clear

that the main events are associated with the injection/combustion processes, and that the amplitude of these events are greatest for the sensors located closest to the cylinder in question. A systematic reduction in energy is evident as the AE propagates to other sensor positions, this attenuation is characterised in Figure 3.7b which shows AE energy level versus injector-sensor distance.

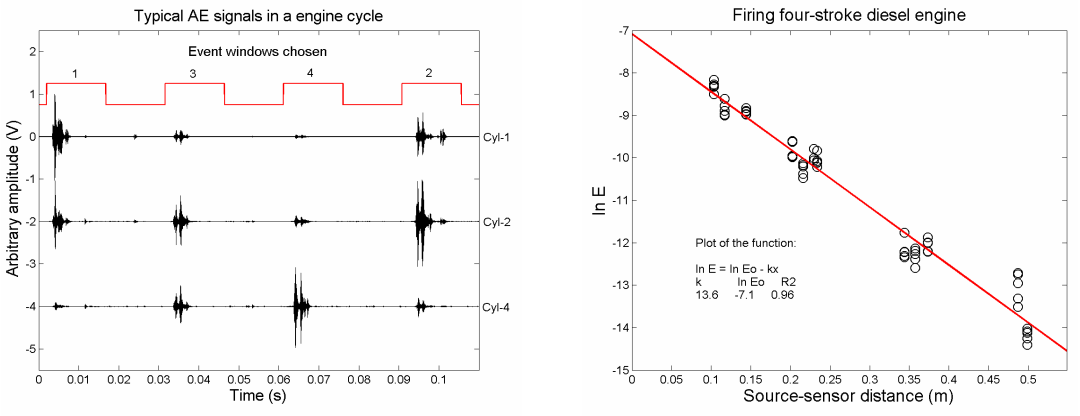

(a) *(b)*

Figure 3.7: Raw AE signals acquired from the cylinder head of a small, HSDI engine, (a) propagation around the head, (b) attenuation characteristics, from Nivesrangsan et al [153].

In order to develop techniques for application on a running engine the authors first investigated AE propagation characteristics, i.e. source-sensor attenuation, wave arrival time differences and frequency modulation, using Hsu-Nielsen simulated sources and a nine sensor array located around the cylinder head [153, 154]. The authors then applied the knowledge gained from these tests towards reconstituting the source AE characteristics, in terms of timing and amplitude, for events associated with injector operation and exhaust valve opening [154]. Good results were reported from the reconstitution process, thereby offering more accurate information regarding event timing and amplitude that could be used as the basis of a diagnostics system. However, the events considered were noted as being the dominant features in the signals, which brings the question as to how this process would fare for lower-strength sources. Further difficulties were noted when an event was itself a composite of multiple sources.

Accurate source location of events was also demonstrated using triangular sub-arrays taken from the aforementioned nine-sensor array [155]. Triangulation methods based upon wave arrival time-of-flight difference and relative energy content were

investigated, with the former found successful for burst-type events and the latter for events which contained multiple sources. A prerequisite for application of these techniques was that the signals should contain strong, well-defined events, with filtering suggested to improve performance for weaker sources. The success of this work opens the path towards complete automatic spatial decomposition of signals using multi-sensor arrays. A possible application could be for the precise location of events of unknown source that may be indicative of a fault, such as events that may originate due to scuffing in large engine cylinder liners.

3.3.5 Monitoring of the piston ring-pack and cylinder liner interface

Pontoppidan and co-workers [8, 9, 156-159] have investigated AE monitoring of the piston ring-pack and cylinder liner interface. This work was conducted to an extent in parallel with the work in this thesis and used some of the same datasets; however the focus of their work was quite different. Their interest lay with developing advanced signal processing techniques for the detection of changes in signals rather than on fundamental interpretation and understanding of the signals. RMS AE data were acquired at 20 kHz from sensors positioned on the cylinder cover and liner of a large, two-stroke diesel running at several loads, and under normal and no lubricating oil supply conditions. Again, the inherent non-stationarity of the signals was overcome through resampling the data to a constant number of samples per engine cycle via the TDC and shaft encoder signals. Techniques such as 'event alignment' were also developed to account for variations in the timing of injection events due to load changes [9, 156, 157].

Statistical techniques such as ICA and PCA were used to investigate the data and it was found that changes in lubricating oil condition could readily be identified [158, 159]. Further work [8] applied a variant of ICA to effectively separate the RMS AE signature into four components, or 'hidden signals'. Three of these signals modelled characteristics of AE generation at three different loads whilst the remaining signal was identified as being representative of friction and wear. These four signals are shown in Figure 3.8a, with source 1 the friction related signal, and data presented from BDC to BDC. The authors noted that features in the friction signal could be related to the engine operation; the amplitude was lower at the beginning and end of the cycle which

was thought possibly due to improved lubricating conditions at around BDC as the cylinder may have received oil indirectly via the common air intake. Figure 3.8b shows the level of each hidden signals presence in the RMS AE signal as the test progressed. Changes in the three load-related signals complied with the load changes. The friction-related signal emerged just after the lubricating oil supply was shut down and increased throughout the experiment until the supply was restored. This resembles what would be expected which would appear to verify to a degree the existence of a friction contribution to the overall AE signal.

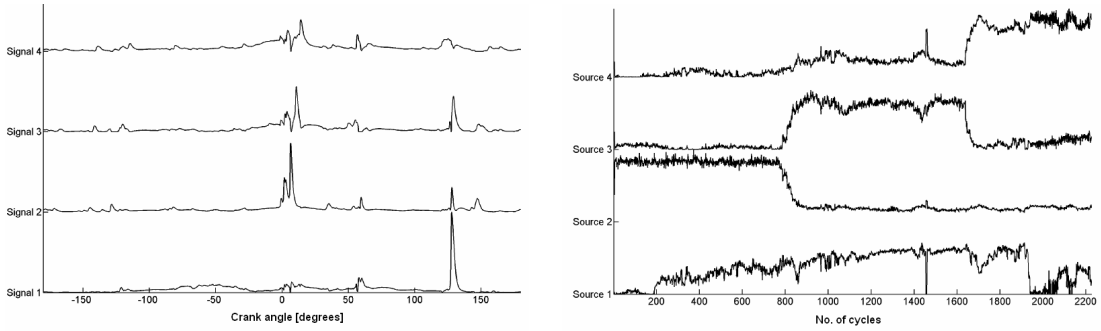

(a) *(b)*

Figure 3.8: (a) Four hidden signals during a cycle, signal 1 attributed to friction, (b) development of four independent components during test, source 1 attributed to friction, from Pontoppidan and Sigurdsson [8].

Sigurdsson *et al* [9] further showed that AE generation was greater during operation with no lubricant supply than for normal conditions. In this case a simple feature was extracted, the total AE energy generated during an engine cycle, and this was found sufficient to discriminate between lubrication conditions at constant load. Figure 3.9a depicts this feature clearly for two engine speeds. However, AE energy was observed to also increase with load, therefore values for fault and no-fault conditions coincide over varying loads, implying that a single overall threshold cannot be used for fault detection. The authors suggested models, founded on supervised and unsupervised learning and with engine load as an input, which could counter this problem by providing non-linear threshold functions, as shown in Figure 3.9b.

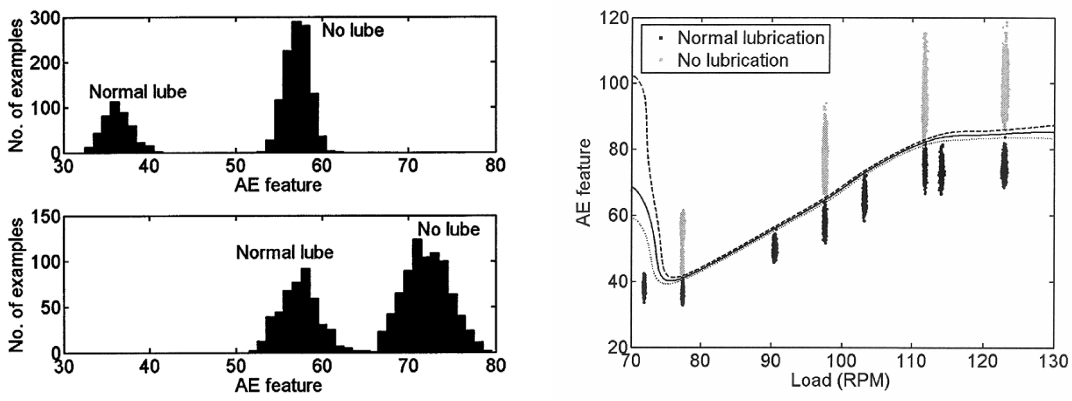

(a) *(b)*

Figure 3.9: (a) Histogram of cyclic AE energy for normal and no lubricant supply conditions, upper and lower panels at 25% and 50 % load respectively, (b) Scatter plot of AE energy versus load with several fault/no fault decision boundaries indicated, from Sigurdsson et al [9].

Carlton [160] alluded to the commercial use of an AE monitoring system to address the problem of cylinder liner scuffing. Although no further information was revealed, and no results or case studies were presented, it can be assumed from the context that this was in relation to large marine engines. This is precisely the problem which the work in this thesis attempts to go someway towards resolving.

3.4 AE monitoring of sliding contact

As has already been stated one of the major objectives of this work is to investigate AE generated from the sliding interface of piston ring-pack and cylinder liner. To provide foundation to this premise it is necessary to review the body of work which has considered AE monitoring of sliding, or interacting, surfaces.

The study of sliding contact encapsulates the topics of lubrication, friction and wear. When two contacting surfaces move relative to each other then a resistance to motion occurs. This resistance, or friction, is due to a combination of various mechanisms such as asperity deformation, adhesion and ploughing by hard asperities or entrapped wear particles, and results in surface and sub-surface deformations, dislocations and fractures which dissipate strain energy in a variety of thermal, kinetic and elastic forms. Monitoring of these effects therefore presents the opportunity to gain insight into the tribological behaviour since they are intrinsically related to the friction mechanisms.

One component of the elastic energy released is in the form of radiated stress waves, including AE.

This possibility of using AE to infer tribological behaviour has been investigated and developed in a numerous published works covering various applications. Precursor to more detailed studies was the initial understanding that AE arises from frictional processes that occur during manufacturing operations such as turning, grinding and forming [161-167]. Fundamental friction and wear characteristics have been investigated on standard wear testing laboratory equipment [168-181]. These have identified systematic relationships between AE activity and the various parameters which govern friction and wear. Further investigations have focused on applying AE monitoring towards a range of industrial situations where interfacial conditions are problematic. This has included a significant body of work on the monitoring of hard disk drive magnetic storage devices [182-201] and also industrial applications such as gearboxes, mechanical seals and bearings [202-215].

3.4.1 Initial identification of AE generation from friction and wear source mechanisms

AE monitoring was initially identified as a technique that could prove useful for investigation of friction and wear phenomena through studies of material cutting and forming processes conducted to investigate whether tool or cutting process condition could be ascertained. The concept behind this is that in order to remove or form material a considerable amount of power is expended in the form of plastic deformation. This is inevitably accompanied by friction acting at the interface of tool and workpiece, and chip in the case of machining processes, the consequence of which is gradual wear of the tool surface that is detrimental to the quality of the workpiece surface finish.

AE generated during turning of aluminium alloy was investigated by Grabec and Leskovar [161]. The spectral content of the signal was examined with audible frequency emissions observed to be discrete whilst emissions in the ultrasonic range, including AE, were continuous. The influences of various cutting parameters were evaluated and although the continuous signal was related to the friction at the tool/workpiece interface no correlation could be identified between tool wear and AE

activity, though the possibility was not dismissed. Tool condition monitoring via AE measurements was also considered by Iwata and Moriwaki [162]. They again focused on the spectral content and reported that features up to 350 kHz were related to the tool wear condition, it was also suggested that AE count parameters may be indicative of tool condition.

Numerous further studies followed these initial works and these have firmly established the effectiveness of AE monitoring of tool condition for manufacturing processes including turning [163, 164], milling [165], grinding [166] and forming [167]. In all of these examples characteristics of AE generation have been related to friction and wear. A number of researchers have associated burst-type AE events to occurrences such as tool fracture and chip break-off whilst continuous AE emissions have been linked to continual shearing and friction. This material is not reviewed in detail here but is used to highlight the role that this research has had in establishing the use of AE monitoring towards understanding interfacial behaviour.

It is appreciated that the material deformation energies associated with manufacturing processes may be considerably greater than for normal wear processes. Nonetheless, it has also been recognised that small energy level deformations generate AE, for instance, Dornfeld *et al* [216] proposed the use of AE to detect the onset of slip between surfaces. Their work consisted of blocks of varying materials and surface roughness pulled in a stick-slip motion against a reference aluminium base block, with pulling speed and normal load varied. For all materials bar a luctite plastic a burst-type AE signal was observed upon the onset of motion, i.e. the transition from static to kinetic friction, with the basis for AE generation identified as deformation of surface asperities in contact. For the plastic material it was thought that there was no AE generation due to a combination of low surface roughness and characteristically poor AE generation capabilities. For steel blocks the AE amplitude was observed to increase with speed whilst an increase in normal load was found to result in increased AE activity for rough surfaces and reduced activity for smoother surfaces. A further application was given of a robotic gripper where burst-type AE signals were observed upon contact of gripper arm with the object and again upon the slipping release.

3.4.2 AE monitoring of sliding contact in laboratory wear tests

To investigate the relationship between AE generation and the friction and wear of sliding contact systems a number of studies have been performed using laboratory test-rigs on which simple testpieces are loaded against each other in relative motion. These test-rigs can take several forms such as a stationary ball on rotating cylinder or reciprocating pin on stationary disc, and typically the speed of relative motion and the applied load can be altered so as to provide a range of wear characteristics. Such tests are routinely used in tribological studies and represent an ideal base for investigation of AE activity from friction and wear. Furthermore, these test-rigs allow other friction and wear parameters to be readily obtained, for instance, measurements of friction force or wear scars, and these can aid interpretation of AE activity and correlation to tribological behaviour.

One of the first investigations of this kind was conducted by Belyi *et al* [168] who examined friction and wear behaviour of polymers sliding against steel using AE and observed that AE parameters could be used to distinguish between different wear mechanisms. Surface roughness of specimens were increased which caused a transition from adhesive and fatigue wear regimes to abrasive wear, and this was found to be accompanied by an increase in AE count rate. This was explained by a greater number of AE generation sites as wear debris surface area increased. A linear relationship between cumulative AE count and wear volume was also presented.

McBride *et al* [169] initiated a body of work which investigated AE generation during rotation of a steel cylinder loaded against a stationary steel ball with both lubricated and unlubricated contact considered. Time-series AE parameters were extracted from the subsequent AE events, namely the peak amplitude and the rise time per given AE signal rise. Clear differences were observed between the two conditions with the lubricated test, Figure 3.10a, exhibiting lower but more consistent peak AE values and no particular rise-time characteristic, whilst unlubricated contact, Figure 3.10b, showed greater peak AE values although with increased spread and a distinctively sharp event rise-time characteristic.

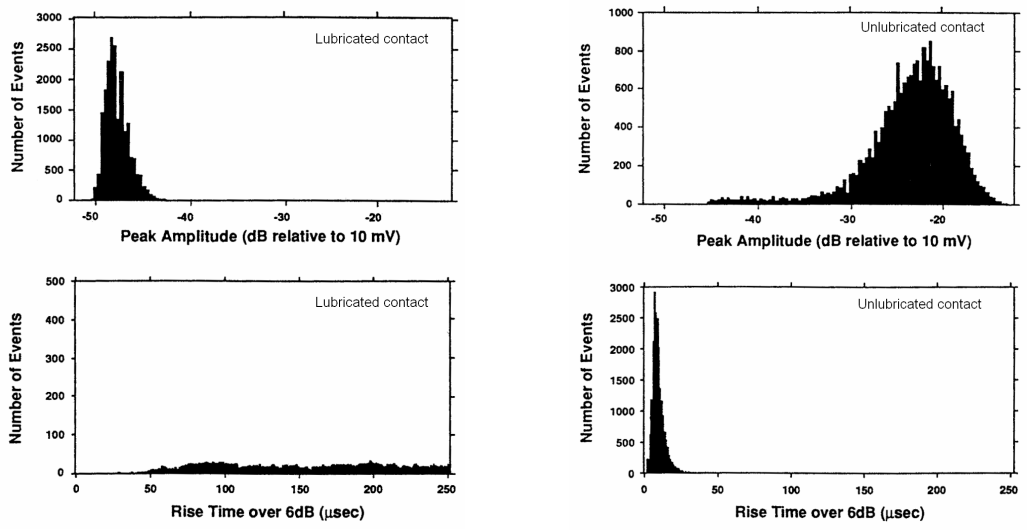

(a) *(b)*

Figure 3.10: AE generation characteristics using a ball and cylinder test-rig for (a) lubricated contact, (b) unlubricated contact, from McBride et al [169].

These observations were correlated to the wear inflicted upon the ball and cylinder surfaces. The unlubricated contact produced a distinct wear scar with evidence of material transfer and wear debris, which led the authors to conclude that the unlubricated AE characteristics were indicative of micro-fracture and material removal. The lubricated case, however, showed smooth wear scars with significant plastic flow, whilst theoretical analysis of the contact zone indicated that mixed lubrication conditions would exist. The authors therefore attributed the AE generation characteristics in this case to asperity contact.

Work in this area was furthered by Boness *et al* [170] who, using a similar set-up, concurred that AE generation was greater from unlubricated contact than lubricated. They also demonstrated the ability to distinguish between different wear mechanisms. Common features in the time-history for lubricated and unlubricated conditions emerged after the data were presented in log-log format as shown in Figure 3.11a. An initial peak observed for both cases was attributed to the initial removal and gross deformation of original asperities. This was followed by a second peak of gradually increasing amplitude. Scanning Electron Microscope (SEM) examination of the surfaces at this point revealed transference of debris from the rough cylinder to smooth ball hence this secondary phase was attributed to adhesive wear. The erratic behaviour exhibited by the unlubricated case after 200 seconds was attributed to predominantly abrasive wear. It was further proposed that for each mechanism; initial contact,

adhesion and abrasion, a linear relationship between wear scar volume and integrated RMS AE signal could be established. This is exemplified in Figure 3.11b for lubricated contact with two grades of paraffin for the initial contact and adhesive wear periods.

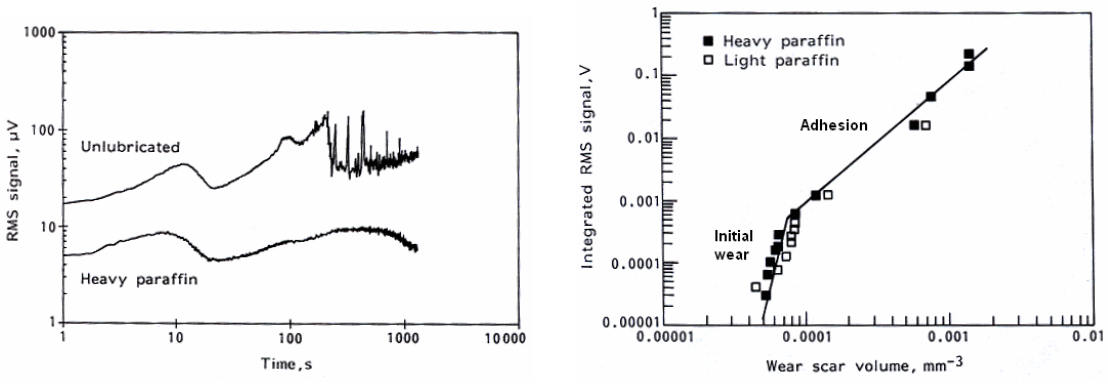

(a) *(b)*

Figure 3.11: (a) RMS AE time history for two different lubrication conditions, (b) linear relationships between integrated RMS AE signal and wear scar volume for different wear regimes, from Boness et al [170].

This relationship was further investigated for lubricated contact by Boness and McBride [171] who reported differing behaviour between a reference lubricated sample and one containing a wear-reducing additive, the latter exhibited less AE generation and a reduced wear volume. Furthermore, they could also distinguish between different concentrations of added aluminium particles. AE activity was observed to increase with particle concentration, and this concurred with increased wear as quantified through examinations of wear scars.

Other authors [172-174] have verified the capability of using AE measurements to detect changes in wear regimes during unlubricated sliding. Jiaa and Dornfeld [172] studied long-distance unlubricated sliding using a pin-on-disk set-up. Through analysis of time-series RMS AE, and substantiation by SEM examinations, they identified distinguishing features for three different wear regimes; running-in, steady-state and self-acceleration. Tests to investigate break-in behaviour after the removal of wear particles indicated a close relationship between AE activity and energy lost through frictional work. Additionally, the response of AE generation to varying sliding speeds and loads was evaluated. The mean RMS AE level during the steady-state wear region was found to be proportional to both, as shown in Figure 3.12 for data scaled to the same range from two different AE measurement set-ups and material pairs. The authors stated that their results were in agreement with a power function relation

between RMS AE and the rate of frictional energy dissipation given by Diei [175].

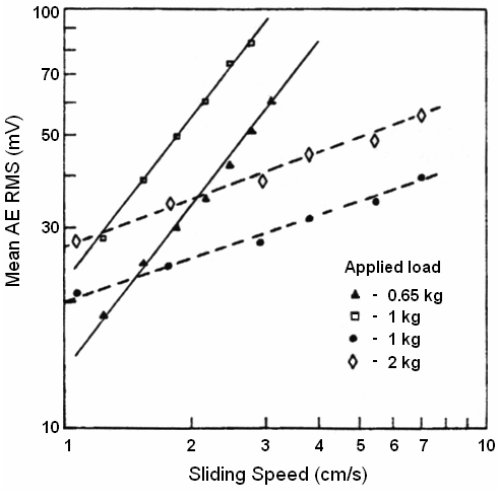

Figure 3.12: Effect of sliding speed and load on RMS AE level for two different set-ups [172].

Similarly, Hamchi and Klamecki [173, 174] investigated the use of AE monitoring to discriminate between different wear mechanisms acting at an unlubricated pin-on-disc interface. Various loads and speeds were considered as well as several pin materials. For most materials the AE count rate and energy content were found to parallel the variation of wear rates across the mild-severe wear transition. It was also found that the different methods of energy dissipation associated with adhesion and micro-cutting (abrasion) wear regimes produced different peak AE amplitude distributions. However, it was noted that the results were dependant upon the material properties, with inconclusive results from tests with a copper pin.

Lingard and Ng [176] investigated AE generation during unlubricated sliding of a rotating disk loaded against a stationary disk. Again, a range of disk materials, loads and speeds were investigated with torque friction measurements and wear scar dimensions recorded to aid interpretation of the AE data. Significant AE activity was observed with AE event count rate and cumulative event count extracted as parameters. No discernible relationships emerged when these were evaluated against measures of wear such as wear rate and volume, although the possibility was not discounted. Instead, relationships were identified between frictional work and cumulative AE event count for all the material pairs examined. Relationships over varying speed and load are shown in Figures 3.13a and 3.13b respectively whilst a further factor was found to be the material pairs used. The form of these relationships were noted as being similar to the power law relationship between the amount of AE generated and the rate of frictional work given by Diei [175] and referenced by Jiaa and Dornfeld [172]. The authors also provided an explanation as to why AE generation would be related to frictional forces rather than parameters of wear. They reasoned that Archard's theory of adhesive wear indicates that only a small proportion of asperity interactions produce a wear particle, whereas all such events contribute to the frictional force.

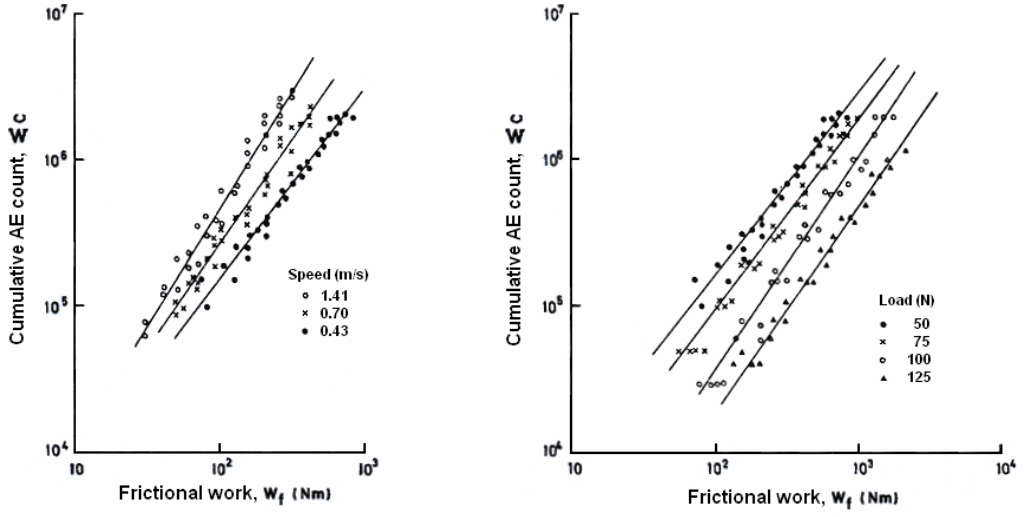

(a) *(b)*

Figure 3.13: Unlubricated ball and cylinder test rig, cumulative AE versus frictional work, (a) effect of speed (b) effect of loading, from Lingard and Ng [176].

Further work by Lingard *et al* [177] led the authors to state that AE output appears to be more sensitive to contact conditions than measurements of either friction force or of the wear rate. Frequency domain analysis showed that certain peak frequencies were associated with different material pairs.

Recent work by Mechefske and Sun [178] considered AE generation from lubricated sliding contact using a ball-on-disk test-rig and a non-contact laser vibrometer. The lubricant contained an anti-wear additive, zinc dialkyldithiophosphate, which was noted as increasing in effectiveness with greater sliding speeds. Similar to other works, their results showed that the peak AE and RMS values increased in accordance with sliding speed and wear surface strain rate. They also reported that AE count rate, in terms of sliding distance, reduced when sliding speed was increased and they related this to the effectiveness of the lubricant and hence wear rates.

AE generation during elastohydrodynamic lubrication has been investigated [170, 177]. Boness *et al* [170] produced these conditions by using a polished surface on a ball-on-cylinder test-rig and noted that for these conditions the RMS AE level was no greater than the base noise level of the equipment. This further confirmed the authors' view that asperity contact was the primary AE source in their work. Lingard *et al* [177] also reported that AE activity was a sensitive indicator of lubrication condition. They observed that when lubricant was introduced to a disc-on-disc interface the AE activity reduced significantly, a reflection of the much reduced wear rates. Moreover,

they found that as conditions were altered so to increase the elastohydrodynamic effect, quantified by the film parameter Λ in Figure 3.14, the AE count rate systematically reduced.

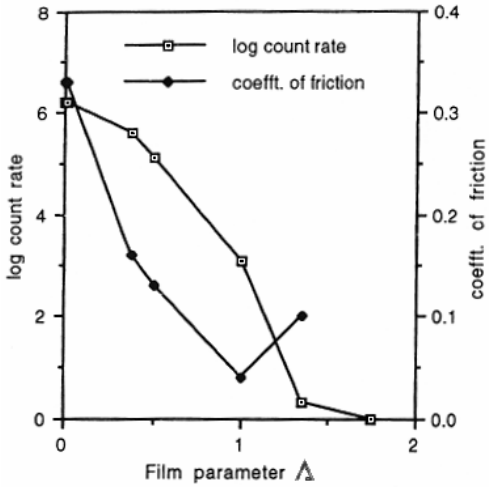

Figure 3.14: Log AE count rate and coefficient of friction versus film parameter, from Lingard et al [177].

Several research groups have indicated that scuffing, severe adhesive wear, can be identified through AE monitoring. Boness [179] investigated normal operation and scuffing inducing conditions using a ball-on-cylinder test rig, with jet fuel and clay-treated jet fuels as lubricants and tests at various loads in both air and nitrogen environments. For both environments an initial peak in the AE activity was observed which was believed to indicate interaction of major asperities during initial wear. For the air environment, under non-scuffing inducing conditions, both AE levels and wear scar diameter gradually increased till the end of the test. Under the same conditions the nitrogen environment case showed no further increase in wear scar or AE level thus indicating that a further oxidative wear mechanism was present for the air environment case.

Regarding scuffing, this could be induced at a critical load in the nitrogen environment, and could be identified through wear scar examination. At this critical load the clay-treated fuel samples exhibited greater AE levels than untreated fuel, as shown in Figure 3.15. Further examination of the wear scars showed that at this critical load the initial adhesive damage in some cases led to progressive deterioration and subsequent failure, i.e. scuffing, which was accompanied by constant high AE levels, labelled as 'scuffed' in Figure 3.15. For others, the surface recovered with both wear and AE levels reduced for the remainder of the test, labelled as 'incipient scuff' in Figure 3.15.

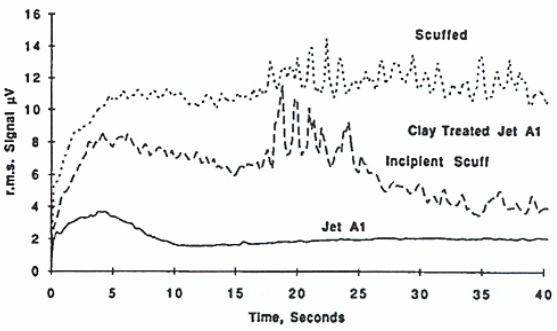

Figure 3.15: Induced scuffing at a critical loading, from Boness [179].

Detection of scuffing through AE monitoring was also an objective of a study by Price *et al* [180] who investigated severe sliding wear in a four-ball lubricant test machine. In this work tests were conducted at incrementally increasing loads. At high loads the lubricant film would fail, causing metal-to-metal contact and localised seizure. Due to wear the contact area would increase, hence contact pressure would decrease. Eventually the pressure would fall to the point where lubricant can re-enter the contact, the system can then recover and scuffing stops. This process was described by the acquired friction force which exhibited a sudden increase upon seizure followed by a drop to a value slightly greater than that experienced before seizure. The corresponding RMS AE level showed the same characteristics as the friction trace which led the authors to state that scuffing conditions can easily be detected through AE measurements. Further, they state that the high signal-to-noise ratio and the large difference between fault and no fault conditions make this suitable for use of simple alarm level monitoring systems.

Shuster *et al* [181] described the use of AE measurements to detect scuffing at the piston ring and cylinder liner interface, albeit with segments of each component loaded against each other in a sophisticated reciprocating rig. Load, temperature and oil flow rate to the interface could be altered to increase the contact severity, and RMS AE and friction coefficient measurements were acquired. Over a range of tests it was found that three regions in the wear history could be identified; running-in, steady-state and self-acceleration. Running-in showed RMS AE increasing gradually. Steady-state showed a constant base level AE with some additional AE spikes that were attributed to surface friction contacts, these were not identifiable from friction coefficient measurements. The self-acceleration period showed multiple AE spikes, of approximately 5-8 times the original level increasing up to 10 times, and this was accompanied by an increase in friction coefficient. It was proposed that there were enough distinguishing features in the AE generation to characterise three different levels of scuffing; origin, irreversible and severe. The authors stated that AE analysis provided more information about scuffing phenomena than measurements of friction coefficient and proceeded to use their findings to evaluate scuffing resistance of different piston ring coatings.

An interesting observation regarding the stability of AE monitoring was made by both Boness *et al* [170] and Lingard *et al* [177]. Using different test-rig and material

arrangements both research groups showed that if a test was interrupted and then restarted, the AE RMS activity resumed at its previous level. This bodes well for the robustness and repeatability of AE monitoring.

3.4.3 AE monitoring of sliding contact in industrial applications

Further developments in AE monitoring of sliding contact can be found from research into interfacial behaviour in commercial applications. A sustained research theme, and one which serves to illustrate a mature application of AE monitoring towards a significant tribological problem, has been the monitoring of Hard Disk Drives (HDD). A further topic which is gaining in interest is the use of AE for condition monitoring of mechanical components such as gears, seals and rotodynamic machinery. Many observations from these works are complementary to, and in some cases an extension of, the findings obtained from the laboratory wear tests. Furthermore, they are testament to the application of AE monitoring towards real problems

3.4.3.1 AE monitoring of sliding contact in magnetic storage devices

One commercial application where friction and wear occurring at a sliding interface is a significant problem and one which has been investigated extensively using AE monitoring is the ultra-sensitive head-slider/disk interface in HDD magnetic storage devices. In this case AE monitoring has proven to be a valuable tool for developmental work, this association is emphasised by the fact that the first research work into AE monitoring of this interface was documented in 1980 [182] whilst the use of HDD in PC's appeared in 1982.

In these data storage devices a disk is rotated underneath a head-slider mechanism with the data stored on a magnetic layer of the disk and protected from damage by carbon material and a further layer of very thin lubricant. During operation the head-slider is hydrodynamically lifted, termed 'flying', to relieve the contact forces acting upon the disk surface. At start-up however, the head-slider slides on the spinning disk in a designated 'landing zone' until sufficient speed is achieved for lift to occur, with a similar process occurring in reverse for shut-down. Inevitably wear occurs during these stop/start actions, and although the landing zone contains no data, wear particles can be

released which contaminate the gap between the head-slider and storage areas of the disk. This can result in accelerated disk surface wear and if the protective layers are breached then irreversible damage can occur possibly resulting in complete failure.

Friction and wear problems have been amplified by the continual evolutionary increase of disk recording densities. This has mainly been due to the reduction of the flying height between the disk and the head-slider, which has allowed weaker magnetic fields and greater storage densities, but has also incurred increasing levels of interaction. Recent developments have been to reduce the flying height further to the point where continuous or intermittent sliding contact is intentionally maintained. For these developments to have taken place tribological issues have had to be investigated and overcome, and a survey of the literature shows that AE monitoring has played a role in this.

The study of AE from head-slider/disk interaction was initiated by Kita *et al* [182] who compared AE activity to interferometry measurements of the slider-head/disk gap and found that the contact intensity during the sliding to flying transition could be inferred from AE measurements. As shown in Figure 3.16a, upon start-up the RMS AE activity increased with sliding velocity, achieved a maximum, and then decreased as hydrodynamic lift was gradually achieved. At full lift no AE activity above the background level was observed, this is similar to observations made for hydrodynamic lubrication conditions in the laboratory wear tests described previously [170, 177].

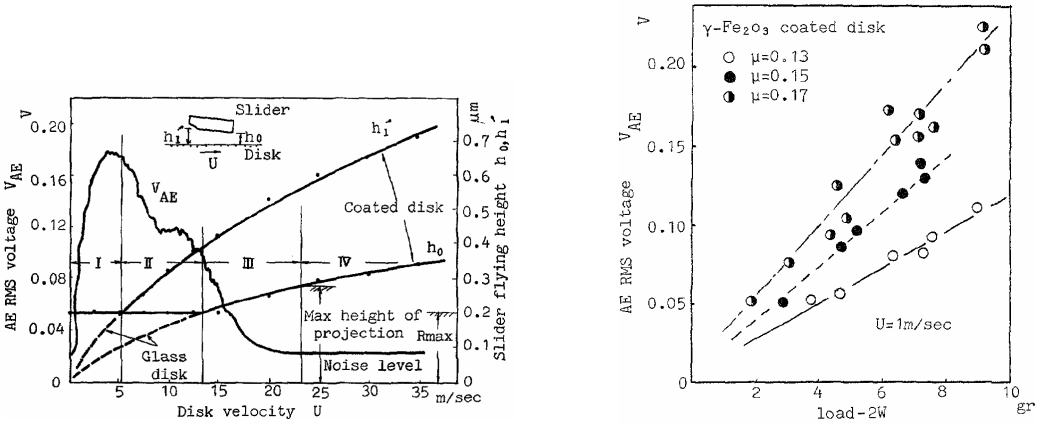

Figure 3.16: (a) Sliding/flying transition, (b) Variation of RMS AE with load at constant sliding speed, from Kita et al [182].

Furthermore, the different contact phases during the take-off process could be characterised from analysis of the acquired raw AE signals. A high level of continuous AE, indicative of continual sliding contact, was evident during the initial sliding phase. Upon initial lifting of the head-slider, as indicated from the interferometry measurements, burst-type AE events were observed and these were attributed to intermittent asperity contacts. During the transitional phase a composite of continuous, although at a lower-amplitude, and burst-type events was observed. As well as time-domain characterisation information relating to the source was also found present in the frequency-domain. Continuous AE from sliding contact was noted to produce a wide spectrum with lower frequencies dominant whilst the burst-type AE events produced a relatively sharp spectrum at higher frequencies. Further tests at a low constant sliding speed so as to maintain continual contact found that in addition to sliding velocity the RMS AE output was proportionally dependant upon the load applied to the head-slider as well as the friction coefficient, as shown in Figure 3.16b. Again, these are similar observations as those made from work on laboratory test-rigs [172].

Similar tests were performed by Khurshudov and Talke [183], they demonstrated that in the absence of hydrodynamic lift the RMS AE level increased proportionally with sliding speed and that when lift was achieved the AE activity reduced, this process is shown in Figure 3.17a. They also identified interfacial loading to be an important parameter in the amount of AE activity generated, Figure 3.17b. Ravikaran and Low [184] further concurred that RMS AE was almost linearly proportional to sliding speed during the initial sliding contact phase.

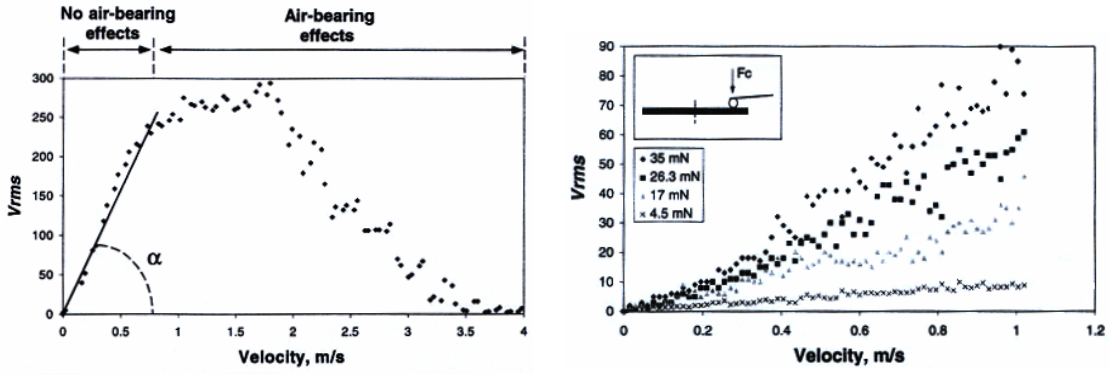

(a) *(b)*

Figure 3.17: (a) Sliding/flying transition, (b) RMS AE versus sliding velocity for varying loads for a ceramic ball/disk interface, from Khurshudov and Talke [183].

The effects of various designs of head-slider have been investigated [183, 185, 186]. Liew *et al* [185] noted that for different designs of head-slider the AE characteristics during both take-off and normal operation were different. The greater level of AE activity displayed by one design was related to its lower flying height, which would incur greater levels of asperity interaction. Similarly, Khurshudov *et al* [183] related differences in AE signatures for 3 designs of tri-pad head-slider to their respective flying heights. An investigation into landing behaviour, Zhu *et al* [186], also concluded that as flying height reduced during deceleration AE activity increased due to increased contact levels. In this study AE measurements were thought of sufficient merit to validate data obtained from a novel optical measurement technique. In this application AE monitoring has been further applied towards validation, as demonstrated by Benson *et al* [187] who used it to qualitatively verify a simulation of head-slider/disk contact.

Ravikiran *et al* [188] raised some interesting points from an investigation into AE activity during take-off using lubricated and unlubricated disks and varying disk accelerations. In all cases AE increased with speed until lift was achieved, and lubricated contact, Figure 3.18a, generated less AE than unlubricated contact, Figure 3.18b. However, when RMS AE at a given velocity was assessed against acceleration it was found that for unlubricated contact RMS AE increased with acceleration whilst for lubricated contact it decreased.

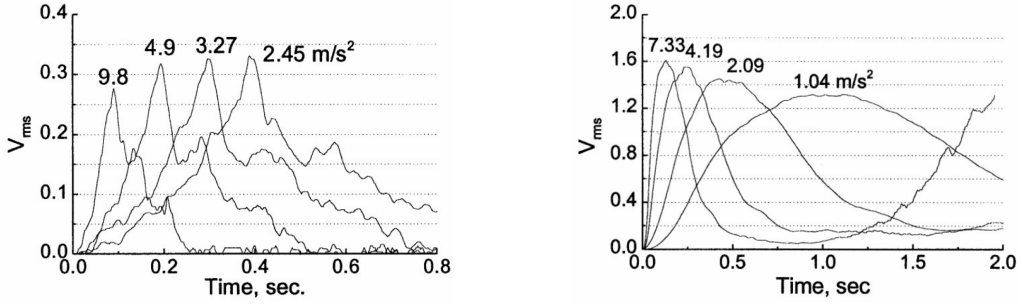

(a) *(b)*

Figure 3.18: Effects of acceleration, (a) slider 1 against lubricated laser textured disk, (b) slider 2 against unlubricated mechanically textured disk, from Ravikiran et al [188].

For the unlubricated case the increased AE activity with acceleration was attributed to a greater number of asperity contacts per unit time at a given speed, assuming parity for other variables such as load and surface roughness. For the lubricated disk the authors suggest that the presence of lubricant reduces asperity interactions and dampens the AE

signal, and that with increasing acceleration greater amounts of lubricant accumulates at the interface causing increased damping and therefore lower AE levels. The authors indicate that to explain further results regarding peak AE levels the effect of this damping may be more dominant that the increase of AE with speed.

In a follow-up study Ravikiran and Low [184] gauged the effect of lubricant thickness, from 0 to 40 Å, on AE activity during the take-off process with all other variables constant. AE activity was found to decrease with increasing lubricant thickness and again this was thought due to increased AE damping caused by lubricant accumulation at the head-slider/disk interface. What is not clear in these studies however, is whether the authors mean that the asperity contact is dampened, i.e. the severity is reduced, or that the resulting AE signal is dampened, i.e. attenuated, by propagation through the lubricant build-up.

Evidence of the effect of lubricant properties on interfacial friction and wear was given by Liu *et al* [189]. Visual observations of disk wear were compared to AE activity for three disks with different lubricant layers operating in a humid environment. At the end of testing one disk was found to have experienced increased lubricant and carbon layer deterioration and this was accompanied by increased amounts of AE activity. This led the authors to conclude that AE is a suitable tool for the detection of degradation events.

A further factor affecting interfacial conditions is the component surface topography. Tanaka *et al* [190] showed that textured and smooth disks generated different AE characteristics at various flying and continuous contact heights. For the greater flying heights the textured disk generated more AE activity but as flying height decreased a steep rise in AE activity from the smooth disk was observed. For both disks, predictions of flying height and friction measurements of the order of mN, supported the conclusion that AE activity is correlated to the contact dynamics and the incurred friction. Further evidence of disk surface roughness influencing AE activity was provided by both Sharma *et al* [191] and Benson *et al* [192].

Particle contamination was studied by Xu *et al* [193] who noted that the introduction of soft particles generated large amounts of AE activity for a head-slider with a relatively large leading edge step (up to 2.4 μm); this was related to damage incurred as particles passed through the interface. A head-slider with a smaller leading edge generated less

AE and this was thought due to the inability of particles to become entrained in the interface due to their relative size.

Other studies have been more concerned with investigating AE propagation characteristics and quantifying the effect of interfacial parameters. For instance, possible sensor positions have been surveyed. In the majority of these studies the AE sensor is located on the sliding arm or on the pivot pedestal. However, Briggs *et al* [194] and Matsuoka *et al* [195] have both shown the merit of expanding the array by instrumenting the disk itself, the latter reporting that head-slider and disk wear can then be evaluated separately.

There would appear to be differences in opinion of which frequency band of the AE spectrum is of most interest, although this may be due to the specifics of the AE transducers or piezoelectric elements used in the individual works, the details of which are rarely given. Kita *et al* [182], in the initial work, investigated a band-pass filtered region between 100 to 500 kHz. Benson *et al* [187] concurred, noting that frequencies in the AE spectrum can be observed up to 500 kHz.

On the other hand Khurshudov *et al* [183] were interested only in AE emissions within the band 600 kHz to 1 MHz as they believed air bearing resonances could be influential at lower frequencies. McMillan *et al* [196] used a high-pass filter above 500 kHz on the raw AE signal and found that well-defined frequencies emerged in the emission spectrum at various disk speeds. These correlated to the first torsional and bending mode frequencies, 730 and 960 kHz respectively, of the head-sliders as determined through finite element analysis. This led the authors to believe that these modes were excited by asperity contacts and furthermore they went on to relate their presence to contacts at different locations on the head-slider. Similar work was reported by O'Brien and Harris [197]. They identified the need to target AE head-slider resonance frequencies by again correlating peaks in the AE spectrum to modelled resonances. Emissions were then compared with and without 500 kHz high-pass filtering and with and without head-slider/disk interaction using a sensor with a resonant frequency of around 250 kHz. They found that when the full spectrum was acquired and with possible contact removed there were significant emissions in the band 200 to 300 kHz. In the absence of any possible contact this AE was attributed to air resistance at the interface with sensor resonance characteristics thought to be heavily influential. The

authors stated that their observations highlighted the inaccuracies possible in using unfiltered or broad-band AE signals for contact detection.

Attempts have been made to quantify the AE activity in terms of contact forces or as an evaluation of wear. Ganapathi *et al* [198] and Khurshodov *et al* [183] both related RMS AE level to contact force through a relationship whereby force could be determined if sliding velocity was known, the former proposing that RMS AE was proportional to the second power of velocity and the latter just velocity. Matsuoka et *al* [195] described a correlation of material removal power at the sliding interface, again using sliding velocity and contact force, to the resulting AE activity. This work built upon previous research quantifying AE activity to sliding contact and wear rates in VCR cassettes [199, 200].

The problem with quantifying the AE activity is that the relationships are specific to particular components and a particular set-up. Therefore, when they are considered for transference over applications the relationships can only be qualitative in nature. Some have proposed overcoming this problem by applying calibration methods. For example, Bhushan *et al* [201] used the dropping of a ball on the disk surface to calibrate AE output to the known input energy and then used this finding to evaluate mechanical frictional losses during disk operation.

3.4.3.2 AE monitoring of sliding contact in mechanical components

The intention of this section is to detail further examples where AE monitoring has been applied towards determining interfacial behaviour in industrial situations.

The monitoring and condition assessment of meshing gears is an important task. Operation of gears in a worn state can result in a loss of performance and premature failure. For some applications, such as helicopter drive gears, knowledge of component condition is of the utmost importance due to critical safety implications. Gear meshing involves a combination of sliding and rolling contact, and common failure modes encountered include micro-pitting, pitting, scuffing and abrasive wear. Other more clinical failure modes include tooth fracture and bending fatigue.

AE monitoring has been considered as a tool through which the contact occurring during gear meshing can be investigated. For instance, Tountzakis and Mba [202] reported that RMS AE level increased with rotational speed. They observed that in addition to a general steady-state increase there was also a further instantaneous increase in activity upon each increase of rotational speed as shown in Figure 3.19a. This extra activity was attributed to the accommodation of changes in the gear contact dynamics. Further results were presented concerning the wear condition of the gears where AE activity was observed to increase in line with increasing amounts of surface pitting and scuffing.

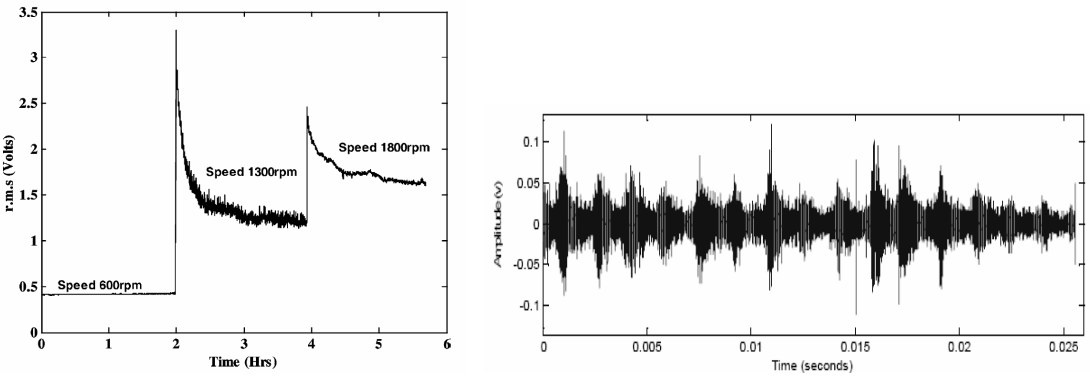

(a) *(b)*

Figure 3.19: (a) RMS AE as a function of gear rotating speed, from Toutountzakis and Mba [202], (b) AE from each gear tooth mesh, from Tan and Mba [204].

Others have also found variations in AE activity when operational parameters have been changed. However, whilst these provide useful knowledge it is of equal, if not greater, importance to investigate the fundamental AE source mechanisms. This was the objective of studies by Tan and Mba [203, 204] who noted from raw AE measurements that transient AE events were generated from each individual gear tooth mesh, the amplitude of which varied during the process of each mesh. This is demonstrated in Figure 3.19b which shows 16 events arising of varying characteristics from 16 separate gear teeth meshes. Source mechanism possibilities were considered and through experimental observations and a process of elimination they determined that these events were due to the changing nature of asperity contact during the meshing process. Theoretical analysis of film thicknesses also indicated that mixed lubrication conditions would exist, further supporting asperity contact as the primary AE source.

Instead of monitoring the contact dynamics themselves a number of researchers have focused on detecting the consequences, i.e. wear defects such as pitting, and have

reported some degree of success. This has been demonstrated for both naturally occurring faults [126, 205], and induced or 'seeded' defects [126-128]. However, not all studies have proved successful; Toutounzakis *et al* [206] could not identify induced defects from the RMS AE signal and stated that attempts to do so were fraught with difficulty. Several of the these works [126-128] compared AE monitoring to more established vibration monitoring, finding in favour of AE for earlier detection of faults.

Other cases of using AE to assess contact behaviour include the monitoring of mechanical face seals [207, 208], shaft seal tips in turbines [209-212] and rolling element bearings [121, 213-215].

During normal conditions mechanical face seals operate in boundary lubrication whilst abnormal excessive leakage results in part-hydrodynamic conditions. Miettinen and Siekkinen [207] tested both cases and with leakage induced they observed 25% lower RMS AE levels than the benchmark normal condition. This was thought to be indicative of the contact characteristics as with leakage, and hydrodynamic lubrication, the contact severity is reduced. A further test showed that when the seal was slowly drained of fluid the face temperature and the RMS AE level rose significantly. In this case the increased activity was attributed in the main to fluid cavitation and vaporisation. Ferguson *et al* [208] further verified the sensitivity of AE to variations in seal interface conditions. An increase in seal face contact force, controlled via the fluid pressure, gave an increase in the mean amplitude of the RMS AE signal. Variation of fluid temperature was also found to impact upon AE activity, again thought to be due to fluid cavitation and vaporisation.

A further example is the monitoring of shaft-seal frictional rubbing in turbines. This detrimental contact has been detected using AE measurements on both laboratory-scale units [209] and large 300+ MW industrial utility turbines [210-212]. It is encouraging to note that this friction contact has been detected in the presence of other strong sources such as bearings, steam flow and blade turbulence.

The well documented case of bearing monitoring provides yet further evidence of the use of AE to monitor interfacial behaviour, although in this case the contact is predominantly rolling motion and not sliding. Choudhury and Tandon [121] provide a review of this topic, and they also evaluate vibration and acoustic monitoring as a

means for defect detection, again finding in favour of AE monitoring for earlier detection. Two primary AE source mechanisms have been identified, subsurface cracking due to Hertzian contact stresses, and impacts as either loaded rolling elements traverse spalls in the races or from defects in the rolling elements. Grease lubrication of rolling element bearings was thoroughly investigated by Miettinen and co-workers [213-215]. Variations in running behaviour; bearing speed, load, grease temperature [213], particle contamination [214] and grease composition [215] were studied and in each case variation in AE generation was observed and related to the interfacial behaviour. In each instance the response of the AE generation to variations in running conditions was similar to that observed from experimentation on wear test-rigs and HDDs as described previously in this Chapter.

3.5 Summary

This section has reviewed AE generation and how it can be measured and analysed to provide information useful for condition monitoring. The measured AE signal is generally dependant upon three main factors; the source generation characteristics, the transmission path from the source to the sensor, and the sensor response characteristics. A variety of processing techniques can then be applied to the measured signal, from the extraction of simple waveform and statistical parameters to complex algorithms.

The use of AE as an engine condition monitoring measurand has been found to offer greater diagnostic capabilities than comparable techniques, due to higher level temporal and spatial resolutions, increased sensitivity and improved signal to noise ratios. It has been established that the mechanical and fluid-mechanical events and processes occurring within engines, e.g. valve contacts, fuel injection, combustion and exhaust, are AE generating sources from which diagnostic information can be garnered. Findings which suggest AE monitoring can be applied towards determining the lubricating condition of the ring-pack/liner interface are particularly relevant to the work in this thesis.

The majority of investigations into engine AE generation have used similar analytical procedures, at least for the initial processing steps. Raw or RMS AE data has typically been converted from the time-domain to an angular base to overcome sign non-

stationarity. In many cases RMS AE has been found adequate; however, to best exploit the extreme temporal resolution available then raw measurements are necessary. The signals are then usually interpreted through mapping of AE events to the mechanical and fluid-mechanical actions occurring within the engine. Both simplistic and advanced signal processing techniques have been used to characterise signals, many researchers have found simple statistical parameters to be sufficient, calculated either from the whole engine cycle or from windowed areas, although improvements have been reported using advanced statistical techniques.

AE monitoring has also proved to be effective for gaining insight into the tribological behaviour of sliding contacts, particularly for evaluation of contact dynamics and frictional behaviour during boundary lubricating conditions. This has been ascertained over several different applications where factors governing contact have been varied and the corresponding effects on AE activity related, including; sliding speed, load, time, surface topography and lubricant characteristics. Various qualitative relationships have been proposed and in some cases these have been found transferable across applications. Tests where hydrodynamic conditions were induced showed little or no AE activity above background noise levels. A variety of primarily time-domain AE parameters have been used to characterise the AE activity, although frequency-domain analysis has also been shown useful. The potential benefit of this work in terms of condition monitoring is that it demonstrates that it may be possible to obtain an on-line measure of friction or wear without the need for direct, intrusive measurements.

In summing up, a review of published work indicates that there are solid foundations for an investigation into AE monitoring of the piston ring-pack and cylinder liner interface in running engines.

Chapter 4

Experimental apparatus, procedures and signal processing

4.1 Introduction

This Chapter describes the test engines, apparatus and procedures used for the experimental work conducted during this research. This has involved testing of different types of engine in various environments including a University laboratory, an industrial research facility and a power station. The features and specifications of these engines and of the apparatus for acquiring AE measurements are first presented. This is followed by a detailed description of the individual tests conducted on each engine. The latter part of this Chapter sets out the processing steps applied to the acquired signals in order to make them suitable for comparative analysis.

The tests performed on each engine are described in brief in the following preface, for some engines these tests were carried out over a period of several years and, unless stated otherwise, they were conducted solely by the author.

Investigation of AE activity generated from the ring-pack/liner interface in a motored, four-stroke, diesel engine

This test specifically investigated the possibility of AE arising from operation of the ring-pack/liner interface. Measures were taken to eliminate other sources of AE thereby simplifying the AE signal and focussing the analysis on any activity generated from the ring-pack/liner interface.

Investigation of AE activity generated from the ring/liner interface in a motored, two-stroke, petrol engine

A limited amount of testing was performed on a small, motored engine in order to further investigate AE possibly generated from the ring/liner interface.

Investigation of AE activity generated from the ring-pack/liner interface in running, four-stroke, diesel engines

This consisted of tests over the operating range of a four-stroke, diesel engine installed in a University laboratory. These were conducted to establish whether AE activity relating to ring-pack/liner interaction occurred under normal conditions and also to investigate changes in this activity over varying engine speeds and torque outputs. Additional tests investigated AE generation as the engine was started from ambient conditions. A limited amount of data were acquired from a further four-stroke, diesel engine (test facilitated by Cummins Recon, Cumbernauld).

Survey of AE generation within a two-stroke, crosshead, diesel engine

This consisted of two series of tests aimed at assessing on a detailed level the spatial and temporal characteristics of AE generated during operation of large, two-stroke, crosshead diesels. The engines tested formed the basis of a power station, and unfortunately this limited the experimentation which could be conducted as no control over engine operation was available. However, a number of features could still be examined such as AE propagation and source location, the mapping of AE signals to mechanical and fluid events, and cyclic and cylinder-to-cylinder variance. These tests were facilitated by Public Power Corporation, Greece, with data from the first set of tests provided by Dr. P. Nivesrangsan, formerly of Heriot-Watt University. The author was jointly responsible for the second set of tests along with further researchers from Heriot-Watt University.

Survey of AE generation and investigation of AE activity arising from the ring-pack/liner interface in a research orientated, two-stroke, crosshead, diesel engine

A number of tests were conducted on a large, two-stroke, diesel engine installed in an industrial research facility operated by MAN B&W Diesel, Denmark. This engine was equipped with a high level of instrumentation and full control was available. This allowed specific tests to be conducted so as to assist all aspects of the AE evaluation process, tests were performed over the engine operating range and with processes removed from the engine cycle. A further series of tests were conducted where the lubricating oil supply to one cylinder was removed in an attempt to deteriorate running conditions and induce scuffing. This consisted of an initial exploratory test, from which data were provided by Dr. T. Fog of MAN B&W Diesel, and a second, more thorough investigation in

which the author was involved collaboratively with MAN B&W Diesel and the Technical University of Denmark.

4.2 Test engine specifications

As already indicated this work entails the instrumentation and testing of different types of reciprocating engines of vastly different sizes. This is emphasised by the engine specifications given in Table. 4.1. Further information regarding each engine is provided in the following Sections.

	Small, four-stroke diesel			Small petrol	Large, two-stroke diesel	
Engine	A	B	C	D	E	F
Operating mode	Motored	Running	Running	Motored	Running	Running
Operating principle	Four-stroke	Four-stroke	Four-stroke	Two-stroke	Two-stroke	Two-stroke
Control system	Mechanical	Mechanical	Mechanical	Mechanical	Mechanical	Electronic
Number of cylinders	4	4	6	1	7	4
Liner type	Dry	Wet	None	None	Composite	Composite
Bore [mm]	98.4	107.9	102	42	600	500
Stroke [mm]	127	120.6	120	36.3	1,650	2,200
Maximum power output [kW]	66	46	97	3	11,500	7,080
Maximum power output per cyl. [kW]	16.5	11.5	16.2	3	1,642	1,770
Maximum operating speed [RPM]	2,000	2,000	2,880	10,000	143	123
Operating speed in this work [RPM]	575	800-2,000	750	1,550	136	57-123

Table 4.1: Engine specifications.

4.2.1 Four-stroke, trunk-piston, diesel engines

Three of this type of engine were tested, with the two principal engines, engines A and B in Table 4.1, installed in a University laboratory. These were fairly typical examples of small, HSDI, four-stroke diesels with both having seen regular use prior to being installed in the test facility. Limited testing was conducted on a further four-stroke engine, engine C, which was a reconditioned engine under test in a manufacturing facility.

For these engines the location of some components such as the starter motor and fuel pump prevented the placement of sensors on some areas of the cylinder block. The remaining block surfaces were surface ground in the case of engine B or spot cleaned with emery paper for engine A in order to prepare clean, flat surfaces for sensor attachment and maximum AE transmission. No surface preparation was afforded to engine C. The cylinder head areas of all these engines were accessible although in some cases the relatively small components limited sensor location possibilities.

4.2.1.1 Engine A

Engine A was a four-cylinder, 3.87 litre, HSDI, Perkins T4.236 diesel engine as used in a number of applications such as agricultural vehicles and generator sets. The cylinders were of the dry-lined variety, i.e. thin liners pressed into bores in the cylinder block, with coolant circulated through passages in the block without coming into contact with the liner. The ring-pack of this engine consisted of three compression rings and an oil-control ring. When running normally this engine would be capable of generating 66 kW, however, in this work the engine was motored at approximately 575 RPM by a Crompton-Parkinson electric motor and pulley arrangement as shown in Figure 4.1. Provision was made for shaft encoding through modifications to the fuel pump gear cover.

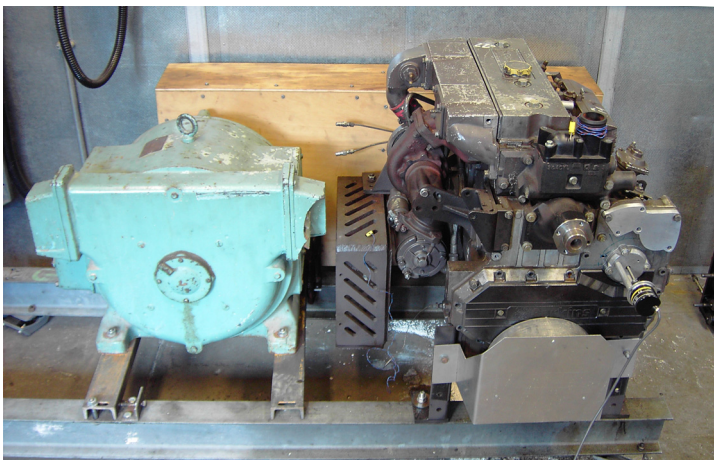

Figure 4.1: Engine A, motored Perkins T4.236 diesel engine.

4.2.1.2 Engine B

Engine B was a 46 kW, four-cylinder, 4.42 litre, wet-lined, HSDI, Perkins A4.270 diesel engine, as shown in Figure 4.2. This model of engine was manufactured between 1958 and 1974 and was typically used for agricultural and marine applications. The engine was naturally aspirated with static injection timing and can be considered as relatively basic when compared to modern engines. The cylinders were of the wet-lined variety, i.e. removable cast iron liners, and had a wall thickness of 6.4 mm. This arrangement means that the external surfaces of the liners are exposed to the coolant. The ring-pack of this engine featured three compression rings and two oil-control rings, situated above and below the gudgeon pin.

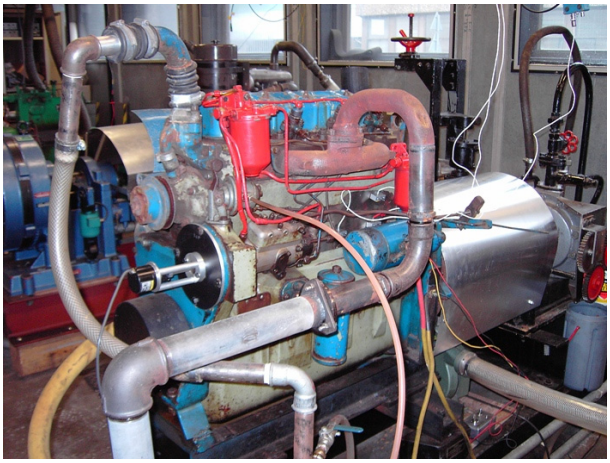

Figure 4.2: Engine B, Perkins A4.270 diesel engine.

To suit the test facility application the engine was modified from its original state. The cooling system components, i.e. radiator, thermostat, pulleys and other fittings, were removed, with cooling instead provided by an open-loop system drawing mains water. Provision was also made for shaft encoding via modifications to the fuel pump gear cover.

In order to simulate actual working conditions the engine was coupled to a Froude & Heenan hydraulic dynamometer (circa. 1919). The dynamometer was modified to allow remote measurements with the original balance weights and dial-gauge torque measurement system replaced by a cantilever load-cell and Wheatstone bridge strain gauge set-up. Therefore, an electrical voltage output was generated in proportion to the strain on the load-cell and this could be calibrated, by applying dead loads and with consideration of dynamometer and load cell geometries, to the torque exerted by the dynamometer main shaft. However, the dynamometer could not permit testing over the

full operating range of engine B. Figure 4.3 shows torque ratings taken from the engine specifications and the experimentally found maximum torque capability of the dynamometer. It is clear that at lower speeds, where torque output of the engine is maximum, there is an area of the engine operating range that cannot be accessed using this set-up.

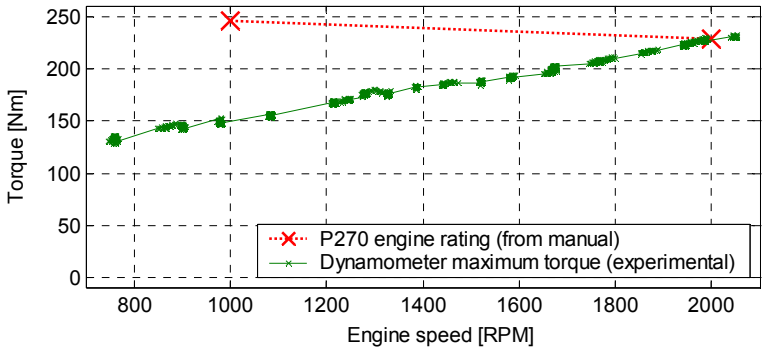

Figure 4.3: Engine B dynamometer capabilities.

4.2.1.3 Engine C

Engine C was a 96 kW, six-cylinder, 5.9 litre, HSDI, Cummins 6BT5.9 diesel engine. This engine was reconditioned as per a new engine and was under post-assembly test coupled to a hydraulic dynamometer in a manufacturing facility. It did not feature cylinder liners; instead the cylinders were integral to the cylinder block, i.e. machined directly from the block. The ring-pack comprised of two compression rings and an oil-control ring. A further feature of this engine was that it incorporated an ancillary reciprocating compressor. Since this engine was a production engine there were no modifications and no provision for shaft encoding.

4.2.2 Two-stroke, petrol engine, engine D

Engine D was a 50 cc, two-stroke, single-cylinder engine removed from a chainsaw. The carburettor components were removed and the remaining crank and piston assemblies were motor driven as shown in Figure 4.4. The piston seal was achieved through a single compression ring. To allow attachment of an AE sensor a flat was introduced to the external cooling fin surface. Given that the engine was of the two-stroke variety it incorporated ports in the cylinder wall instead of poppet valves to facilitate the processes of intake, exhaust and scavenging.

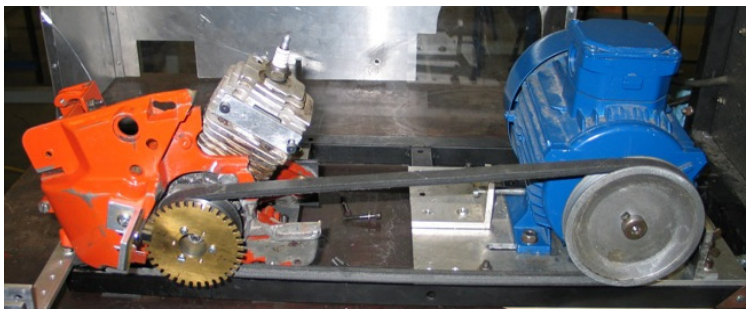

Figure 4.4: Engine D, motored, small, petrol engine.

4.2.3 Two-stroke, crosshead, diesel engines

A series of tests were performed on two different models of this engine type. Three, stationary, seven-cylinder engines attached to generators were available to test in an industrial power station, these are collectively denoted as engine E in Table 4.1. A further four-cylinder, highly instrumented engine, installed in a research facility, was considered, engine F. For both engines the ring-pack consisted of four compression rings. Due to the large size of these engines the component surfaces are very open and accessible. Therefore, it was possible to locate sensors on most surfaces of the cylinder head area and also on some external positions in the upper liner area; these are identified in the liner schematic shown in Figure 4.5.

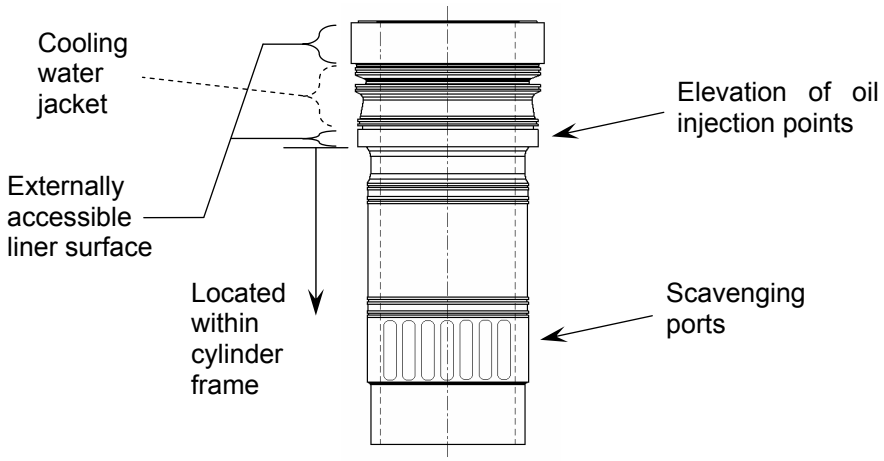

Figure 4.5: Cylinder liner of a two-stroke diesel engine with structural features and accessible external surfaces indicated.

4.2.3.1 Engine E

Engine E was a 11.5 MW, seven-cylinder, mechanically governed, MAN B&W engine installed in an industrial power station, as shown in Figure 4.6. It was coupled directly to a 50 Hz electrical generator and thus operated solely on the generator curve at a constant speed. Three engines of this type were available to test, although only one was fitted with a shaft encoding system.

Figure 4.6: Engine E, MAN B&W, seven-cylinder, crosshead, two-stroke, diesel engine.

4.2.3.2 Engine F

An electronically governed, four-cylinder, MAN B&W engine installed in a research facility and attached to a water-brake dynamometer was investigated, engine F, shown in Figure 4.7. At Maximum Continuous Rating (MCR), i.e. maximum load, this engine was capable of generating over 7 MW at 123 RPM and could operate in propeller or generator curve modes; operating parameters at various loads on both curves are given in Table 4.2. Due to its function as a dedicated research tool this engine was more highly rated than comparable engines and utilised a cylinder bore of 500 mm and a stroke of 2200 mm. It was also highly instrumented with dedicated in-cylinder pressure, fuel pressure, and valve lift measurement transducers. The engine and dynamometer set-up have been designed to simulate as close as possible the behaviour of an operational installation, with the only exceptions being the lack of the natural movement of a ship and perhaps some fuel-oil mixtures not allowed by local environmental regulations [82].

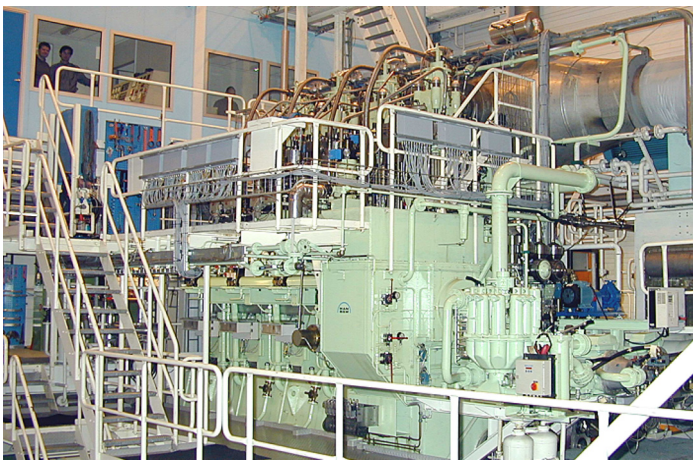

Figure 4.7: Engine F, MAN B&W, four-cylinder, crosshead, two-stroke, diesel engine.

Propeller curve			
% of MCR	Speed [RPM]	Torque [kNm]	Power [kW]
100	123	549.7	7080
90	118.8	512.2	6372
80	114.2	473.6	5664
75	111.8	453.5	5310
60	103.7	391.2	4248
50	97.6	346.4	3540
40	90.6	298.5	2832
25	77.5	218.1	1770
20	71.9	188.1	1416
10	57.1	118.4	708

Generator curve			
% of MCR	Speed [RPM]	Torque [kNm]	Power [kW]
90	123	494.7	6372
75	123	412.3	5310
50	123	274.8	3540
25	123	137.4	1770
10	123	55.0	708

Table 4.2: Engine F operating parameters at various loads on propeller and generator operating curves.

4.3 Data acquisition equipment

Several different systems were used throughout this work in order to acquire, digitise and store data for further processing and analysis, an example of a typical Data AcQuisition (DAQ) system used is outlined in Figure 4.8. The system consisted of externally located AE sensors and pre-amplifiers, a Signal Conditioning Unit (SCU) and a DAQ card installed in a standard PC. The number of AE sensors used per test, i.e. the sensor array, was dependant upon the specification of the DAQ card (i.e. maximum number of input channels) and specific test requirements. The inputs to the DAQ card were not necessarily all AE, throughout these tests other signals relating to engine operation were acquired at the expense of one or more AE channels. This is the case in

the example DAQ set-up described in Figure 4.8, which shows a shaft encoder signal acquired in addition to a three-sensor array.

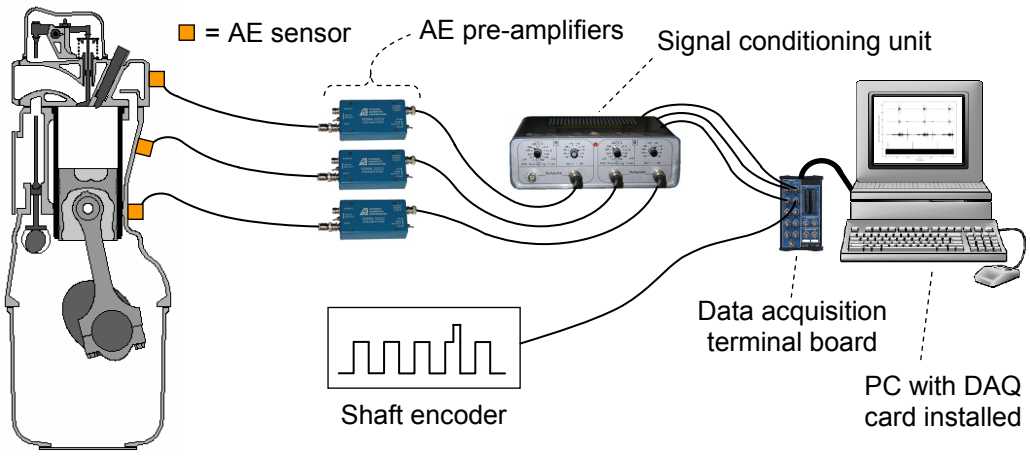

Figure 4.8: Outline of typical data acquisition system used in this work.

Although the principle of the DAQ acquisition system remained the same throughout the experimentation the actual component elements and system set-up varied test to test, dependant mainly upon equipment availability and suitability. One particular set-up was used for the majority of the work. Details of this system and of the others used shall be given in later Sections of this Chapter which detail apparatus set-ups and experimental procedures used for each individual test.

4.3.1 AE sensors

All the AE sensors used in this research were of the commercially available peizoelectric element type, based on the ceramic, lead zirconate titanate (PZT). These generate small voltages in relation to nanometre amplitudes of surface waves and can be manufactured so as to provide different bandwidth responses and sensitivities to suit a variety of applications.

For the majority of testing Physical Acoustics Corporation (PAC) Micro-80D AE sensors were used. These are 10 mm in diameter, 12 mm in height and are specified as having an operating frequency range from 175 to 1000 kHz whilst being resonant at 250 and 325 kHz. They are of differential configuration and therefore when combined with a differential pre-amplifier they provide 24 dB common mode rejection of unwanted signals in areas of high electromagnetic interference. These sensors are rated for

operation up to 177 °C which comfortably exceeds the maximum surface temperatures experienced in this work of approximately 90 °C.

For early experiments on engine F, PAC WD sensors were used. These have a wider operating range than the Micro80D sensors of between 100 to 1000 kHz (resonant at 125 and 650 kHz) and are slightly larger at 18 mm diameter and 17 mm height. A further type of sensor was used for one of the latter experiments on engine F. This was a prototype sensor, specifically designed and optimised for engine monitoring [217], and shall be designated as an Env sensor in this work. The sensor bandwidth was reported as being similar to that of a PAC WD sensor with the advantage of improved performance at elevated temperatures whilst the structure of the sensor was also considered to be more robust.

Coupling of the AE sensors to the engine surfaces was typically achieved through magnetic hold-downs, although in some cases the sensors were held in place by means of screw threads or pressure applied to the back plate. In all cases, to ensure good transmission of the AE signal, a thin layer of vacuum grease was applied between the engine surface and the sensor face plate.

4.3.2 AE pre-amplifiers

Amplification of the raw AE signals were generally provided by PAC 1220A pre-amplifiers, these supplied gains of either 40 or 60 dB and also band-pass filtering within the range 100 to 1000 kHz. In some later experiments PAC type 0/2/4 pre-amplifiers were also used. These offered gains of 0, 20 or 40 dB and again band-pass filtered the signals but within the frequency range 20 to 1000 kHz. For both amplifier types a single BNC connection provided the means for 28 V power supply and also for the signal output.

4.3.3 Signal conditioning units

As well as providing a power supply to the pre-amplifiers the purpose built in-house Signal Conditioning Units (SCU) provided further signal amplification or attenuation as necessary dependant upon source AE levels. In addition to raw signal throughput these

units also provided an analogue RMS output with selectable RMS averaging times for situations in which the full detail of raw data was unnecessary and/or longer time durations were required.

4.3.4 Data acquisition cards

Several different DAQ cards were used to acquire and digitise the analogue input data. For the majority of testing a 12-bit, 4-channel, National Instruments (NI) PCI-6115 DAQ card installed in a standard PC was used. This board was capable of digitising four inputs simultaneously up to a sampling rate of 10 MHz, although in this work typical sampling rates used were 2.5 or 5 MHz for raw data and 20 or 100 kHz for RMS data. The amplitude limits for each channel could be adjusted individually from ± 200 mV to ± 42 V in order to maximise the 12-bit resolution. This board benefited from an onboard buffer memory of 32 Mb which meant that it was possible to acquire a full engine cycle of data acquired at 2.5 MHz even at the slowest running speeds of the large, two-stroke, marine diesels. The board was controlled via a custom-built program developed with National Instruments LabVIEW software by Dr. P. Nivesrangsan, formerly of Heriot-Watt University. This program acquired data in batches utilising the onboard memory and allowed all important acquisition parameters to be adjusted according to requirements. Data streaming was not facilitated.

A further DAQ system was used for some of the tests conducted on Engine F at the industrial research facility. This system acquired RMS AE data at a sampling rate of 20 kHz using a 12-bit NI PCI-6071E DAQ card and a NI SC-2345 signal conditioning carrier interface unit. The advantage of this system was the large number of input channels that could be acquired, up to 16, which therefore allowed a number of other signals relating to engine operation to be acquired simultaneously. This system was used standalone and also in some cases to supplement the 4-channel NI system.

A limited amount of testing was conducted on engine D, the small, motored engine, using a 12-bit, Compuscope CS512 DAQ card. This board was capable of acquiring data from two channels at 5 MHz and was controlled via commercial Gagescope software. The buffer memory size of 2 Mb limited acquisition times to 0.1 seconds for raw AE data sampled at 5 MHz.

4.3.5 Shaft encoders

Shaft encoders are electromechanical devices that can be used to monitor angular position. They were employed in most of the motored and running engine tests in order to monitor crankshaft position, directly for the case of the large, two-stroke engines and indirectly via the crankshaft driven fuel pump gear for the small, four-stroke engines. This is a valuable parameter to acquire as it is useful for both signal processing and for event mapping and interpretation. For engine monitoring it is advantageous to have two shaft encoding signals. The first is a simple one pulse per revolution signal which allows identification of an angular reference point every cycle, typically calibrated to correspond to Top Dead Centre (TDC) of a particular cylinder and referred to as a TDC marker or TDC signal.

The second shaft encoding signal is one which generates a number of circumferentially equally spaced pulses per revolution. The function of this is two-fold. Primarily, it provides a means for conversion of the AE, or other, data from the time-domain into the angular-domain, which is essential when dealing with non-stationary signals such as those produced by reciprocating machinery. This allows accurate reference of AE to crankshaft position and thereby also piston position in the liner. Secondly, it permits the angular position of the crankshaft, and hence the angular velocity, to be monitored with high resolution, providing a further engine monitoring opportunity.

A number of different shaft encoding systems were used in this work; these shall be described in the following Sections which detail the individual tests conducted on each engine. For all of the small engine work and a limited amount of the large engine testing it was possible to use encoders which generated an integrated TDC marker and shaft encoder signal. This increased the number of channels available for AE acquisition which was beneficial when testing with the 4-channel NI DAQ system.

4.4 Details of tests conducted on each engine

4.4.1 Investigation of AE activity generated from the ring-pack/liner interface in a motored, four-stroke, diesel engine, engine A

This test represents the initial investigation into possible AE activity generated at the ring-pack/liner interface in small, diesel engines. The benefit of performing this test on a motored engine was that the resulting AE activity would be expected to be simpler than that acquired from a running engine due to the lack of injection and combustion processes and associated AE events. Further isolation of the ring-pack/liner interface was achieved through removal of the cylinder head and pushrods, thereby removing any AE activity that may have been generated from valve operation and from sources related to the in-cylinder pressure. The only remaining moving parts in the engine were the crankshaft and connected piston assemblies, fuel pump gear, oil pump, main bearings and seals, and the camshaft and followers. Lubricant circulation was as normal bar the sealing of oil galleries leading to the cylinder head.

Two sensor arrays were considered on the cylinder block, with sensor positions as illustrated in Figure 4.9. For array 1 sensors were located on the centre-line of cylinder 1 with the uppermost sensor located 105mm from the top of the block, the mid position sensor 50mm below this and the lower position a further 40mm below. For array 2 sensors were located at the upper position on the centre-lines of cylinders 2 and 3 with a further sensor located at the lower position of cylinder 3.

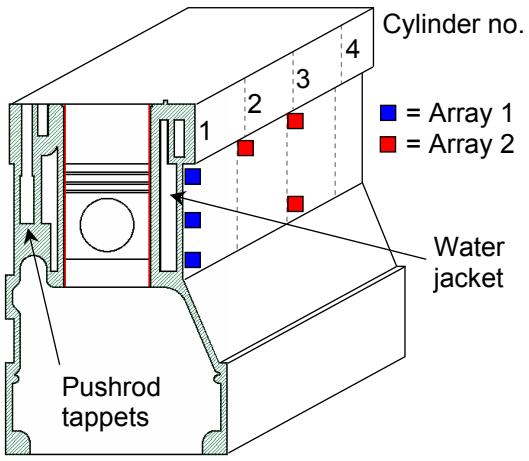

Figure 4.9: Engine A cross-section showing AE sensor positions.

For both sensor arrays over 30 engine cycles of raw AE data were acquired at a sampling rate of 2.5 MHz using PAC Micro80D sensors together with the 4-channel NI DAQ system.

In order to provide a comparison the engine was also motored with the cylinder head in place, thereby introducing events that may arise due to the in-cylinder pressure and valve operation. In this case, raw AE measurements were acquired from the upper sensor position on the centre-line of cylinder 1 using the same DAQ apparatus as the previous test.

For both the cylinder head on and off tests, a shaft encoding signal of 360 ppr (pulses per revolution) relating to the fuel pump gear was acquired in addition to the AE measurements. This was provided by attachment of an Omron E6C2-CWZ6C optical shaft encoder with integrated TDC marker. Since the fuel pump gear rotates at half the speed of the crankshaft a TDC signal was generated every two crank revolutions, i.e. one full engine cycle, and a shaft encoder pulse every 2 degrees of crank rotation.

4.4.2 Investigation of AE activity generated from the ring/liner interface in a motored, two-stroke, petrol engine, engine D

The objective of this test was to investigate if findings obtained from this smaller engine would substantiate those from the motored diesel engine tests.

For this test a PAC Micro80D sensor was used in conjunction with the 2-channel CompuScope DAQ system with raw AE data acquired at a sampling rate of 5 MHz. The sensor was located on a flat introduced to the cylinder head/barrel at the position indicated in Figure 4.10 and was held in place by pressure applied to the sensor backplate. Over 20 cycles of raw AE data were acquired with the engine motored at approximately 1550 RPM and the spark plug removed. Since under normal conditions the engine would operate with lubricating oil mixed with the fuel supply then for this test it can be considered as operating in an unlubricated condition. A 35 ppr shaft encoding signal generated by a slotted disk and photoelectric pickup system fitted to the driveshaft was simultaneously acquired; this incorporated a TDC marker which could be identified via a missing slot

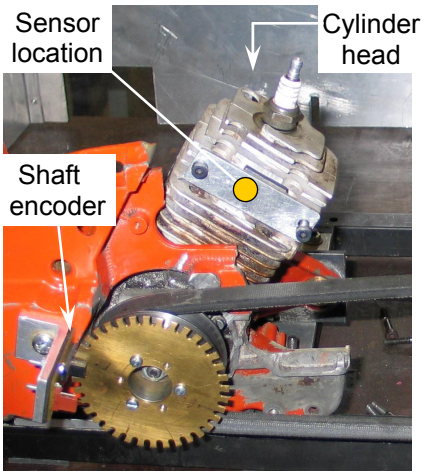

Figure 4.10: Engine D, showing AE sensor position.

4.4.3 Investigation of AE activity generated from the ring-pack/liner interface in running, four-stroke, diesel engines, engines B and C

There were two main objectives to these tests. Firstly, tests on both engines aimed to establish whether AE activity relating to the ring-pack/liner interface occurred under normal operating conditions. Secondly, tests performed on engine B aimed to examine the variance of this activity over the engine operating range. This may allow an indication as to the source mechanisms responsible for AE generation at the ring-pack/liner interface, and therefore, the aspects of tribological behaviour which can be monitored.

For all the tests on engine B raw AE signals were acquired using PAC Micro80D AE sensors and the 4-channel NI DAQ system at a sampling rate of 5 MHz. Furthermore, a sensor was consistently located on the cylinder block surface, on the centre-line of cylinder 1 at the elevation indicated in Figure 4.11. This location was selected on the basis that it would appear to offer the greatest chance of investigating AE arising from the ring-pack/liner interface as it was located immediately next to the internal position where the liner pressed against the cylinder block casting. Shaft encoding was again provided by the Omron 360 ppr shaft encoder with integrated TDC marker fitted to the fuel pump gear as shown in Figure 4.12. The dynamometer load cell output was also acquired in order to provide a measure of the applied torque load.

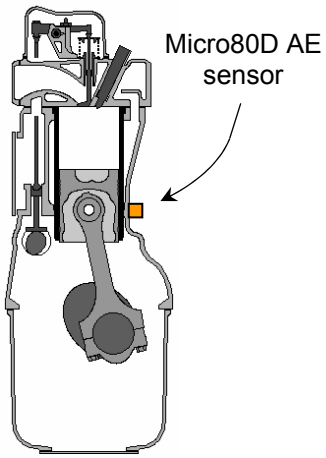

Figure 4.11: Engine B cross-section showing sensor location.

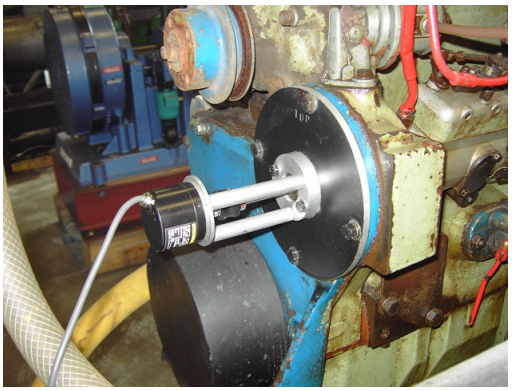

Figure 4.12: Optical shaft encoder fitted to fuel pump gear of engine B.

A preliminary test to briefly assess some basic AE generation and propagation characteristics was conducted at 800 RPM with no load applied to the engine. Raw AE measurements were acquired from one of the strongest anticipated sources of cylinder 1, the fuel injector surface, in addition to the lower cylinder block position.

AE generation over the accessible operating range of the engine/dynamometer set-up was investigated. The engine was operated at numerous loading points, as indicated by the speed/torque test matrix shown in Figure 4.13, with 40 engine cycles of raw AE data acquired at each point. The loading points considered were such that AE activity could be examined over varying load at constant engine speeds, and over varying speed at constant loads.

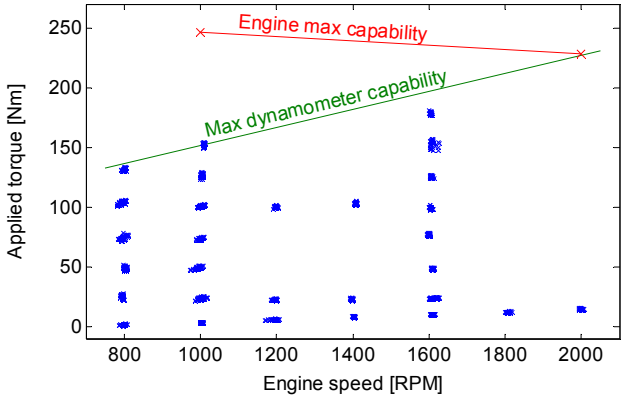

Figure 4.13: Engine B, tests over engine operating range.

Data were acquired first with the engine speed maintained at around 800 RPM and the applied torque increased by increments of approximately 25 Nm till 125 Nm, the maximum torque load possible at 800 RPM. This process was repeated for engine speeds of 1000 and 1600 RPM. Data were then acquired from further loading points in order to fill the matrix and allow comparisons over varying speed and constant torques at increments of 200 RPM. As a result data were available over the range 800 to 2000 RPM with minimum torque applied via the dynamometer (varying from 1.5 Nm at 800 RPM to 13.5 Nm at 2000 RPM), and over the range 800 to 1600 RPM at constant applied torques of 25 and 100 Nm.

Two further tests were performed to investigate changes in AE activity as the engine warmed up from ambient conditions. For both tests engine B was run for over 35 minutes at approximately 1200 RPM with minimum load applied. AE measurements were again acquired from a sensor located on the centre-line of cylinder 1 and the sump

oil temperature was measured by a thermocouple. The engine speed fluctuated slightly over the course of both tests and continual throttle adjustments were necessary to maintain an approximate constant speed.

For the first test the initial oil temperature was 17.9 °C. However, problems with the apparatus meant that two minutes elapsed before the engine was set to run at approximately 1200 RPM, at which point the oil temperature was 22.2 °C. Data were then acquired at a maximum rate of one engine cycle of data per second for a period of 37 minutes. Oil temperature at the end of the test was 59.2 °C. The development of sump oil temperature and the variance of engine speed over the course of this test are shown in Figure 4.14a.

For the second test the initial sump oil temperature was 18.5 °C. The first cycle of data was acquired 45 seconds after initial cranking of the engine at which point the temperature was 19.6 °C. Data were then acquired intermittently for 49 minutes with 2000 cycles of data acquired in total and a final oil temperature of 62.9 °C. Variance of sump oil temperature and engine speed during this test is shown in Figure 4.14b.

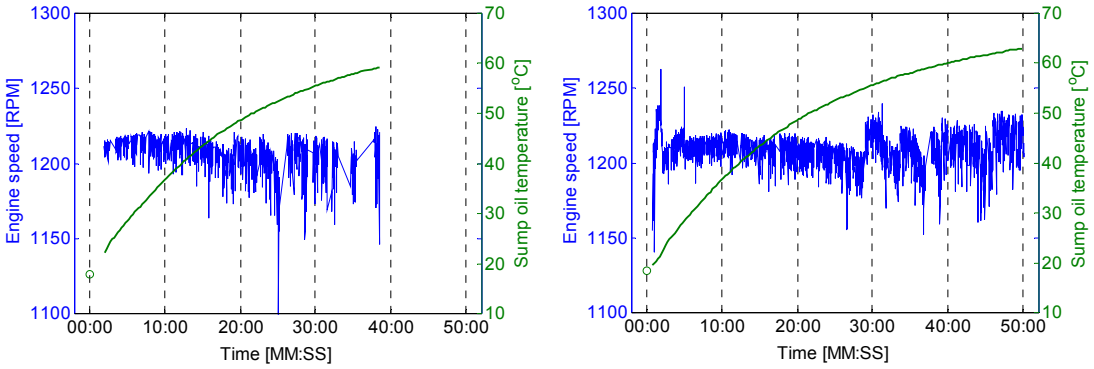

(a) *(b)*

Figure 4.14: Sump oil temperature and engine speed fluctuations during, (a) test 1, (b) test 2.

AE generation from the ring-pack/liner interface was further evaluated through measurements acquired from engine C. In this case the engine was in its first minutes of operation after being reconditioned and was operating at 750 RPM with minimal load applied. Raw AE data were acquired at 2 MHz using the 4-channel NI DAQ system with PAC Micro80D sensors located close to the top of the cylinder block on the centre-lines of cylinder 3 and 6, with a further sensor located at the base of the ancillary reciprocating compressor.

4.4.4 Survey of AE generation within a two-stroke, crosshead, diesel engine, engine E.

Two series of tests were conducted on engine E. Both were aimed at evaluating the characteristics of AE generation during normal operation. Tests were performed so that many aspects could be examined including; source location and event mapping of AE events, consistency of events (cyclic and cylinder-to-cylinder), and changes in the AE signals over varying load on the generator operating curve.

Since these three engines were used for power generation their loading was determined by the power grid demand. Unfortunately this meant no loading control was afforded to the investigator and this obviously impacted upon the testing possibilities. Nevertheless, a number of tests were conducted and the loading applied to the engines was observed to fluctuate therefore providing opportunity to investigate the effect this had on the AE signals. In all cases the engine speed remained constant at approximately 136 RPM.

A number of sensor positions around the cylinder head and liner area were selected for investigation. These are indicated in Figure 4.15 and were chosen on the basis of accessibility and the perceived ability to provide monitoring of anticipated sources such as injector and valve operation. Comparison of signals acquired from these positions would allow source location and AE propagation characteristics to be investigated, as was demonstrated by Nivesrangsan *et al* [152, 154, 155] for AE activity occurring within a small engine.

For both series of tests PAC Micro80D sensors and the 4-channel NI DAQ system were used. Only one of the three engines available for test was fitted with a shaft encoding system. For the first set of tests access restrictions limited the installation to that of a simple zebra-tape and photoelectric pick-up system with TDC and 1015 ppr shaft encoding signals generated on separate channels. This restricted acquisition to two-channel AE arrays. For the second set of tests a more accurate Phoenix optical shaft encoder was installed which provided 1024 ppr and an integrated TDC marker, thereby permitting acquisition of three-channel AE arrays.

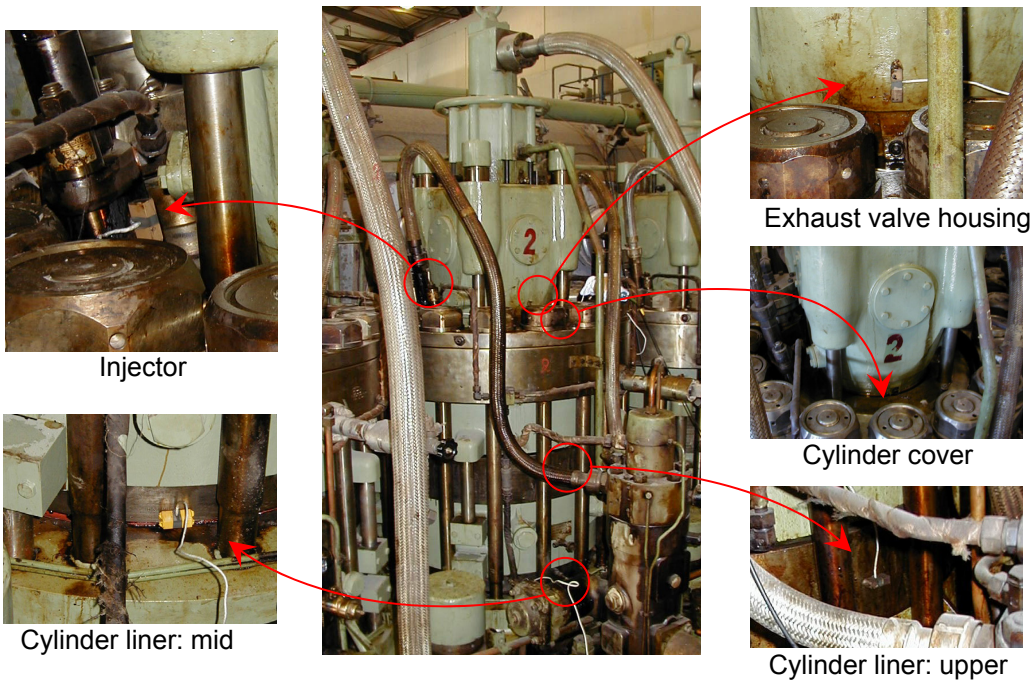

Figure 4.15: Upper cylinder area of engine E with sensor positions indicated.

In order to cover most combinations of sensor positions two or three different sensor arrays were used per cylinder. For each array the quantity of data acquired typically amounted to 10 engine cycles of raw AE data sampled at 2.5 MHz and 100 engine cycles of RMS AE data sampled at 100 kHz. To assess cylinder-by-cylinder variance this process was repeated for all cylinders of the engine fitted with the shaft encoding system.

For the two engines not fitted with a shaft encoding system data were acquired from 4-channel AE arrays covering 4 of the 5 sensor positions detailed in Figure 4.15. Similar quantities of raw and RMS AE data were acquired per cylinder as in the previous tests; however, this was limited to several cylinders each from the two engines.

4.4.5 Survey of AE generation and investigation of AE activity arising from the ring-pack/liner interface in a research orientated, two-stroke, crosshead, diesel engine, engine F

A number of tests were conducted on engine F in order to further evaluate AE generation within large, two-stroke diesels and also to specifically investigate the potential for monitoring of the ring-pack/liner interface. The increased levels of instrumentation and control available for engine F meant that more purposeful tests

could be carried out. These were envisaged to provide greater insight into the AE activity and would also allow comparisons to be made with the power plant engines, engine E, i.e. of a similar type but different in size and specification.

The flexible control of engine F enabled operation with the injection and exhaust valve activity of the instrumented cylinder 2 turned off. In the case of the injection process this meant that cylinder 2 was effectively motored by the remaining cylinders, thereby somewhat simulating extreme misfire conditions. Data acquired from operation in these modes, alongside that relating to normal operation, were anticipated to aid understanding of each processes contribution to the overall AE activity. For each operating mode RMS AE measurements were acquired at 20 kHz from PAC WD AE sensors located at the cylinder cover and mid liner sensor positions using the 16-channel NI DAQ system. Shaft encoding signals, both TDC and 2048 ppr, were also acquired in addition to measurements of valve lift, fuel line injection pressure and in-cylinder pressure. For these tests the engine was restricted to operating at loads of 10 and 25 % of MCR in propeller mode in order to prevent damage.

Two series of tests were conducted to investigate changes in AE generation in response to variation of lubricating condition at the ring-pack/liner interface. Both of these involved the suspension of lubricant supply to cylinder 2. It was expected that this would have an adverse affect on ring-pack lubrication and if AE monitoring were to be a viable tool then it is to be hoped that these condition changes would be detectable.

Data from the first lubricant starvation test were provided by Dr. T. Fog of MAN B&W Diesel. RMS AE measurements were again acquired from the cylinder cover and mid liner positions of cylinder 2 at a sampling frequency of 20 kHz using PAC WD sensors and the 16-channel NI DAQ system. Other engine operating parameters were also acquired as described previously. The structure of this experiment is indicated in Figure 4.16. Engine F was run initially at 25% of MCR for a sufficient period of time to allow acquisition of approximately 200 cycles of data. The lubricating oil supply to cylinder 2 was then stopped and approximately 2000

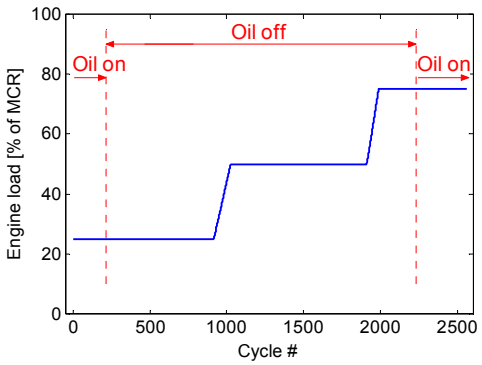

Figure 4.16: Structure of first lubricant starvation test on engine F.

cycles of data were acquired at loads of 25, 50 and 75 % of MCR, including the intermediate ramp-up periods. Lubricant supply then recommenced at 75 % of MCR and a further 300 cycles of data were acquired.

A second lubricant starvation test was performed several years after the initial test with an increased level of instrumentation and a more thorough experimental procedure. A schematic of the complete DAQ system used is given in Figure 4.17 and shows sensor positions, sensory inputs to DAQ cards and the intermediate signal processing stages. Both 4- and 16- channel NI DAQ systems were employed, as well as sensors of both Micro80D and Env types. As in previous tests, sensors were located at the cylinder cover and mid liner positions of cylinder 2. Further sensors were also located at the upper liner position and an Env sensor was affixed internally just below the scavenging ports at the lower area of the liner, as indicated in Figure 4.18, with the sensor cable extracted through a tapping in the frame. It was expected that the increase in sensor array coverage gained by these sensors would benefit the investigation by increasing source location potential. The internal location of the Env sensor also functioned as a check of the robustness of this developmental sensor.

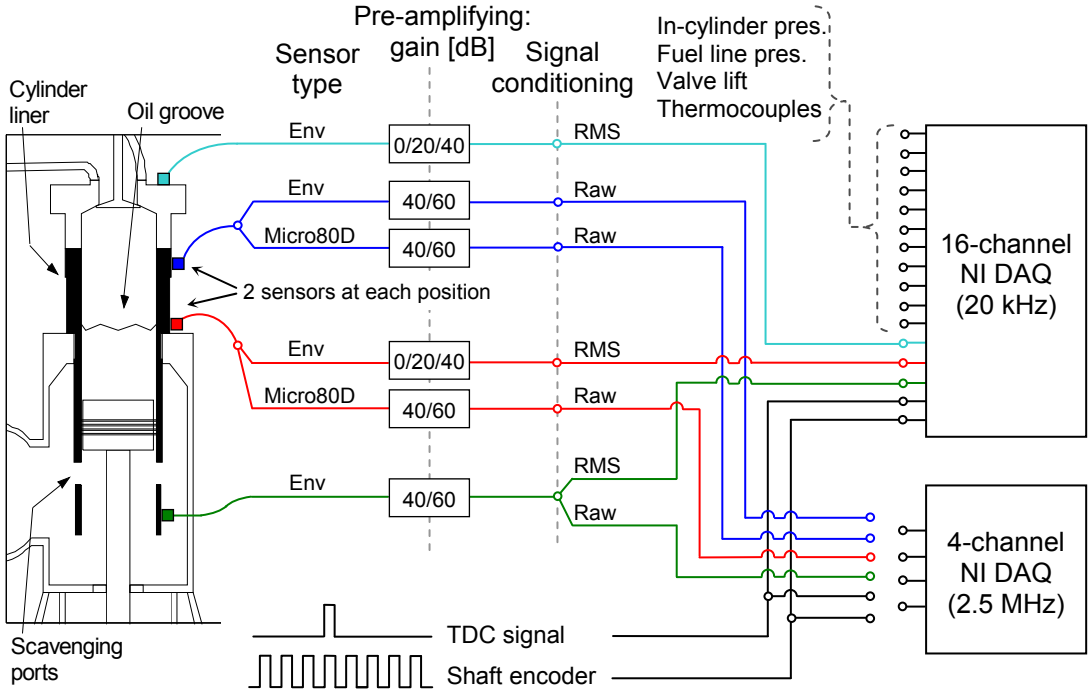

Figure 4.17: Schematic of DAQ set-up for second lubricant starvation test on engine F.

The 16-channel DAQ system used a stable set-up throughout with 20 kHz RMS data acquired from Env sensors located at the cylinder cover, mid liner and lower liner sensor positions. Pre-amplification was provided by PAC 0/2/4 pre-amplifiers for the

cylinder cover and mid liner sensors and by a PAC 1220A pre-amplifier for the lower liner sensor. Shaft encoding signals, both TDC and 1024 ppr, were acquired in addition to measurements of in-cylinder pressure, fuel injection pressure and valve lift. Each acquisition of RMS data was for 8 seconds, corresponding to a least 9 engine cycles at the lowest operating speed.

Figure 4.18: Attachment of Env sensor to lower area of liner.

The 4-channel DAQ system was used to acquire raw AE data at 2.5 MHz from a number of sensor position combinations at repeated intervals throughout the tests. Since TDC and shaft encoding signals were provided on separate channels only two raw AE channels could be acquired simultaneously, or 3 AE channels and just the TDC signal. As indicated in Figure 4.17 the available raw AE channels were Micro80D sensors located at the upper and mid liner positions, and Env sensors at the upper and lower liner positions. The length of each raw data acquisition was varied to correspond to just over one engine cycle and typically for one batch of data, i.e. one combination of sensor positions and shaft encoding signals, 20 cycles of data were acquired.

The structure of the second lubricant starvation test, summarised in Figure 4.19, was more thorough than the initial test. Firstly, to establish variation of AE activity under normal operating conditions, data were acquired at various loading points on both the propeller and generator curves. The engine was then run for a period of several days for purposes unrelated to this work before the lubricant starvation test was performed. For this the engine was operated at 25 % of MCR for a short period before the oil supply to cylinder 2 was removed. The engine was then run for approximately 15 hours at various loading points on the propeller curve as shown in Figure 4.19. After this period the oil supply was reconnected and the engine was operated for a short time at 100% of MCR before the test was stopped. Throughout this test, after each change in load, the engine operation was allowed to stabilise before acquisition of data commenced. Over 400 cycles of RMS data were acquired at each load in addition to batches of raw AE from various sensor combinations.

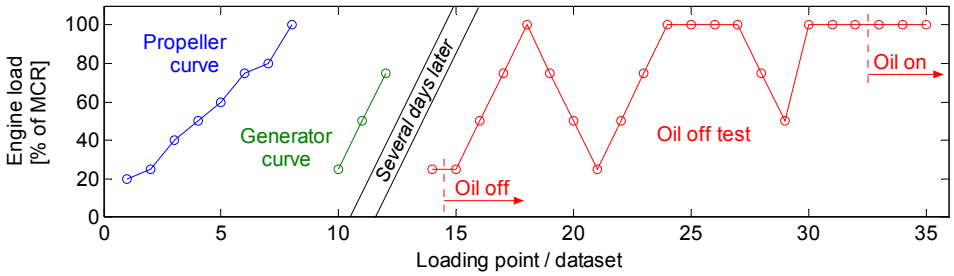

Figure 4.19: Structure of second lubricant starvation test on engine F.

During this test the opportunity was taken to acquire data from other cylinders of the engine which were operating under normal lubricating conditions. Raw AE data were acquired using the 4-channel NI DAQ system and Micro80D AE sensors at the mid liner positions of cylinders 3 and 4 at full load.

For both lubricant starvation tests visual inspections of cylinder 2 identified that conditions at the ring-pack/liner interface had not degraded to the point where scuffing was initiated, thought due in the main to entry of an oil mist via the scavenging ports. However, for the second test, it was noted that the crests of the liner wave cut surface had worn down. Approximately one month after the second lubricant starvation test all the liner conditions were inspected. This revealed that the cylinder 4 liner had deteriorated to the extent where a cylinder overhaul was necessary.

4.5 Signal processing

This Section outlines the processing steps applied consistently throughout this work in order to transform the acquired AE signals into a format where they can be compared and analysed on a common basis. This predominantly involves the resampling, or conversion, of data from time-domain into angular-domain signals but also includes other processing steps such as the identification of engine cycles, calculation of RMS AE signals and simple statistical analysis. These procedures are fairly straightforward and are described in detail in this Section as in subsequent Chapters which present and discuss the AE signals there is little reference made as to the processing steps used.

4.5.1 Conversion of time-series data into angular-domain signals

All the signals acquired during this work are similar in the respect that they are acquired as time-series data, be it with sampling rates of 20 kHz or 5 MHz. However, time-domain signals from reciprocating machinery are not ideal for comparative analysis on a cyclic basis as they are highly non-stationary [82]. Assuming a constant sampling rate the number of data samples during an engine cycle will increase in proportion to its duration; this will vary even at apparent constant engine speeds due to small fluctuations. Accelerations of the crankshaft during the engine cycle represent a further source of non-stationarity.

A further option is analysis of signals in the crank angle domain. In this case, the signals are inherently tied to the engine cycle and each cycle therefore consists of an equal number of data samples. This is more favourable in terms of signal stationarity and it also nullifies any effects of crankshaft angular accelerations during the cycle. Signals which were originally acquired as time-series data have to be converted into angular domain signals. For the signals acquired in this work the obvious means to achieve this was to use the information contained in the shaft encoder signals as these consisted of a number of angular equidistant pulses that were effectively stationary markers of angular displacement. The AE data within these markers could then be resampled to an equal length so that each engine cycle of data comprised an equal number of sample points.

The use of a shaft encoder signal to resample time-series data is a common processing step employed in many previous works [8, 82, 152]. In many cases the original AE signals have been resampled down to a single value per encoder pulse in order to dramatically reduce their size and make them more suitable for various forms of advanced statistical analysis. However, since the work in this thesis is concerned mainly with interpretation of the signals the aim of the resampling process was not to reduce the signals to such a coarse resolution but rather to preserve as much of the original signal structure as possible.

The resampling and other processing actions are best described by outlining each step on some example raw AE signals. Figure 4.20 shows typical time-series data acquired from the running, four-stroke diesel, engine B, at a sampling rate of 2.5 MHz using the 4-channel NI DAQ system. The signals consist of 1.2 million sample points, i.e. a time

period of 0.48 seconds, and correspond to a three sensor AE array located on cylinder 1 and a shaft encoding signal (signals are shown with offsets introduced in Figure 4.20 simply for presentation purposes). The shaft encoder signal contains both a 360 ppr pulsetrain, the detail of which cannot be seen in Figure 4.20, and a TDC marker which was calibrated to cylinder 1 TDC on the exhaust/intake strokes and is evident as a short pulse above the bulk of the signal. The TDC markers allow each engine cycle to be identified, for this acquisition the engine speed and DAQ parameters were such that it contained four complete engine cycles. The AE signals are as expected in that they show AE events of varying amplitudes and durations which appear in a recurring pattern every engine cycle.

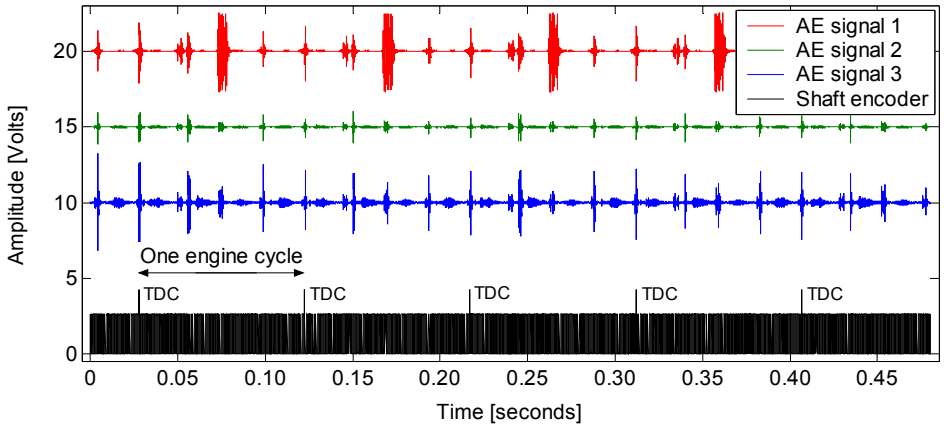

Figure 4.20: Typical signals acquired from engine B from a three sensor AE array and a shaft encoder.

The first processing step was to account for signal amplification and/or attenuation introduced by the DAQ apparatus at the pre-amplifier and SCU stages. The aim of this procedure was to revert the signal amplitudes back to that measured at the sensor, excluding the effects of band-pass filtering at the pre-amplifiers, in order to allow comparison of amplitudes over sensor arrays where different gains have been used. To provide an example of typical gains used, AE signal 1 in Figure 4.20 was acquired with gains of 40 dB at the pre-amplifier and -6 dB at the SCU, hence a total gain of 34 dB. This is related to the ratio of signal amplitudes before and after amplification through Equation 4.1 [7].

$$A = 20\log(U_{out}/U_{in}) \tag{4.1}$$

where A is signal gain expressed in dB and U_{out}/U_{in} is the ratio of output to input signal amplitudes.

Therefore, in this case, with *A* equal to 34 dB, the signal has been amplified by a factor of approximately 50. In order to regress it back to that measured at the sensor the amplitude of the acquired signal was therefore simply divided by 50. In contrast, AE signal 3 was acquired with gains of 40 and -12 dB; a total gain of 28 dB, or an amplification ratio of 25. Once the signal gains have been accounted for the signal amplitudes can then be compared. However, this can still produce misleading results since differences in sensor coupling and sensor sensitivity, even between sensors of nominally the same type, may have a significant effect. Nevertheless, all the signals presented in the following Chapters are shown with the signal gains accounted for.

If the original signals were raw AE, as is the case for the example data, then the corresponding analogue RMS AE signals were calculated in order that both forms of the signal were available for further analysis. RMS AE signals are sufficient for comparison of signal energy content; however, if spectral content or wave arrival time differences over sensor arrays are under scrutiny then the use of raw AE may be essential. The method used to calculate the RMS AE signal was similar to the function of the SCU hardware in the DAQ apparatus. Initially an analogue RMS AE signal was calculated using a sliding window of specified time duration; this was then resampled at a much lower rate, typically 100 kHz. RMS AE signals corresponding to the raw AE data shown previously in Figure 4.20 are given in Figure 4.21, these were calculated using a time constant of 120 µs, a resampling rate of 100 kHz and with DAQ system gains accounted for; the signals are again shown with offsets introduced for presentation purposes.

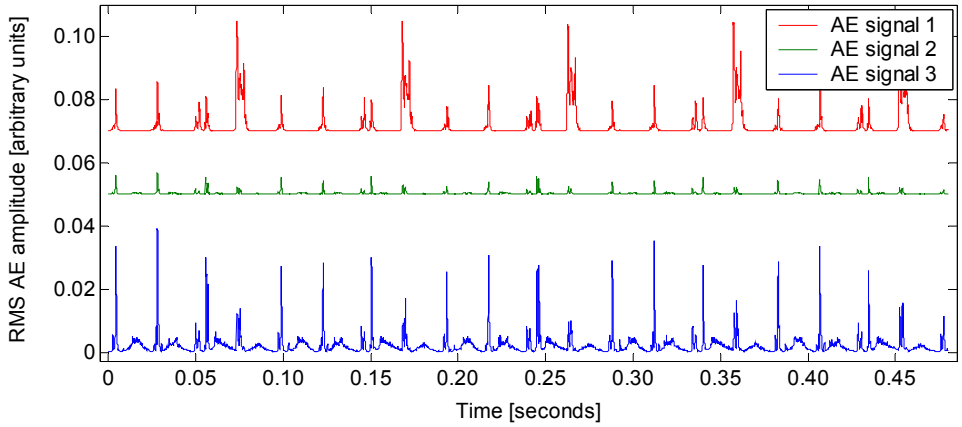

Figure 4.21: Calculated RMS AE signals from raw AE data.

The next step in the process was the identification of TDC and pulsetrain pulses in the shaft encoder signal. Figure 4.22 shows the structure of the shaft encoder signal in the vicinity of a TDC pulse. The pulsetrain was simply a square wave signal with a wavelength equal to two degrees of crank rotation which was modified by the presence of the TDC pulse. The timing of pulsetrain and TDC pulses were determined through identifying where the signal crossed thresholds with a positive gradient, as indicated in Figure 4.22. In addition to being an essential element of the resampling process the TDC pulses also allowed the duration of the engine cycle, and therefore the engine speed, to be accurately determined. Similarly, the variation of crank angular velocity, i.e. the ICAV waveform, could be determined from the duration between the pulsetrain pulses.

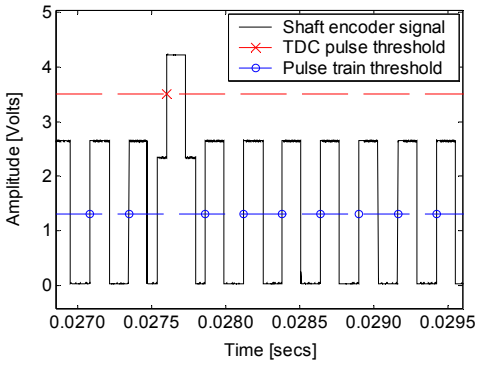

Figure 4.22: Structure of shaft encoder signal around TDC.

The raw and RMS AE signals were separated into individual engine cycles of data using the location of the TDC pulses. Within each cycle the signals were further segmented in relation to the timing of the pulsetrain pulses. Each segment of data was then resampled down from its original number of sample points to an equal number of points using a nearest neighbour interpolation process. The principle of this process is illustrated in Figure 4.23 for a 30 sample point signal resampled down to 17 sample points. The data were resampled down rather than up in order to avoid introducing two successive points that relate to the same original point.

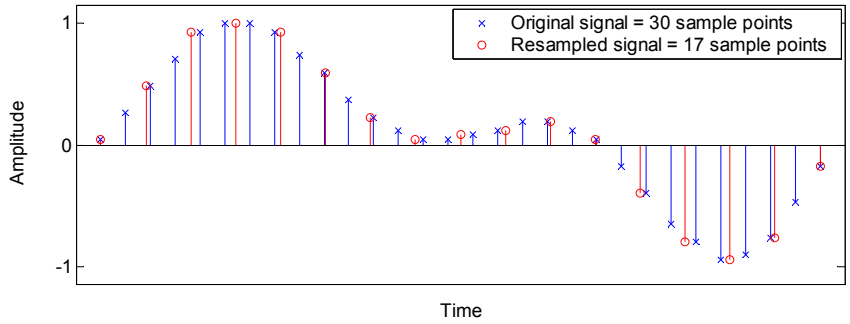

Figure 4.23: Example showing principle of nearest neighbour resampling process.

A comparison of original and resampled raw AE segments for the example data is provided in Figure 4.24. The original data corresponding to the first 2 degree segment of data after the first TDC pulse for AE signal 3 is shown in Figure 4.24a; it consists of

647 sample points. The equivalent resampled signal, of 500 sample points, is shown in Figure 4.24b. It is clear that in this case the resampled signal preserves the structure of the AE waveform.

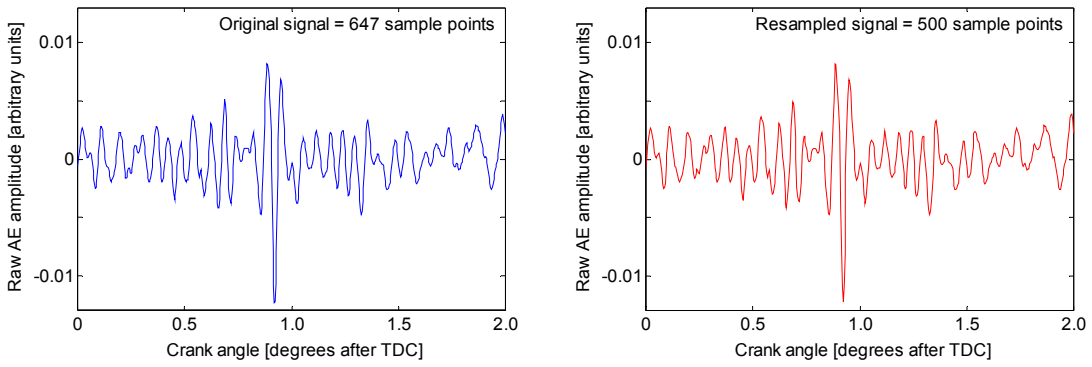

(a) *(b)*

Figure 4.24: Segment of raw AE signal, (a) original signal, (b) resampled signal using nearest neighbour interpolation.

This may have been expected from consideration of the sampling rate and the frequency content of the AE signals. Since in this case the original raw AE sampling rate was 2.5 MHz and the data segment was resampled from 647 to 500 points, i.e. a reduction factor of 1.29, the effective sampling rate of the resampled segment was therefore 1.94 MHz. Although the general range of AE activity is 0.1 to 1 MHz the response of the Micro80D sensors used in this test was such that the highest significant frequency was around 600 kHz, with any component above this of negligibly low energy. Given the Nyquist theorem which lays down the fundamental rule of analogue to digital digitisation [218], the required sampling rate to acquire the highest significant frequency of a signal without introducing aliasing effects is double this frequency, i.e. 1.2 MHz. Although for each test on the different engines the original raw AE data was resampled down by varying extents the effective sampling frequency of the resampled raw data was always greater than 1.2 MHz thus ensuring that the structure of the raw AE signal was maintained.

There are further effects of resampling time-series data into the angular domain, which particularly affect burst-type events. With increasing engine speed the amount of crank rotation in a specific time period will increase and since AE events are functions of time then events of similar time duration, when resampled, will appear over broader angular periods for greater speeds. This is exemplified in Figure 4.25. A time-series RMS AE signal of a burst-type event is shown in Figure 4.25a and the corresponding resampled

angular-domain signals if this event had occurred at 800 and 2000 RPM are given in Figure 4.25b. As expected, the event appears over a broader angular period for the higher engine speed. This may have implications when characteristics of burst-type events in resampled signals are compared over different engine speeds.

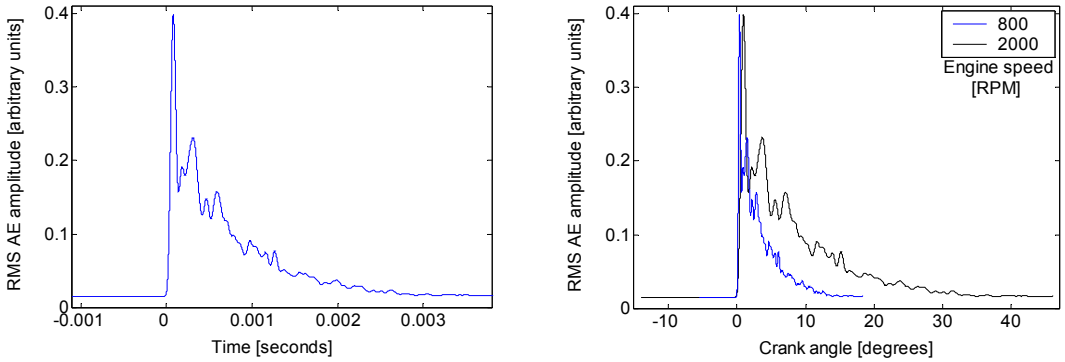

(a) *(b)*

Figure 4.25: Effect of resampling signals containing burst-type events, (a) original RMS AE signal, (b) resampled signal at two different engine speeds.

Each segment of both the raw and RMS AE signals were resampled in turn, and then concatenated to form complete resampled cycles in the angular-domain, as shown for the first cycle of data for AE signal 3 in Figures 4.26a and 4.26b for raw and RMS AE signals respectively. The signal is presented with TDC firing in the centre of the plot; this form of presentation is consistent throughout this thesis.

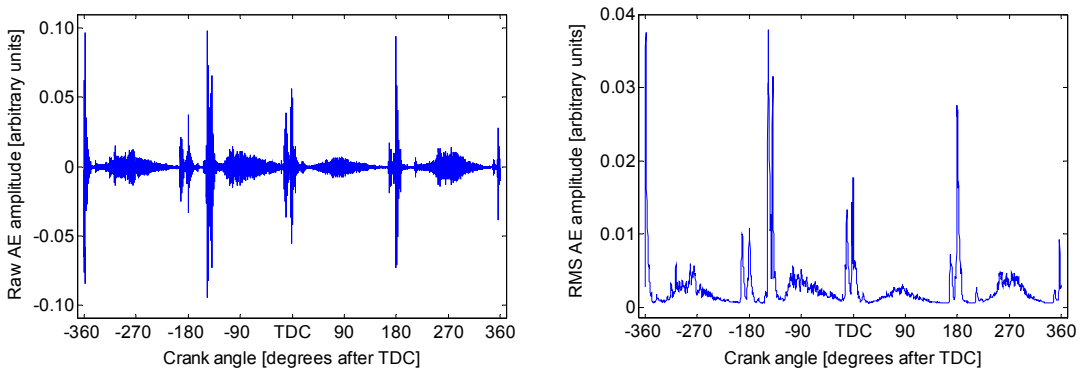

(a) *(b)*

Figure 4.26: Resampled cycle of data corresponding to the first cycle from AE signal 3, (a) raw AE, (b) RMS AE.

Each individual resampled cycle was then grouped together with other cycles acquired at the same operating conditions to form a dataset. For the work in this thesis this consisted of anything from 10 cycles of raw AE data to over 400 cycles of RMS AE data per dataset. For instance, the example data acquisition in Figure 4.20 contained 4

full cycles. These were added to the resampled data from a further 19 acquisitions to form a dataset consisting of 80 cycles.

4.5.2 Statistical analysis of datasets

Within each dataset the AE signals contain consistent cyclic features in addition to fluctuations of amplitude, timing and duration of particular events. This is demonstrated to an extent in Figure 4.27a. It shows 80 resampled cycles of RMS AE corresponding to AE signal 3 of the example data with each cycle superimposed in a different colour. From such plots an indication of cyclic consistency and the range of cyclic fluctuations can be gained.

Although the cyclic fluctuations may well contain information relevant to the engine operation it is of greater importance to establish the typical, or mean, AE signal based upon statistical analysis of the dataset. Analysis of mean signals is a common approach that is more reliable than single cycle analysis and has been used for other engine condition parameters including the in-cylinder pressure [14, 53]. In this work for each dataset of RMS AE signals simple statistical analysis has been performed whereby the mean, maximum, minimum and standard deviation at each sampling point during the cycle have been calculated. Figure 4.27b shows the mean, maximum and minimum values for the dataset shown in Figure 4.27a. From this a more succinct evaluation of the range of the data can be made and the mean signal can be used in further comparative analyses over varying engine conditions.

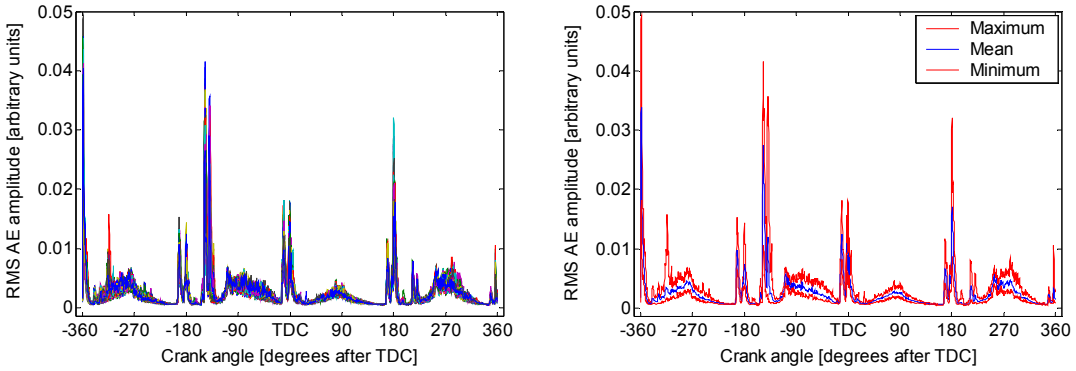

(a) *(b)*

Figure 4.27: Dataset of resampled RMS AE signals consisting of 80 engine cycles, (a) all cycles superimposed, (b) maximum, mean and minimum values at each sample point during the cycle.

Chapter 5

Four-stroke, trunk-piston, diesel engines

5.1 Introduction

This Chapter presents and discusses the results of tests on the smaller engines, engines A to D in Table 4.1. Initial investigations considered motored engines and were geared towards identifying whether or not AE activity was generated at the ring-pack/liner interface. Subsequent tests on running engines were aimed at investigating if ring-pack/liner AE activity occurred under normal operating conditions and at establishing the variation of such activity over the engine operating range. In the final section the experimental evidence is compared with typical ring-pack behaviour in order to determine what this AE activity relates to in terms of the source mechanisms active at the ring-pack/liner interface.

Previous work has indicated a sound basis for this investigation. It has been established that AE monitoring can be applied successfully towards evaluation of other engine processes [82, 122, 123, 137-150] as well as towards investigating tribological behaviour in a range of laboratory and industrial applications [168-181, 202-215]. Furthermore, it has been shown [152] on an engine similar to that considered in this work that simulated Hsu-Nielsen AE sources propagate from the internal liner surface to the external surface of the cylinder block.

5.2 Motored engines

AE signals acquired from reciprocating engines are a composite of burst and continuous type events that originate from mechanical impact, fluid, combustion and wear processes within engines [6, 152]. Since the timing of these processes often coincide or overlap, particularly in small, multi-cylinder engines where the relatively small dimensions permit extensive cross-cylinder propagation, it can be difficult to decipher the AE signals with regards to identifying AE events that correspond to specific sources. Nevertheless, previous work on small, four-stroke engines [138, 152] has

indicated that most of the major AE events can be attributed to impacts occurring during normal operation of the fuel injectors and valves. Furthermore, there has been little recognition that AE signals from engines contain a contribution arising from the ring-pack/liner interface which suggests that if any is present then it is of relatively low amplitude. One of the main aims of this work is to move beyond the more obvious AE sources and, using previous knowledge, find ways to identify and understand AE generated from the ring-pack/liner interface.

For this reason the initial investigation considered two motored engines, engines A and D in Table 4.1. Testing on motored engines eliminates contributions to the AE signal from the injection and combustion processes and thereby focuses attention on the remaining AE generating sources. In the case of engine A further isolation of the ring-pack/liner interface was achieved by motoring the engine with the cylinder head removed. This would eliminate any AE activity associated with the in-cylinder pressure and also from valve impacts and pushrod interactions.

5.2.1 Engine A

5.2.1.1 Comparison of signals acquired with the cylinder head on and off

Raw AE signals acquired from approximately the same sensor position on engine A, the motored, four-stroke engine, with the cylinder head on and off are shown in Figures 5.1a and 5.1b respectively. The signals correspond to one full cycle of operation, i.e. two crankshaft revolutions, with the crankshaft motored at approximately 575 RPM.

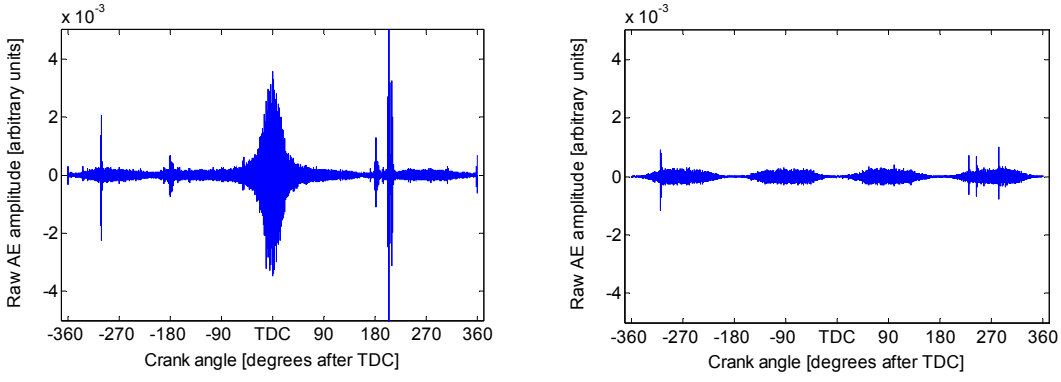

(a) *(b)*

Figure 5.1: Engine A, signals acquired from the cylinder block with (a) cylinder head on, (b) cylinder head off.

There are some significant differences between the signals. The signal acquired with the cylinder head on, Figure 5.1a, shows several burst-type events and a continuous component which rises and falls about TDC. This feature would correlate well to the development of in-cylinder pressure and because it appears in one cylinder only it is likely attributable to fault-related leakage of some form. With the cylinder head removed the signal shows different characteristics. There are again several burst-type events and a continuous background feature, however, the burst-type events are much reduced in amplitude and the continuous feature in this case consists of four pulses, or envelopes, during the engine cycle; the amplitudes of which are maximum at around the piston mid-strokes and minimum at the dead-centres. In the absence of other moving components these envelopes can be surmised as relating to the four strokes of the cycle, and therefore to an aspect of the piston assemblies movement against the cylinder liners.

Closer inspection of the signal acquired with the cylinder head on reveals that the four envelopes per cycle characteristic is also present in the relatively low-level background AE, although, on the compression and expansion strokes around TDC it is overwhelmed by the continuous AE activity relating to the in-cylinder pressure. The identification of this feature in both signals indicates to an extent the relative level of the presumed piston assembly/liner AE activity compared to that generated from other engine processes.

5.2.1.2 AE activity generated with cylinder head off

This Section investigates some propagation characteristics and the cyclic consistency of the distinct, continuous AE events observed when engine A was motored with the cylinder head removed and which were presumed to relate to the piston ring-pack/liner interfacial behaviour.

Examples of AE signals acquired during an engine cycle from a number of sensor positions on the cylinder block are shown in Figure 5.2. These were acquired from two sensor arrays, with the signals from cylinder 1 acquired separately from those relating to cylinders 2 and 3. All the signals show, to varying amplitudes, the four continuous AE envelopes generated during the engine cycle. Comparisons of signal amplitudes should

be valid since the same type of instrumentation was used, however, this cannot be confirmed as there remains the possibility of differences in sensor sensitivity and coupling quality. The cyclic consistency of the energy content of each signal is examined in Figure 5.3; it shows the angular-domain AE energy per cycle calculated using Equation 3.2 over 30 cycles of data. For each sensor position the amount of AE energy per cycle was generally consistent and the relative energy levels were in accordance with the signal amplitudes observed in Figure 5.2.

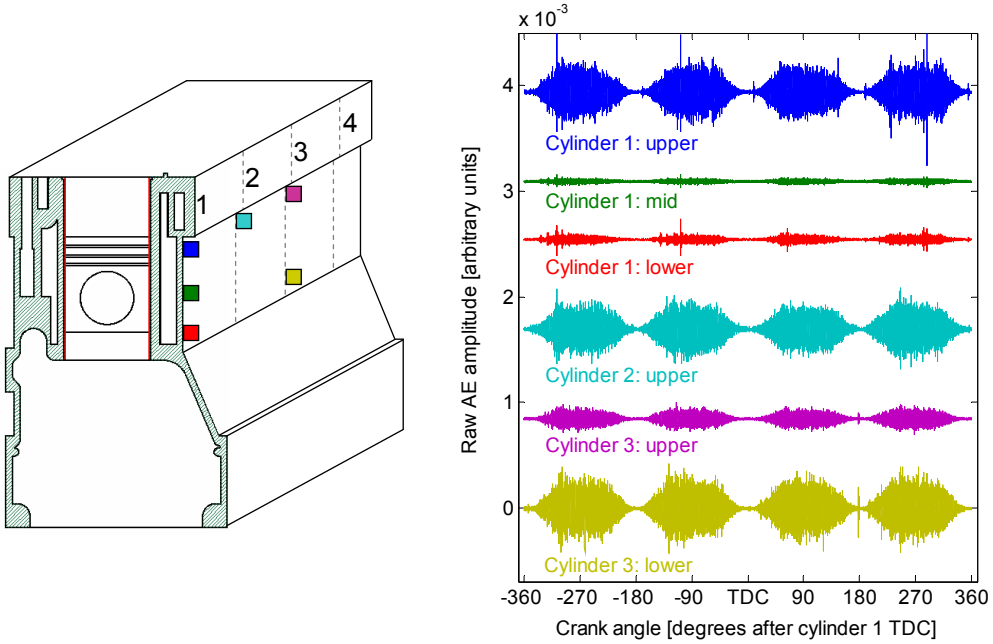

Figure 5.2: Engine A, raw AE signals acquired from sensor positions on the cylinder block over two sensor arrays.

Since the amplitude of the measured signal at each sensor position in Figure 5.2 is a function of the source intensity and the source to sensor AE transmission properties then, barring differences in sensor response as described earlier, the relative amplitude levels must be due to the differing transmission paths for each sensor. This also suggests that the differences in signal amplitude can be used to locate the source of the activity.

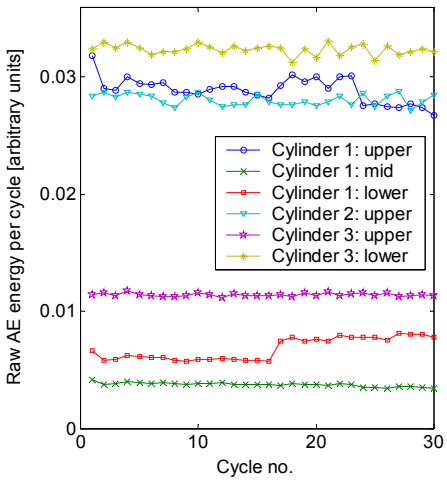

Figure 5.3: Engine A, AE energy per cycle.

However, there appears to be no consistent pattern of signal amplitudes with regards to sensor location on the cylinder block. For the case of signals acquired from the centre-

line of cylinder 1 the greatest AE levels are observed at the upper position, followed by the lower then the mid positions. This indicates that AE propagation from the liner to the external surface of the cylinder block occurs both above and below the water jacket. The upper position on cylinder 2 shows similar levels as the upper position on cylinder 1, however, this is not consistent for cylinder 3 as greater signal amplitudes are observed at the lower position than the upper. The inconsistent nature of the AE energy distribution means that there is little in the way of immediate deductions that can be made regarding the location of the source. This may have been expected given that the source appears to be related to an aspect of the ring-pack/liner interfacial behaviour. Assuming that AE generation from this interface is a normal characteristic, rather than fault related, then the ring-packs of all four cylinders would be sources of AE and therefore the AE signals at each sensor position would contain a contribution to varying extents from each.

To fully understand the AE measured at the sensor positions would be a considerable task. It would require knowledge of the complex, three-dimensional transmission properties of the cylinder block geometry and consideration of multiple, continuous, non-stationary sources of varying amplitudes. The cylinder block geometry is particularly intricate, it is not uniform (the cross-section shown in Figure 5.2 is only an example) and contains variations and discontinuities in thickness and surface curvature. It also includes internal webs which may aid or impede wave propagation to particular areas on the external cylinder block surface. AE transmission in this case will also be affected by propagation over material boundaries since engine A is dry-lined, i.e. thin-walled liners pressed into place. As a result the contact level between a liner's external surface and its housing within the cylinder block may vary both axially and circumferentially with consequential AE transmission discrepancies.

Developments towards understanding AE transmission in cylinder blocks and heads have been instigated by Nivesrangsan *et al* [152]. AE transmission characteristics were established through the use of Hsu-Nielsen sources and an array of sensors. This information was then used in conjunction with source location techniques to decompose a multisource signal from a running engine by reconstituting the individual signals attributable to the source events. However, the signals of interest were relatively strong, burst-type events originating from injector or valve activity; it is possible that this approach may not be transferable to the continuous, lower-amplitude AE activity arising

from the ring-pack/liner interface. A further novel method of determining AE attenuation in cylinder blocks is to estimate it through the use of 3D solid modelling and ray tracing techniques [219]. This has shown promising initial results with good agreement to experimental work.

5.2.1.3 Influence of piston sliding speed

Regardless as to whether or not the transmission properties of the cylinder block can be understood, further investigation of the signals is still constructive as it may reveal information about the factors which govern the amount of AE generated.

The consistency during the cycle of the continuous events proposed to relate to the ring-pack/liner interface is examined in Figures 5.4a and 5.4b for data acquired from the upper sensor positions of cylinders 1 and 3 respectively. These plots show the amount of AE energy generated per degree of crank rotation for 20 engine cycles. For both sensor positions the background activity was relatively consistent and there also occurred at consistent angular timings AE activity greater than the background level, these largely relate to transient, burst-type events.

Figures 5.4a and 5.4b also show information regarding the piston trajectory of the cylinder on which each sensor is located. The piston speed is shown above the main body of AE data whilst the direction of piston acceleration is inferred by colour, acceleration towards the crankshaft is defined as positive (red) and towards the cylinder head as negative (blue). The piston trajectories for cylinders 1 and 3 are essentially the same although the engine firing order dictates that the trajectory for cylinder 3 is 180 degrees out of phase from cylinder 1. The firing order further determines that cylinder 2 follows the same trajectory with cylinder 3, although 360 degrees out of phase in terms of the engine cycle, and similarly cylinder 4 and cylinder 1 are 360 degrees out of phase.

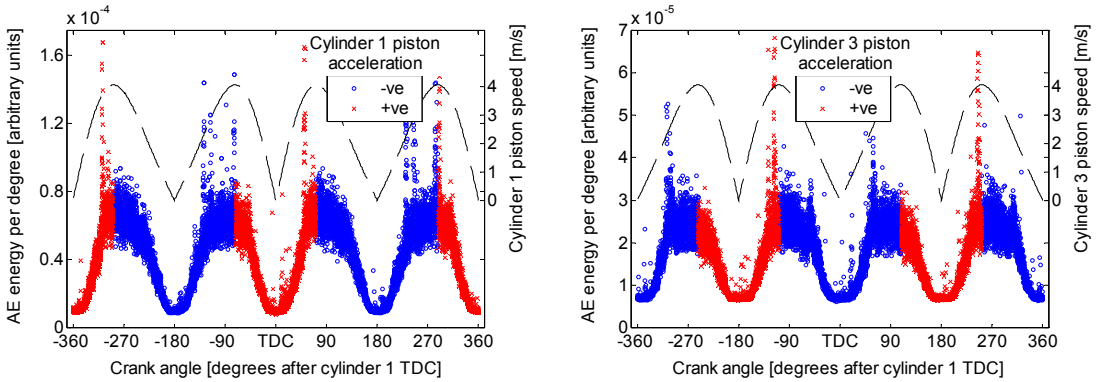

(a) *(b)*

Figure 5.4: Engine A, AE energy per degree for 20 cycles of data acquired from upper sensor positions on (a) cylinder 1, (b) cylinder 3.

The background AE activity would appear to be related to the piston sliding speed. This proposition is examined further in Figures 5.5a and 5.5b where the AE energy per degree is plotted against the piston velocity of the cylinder on which each sensor is located. Due to the four-stroke cycle strokes 1 and 3 follow the same motion and similarly strokes 2 and 4 are grouped together. These plots emphasise that AE activity is related to piston velocity. It is also clear that there is a distinction between the directions of piston acceleration; at a given piston velocity the AE energy is greater for acceleration towards the cylinder head (-ve) than towards the crankshaft (+ve). Figure 5.5 also suggests that the background AE activity is symmetrical about zero piston velocity indicating little difference between the piston upstroke and downstroke.

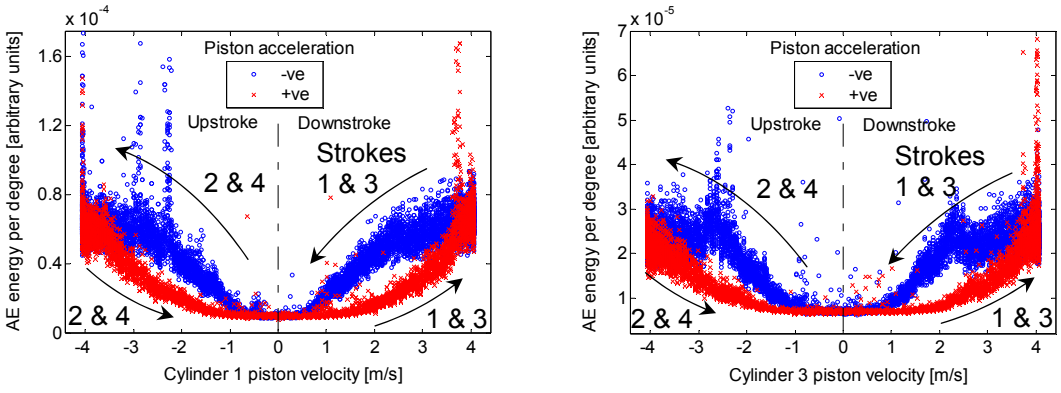

(a) *(b)*

Figure 5.5: Engine A, piston velocity versus AE energy for data acquired from the upper sensor positions on (a) cylinder 1, (b) cylinder 3.

The instances where the AE activity is greater than the background level, i.e. the burst-type events, are noted to occur at maximum piston speeds when the direction of piston acceleration changes and also at certain angles on the piston upstroke. The precise

source origins of these events are unknown. One possibility is that they occur due to disruption of the ring-pack/liner interface as the direction of piston acceleration changes; another is that they result from impacts caused by movement of the pushrod tappets.

There are also two possible explanations identified for the difference in the amount of AE generation between acceleration directions. Firstly, the direction of acceleration may impact upon the piston ring dynamics causing a change in the tribological behaviour and consequently a change in the AE generation properties. This is obviously dependant upon the AE generation being sensitive to changes in the ring-pack sliding contact behaviour, this has been proven in other applications, for instance, differing AE generation characteristics have been observed for different contact areas at the head-slider/disk interface in HDDs [191, 196]. This explanation is also further reliant upon the AE measured at the centre-line of a cylinder being dominated by the ring-pack/liner interaction in that particular cylinder.

The second explanation concerns cross-cylinder propagation. Taking cylinder 1 as an example, AE arising from the ring-pack/liner interfaces of cylinders 2 and 3, whose piston trajectories do not follow that of cylinder 1, will likely propagate to the sensor located on the centre-line of cylinder 1. Given the apparent relationship between piston speed and AE activity the effects of any cross-cylinder propagation will be most obvious when the piston velocities for cylinders 2 and 3 are greater than cylinder 1. The piston kinematics are such that these circumstances occur when the direction of cylinder 1 piston acceleration is towards the crank, i.e. negative in Figures 5.4 and 5.5. This therefore provides a plausible explanation for what seemingly appeared to be an acceleration related feature. The issue of cross-cylinder propagation is significant as it suggests that to achieve focussed monitoring of specific cylinders it may be necessary to develop spatial reconstitution techniques to decompose the signal into its constituent parts.

Considering that the AE measured at the centre-line of cylinder 1 will likely involve contributions from each of the four cylinders then the comparisons shown previously in Figures 5.4a and 5.5a which related AE activity to solely the motion of piston 1 are inaccurate. Rather, the AE data should be compared to a combination, to varying extents depending upon their relative influence, of all the piston motions. As described

previously, determination of each cylinders contribution would require knowledge of the complicated transmission properties of the cylinder block and of the source AE levels at each ring-pack/liner interface. The complexity of this task limits what can be achieved here and instead the mean piston speed of all four pistons is used as an approximation. This is shown in Figure 5.6a above the main body of the AE energy data corresponding to the upper sensor position on cylinder 1. No distinction is made between directions of piston acceleration since the objective in this case is to compare the AE activity with the overall piston speed characteristics. It is observed that the mean piston speed resembles more accurately the profile of the AE energy during the cycle than the individual cylinder 1 piston speed, which may imply that it offers a more realistic representation of the signal composition. Figure 5.6b shows a comparison of the mean piston speed against AE energy.

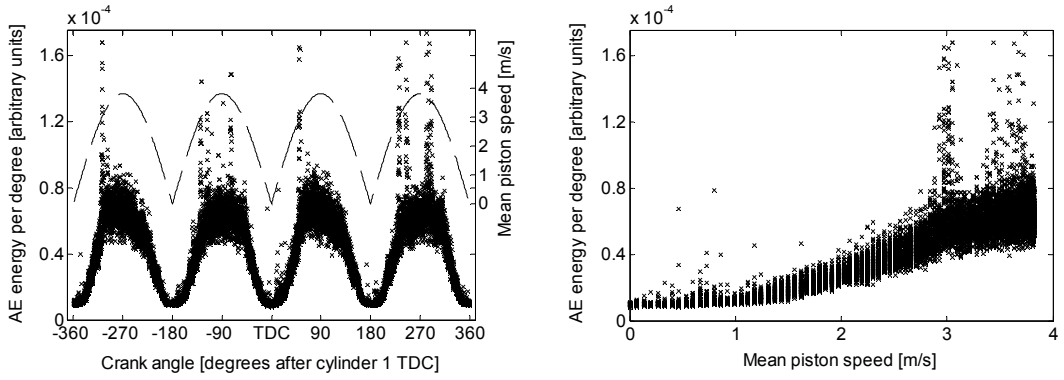

(a) *(b)*

Figure 5.6: Engine A, upper position on cylinder 1, (a) AE energy per degree for 20 cycles with mean piston speed shown, (b) mean piston speed versus AE energy.

The principal observations from motoring tests on engine A are that AE activity does appear to be generated from the ring-pack/liner interface and that the selection of sensor position greatly affects the measured strength of this activity. The identification of the ring-pack/liner interface as an AE generating source within four-stroke engines is, to the author's knowledge, a new finding not reported elsewhere in the literature. Furthermore, it has also been established that for this activity there is a relationship between piston sliding speed and the amount of AE generated. This is consistent with findings reported previously from AE monitoring of sliding contact in other applications such as materials testing [172] and the head-slider/disk interface in HDDs [182-184].

5.2.3 Engine D

A further motored engine was investigated in order to evaluate the repeatability of the findings from engine A. Figure 5.7 shows an example of raw AE measured from the cylinder barrel of engine D, the small, single-cylinder, two-stroke engine. During one cycle, i.e. one crank revolution, two envelopes of continuous AE are evident and similarly to the motored four-stroke engine these occur at the piston mid-strokes. Additional burst-type events occur at precisely TDC and BDC and are assumed to arise from impacts between the piston and cylinder barrel due to the directional change of the piston, i.e. piston slap. Similar events, although of a far lower relative amplitude when compared to the mid-stroke AE, were observed in some signals acquired from engine A. The relative strength of these events for engine D may simply be a reflection of the lesser precision of this engine and increased clearance at the ring/liner interface.

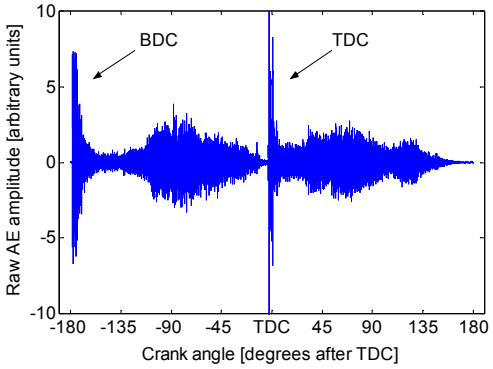

Figure 5.7: Engine D, example of raw AE during a cycle.

Similar analysis as to that of the motored, four-stroke engine was conducted on the AE data acquired from engine D. The consistency of the cyclic AE activity over 20 cycles is shown in Figure 5.8a, and again the piston speed is shown above the main body of AE data and direction of piston acceleration is inferred by colour. A comparison between piston velocity and AE energy is given in Figure 5.8b.

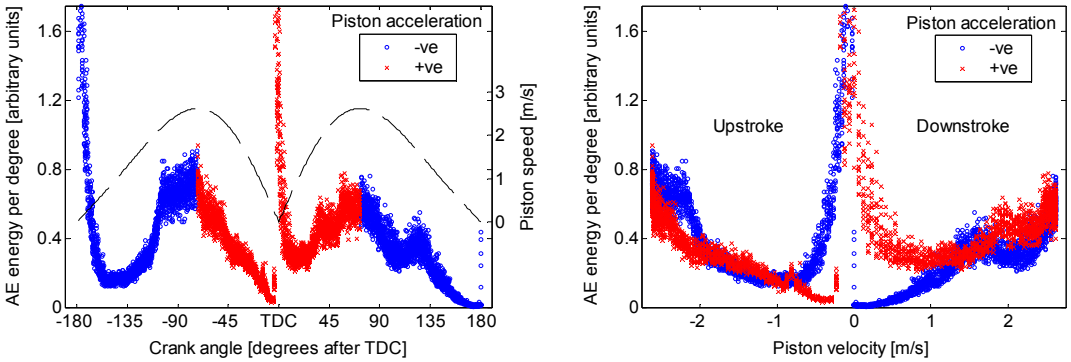

(a) *(b)*

Figure 5.8: Engine D, (a) AE energy per degree over 20 cycles, (b) AE energy versus piston velocity.

This analysis supports the findings from engine A in that the AE activity is consistent on a cyclic basis and the amount of the mid-stroke continuous activity proposed to relate to the ring/liner interface increases with piston speed. One difference is that there is no apparent distinction in the levels of AE activity between the directions of piston acceleration. This strengthens the argument that for engine A cross-cylinder propagation was responsible for the difference in AE activity between acceleration directions.

5.3 Running, four-stroke engines

Whilst the observations from the motored engine tests give an indication as to the characteristics of AE generation from the ring-pack/liner interface they also invite an element of doubt as a motored engine represents an unrealistic operating condition. Therefore, tests were conducted on running, four-stroke engines to assess whether similar features were present under normal conditions. This primarily involved experimentation on a wet-lined, HSDI, diesel engine, engine B in Table 4.1, and consisted of preliminary tests, a series of tests over the engine operating range and tests as the engine warmed from ambient conditions. Data were also acquired from another four-stroke engine, engine C in Table 4.1, in order to further evaluate AE generation from the ring-pack/liner interface.

5.3.1 Engine B

5.3.1.1 Identification of AE activity relating to the ring-pack/liner interface

Figure 5.9 shows raw AE signals acquired from sensors located on the cylinder 1 fuel injector and directly below on the cylinder block of engine B operating at 800 RPM and with no load applied. The signals are evidently quite different; the injector signal consists of a series of burst-type events whilst the signal from the cylinder block surface contains burst-type activity and also a further continuous component.

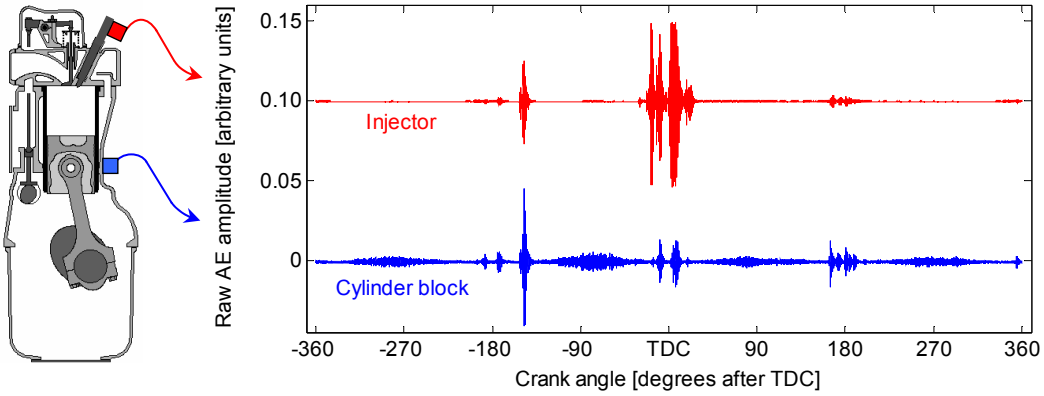

Figure 5.9: Engine B, AE signals acquired from the fuel injector and cylinder block.

Unsurprisingly, the strongest events in the injector signal are observed at around TDC and are assumed to relate to operation of the injector and consequent fuel combustion. AE generation during the injection process, although for the case of large, two-stroke engines, is considered further in Chapter 6. Additional burst-type events in the injector signal occur at around the other dead-centres; these have typically been found by other researchers to be associated with valve activity and the injection processes of other cylinders [153].

The burst-type events around TDC are also present in the signal acquired from the cylinder block, although the amplitudes are considerably lower. This is consistent with findings by Nivesrangsan [152] who reported that there was generally a significant reduction in AE energy over the head to block interface and that propagation via the cylinder bolts was the principal means for this transmission. Importantly, the cylinder block signal also contains the continuous events at around the piston mid-strokes that were observed previously from the motored engine tests and were proposed to originate from the ring-pack/liner interface. For these events there again appears to be a correlation between the amount of AE activity and piston velocity in that maximum amplitudes occur at around the mid-strokes, this characteristic shall be investigated more fully in the following Section.

5.3.1.2 Variation of ring-pack/liner AE activity over engine operating range

Data were acquired over the operating range of engine B from a sensor located on the centre-line of cylinder 1 on the cylinder block surface. The loading points used provided a series of datasets whereby either the engine speed or applied torque varied

and the other remained approximately constant. Data were acquired first at constant speeds with torque incrementally increased and then from further loading points to fill the matrix and allow comparisons over varying engine speeds. These tests are described more fully in Section 4.4.3 and by the matrix of speed/torque permutations given in Figure 4.18, and can be summarised as:

Minimum applied torque with varying speed from 800 to 2000 RPM
Constant torque of 25 Nm with varying speed from 800 to 1600 RPM
Constant torque of 100 Nm with varying speed from 800 to 1600 RPM
Constant speed of 800 RPM with varying torque from minimum to 125 Nm
Constant speed of 1000 RPM with varying torque from minimum to 150 Nm
Constant speed of 1600 RPM with varying torque from minimum to 175 Nm

5.3.1.2.1 Tests with constant torque and varying speed

Examples of raw AE measured during an engine cycle at four engine speeds with minimum possible torque applied are shown in Figure 5.10. In these examples the AE activity generally increased with engine speed, both for the burst-type events thought to originate from injector and valve activity and the continuous mid-stroke activity presumed to relate to the ring-pack/liner interface.

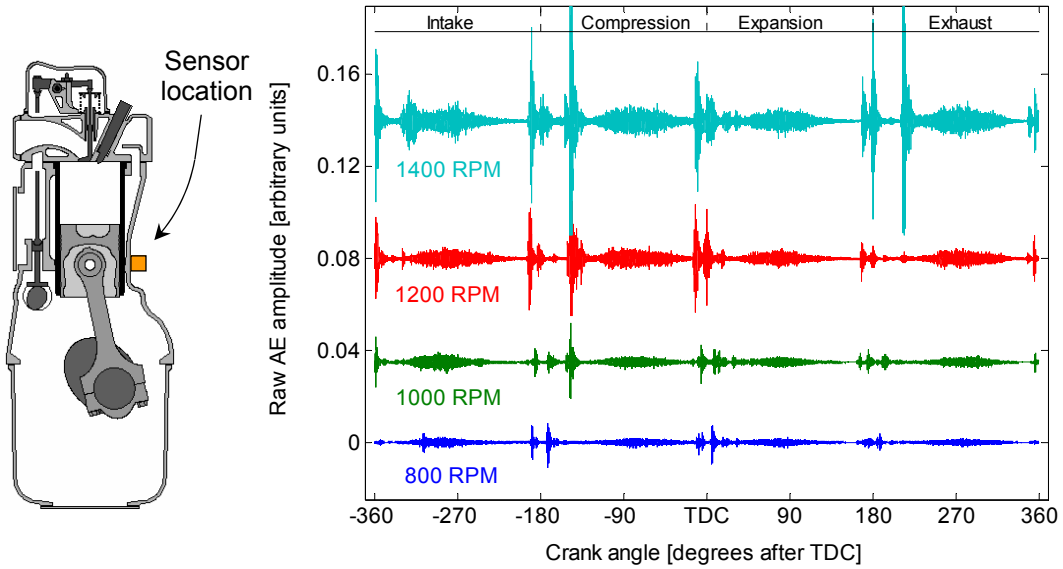

Figure 5.10: Engine B, example cycles of AE from four speeds with minimum applied torque load.

A more reliable representation of the change in AE activity over the full range of the minimum torque and varying speed dataset is given in Figure 5.11 as it shows the mean RMS AE signals of the 40 cycles acquired at each engine speed. Again, the amount of mid-stroke AE activity is observed to increase with speed. The influence of the burst-type events also increases with speed, due in part to the amplitude of the events, but also because the event decay period occurs over greater angular durations with increasing engine speed.

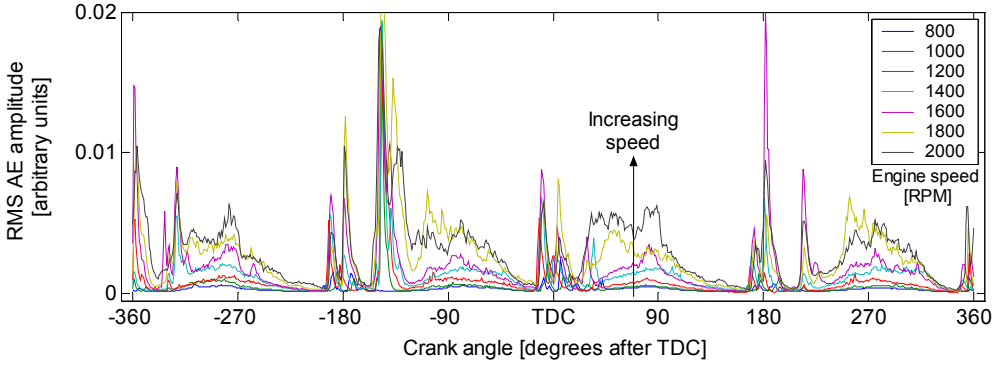

Figure 5.11: Mean RMS AE signals from minimum torque, varying speed dataset.

The relationship between piston sliding speed and mid-stroke AE activity is investigated in Figures 5.12 and 5.13. The former shows an example of raw AE acquired at 1200 RPM with minimum load applied and also the piston speed for cylinder 1 during the cycle. The profile of the mid-stroke AE appears to correlate well with the piston speed. Furthermore, the correlation to cylinder 1 piston speed is better than that which could be achieved with the mean engine piston speed. A simplistic means of identifying this is that the mid-stroke AE events are grouped closer together around TDC than BDC. This parallels the development of cylinder 1 piston speed during the engine cycle and suggests that the mid-stroke AE at this sensor position was dominated by the ring-pack/liner source in this cylinder.

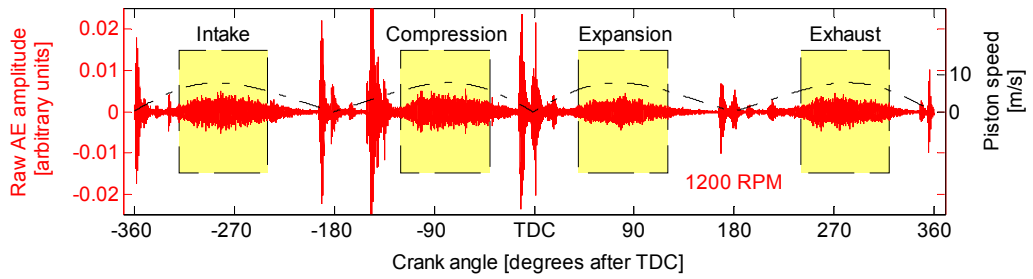

Figure 5.12: Raw AE activity at 1200 RPM with minimum load applied, piston speed shown above AE data and angular windows for each stroke identified.

Figure 5.13 further examines the relationship between piston sliding speed and AE energy. The AE energy per degree for the mean AE signal from each engine speed is shown against the corresponding piston sliding speed. Over all engine speeds the baseline energy level follows a very consistent trend. This is similar to the findings from tests on the motored engines, although in this case there is a greater amount of AE activity above the baseline level. This is to be expected given the presence of burst-type events originating from other sources. The range of the baseline energy also increases with engine speed which simply indicates that at greater speeds the mid-stroke AE activity is less cyclically consistent.

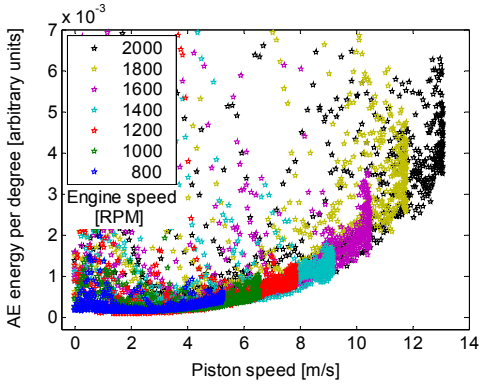

Figure 5.13: Engine B, minimum torque and varying speed, AE energy per degree versus piston speed.

A further method of examining changes in the mid-stroke AE activity is to compare the AE energy in selected areas of the cycle which contain predominantly continuous AE activity. Such angular windows were selected for each piston stroke as indicated in Figure 5.12. Each window is identical in terms of the mid-stroke area on the liner that it relates to, and therefore, the piston sliding speeds during the windows are equal and the amounts of AE energy generated are comparable over the different strokes.

For the minimum torque and varying speed dataset the AE energy in each window is shown in Figure 5.14, the error bars at each value indicates the standard deviation of the energy over each batch of 40 cycles. As expected considering the previous analysis the AE energy contained in each window increases with speed. The only exception to this is the compression and exhaust strokes which show a small drop in energy when engine speed was increased from 1800 RPM to 2000 RPM. Since these are both piston upstrokes this tenuously suggests that stroke direction is a factor. Asides from this feature there is generally little difference between each stroke although for the majority of the speed range the energy is greatest for the

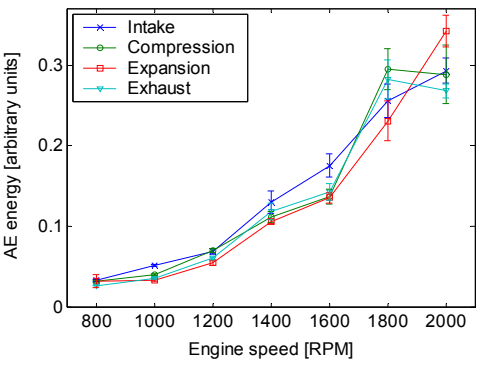

Figure 5.14: Engine B, minimum torque and varying speed, AE energy in windowed areas versus engine speed.

intake stroke and least for the expansion stroke. As identified previously the range of the AE energy over the 40 cycles at each operating point increases with speed.

Similar analysis is provided for the constant load and varying speed datasets at 25 and 100 Nm. Figure 5.15a shows mean RMS AE signals for the 25 Nm data whilst Figure 5.15b shows the AE energy in each windowed stroke. Likewise, Figures 5.16a and 5.16b relate to the 100 Nm data. For both datasets the AE energy generally increases with speed, although it would appear that with load applied this relationship is not as consistent as was observed from the minimal load data. In both cases the values for 1200 RPM are greater than would be expected given the overall trend and the relationship cannot be examined over the full engine range since data were not available for the higher engine speeds. For all operating conditions considered the expansion stroke consistently shows the lowest AE energy levels.

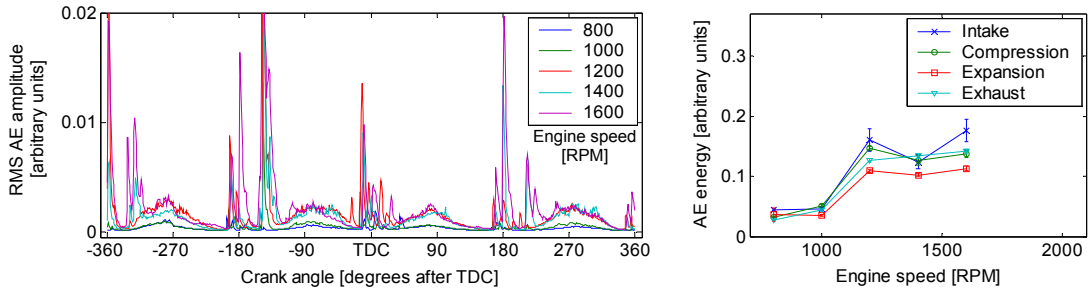

(a) *(b)*

Figure 5.15: Constant torque of 25 Nm and varying speed, (a) mean RMS AE signals, (b) AE energy in windowed areas of each stroke versus engine speed.

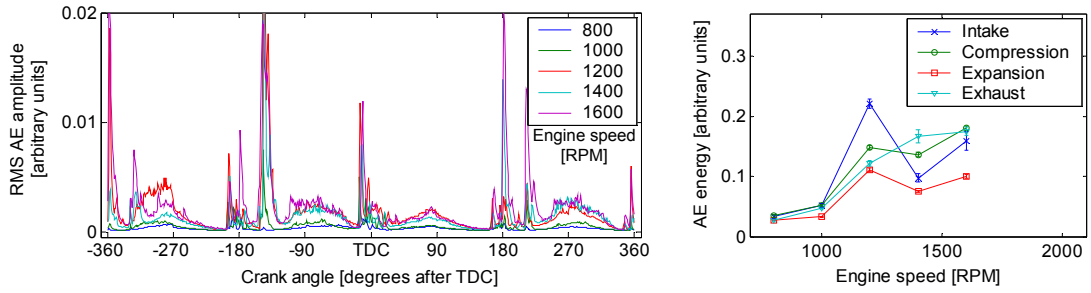

(a) *(b)*

Figure 5.16: Constant torque of 100 Nm and varying speed, (a) mean RMS AE signals, (b) AE energy in windowed areas of each stroke versus engine speed.

5.3.1.2.2 Tests with constant speed and varying torque

Similar analysis was conducted on the data from the constant speed and varying torque tests. Mean AE signals for each load at 800 RPM are shown in Figure 5.17a; these are presented on the same scale as signals from the previous tests to allow straightforward comparisons. With increasing load there is little difference in the amount of mid-stroke AE activity, this is further indicated in Figure 5.17b which shows the AE energy in the windowed areas of each stroke

The signals for the 1000 RPM data and the windowed AE energy per stroke are shown in Figures 5.18a and 5.18b respectively. Again, there is little variation in mid-stroke activity with increasing torque load, although the energies are slightly greater than the 800 RPM data. For the 1600 RPM test, Figure 5.19, the energies are greater still and they remain relatively constant over the load range, albeit with greater variance than the lower speeds. In this case, the compression and exhaust strokes show the same characteristics which again suggests that a factor in the AE generation is the direction of piston stroke. Similarly to the varying speed tests the expansion stroke is observed to generate the lowest amount of AE activity during both the 1000 and 1600 RPM tests.

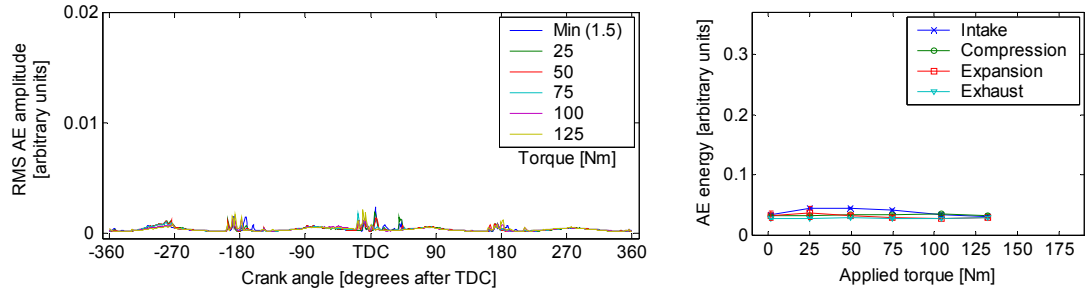

(a) *(b)*

Figure 5.17: Constant speed of 800 RPM and varying torque, (a) mean RMS AE signals, (b) AE energy in windowed areas of each stroke versus engine speed.

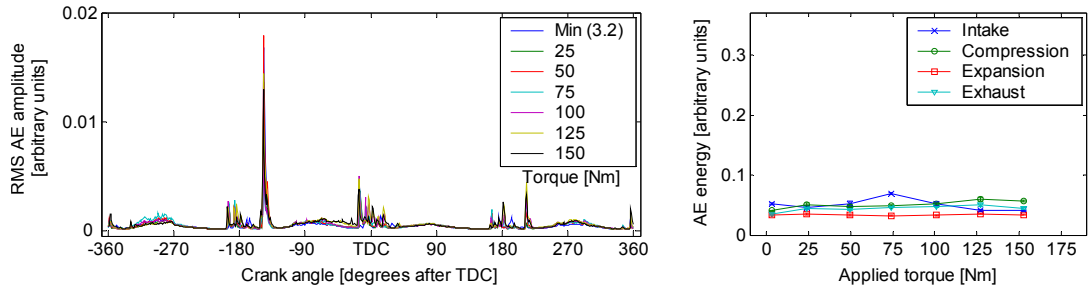

(a) *(b)*

Figure 5.18: Constant speed of 1000 RPM and varying torque, (a) mean RMS AE signals, (b) AE energy in windowed areas of each stroke versus engine speed.

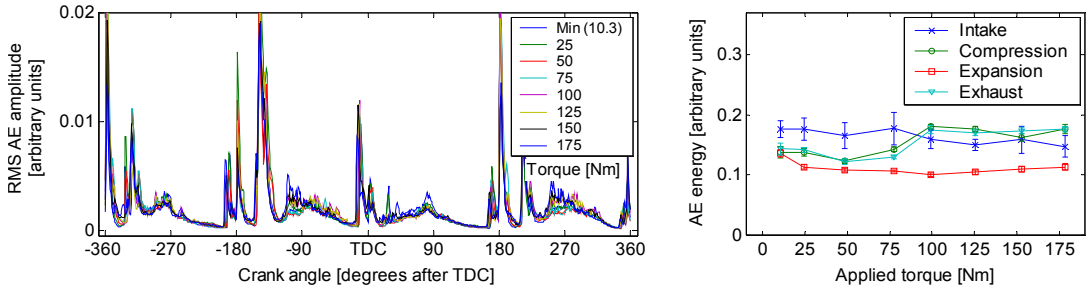

(a) *(b)*

Figure 5.19: Constant speed of 1600 RPM and varying torque, (a) mean RMS AE signals, (b) AE energy in windowed areas of each stroke versus engine speed.

5.3.1.2.3 Comparison of all data

For each stroke the results from both sets of tests can be combined in a single plot so to provide an overall review of the characteristics of the mid-stroke AE activity over the engine operating range. The AE energy in the windowed areas for each cycle of data is shown against applied torque in Figures 5.20a, 5.20b, 5.20c and 5.20d for the intake, compression, expansion and exhaust strokes respectively, with engine speed differentiated by colour.

These plots reinforce the observations made previously, with AE activity generally increasing with speed and remaining approximately constant with load. There are exceptions, particularly some data acquired at 1200 and 1400 RPM which do not agree completely with the overall characteristics.

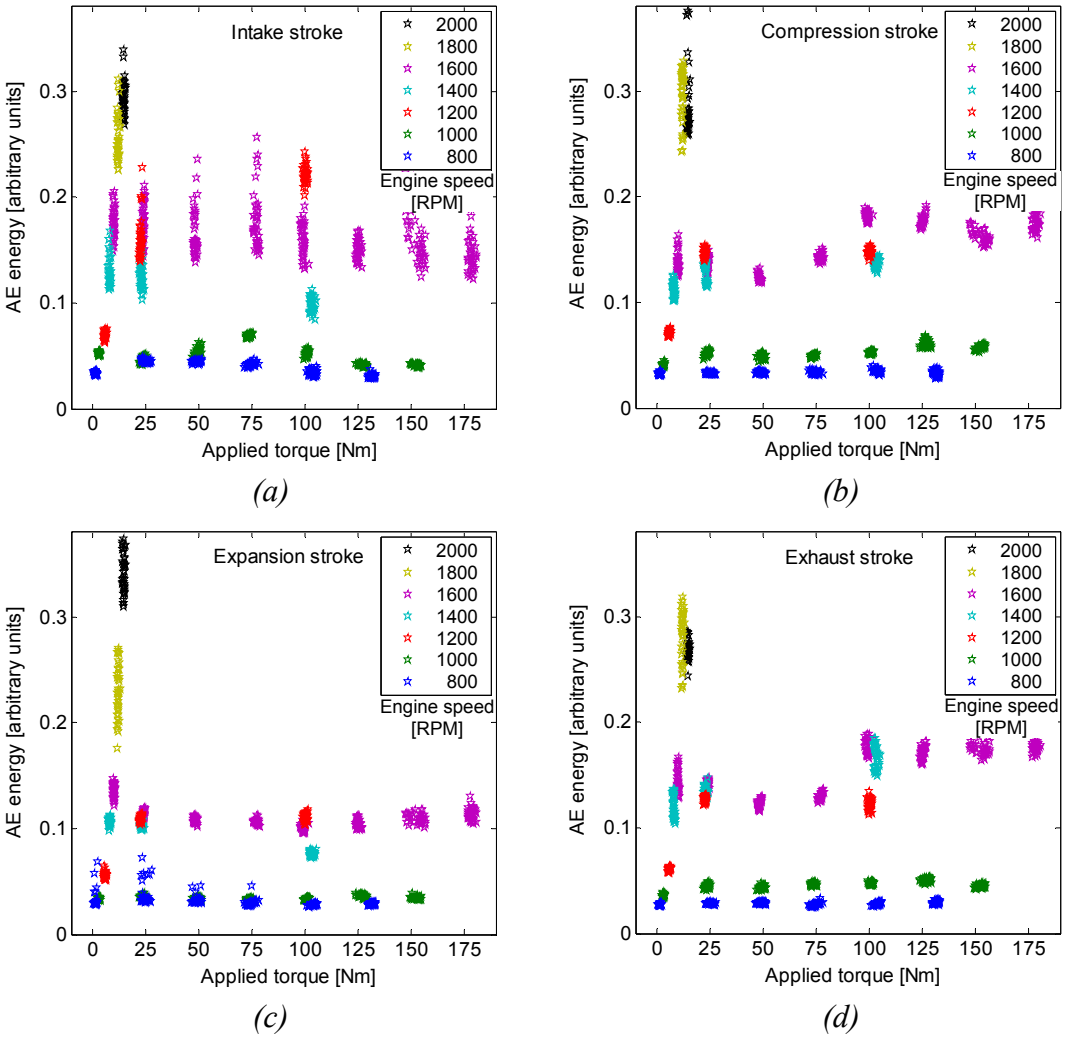

Figure 5.20: Engine B, windowed AE energy in each stroke with varying speed and torque, (a) intake, (b) compression, (c) expansion, (d) exhaust.

5.3.1.3 Variation of ring-pack/liner AE activity as engine warmed up

Variance of the mid-stoke AE activity believed to relate to the ring-pack/liner interface was investigated for engine B warming up from ambient conditions. Two tests were conducted, for both raw AE data were acquired intermittently for over 35 minutes with the engine operated at 1200 RPM and with minimum torque applied. Further details regarding these tests were given in Section 4.4.5.

The AE energy per cycle during the first test is shown in Figure 5.21a with the windowed AE energy for each stroke shown individually in Figure 5.21b (windows as identified previously in Figure 5.12). Due to problems with the instrumentation AE data were not acquired until two minutes after the engine was started. For both plots the

increase of the sump oil temperature with time is also shown. However, the cyclic and individual AE energies within each stroke do not show any particular trends that correspond to this increase of temperature. The cyclic AE energy initially increased and thereafter remained relatively constant with a small degree of fluctuation. The energy contained in the individual strokes fluctuated more, particularly the intake stroke which showed a peak at the start at the test.

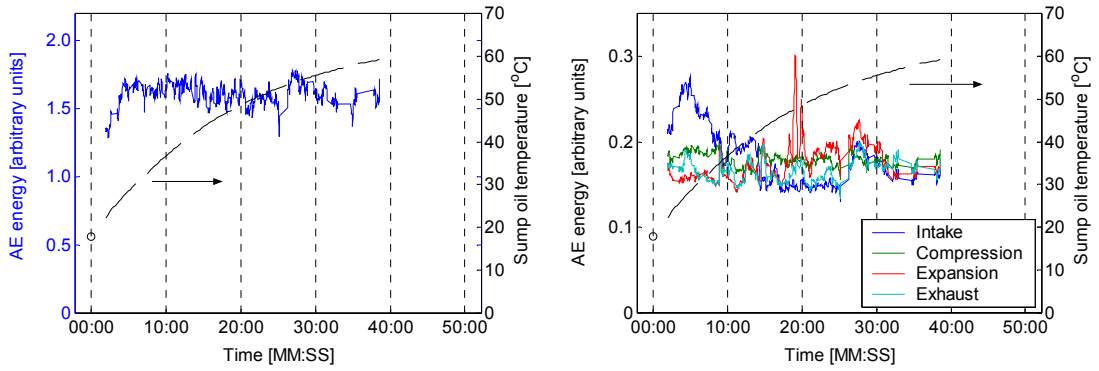

(a) *(b)*

Figure 5.21: Engine B, first warming up test, (a) total cyclic AE energy, (b) AE energy in windowed areas of each stroke.

The set-up for the second test was identical although the engine was run for a longer period and data were acquired from 45 seconds after the engine was started. The total cyclic AE energy and the energy content of each windowed stroke are shown in Figures 5.22a and 5.22b respectively. These results are different from the first test in that there is generally a slow reduction in the cyclic AE energy as the engine warmed up. The AE energy in the individual strokes shows a similar slow reduction although with a greater initial decrease in activity in the first few minutes of the test.

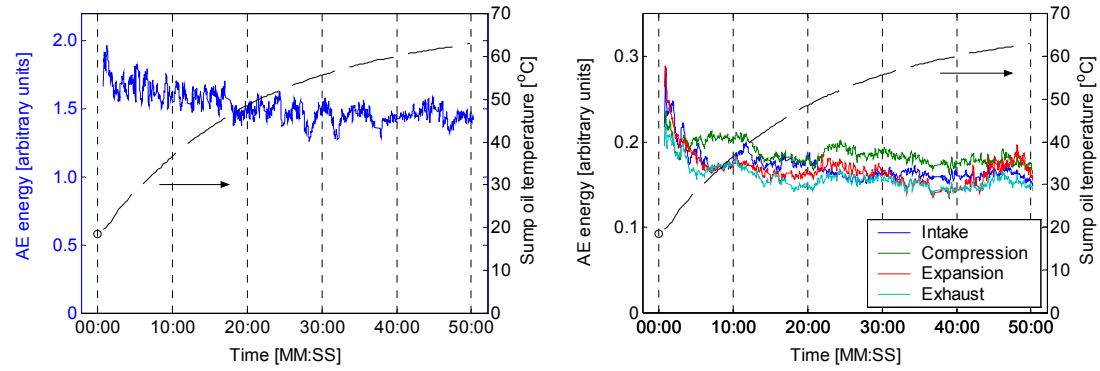

(a) *(b)*

Figure 5.22: Engine B, second warming up test, (a) total cyclic AE energy, (b) AE energy in windowed areas of each stroke.

5.3.2 Engine C

Measurements were also acquired from a further four-stroke, diesel engine, engine C, immediately after it had been completely overhauled. All piston assembly components were new and the cylinders were re-bored and finished to the same specification, in terms of surface topography, as a new engine. Consequently, during the period when the AE signals were acquired, i.e. the first minutes of operation, an increased amount of wear would be expected as the major asperities are removed and the components begin to conform to each other. The engine featured cylinder bores integral to the cylinder block and therefore it would be expected that AE transmission between the internal cylinder bore and the external block surface would be more favourable than in engines A and B since there would be no losses incurred due to transmission over material boundaries.

Raw AE data corresponding to just over one engine cycle are shown in Figure 5.23 for AE sensors located on the centre-lines of two cylinders on the block and from the base of an ancillary, crank-driven, reciprocating compressor. For these measurements the engine was run at low idle conditions at approximately 750 RPM with minimal torque load applied. No shaft encoding was available hence the data is shown in time-domain format, although the duration of an engine cycle is indicated.

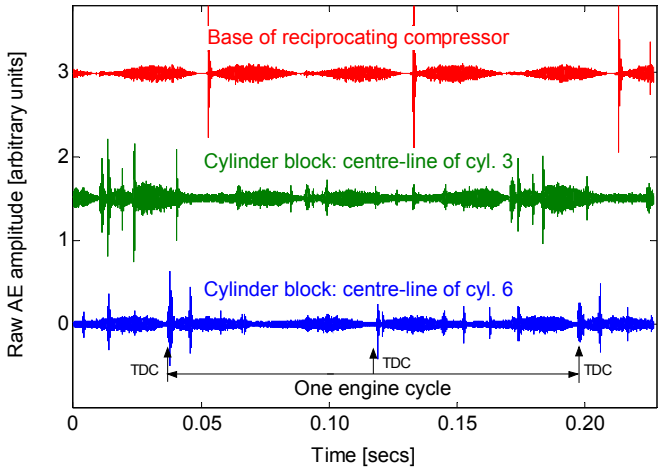

Figure 5.23: Engine C, raw AE signals acquired for just over one engine cycle.

The signals acquired from the two positions on the cylinder block are again composites of burst-type events and continuous background components. Similar to engines A and B the continuous components fluctuate and during one engine cycle four envelopes are discernible in both signals which are presumed to relate to the ring-pack/cylinder bore

interface. Through the relative location and profile of these envelopes, and the relationship established previously between piston speed and AE activity, an estimation of TDC can be made for each cylinder, as indicated in Figure 5.23 for the signal acquired from the centre-line of cylinder 6. However, the continuous components are not as clear as was observed from engine B. This is likely due to engine C comprising of six cylinders and the motion of each piston being at multiples of 120 degrees out of phase with each other rather than 180 degrees as was the case for the four-cylinder engine B. The implication of this is that at any point in the engine cycle there are at least four pistons moving, and thus four AE sources which may obscure the profile of mid-stroke AE activity from the cylinder under scrutiny. That AE activity relating to one cylinder can be distinguished in each signal suggests that in these examples the AE activity measured at a cylinder centre-line is dominated by piston movement in that cylinder.

The signal from the reciprocating compressor clearly displays the continuous events relating to the compressor piston strokes with a further burst-type event occurring consistently at one of the piston dead-centres. Asides from these events there is little other AE which indicates minimal propagation from the adjoining cylinder block.

5.4 Discussion of possible AE source mechanisms

The results presented in this Chapter have shown that AE signals acquired from the cylinder blocks of small engines contain continuous-type AE events occurring at around the piston mid-strokes which are believed to originate from the ring-pack/liner interface. This activity appears to be a normal characteristic of the overall AE generation as it has been observed consistently from engines of differing sizes and also from engines which feature different forms of cylinder bores; dry-lined, wet-lined and integral to the cylinder block.

This continuous mid-stroke AE activity was identified initially in measurements from a motored engine where measures had been taken to isolate the ring-pack/liner interface from other known AE sources. Testing of running engines confirmed that these events were also present under normal operating conditions. A correlation was identified between piston speed and the amount of AE activity generated, whilst tests over

increasing load at constant speeds had relatively little effect. Tests on an engine started from ambient conditions investigated the effects of increasing oil temperature, hence reduced oil viscosity. However, the results were inconclusive, although it has been noted in previous work that measurement of bulk oil temperature from the sump may bear little relation to conditions at the ring-pack/liner interface [94].

In summary, it appears that an aspect of ring-pack operation is represented in the AE signals, thereby implying that this feature can be monitored to provide information about changes in interfacial behaviour. To evaluate the capabilities of this monitoring opportunity a greater understanding is required of the source mechanism(s) of the mid-stroke AE activity. This necessitates a more detailed interpretation of the experimental results. However, this is problematic as in these tests there were no other parameters acquired which would describe ring-pack behaviour and could be used towards a comparative analysis. This is representative of the overall problem, i.e. there are no simplistic means of evaluating ring-pack behaviour in running engines. The remaining option is to compare the experimental evidence against typical ring-pack/liner interfacial behaviour, as ascertained from experimental and modelling work by other researchers. Although this approach may provide an indication as to the likely AE sources it is limited in that the outcomes cannot be validated.

A brief review of experimental and modelling work on ring-pack behaviour has been given in Section 2.4.5. The dynamics of the contact area are complex, emphasised by the number of factors which may bear influence, including amongst others; piston motion (both primary and secondary), gas pressures, ring twist motions, ring end gap effects, elastic and thermal deformations, component condition, and lubricant characteristics and availability [63, 64]. The result is that there are a number of possible source mechanisms of continuous AE activity, primarily consisting of asperity contact, blow-by and hydrodynamic lubrication sources.

It has been established that compression rings benefit from full-film lubrication throughout most of the cycle, the exceptions being at around the dead centres where piston velocities and thus oil entrainment velocities are close to zero. Considering this, the possibility of asperity contact between compression rings and liner as the source of the mid-stroke AE activity would appear unlikely since at these positions the hydrodynamic effect and thus ring/liner separation would be at a maximum. However,

this possibility cannot be discounted entirely due to circumstances such as oil starvation and particulate contamination. Further evidence against compression ring asperity contact as the source of the mid-stroke AE source is that the AE activity remained relatively constant when load was increased at constant engine speeds. This is not what would be expected if the source were asperity contact as previous work on monitoring of interfacial behaviour has indicated that AE activity increases with load due to the increasing severity of asperity contacts [172].

It is possible that phenomena relating to hydrodynamic lubrication of the compression rings and resulting viscous friction are responsible for the mid-stroke AE activity. This is consistent with the relationship identified between AE activity and sliding speed since oil-film thickness increases with speed, whilst an increase in gas-sealing pressure, as in the constant speed, increasing torque test, would not have as significant an effect. Within the hydrodynamic lubrication process the convoluted oil flow characteristics results in possible AE generating sources such as turbulence, oil shear, and oil film cavitation. However, prior work which has considered AE monitoring of sliding contact has found that as lubrication tends towards full-film conditions the resulting AE activity reduces to the noise floor of the DAQ equipment [170, 177]. This suggests that the processes within hydrodynamic lubrication are unlikely to be the principal AE source, although there remains an element of doubt as to the transferability of findings from relatively simple tribological set-ups to the complexity of a piston ring-pack.

A further possibility is that the mid-stroke AE activity is related to operation of the oil-control ring. Modelling and experimental work has indicated that this ring behaves differently to the compression rings; it has been identified, although not universally agreed, that the narrow rails of the oil-control ring cannot generate sufficient hydrodynamic load carrying capacity and therefore mixed lubrication conditions exist for the majority of the piston stroke [65]. Mixed lubrication implies that a proportion of the load acting on the ring is supported by asperity contact and given that the material deformations occurring during such contact have long been established as an AE source then this represents a credible source mechanism of the mid-stroke AE activity.

With boundary or mixed lubricating conditions there may be a relationship between the factors which govern the tribological behaviour and the amount of AE generated. This has been investigated in previous work on applications such as fundamental materials

testing [168-181], the head-slider/disk interface in HDDs [182-198] and the meshing of gears [202-204]. Attempts have been made to correlate AE activity to various parameters of friction and wear. Most successful have been those which have related AE activity to the frictional work or frictional power loss due to asperity contact at the interface, two major factors of which are the relative sliding speed and the applied load.

The experimental evidence is consistent with a relationship between mid-stroke continuous AE activity and power loss due to boundary friction. The amount of AE activity was observed to be highly dependant upon piston speed, both during the engine cycle and over the constant load, varying speed test. The observation that AE activity varies with piston speed during the cycle is significant as it infers that it relates to the frictional power loss rather than the friction force. This possibility is further corroborated by the predicted frictional power losses of each ring during an engine cycle shown in Figure 2.30c [65]. The loss attributed to the oil-control ring at around the piston mid-strokes is evidently related to piston speed and is therefore very similar to the profile of the continuous AE activity.

Furthermore, modelling of ring behaviour over increasing load at constant speed [65] indicated that the loading on the oil-control ring was independent of the in-cylinder pressure since the ring was vented to the crankcase, i.e. the load was mostly due to ring tension. Therefore, unlike the compression rings, the frictional losses attributable to the oil-control ring would remain constant with load, as shown in Figure 2.31b. The experimental results parallel this behaviour with mid-stroke AE activity varying little during the constant speed, varying load tests. This further supports the proposition that the mid-stroke AE was indicative of asperity contact and boundary frictional losses at the oil-control ring/liner interface.

Blow-by is a further AE source possibility that would be expected to generate AE of a continuous nature. However, if this source were active it would be most evident when large pressure differences exist over the rings, i.e. at around TDC on the compression and expansion strokes, and not at mid-stroke every stroke. Therefore, blow-by is considered unlikely to be the source mechanism. The piston skirt represents a further possible source, and accounts for a significant proportion of total piston assembly friction, estimated at approximately 30 % [61], but under normal conditions at mid-strokes it would be expected to operate under full-film lubrication [220].

Of the potential AE sources a comparison of the experimental evidence to the expected ring-pack behaviour indicates that asperity contact at the oil-control ring/liner interface offers the most reasonable explanation for the mid-stroke AE activity. If this could be verified then this would represent a significant monitoring opportunity. The oil-control ring has been estimated as responsible for between 50% and 75% of total ring-pack friction [62], hence, a technique which can provide a qualitative measure of the frictional losses may prove useful in developmental work aimed at minimising these losses.

Since the AE signals appear to contain information about asperity contact at mid-strokes then there may also be information available regarding continuous interaction at around the dead-centres. It is in these regions, particularly around TDC, that the majority of liner wear occurs due to asperity contact between compression rings and the liner. In the example signals given in this Chapter for diesel engines there was no significant continuous AE activity at around TDC. This is consistent with the notion that continuous AE activity is related to frictional power loss since the piston speed reduces to zero around the dead-centres. On the other hand, it may simply reflect that there was little continuous asperity contact at around TDC in the engines tested. There is also the possibility that some of the burst-type events occurring at around TDC may be related to interaction at the ring-pack/liner interface, as was observed in signals acquired from the small, motored engine D and the ancillary compressor of engine C.

A further consideration is that, with regards to monitoring ring-pack/liner interaction within engines A and B, there are likely more informative AE signals available from the external surfaces of the liners as this would minimise transmission losses inherent to signals acquired from the cylinder block. For both engines there may be problems to overcome regarding access to the appropriate surface, isolation of the sensor from the engine water jacket and disruption of the liner cooling, although these issues have not overly inhibited the application of other intrusive liner instrumentation in other engine experimental work [95-97].

5.5 Summary

Tests conducted on small, four-stroke, diesel engines have established for the first time that AE activity is generated at the ring-pack/liner interfaces within these engines. AE events of similar characteristics occurring at the piston mid-strokes were consistently observed in signals acquired from all of the engines tested. Analysis of signals from motored engines identified a relationship between piston speed and AE activity and also showed that sensor position could greatly affect the measured AE parameters. Experimentation on running engines verified that these observations applied for normal operating conditions and also allowed the variation of the ring-pack/liner AE activity to be ascertained over the engine operating range.

The observations from the experimental work were then compared to knowledge of typical ring-pack behaviour and of AE monitoring of other tribological processes in order to gain understanding of the source mechanism of the mid-stroke activity. A number of possible sources were considered with the most likely determined to be asperity contact and boundary friction at the oil-control ring/liner interface. The ability to monitor boundary frictional losses may prove useful in engine developmental work, although doubts remain over the ability to monitor specific cylinders of a multi-cylinder engine. This would benefit from a greater understanding of the cylinder block transmission properties and the application of more advanced spatial location techniques.

The observations and findings developed in this Chapter will be compared to results from testing on large, two-stroke engines in order to arrive at a more general assessment of the potential for AE monitoring of ring-pack/liner interaction.

Chapter 6

Two-stroke, crosshead, diesel engines: survey of AE generation

6.1 Introduction

This Chapter investigates AE generation within large, two-stroke diesel engines, engines E and F in Table 4.1, under normal operating conditions. The main objectives are to characterise the AE signals and to establish the physical meaning of the various signal components as this ultimately determines the aspects of engine operation which can be monitored. This involves identifying the sources of the major AE events through information gained from sensor arrays and mapping of the AE signals against the processes occurring during the engine cycle. This task is somewhat simpler for these large engines than the smaller engines considered in Chapter 5 as AE transmission between cylinders is severely attenuated due to the relatively large distances and significant material boundaries. Steel and Reuben [6] have reported attenuation levels between cylinder heads on engine E of between 35 to 40 dB, therefore, AE signals acquired from the upper area of a cylinder are likely to relate only to operation of that cylinder.

Figure 6.1 shows example raw AE signals acquired from sensor positions on one cylinder of engine E during an engine cycle. A series of AE events of varying amplitude, duration and spectral content are generated, the full detail of which can only be appreciated by examining the signals on an enlarged scale, as per the inset in Figure 6.1. For each individual event, comparison of signal attributes over sensor arrays yields information such as relative energy levels and event arrival time differences. This combined with knowledge of the processes occurring within the engine can enable the origin of the event to be determined with a degree of confidence. This methodology allows the majority of events in Figure 6.1 to be attributed to mechanical or fluid source events, as shall be detailed in this Chapter.

Having identified the main sources of AE it is then possible to focus on the remaining activity, some of which may be related to the ring-pack/liner interface. Therefore, the

survey of AE activity in this Chapter also functions as a precursor to investigation of AE generation from the ring-pack/liner interface, which is considered in Chapter 7.

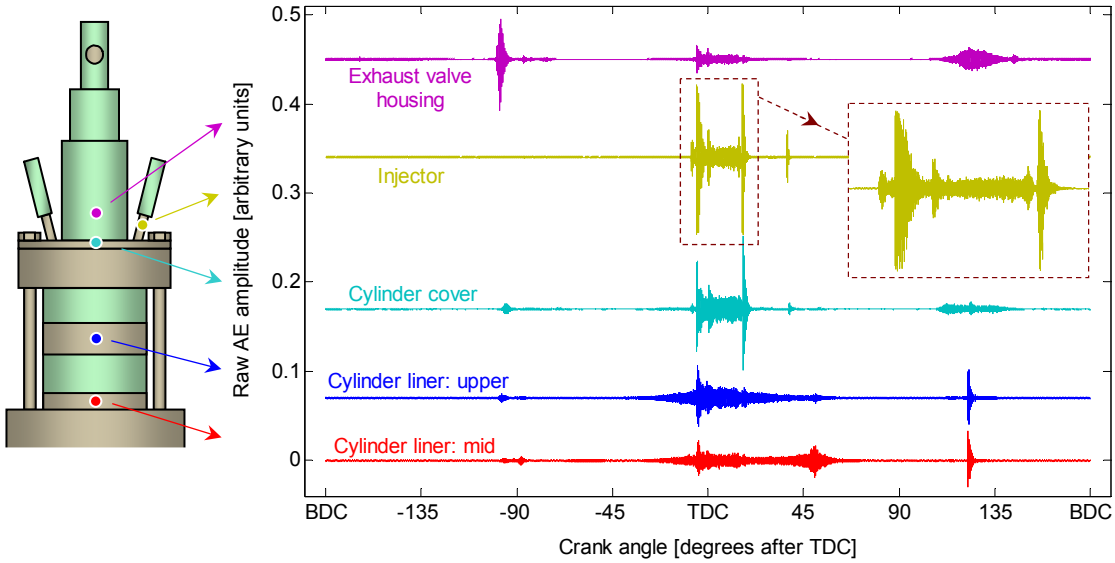

Figure 6.1: Engine E, review of sensor positions and examples of raw AE signals acquired during an engine cycle.

6.2 Fuel injection period

AE activity during the period around TDC in Figure 6.1 is the strongest in the cycle and features to some degree at all the sensor positions, although it is observed at maximum intensity in measurements acquired from the injector and cylinder cover surfaces. Closer examination of the signal acquired from the injector surface, the inset in Figure 6.1, shows that a distinct series of AE events are generated.

As was shown in the schematic of a two-stroke engine cycle given in Figure 2.2 the period around TDC is when fuel injection into the cylinder takes place. Indeed, in previous work on this type of engine [82] two burst-type events occurring around TDC have been interpreted as indicative of the start and end of this process. This was established from RMS AE signals acquired from the exhaust valve housing during normal running and simulated misfire conditions. It was further stated that there was little evidence to suggest AE activity was generated from the combustion process with the possible exception of high-frequency activity between the injection start and stop events.

This Section aims to substantiate the deduction that AE activity results from the injection process and endeavours to further develop understanding by determining more precisely what this activity relates to in terms of the mechanics of injector operation. To achieve this, data from several tests shall be investigated including; consideration of several sensor arrays, tests with the injection process removed from the engine cycle and correlation of AE activity to both anticipated fuel injector behaviour and measurements of fuel injection pressure.

As a result of this investigation the structure of the AE generated during the fuel injection period has been carefully examined. This has led to the identification of AE parameters that can be used in conjunction with information about the fluctuations of crankshaft speed to indicate the load, or power generated, of these engines and also to provide diagnostic information regarding cylinder performance. These findings are reported in greater detail in Chapter 8.

6.2.1 Cylinder-by-cylinder and cyclic repeatability

The first task is to establish the typical characteristics of AE activity during the fuel injection period through an investigation of cylinder and cyclic consistency. RMS AE signals acquired from the injector body during the injection period for four cylinders of engine E, operating in the range 7.5 to 9 MW, are shown in Figures 6.2a to 6.2d. In each case the AE signal is presented in relation to the angular position of the monitored cylinder.

It is clear that each injector possesses its own individual AE signature, most likely due to variations in fuel delivery and injector condition characteristics; nevertheless, there are some common features in the signals and these are identified as events A, B, C and D. These events exhibit characteristics typical of burst-type events, with sharp event rises and exponential decays, such as may occur from impact-type sources. For each cylinder the greatest amplitude during the injection period is observed at event B. This event also contains additional activity during the event decay period which may be indicative of further source generation. The period between events B to C also consistently features lower amplitude continuous AE activity and, with the exception of

cylinder 4, a further burst-type event occurring just after TDC (labelled as event E in Figure 6.2).

Event D occurs some time after the main injection period, this event was also identified in previous work [82] and was believed to be related to the injection process although the exact source could not be identified.

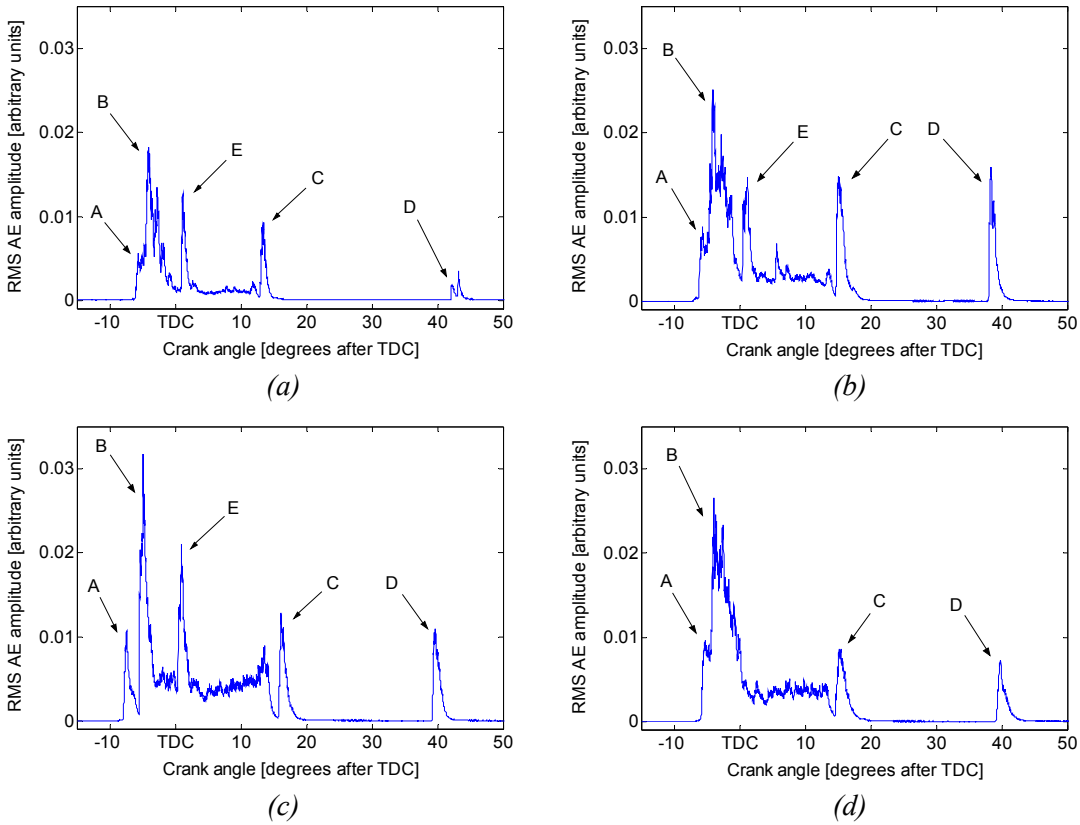

Figure 6.2: Engine E, examples of RMS AE signals acquired from the injector sensor position during the fuel injection process, (a) cylinder 1, (b) cylinder 2, (c) cylinder 3, (d) cylinder 4.

The cyclic repeatability of the AE activity generated during the injection process under steady-state loading conditions can be assessed from Figure 6.3. Each plot shows the mean, maximum and minimum amplitudes measured from the injector sensor position over a dataset of 50 RMS AE cycles for each cylinder. It is apparent that under steady-state conditions the AE generated during the main body of the injection period, from event A to event C, displays a high level of cyclic consistency. Event D, however, varies substantially in both timing and amplitude.

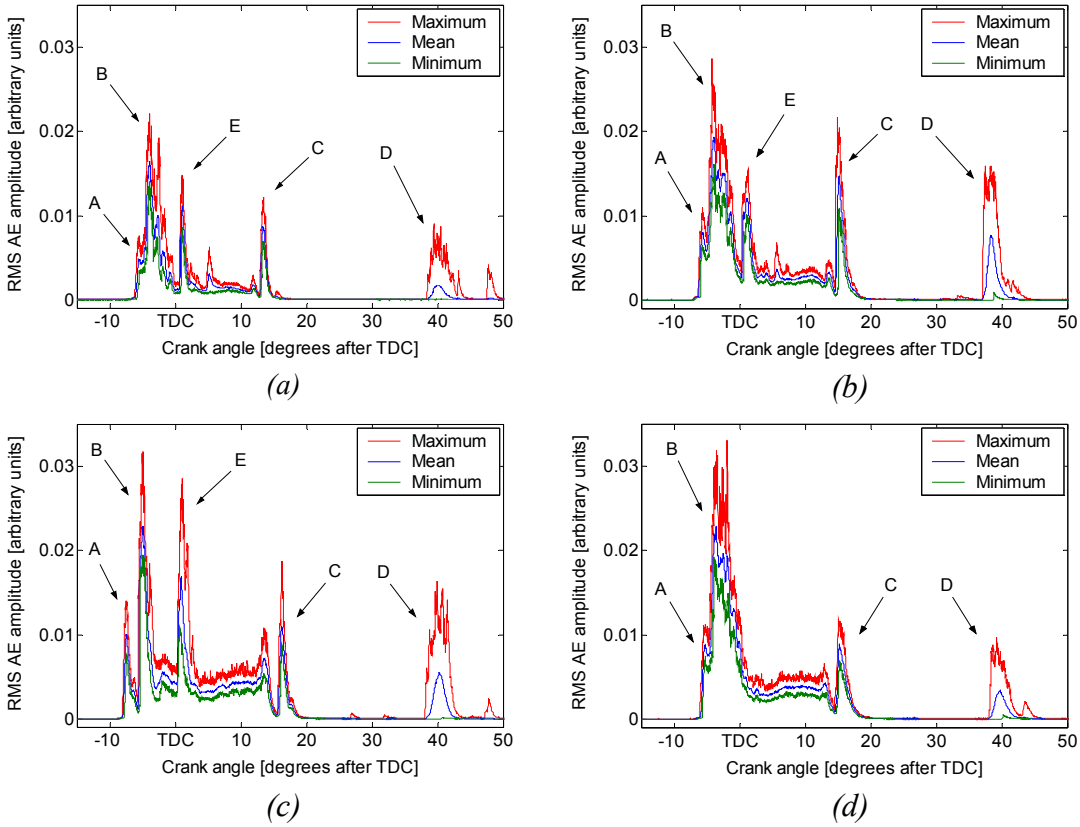

Figure 6.3: Engine E, range of AE activity over 50 cycles at steady-state operating conditions, (a) cylinder 1, (b) cylinder 2, (c) cylinder 3, (d) cylinder 4.

6.2.2 Observations from AE sensor arrays

As shown in Figure 6.1 some of the AE events generated during the fuel injection period are observable at all the sensor positions. Since AE signals propagate with a velocity through a material and attenuate as they do so then consideration of relative energy levels and event arrival times can give an indication as to the event origin, i.e. events should arrive earlier and with greater intensity at locations closer to the source. In this Section sensor arrays on engine E are considered in order to investigate whether the relative signal characteristics substantiate the source as being injector operation. For these arrays nominally identical AE sensors and pre-amplifiers were used hence signal amplitudes should be comparable. However, there remains the possibility of differences in sensor sensitivity and coupling quality and for this reason source location based upon comparisons of signal amplitudes should be regarded as indicative rather than conclusive.

A thorough example of how sensor arrays can be used to locate the source of AE events in engines has been provided by Nivesrangsan *et al* [155]. Source triangulation methods were developed using multi-sensor arrays based upon relative event arrival times and energy contents. The former was found generally more successful, particularly for location of burst-type sources, whilst the latter was effective when multiple source signals were present and accurate identification of discrete events was difficult. The work presented here is not intended to be as comprehensive but does serve to illustrate the principle of source location.

Due to the complex structure and varying nature of AE signals the identification of a point in the signal that consistently represents the occurrence of an event can be difficult and is open to interpretation, particularly when the signals are heavily distorted from the effects of propagation or when multiple overlapping sources are present. Ding *et al* [118] surveyed a number of methods for determination of arrival time of burst-type events arising from simulated sources and recommended a process based upon a combination of wavelet decomposition, filtering and threshold-crossing. However, this method is not used in this work due to the signals being rather more complex and instead a process based upon the gradient of the smoothed RMS AE signal and threshold-crossing is employed.

6.2.2.1 Array consisting of injector, cylinder cover and mid liner sensor positions

An example of raw AE signals acquired during the injection period from an array consisting of injector, cylinder cover and mid liner sensor positions on cylinder 3 of engine E is shown in Figure 6.4. For the injector signal, with the exception of injection event D, there was no other AE activity during the entire engine cycle. Both the cylinder cover and mid liner positions displayed AE activity at other parts of the cycle, particularly the mid liner signal which contained a low-amplitude continuous component present before, during and after the injection process. Possible origins for this continuous activity shall be discussed in Chapter 7.

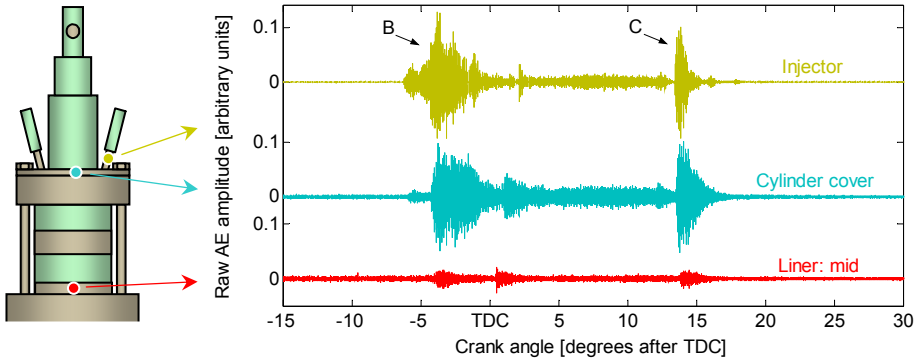

Figure 6.4: Engine E, cylinder 3, raw AE signals acquired from the injector, cylinder cover and mid liner sensor positions during the fuel injection period.

The events labelled B and C in Figure 6.4 are observed at all three sensor positions. In both cases the relative event amplitudes signify that the AE source is much closer to the injector and cylinder cover than the mid liner position. A better comparison of relative event attributes can be obtained from a plot of the smoothed analogue RMS AE signals (without resampling to a lower rate) that correspond to the original raw AE data. This is shown in Figure 6.5a for the whole injection period, with enlargements of events B and C given in Figures 6.5b and 6.5c respectively. Vertical lines indicating the calculated event arrival times for each sensor position are also shown.

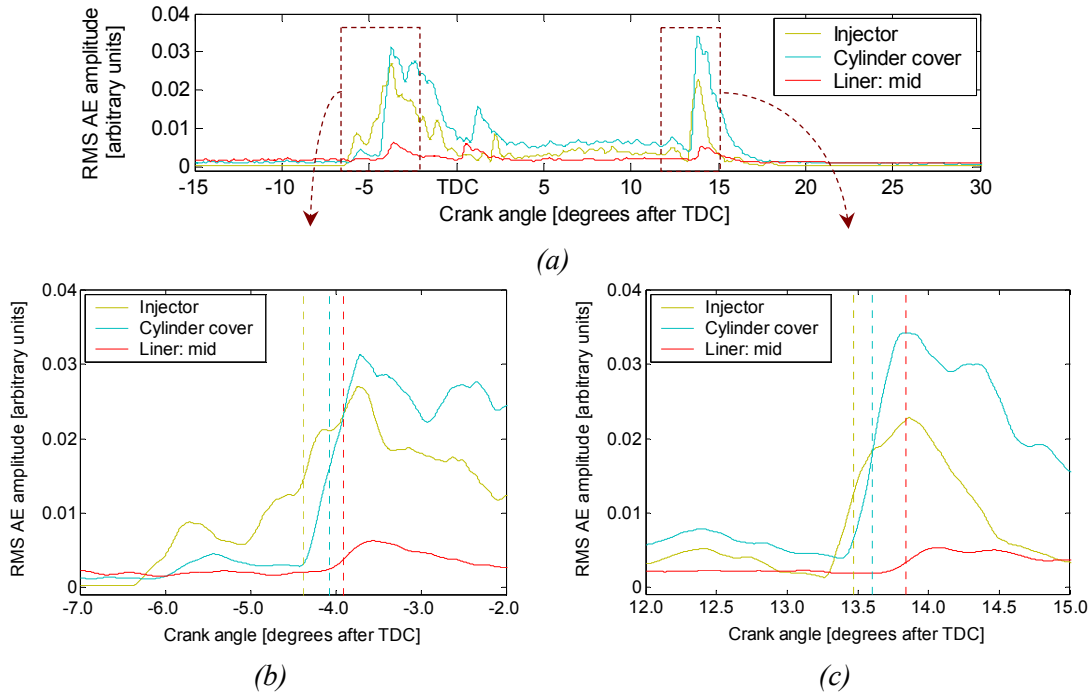

Figure 6.5: Engine E, cylinder 3, smoothed RMS AE signals during, (a) fuel injection period, (b) AE event B, (c) AE event C.

In this example, for both events, the cylinder cover signal displays the greatest amplitude. This would initially seem to be inconsistent with the presumed source of injector operation. However, this can be accounted for when it is considered that each cylinder consists of two fuel injectors. It would therefore be expected that the AE measured at the cylinder cover would be a combination of AE activity arising from both injectors and, depending upon the attenuation of the activity from each source, the combined amplitude may well be greater than the signal measured at one of the injectors. Again, it is also possible that a factor in the differences in amplitude is the variance of sensor response characteristics over the array.

The other approach for locating the source of AE events B and C is to consider the relative event arrival times. For both cases the AE activity is observed first at the injector followed by the cylinder cover and then the mid liner position. This is indicative of a source origin closest to the injector sensor position which is consistent with the presumed source. Figures 6.6a and 6.6b show the consistency of event arrival timings over 10 cycles for events B and C respectively. In both cases, even though the angular timings vary, the relative timings are very consistent. It is also evident that the variance in timing of the events, and hence of the originating sources, is as much as a degree even over just 10 cycles. However, as this was from testing on engine E there was no control available over engine operation and therefore steady-state conditions could not be assured during acquisition of this data.

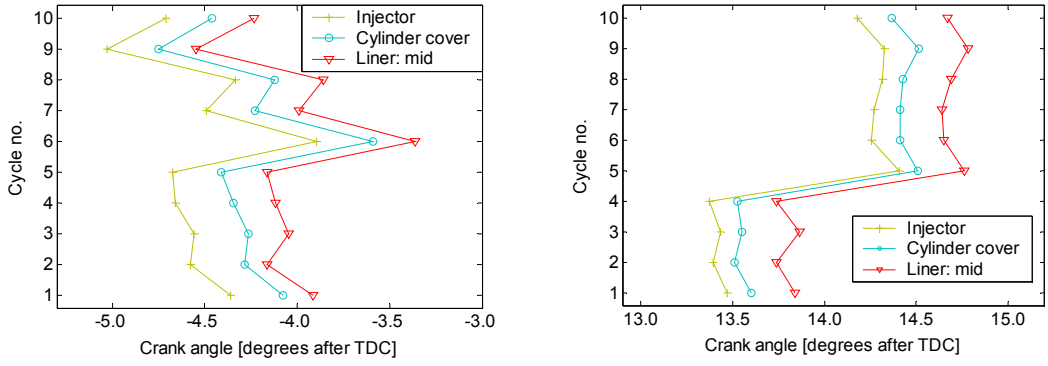

Figure 6.6: Engine E, cylinder 3, angular timing of events at each sensor position over10 cycles, (a) event B, (b) event C.

6.2.2.2 Array consisting of exhaust valve housing, cylinder cover and mid liner sensor positions

A further sensor array considered the exhaust valve housing, cylinder cover and mid liner sensor positions, again on cylinder 3 of engine E. Figure 6.7 shows an example of raw AE signals acquired from this array during the fuel injection period. AE event arrival times for events B and C over 10 cycles are shown in Figures 6.8a and 6.8b respectively, with similar analysis for the same array on cylinder 1 shown in Figure 6.9.

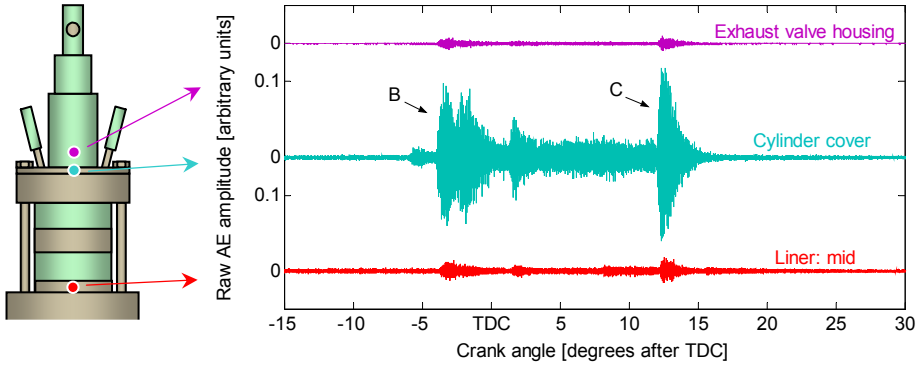

Figure 6.7: Engine E, cylinder 3, raw AE signals acquired from the exhaust valve housing, cylinder cover and mid liner sensor positions during the fuel injection period.

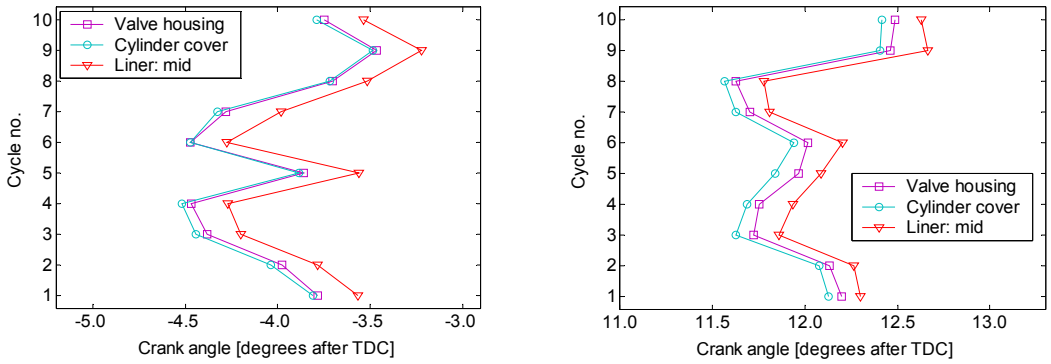

(a) *(b)*

Figure 6.8: Engine E, cylinder 3, angular timing of events at each sensor position over10 cycles, (a) event B, (b) event C.

These results show, for events B and C over both cylinders, that AE activity propagates first to the cylinder cover, shortly followed by the exhaust valve housing and finally the mid liner position. The cylinder cover signal also displays by far the greatest amplitude for both events. Both these observations are again consistent with the anticipated injector operation source. A further comment is that the event amplitudes are slightly greater for the mid liner signal than at the exhaust valve housing. This is likely a reflection of a more complicated source to sensor transmission path, as although the

valve housing position is closer to the anticipated injector source there are several significant material boundaries in between.

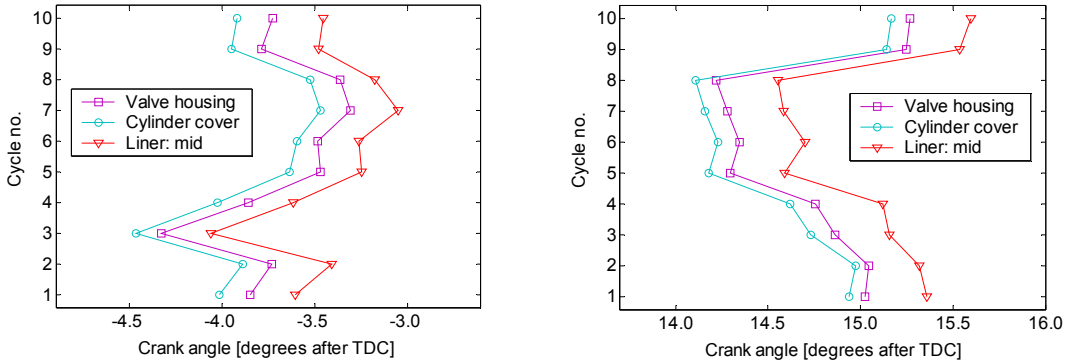

Figure 6.9: Engine E, cylinder 1, angular timing of events at each sensor position over10 cycles, (a) event B, (b) event C.

Results from further sensor arrays to that presented here have been considered and generally the findings are consistent in that they indicate the origin of the principal events during the injection process, events B and C, to be injector operation.

6.2.3 Comparison of normal running and simulated misfire tests

Tests were conducted on the electronically controlled engine F operating under normal conditions and with the injection process for cylinder 2 turned off in order to simulate extreme misfire conditions, i.e. the cylinder was effectively motored. Figure 6.10 shows comparisons of RMS AE signals acquired from the cylinder cover position for both operating conditions at loads of 10 % and 25 % of MCR. Although the structure of the signals are different to those shown previously for the cylinder cover position of engine E it is clear that when the injection process is removed from the cycle the AE events do not appear, thereby offering further confirmation that these events result from injector operation. The findings from these tests are in close agreement with results reported by Fog [82].

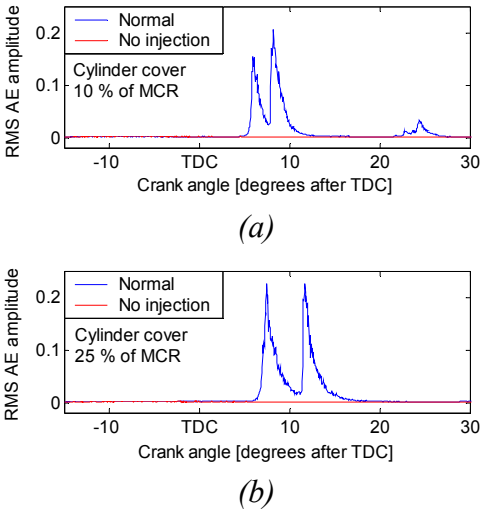

Figure 6.10: Engine F, comparison of normal and simulated misfire tests, (a) 10 % of MCR, (b) 25 % of MCR.

6.2.4 Correlation between AE activity and injector mechanics

To determine more precisely the source of each AE event during the injection process a detailed examination of the mechanics of injector operation is required.

The traditional method for controlling injectors in large, two-stroke diesels is through the fuel line pressure generated by an in-line pump for each cylinder. The fuel injectors used in engine E were of the two-stage type, a cross-section of a complete assembly and a breakdown of components is given in Figure 6.11a. Figure 6.11b shows cross-sectional schematics of the three possible positions of the injector components. Within the spindle guide **A** there consists the spindle **B**, thrust piece **C**, inner spindle **D** and spring **E**. With the injector at rest (position *I* in Figure 6.11b) the spindle **B** is pressed against the valve seat of the spindle guide **A** through pressure exerted by the thrust spring and transmitted via the slotted thrust foot. The stiffness of the thrust spring determines the opening pressure of the injector. A valve to allow fuel oil circulation is contained within spindle **B.** At rest the inner spindle **D** is pressed by spring **E** against the valve seat of spindle **B**. In this position the top of the inner spindle **D** uncovers a small bore in thrust piece **C** which allows fuel oil to circulate through the injector; this feature is shown more clearly in Figure 6.11b.

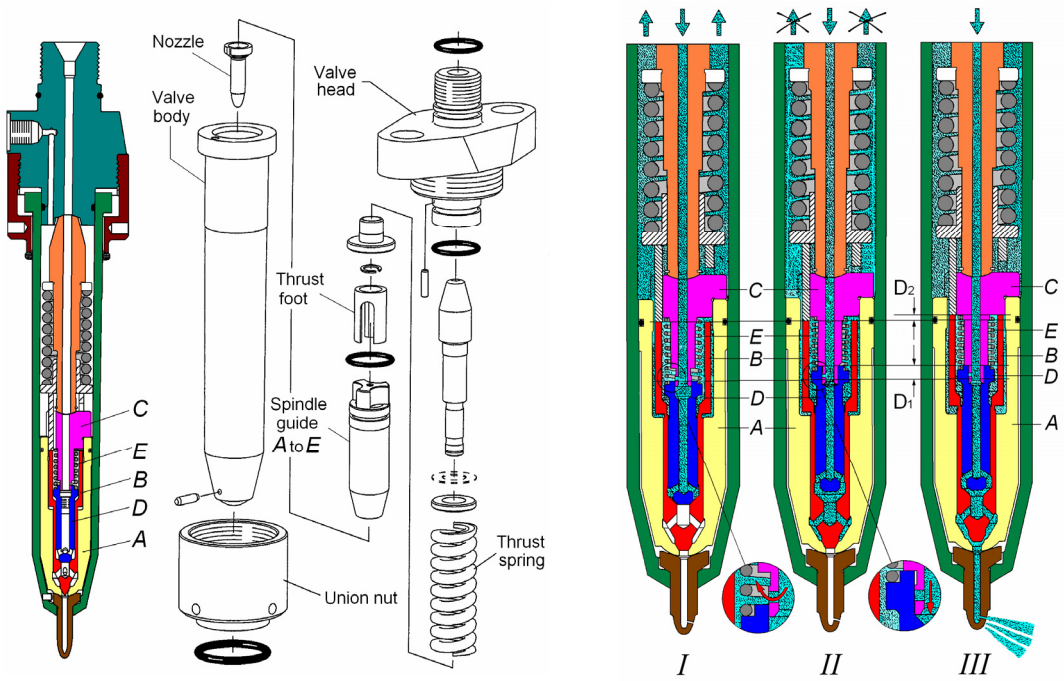

Figure 6.11: Cross-sectional schematics of fuel injector from engine E, (a) complete assembly [221], (b) three positions of injector operation [222].

The functioning of the fuel injector can be described by the profiles of injection pressure and spindle/needle lift during the injection process. Typical fuel pump delivery and injection pressure profiles, and resulting spindle/needle lift, are shown in Figure 6.12a. In this work there were no measurements of spindle lift, although fuel line pressure measurements were available for some tests on engine F. An example for operation at 25 % of MCR on the propeller curve is shown in Figure 6.12b along with simultaneously acquired RMS AE from the cylinder cover position. The AE signal in this case shows similarities with that acquired previously from engine E and the sequence of AE events are labelled accordingly.

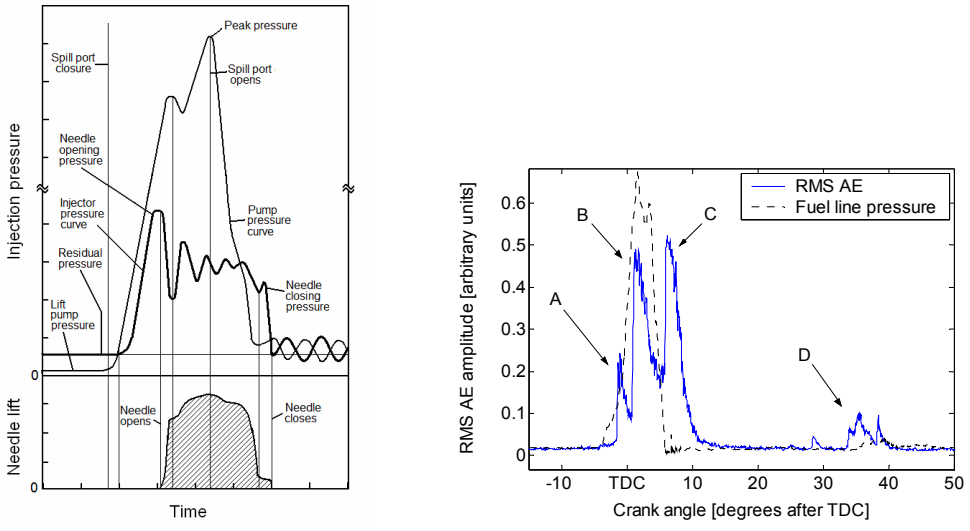

(a) *(b)*

Figure 6.12: (a) Pump pressure, injector pressure and needle/spindle lift versus time for a typical in-line injection system [223], (b) Engine F, fuel line pressure and RMS AE signal acquired from the cylinder cover position at 25% of MCR.

Through knowledge of the expected injector behaviour and correlation between injection pressure and AE activity precise origins for the series of AE events during the injection period can be determined. These are set out in the following which describes the AE activity with regards to five phases of injector operation [224] and the corresponding positions of the injector components (as shown in Figure 6.11b).

Injection phase *I*, position *I* - fuel oil circulation:

Fuel oil is circulated through the fuel pump and injector. Within the injector the oil passes through the central bore of the valve head and continues down to the bottom of thrust piece **C**. Here it passes through the circulation bore before rising back up the

interior of the valve body and exiting via an outlet pipe on the side of the valve head. The space around the tapered valve seat of the inner spindle **D** is also filled with fuel oil, but the circulating pump pressure is insufficient to overcome the force of spring **E**.

Injection phase *II*, position *II* - beginning of fuel delivery:
When, at the beginning of the fuel pump delivery stroke, the fuel line pressure has risen to about 10 bar, the force of spring **E** will be overcome and the inner spindle **D** is pressed back the distance $\mathbf{D_1}$ in Figure 6.11b onto the shoulder of thrust piece **C**. This impact is thought to be the likely origin of the first burst-type AE event A in Figure 6.2. The fuel line pressure profile in Figure 6.12b also shows a close alignment between the initial rise in fuel pressure and AE event A. The upward movement of spindle **D** also closes the circulation bore and fuel oil enters the space around the seat of spindle **B**.

Injection phase *III*, position *III* - fuel delivery:
The fuel line pressure rises sharply and when the preset opening pressure of the fuel valve is reached, i.e. the force of the thrust spring is overcome, spindle **B** is lifted the distance $\mathbf{D_2}$ on Figure 6.11b and hits the thrust piece **C**. This impact is thought to be the initial cause of AE event B. It also signifies the commencement of fuel injection into the cylinder with fuel forced through the nozzle under high pressure at the moment of spindle lift. This fuel is ignited in the cylinder and a period of rapid uncontrolled combustion ensues accompanied by a large energy release. AE event B is generally broader than a typical AE impact response and it may be that further activity arises from the initial rapid combustion or the initial rush of fuel through the nozzle under very high pressure. A further possibility is that AE propagation between the two injectors gives the impression of an extended event duration.

Fuel oil is then delivered continuously at high pressure. As is evident from the examples for engine E in Figure 6.2 during the period from event B to event C there is continuous AE activity of an amplitude greater than the background noise level but lower than the impact related AE. Possible sources for this activity are limited and it is presumed that it arises from either high-pressure fuel flow through the injector passageways and nozzle or from the combustion of fuel as it enters the cylinder. In some examples there is a further burst-type event during this period, labelled event E, possible sources for which shall be discussed later.

Injection phase *IV*, position *II* - end of injection:
The opening of the spill port within the fuel pump causes a sudden collapse in fuel line pressure that signifies the end of fuel delivery. Fuel contained in the region of the spindle seat and nozzle area will continue to discharge until its pressure energy is exhausted. This is signified in the example AE signals in Figure 6.2 by the period that precedes event C which shows a reduction in AE activity to background noise levels. At this point the fuel pressure can no longer maintain compression of the thrust spring which causes the valve spindle **B** to snap down on its seat, **A**, i.e. the injector reverts to position *II*. This impact signifies the end of fuel injection and is thought to be the origin of AE event C. The alignment of the fuel injection pressure collapse with AE event C in Figure 6.12b supports this belief.

Injection phase *V*, position *I* - fuel oil circulation:
There is uncertainty regarding AE activity arising from the final action in the injection process, the opening of spring **E** and resulting closure of inner spindle **D** against its seat in **B**. This causes the injector to revert back to position *I* and therefore allows oil to circulate through the injector again. It is presumed that an impact occurs between the inner spindle **D** and its seat which would be responsible for AE generation. However, there is uncertainty as to when this occurs as there is no AE event immediately proceeding AE event C.

There is though the highly variable AE event D to account for. There is the possibility that some residual pressure remains in the area of the spindle seat that causes the opening of spring **E** to be delayed somewhat from the main injection period. This would then relate AE event D to the eventual closing impact, however, this is a tenuous conclusion which would require further investigation. There is limited further evidence available from the measured injection pressure profile. Figure 6.12b does show that AE event D appears to precede a small rise in injection pressure. It is possible that this is caused from fluid disturbances arising from the opening of spring **E**; it also may be due to pressure waves travelling down and up the fuel line.

In summary, although full validation cannot be achieved in the absence of spindle lift measurements, the AE events during the injection period would appear to correlate well with the sequence of mechanical and fluid events that occur within the injector and which define its operation. Furthermore, the resolution of AE measurements allows

very precise crank angular timings to be obtained for each individual impact between spindle and injector body which could prove useful for diagnostics purposes.

6.2.5 Variation of AE activity with load

Investigation of AE activity from injector operation over varying loads shows that it parallels the changes in injector behaviour. This is demonstrated in Figures 6.13a and 6.13b for signals acquired at different loads from the cylinder cover positions on engines E and F respectively. From both examples it is clear that with increasing load the timing of event C (presumed injection end) occurs later in the cycle. This is consistent with the assumed source since to meet increased loads the control action of the engine is to extend the injection duration. Figure 6.13c further clarifies the ability to determine injection duration from AE measurements. It clearly shows the development of injection timings over the three loads and intermediate periods during the first lubricant starvation test conducted on engine F. Further examination of the variation of AE activity during the fuel injection period with load is presented in Chapter 8.

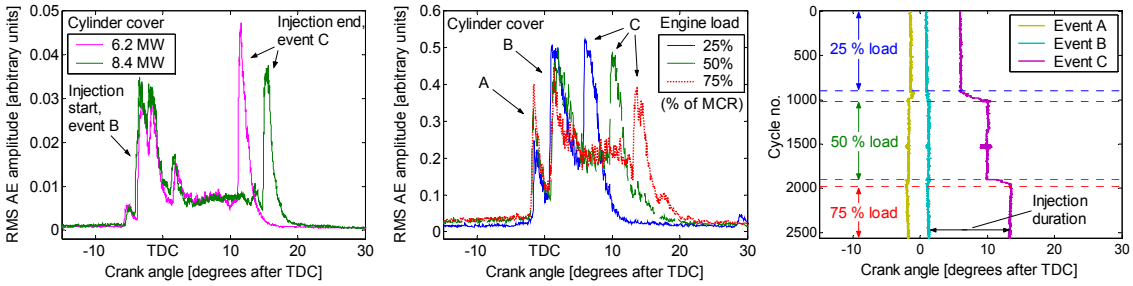

(a) *(b)* *(c)*

Figure 6.13: Variation of AE activity from injector operation with load, (a) engine E, (b) engine F, (c) angular timings of events during the first lubricant starvation test on engine E.

6.3 Exhaust valve activity

AE activity can also be identified as arising from operation of the exhaust valve. Figures 6.14a and 6.14b show RMS AE signals acquired from the cylinder cover and mid liner sensor positions during the valve opening and closing periods over three loads on engine F; simultaneously acquired exhaust valve lift measurements are also shown.

Engine F featured variable valve timing and it is clear that with increasing load the initial point of valve opening occurred earlier and valve closing occurred later.

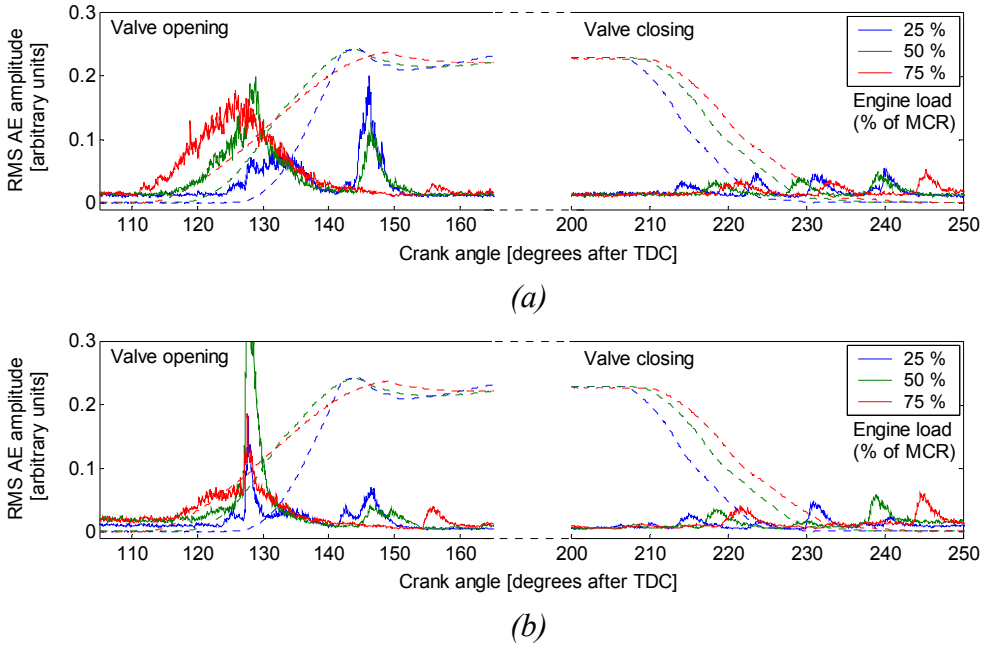

Figure 6.14: Engine F, RMS AE signals and simultaneous valve lift measurements during exhaust valve opening and closing periods, (a) cylinder cover, (b) mid liner.

6.3.1 Exhaust valve opening

Significant AE events are generated during the valve opening period. The first of these appears to be related to the initial point of valve opening since for both the cylinder cover and mid liner signals there is continuous-type AE activity that correlates well with the initial valve opening, and this remains true irrespective of the timing advance with load. This strongly suggests that the source of this AE is the initial rush of exhaust gas past the valve as it opens. This activity is observed to be of greater strength at the cylinder cover position which is in agreement with the presumed source since the mid liner position is located farther away. Furthermore, gas flow through a confined space is a known source of AE with the amount of activity generated observed to increase in proportion to flow-rates [225].

The varying amplitude of the continuous AE activity may then be related to the properties of the gas flow as the valve opens. This is governed by the pressure differential over the valve and the valve lift, as the valve opens increased gas flow rates are possible before the pressure quickly becomes equalised and gas flow reduces to

relatively low flow-rate scavenging conditions. The characteristics of the continuous AE activity in Figure 6.14a parallels the anticipated gas flow-rates as it displays a gradual increase to a maximum level shortly after initial valve opening before reducing to background levels. A further feature is that the strength and duration of this event increase with load. Again, this is consistent with the assumed gas flow source since at increased loads, and with advanced opening, the in-cylinder pressure at opening would be greater. Fog [82] also attributed a broad, load dependent AE event in a similar area of the cycle to the initial release of exhaust gas as the valve opened.

Much use has been made of the high sensitivity to gas flow inherent to AE monitoring to investigate exhaust gas leakage due to valve burn-through in large, two-stroke diesels [82, 146, 147]. Similar to the observations made here for exhaust gas flow during normal operation it was reported that the amount of AE activity due to leakage was a function of the load. El Ghamry *et al* [122] also reported that it may be possible to infer information from AE activity generated during valve opening regarding; the in-cylinder pressure, whether the valve is leaking and whether deposition is restricting the smooth passage of exhaust gas. Sasaki [35] further found that activity relating to valve opening was present in vibration signals acquired from the valve housing and cylinder cover areas of large, two-stroke diesels.

The signals acquired from the mid liner position, Figure 6.14b, during the opening period exhibit a further burst-type event of higher amplitude occurring coincident with the gas flow event at around 127 degrees after TDC. This event occurs at a consistent timing regardless of load change and valve timing advance, and is observed with greater intensity at the mid liner position than the cylinder cover. Therefore, it is presumed that it does not originate from valve activity. The likely source of this event shall be discussed later in this Chapter.

The exhaust valve does not open instantaneously. Figure 6.14a shows that it takes approximately 30 degrees of crank rotation to fully open and then further time for the valve to come to rest. In both the cylinder cover and mid liner positions there are further AE events which appear to relate to the exhaust valve reaching the fully open limit.

6.3.2 Exhaust valve closing

A series of smaller scale AE events in both the cylinder cover and mid liner signals in Figure 6.14 are observed to occur coincident with the closure of the exhaust valve. This sequence of events occurs later in the cycle with increasing load, which again reflects the changes in valve timing. This relationship is shown more clearly in the intensity plot of cylinder cover AE signals during the valve closing period given in Figure 6.15. The y-axis in these plots represents the progression of time during the first lubricant starvation test conducted on engine F and changes in load are clearly labelled.

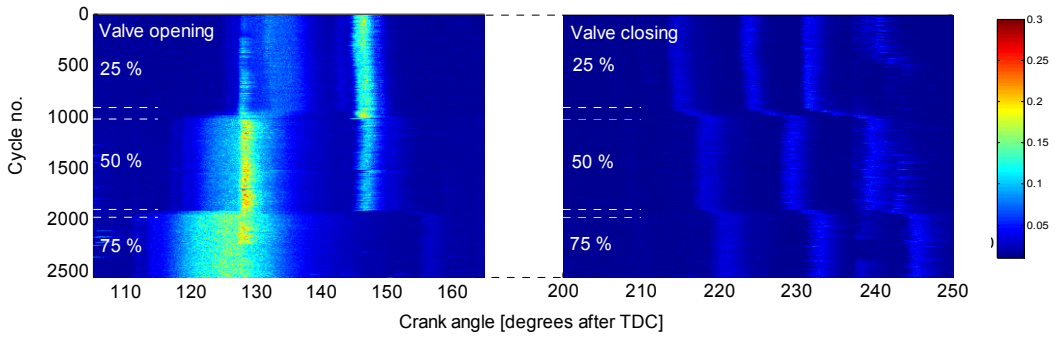

Figure 6.15: Engine F, cylinder cover, intensity plots of RMS AE signals during valve opening and closing periods.

Referring to the comparison of AE signals and valve lift shown in Figure 6.14a, the first AE event for each load occurs just after the initial movement of the valve away from the fully open position. The amplitudes of these events are similar for each load and for both sensor positions. The second event aligns with an abrupt reduction in valve velocity as the valve approaches the closed position, which is perhaps indicative of contact between the valve and the air spring which cushions the closure. Further, this event is stronger at the cylinder cover position which is consistent with a source in the valve housing area. The third event occurs later, when the valve reaches the fully closed position and is brought to rest, in this case the mid liner position shows slightly greater amplitudes.

Events relating to valve activity can also be observed in signals acquired from engine E. Figure 6.16 shows RMS AE signals during the valve opening and closing periods from an array consisting of cylinder cover, mid liner and valve housing sensor positions. During valve opening there are similar events present at the cylinder cover as was observed for engine F, this activity is also seen clearly at the valve housing position. The mid liner signal also displays the strong burst-type event seen at a similar position

on engine F which was thought not to be valve related. During the valve closing period, in this example, there is one principle event that originates closer to the valve housing in addition to some lower level activity. However, for other cylinders tested on engine E there were several events generated in a similar manner to engine F. For these events there is again AE propagation to the mid liner position but signal attenuation is such that identification of events can be difficult.

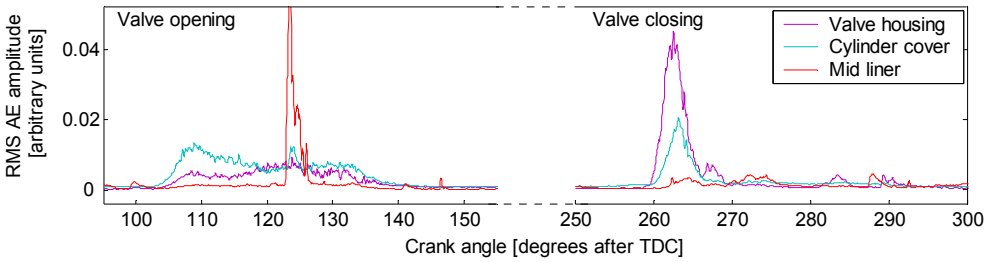

Figure 6.16: Engine E, RMS AE during valve opening and closing periods.

6.4 Piston ring-pack and cylinder liner interface

A major objective of this thesis is to investigate whether or not AE activity is generated from the ring-pack and cylinder liner interface in large, two-stroke diesels, and if so, a further objective is to determine what this activity represents in terms of its physical origins. For these intentions the signals of foremost interest are those acquired from sensor positions closest to the anticipated source, i.e. the sensors located on the cylinder liner. Examples of raw AE signals acquired from the liner sensor positions of engines E and F during an engine cycle are shown in Figures 6.17 and 6.18 respectively.

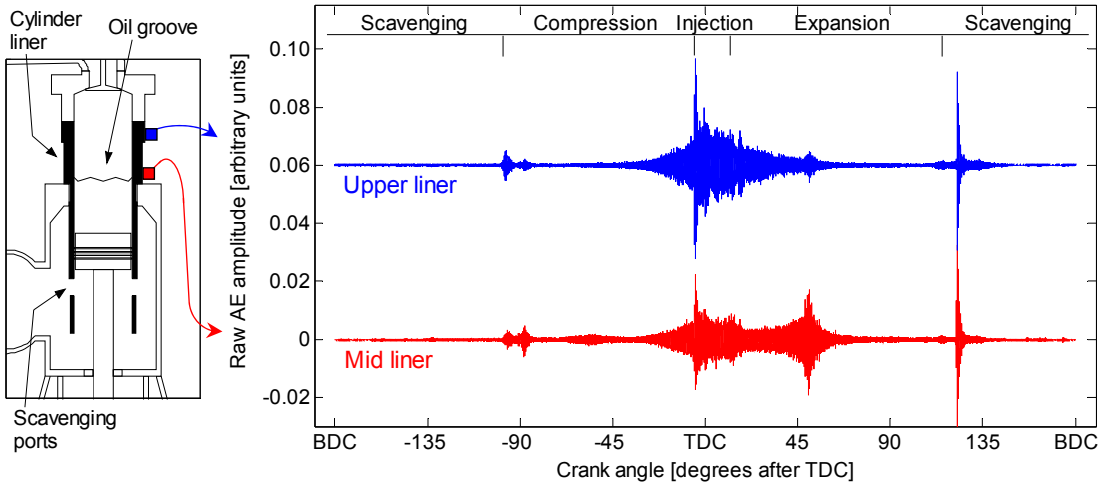

Figure 6.17: Engine E, review of sensor positions and examples of raw AE signals acquired during an engine cycle.

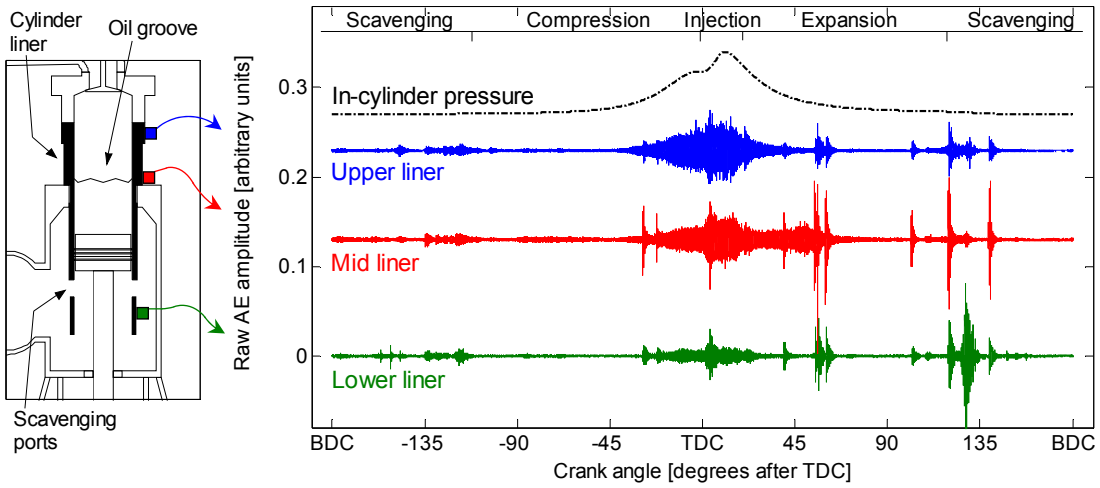

Figure 6.18: Engine F, review of sensor positions and examples of raw AE signals acquired during an engine cycle at 100 % of MCR.

All the liner signals from both engines contain burst- and continuous- type events. As already identified some of these events relate to the normal operation of the fuel injectors and exhaust valve, although at the liner positions these events are observed at a reduced amplitude when compared to signals acquired from closer to the respective sources. There are a number of other possible source mechanisms that may account for the remaining AE activity, some of which involve the ring-pack and liner interface. These include mechanisms associated with the continuous sliding interfacial behaviour, and also from impacts occurring at the interface due to interaction between rings and non-continuous features of the liner surface, combustion shockwaves and other phenomena which may unsettle the rings. Further possible sources which are not directly related to the ring-pack/liner interface include exhaust valve leakage, bearing related sources (both main and crosshead bearings), and interfacial behaviour at the stuffing box/piston rod interface.

6.4.1 Burst-type AE activity

Significant burst-type events can be observed in the signals acquired from the liner sensor positions. It is believed that some of these events are attributable to the passing of the ring-pack over non-continuous features of the liner surface. An example where these events are prominent is given in Figure 6.19 which shows over 100 cycles of RMS AE data superimposed on one plot. In this case, the signals relate to the mid liner

position on cylinder 5 of engine E. The events thought to originate from ring-pack interaction with non-continuous features of the liner surface are indicated.

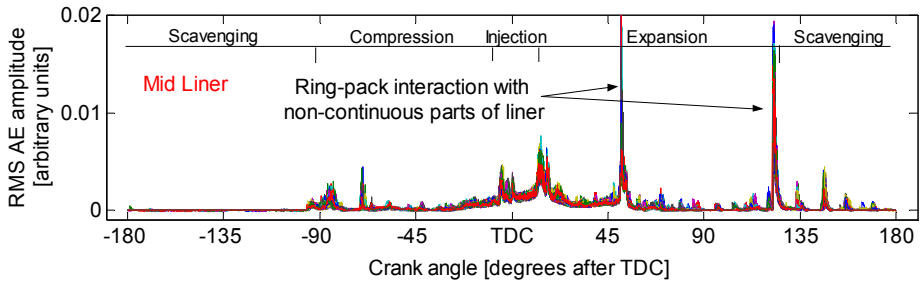

Figure 6.19: Engine E, burst-type activity believed to originate from ring-pack passing over non-continuous features of liner surface.

6.4.1.1 Oil groove related events

As described previously in Section 2.2.1 the inner surface of the liner features a machined groove which aids the circumferential distribution of lubricating oil. This groove is located at approximately the same elevation as the mid liner sensor position and is structured in a criss-cross form as indicated in Figure 6.20 and in previous cross-sectional schematics.

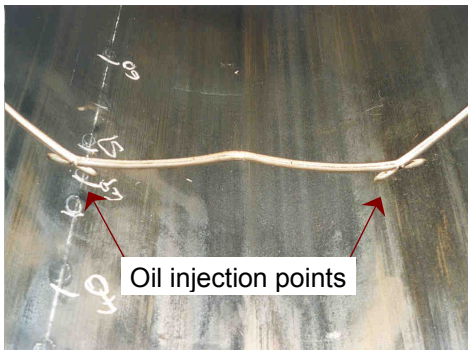

Figure 6.20: Engine E, oil groove.

Examination of the mid liner signals in Figures 6.17, 6.18 and 6.19 shows an increase in AE activity in the regions from approximately 45 to 60 degrees after TDC on the piston downstroke. This region in the cycle coincides with the ring-pack passing over the oil groove. The mechanical effects brought about by this disruption to the sliding contact are believed to be responsible for the burst-type AE activity. Other researchers have come to similar conclusions, particularly Sasaki [35] who noted that impulsive vibrations occurred symmetrically before and after TDC at crank angles corresponding to the top ring running across the oil groove.

It can be observed that the occurrence and characteristics of this event varies for different cylinders of engine E. The example in Figure 6.17 shows an event only slightly above the background level whereas the example in Figure 6.19 for a different cylinder shows an event of significant amplitude. This is presumably a reflection of

differences in the source mechanism for each cylinder; although it is not known precisely what the source is and what effect it has on the operation and reliability of the engine. One possibility is that the ring clips the oil groove; the occurrence of this would be determined by the orientation of the ring relative to the liner, which is itself a function of many factors including ring twist, ring profiles, secondary motions and deposition. A further consideration is that the rapid flow of high pressure gas into and around the oil groove may unsettle the ring(s) causing them to impact against the liner and increasing the likelihood of their becoming clipped by the oil groove.

A degree of validation of the presumed ring/oil groove source is offered through comparison of the upper and mid liner signals. This shows that this event contains far greater energy at the mid liner position. Since AE decays exponentially a large energy difference suggests that the source is much closer to the sensor showing the greatest activity, i.e. the mid liner position, which is consistent with the presumed source. The example given for engine F in Figure 6.18 shows several events that appear to originate in the vicinity of the mid liner position, in this case the events may be related to the passing of different rings over the groove although no means to substantiate this can be provided. A further characteristic over both engines is that smaller scale events have been observed in some cylinders to correspond with the timing of the ring-pack passing the oil-groove on the piston upstroke. The reduced amplitudes of these events compared to those on the downstroke may be related to the lower in-cylinder pressures on the upstroke and corresponding effects regarding ring orientation.

6.4.1.2 Scavenging port related events

Further non-continuous features of the liner surface are the scavenging ports in the lower area of the liner. On the downstroke the piston rings sequentially uncover these ports thereby allowing fresh charge to enter the cylinder. As the rings traverse the port area they are supported only by the port bars as shown in Figure 6.21. The passing of the ring-pack over these ports, or to be more specific, the entering and exiting

Figure 6.21: Ring-pack passing over scavenging ports.

of the port area, are thought to result in AE activity. Evidence to support this shall be presented in this Section.

In the example liner AE signals given for engines E and F in Figures 6.17, 6.18 and 6.19 there is relatively high-amplitude burst-type activity on the piston downstroke during the period 110 to 140 degrees after TDC. This period of the cycle corresponds to the end of the expansion phase through the opening of the exhaust valve, and the beginning of the scavenging process as the ring-pack uncovers the scavenging ports. It was established previously that these burst-type events were not directly related to valve opening as sensor array characteristics indicated a source much closer to the mid liner than the cylinder cover and valve housing positions. It is possible that valve opening may still indirectly be the origin through the ring-pack/liner interface being disrupted by the abrupt drop of in-cylinder pressure upon opening. However, a more likely scenario is that the activity is related to the ring-pack passing over the scavenging ports.

Further source location of these events can be achieved from comparison of signals acquired simultaneously from the upper and mid liner sensor positions. An example of time-series raw AE data over two cycles on engine E is given in Figure 6.22a (data presented in the time-domain since these measurements were taken from one of the engines not fitted with a shaft encoder, although the approximate position of TDC is indicated). The events proposed to relate to ring-pack/port interaction in both cycles are windowed with enlargements of these areas shown in Figure 6.22b. It is clear that the event arrives first at the mid liner followed by the upper position; which is consistent with the presumed source as it indicates a source closer to the mid liner position.

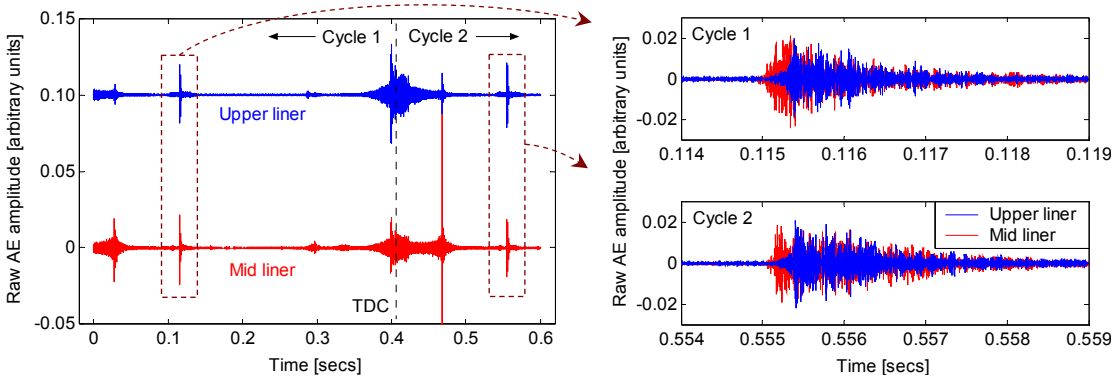

(a) *(b)*

Figure 6.22: Engine E, (a) time series raw AE signals from upper and mid liner sensor positions, (b) enlarged views of windowed AE events.

The consistency of this event is examined in Figure 6.23. Two sets of measurements are shown which were acquired seven months apart. Each plot relates to a single cylinder and shows 50 superimposed cycles of windowed RMS AE data from the mid liner position. In all the signals, with the exception of cylinder 4, the event occurs consistently at approximately 123 degrees after TDC. For cylinder 4 for the first set of measurements the event did not occur at all and for the second set it did occur although at a much reduced amplitude. The reason for this discrepancy is unknown but it obviously indicates that the characteristics of the AE source mechanism were different for this cylinder.

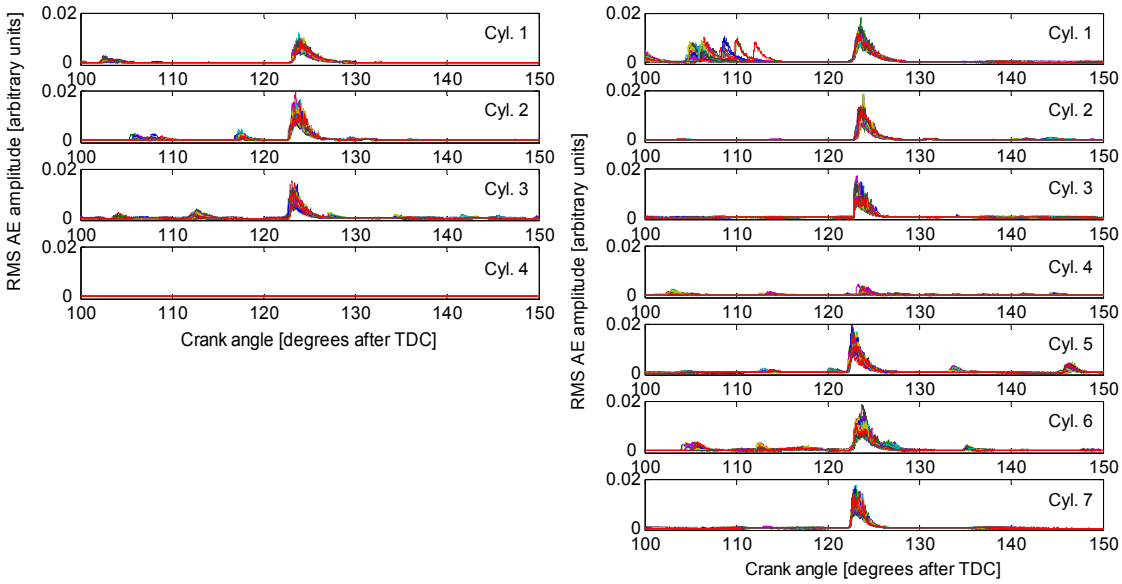

(a) *(b)*

Figure 6.23: Engine E, mid liner position, events believed to originate from ring-pack/scavenge port interaction, two sets of measurements seven months apart, (a) cylinders 1 to 4, (b) cylinders 1 to 7.

The occurrence of this event can also be highly cyclically irregular within data acquired from one cylinder. This is demonstrated in the time-series data acquired over two cycles shown in Figure 6.24, during the first cycle the event was absent although it appears as normal in the second cycle.

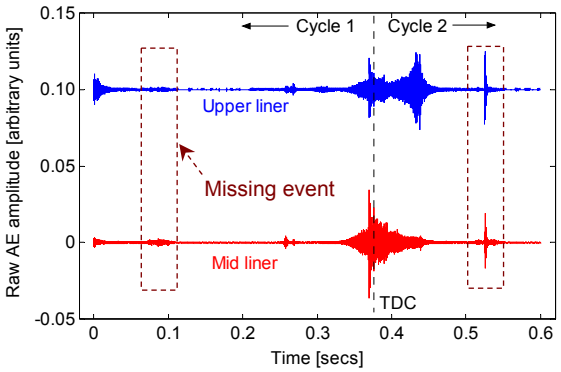

Figure 6.24: Engine E, time series raw AE signals from upper and mid liner sensor positions showing missing event.

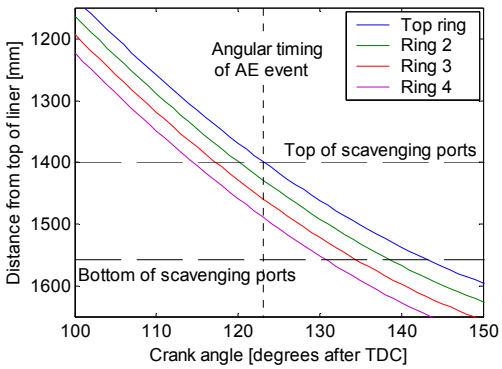

Figure 6.25: Engine E, timing of AE event compared to the location of the ring-pack and scavenging ports.

Approximate dimensions of the ring-pack and its location relative to the top of the liner at TDC were known. This allowed a comparison to be made in Figure 6.25 between the position of the mid point of each ring during the downstroke, the location of the scavenge ports and the angular timing of the AE event. The event was found to be coincident with the top ring entering the scavenge port area at approximately 123 degrees after TDC, therefore providing further evidence that ring/port interaction was the likely source.

Data acquired from engine F during the first lubricant starvation test similarly displayed a significant burst-type event in the region 125 to 130 degrees after TDC. An example cycle of data acquired from the mid liner position is shown in Figure 6.26a with the event in question windowed. The timing and amplitude of this event over the three loading conditions of the test are indicated in the intensity plot shown in Figure 6.26b. It is observed at greatest amplitude during the periods where the lubricating oil supply was removed and at loadings of 50 and 75 % of MCR, suggesting that the source mechanism may be further related to lubricating condition and load.

The occurrence of the event was again cyclically inconsistent as there were several periods during the test when the event did not occur, most notably immediately after reconnection of the lubricating oil supply. A further observation from Figure 6.26b that discounts indirect consequences of valve opening as the source and supports ring/port interaction is that throughout the test over the three loads, the event, when it occurred, did so at a consistent angular timing. This is in contrast to the opening of the exhaust

valve, and resulting abrupt change of in-cylinder pressure, which has been shown previously in Figure 6.14 to advance with load.

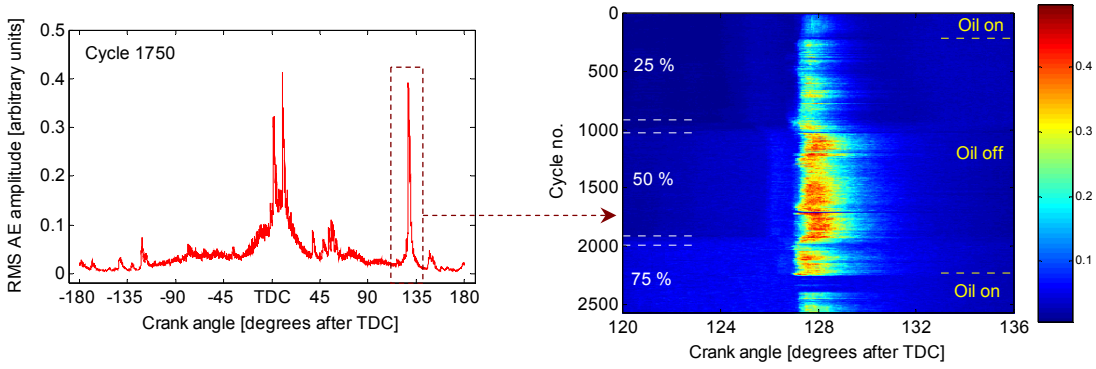

(a) *(b)*

Figure 6.26: Engine F, mid liner position, (a) example with ring/scavenge port event windowed, (b) intensity plots of windowed period during first lubricant starvation test.

The reason why interaction may occur from the ring-pack traversing the scavenging ports has been identified by Henshall [226]. It was recognised that as a ring crosses the ports the unsupported sections of the ring will be blown outwards by the gas pressure acting behind the ring. This effect would be greater for the ring ends if they come opposite a port due to their then being cantilevered instead of bridging the port. The disturbances and interaction caused by this may then be responsible for the generation of burst-type AE activity. In this respect the second ring is often treated more harshly than the top ring since the pressure acting on the second ring lags behind that in the cylinder and is often greater at the point where the ring crosses the ports [226]. For engine E the timing of the ring/port AE event was estimated as coincident with the top ring entering the scavenge ports. However, errors in the dimensions used to determine this mean that there is a slight possibility the source mechanism may have been the second ring entering the ports. Further ring/port interaction may be incurred through a ring becoming snagged as it returns to the full support of the liner. The ring ends are far more susceptible to this and for severe or repeated occurrences there is the possibility that it may lead to breakage [226].

Work by Sasaki [35] concurs with the proposed source mechanism of ring/port interaction. In this case, transient events in vibration signals were noted to arise from the ring-pack passing over the scavenging ports. Similar to the results presented here, the occurrence of this event was found to be cyclically inconsistent and this was

attributed to the varying positional relationship between the scavenging ports and ring ends.

Further data acquired during the second lubricant starvation test from the lower liner sensor position on Engine F, located internally below the scavenging ports, shows a sequence of four events occurring both just before and just after BDC. This is demonstrated in Figure 6.27 which shows the mean RMS AE signals of datasets for three loads on the generator curve. The sequence of AE events displays a high level of symmetry about BDC, particularly regarding the angular timings of each event, as signified by the sharp event rises, and also to an extent the event amplitudes.

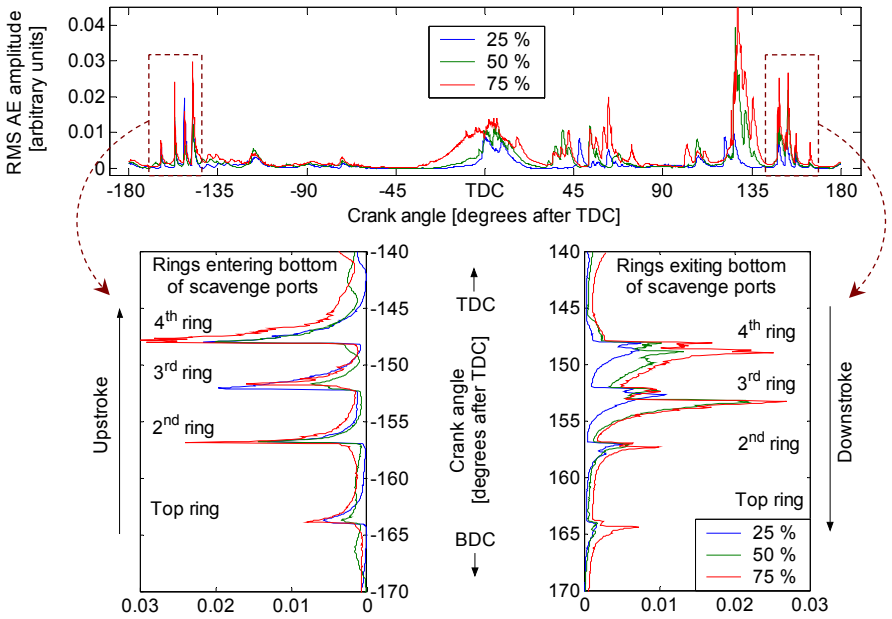

Figure 6.27: Engine F, lower liner sensor, AE events from interaction between each ring and bottom of scavenge ports for three loads on generator curve.

Through knowledge of the piston motion and ring-pack dimensions the relative timing of the events was found to correspond well to each ring sequentially entering on the upstroke, and exiting on the downstroke, the bottom of the scavenge port area. Furthermore, all these events were observed to be sharper and with greater amplitudes in signals from the lower liner sensor. These observations provide ample evidence that these events originated from ring/port interaction. A further characteristic was that the amplitude of these events was generally greater the farther away from BDC they occurred. This was presumably a reflection of the increased severity of interaction due to greater sliding velocities. Similar analysis on signals acquired at various loads on the

propeller curve was consistent in that it showed that the amplitude of these events increased with load and thus engine speed.

6.4.1.3 Events of unknown origin

In many instances there have been observed further burst-type activity that occurs in addition to anticipated activity from ring-pack interaction with the oil groove and scavenge ports. For instance, Figures 6.28a and 6.28b show examples of raw AE signals acquired from the mid liner positions of engines E and F in which there are a number of additional burst-type events. The source mechanisms of these events are unknown, although analysis of sensor arrays suggests that they are likely to originate on the liner surface and therefore be related to ring-pack/liner interaction.

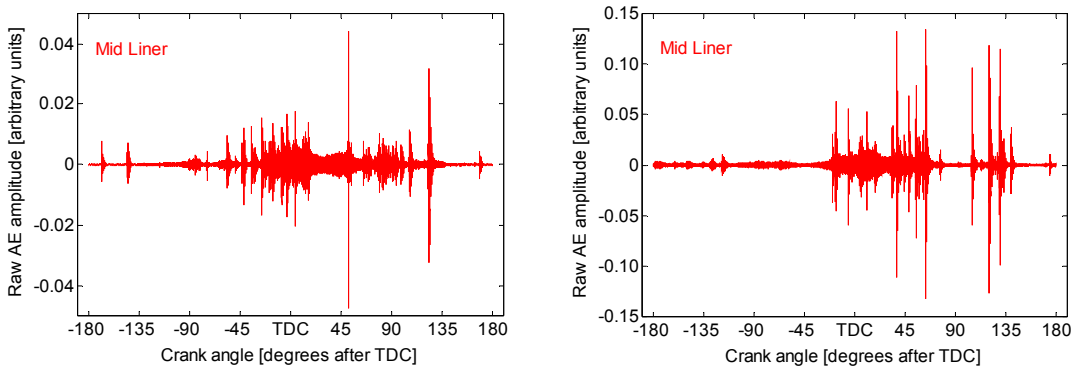

(a) *(b)*

Figure 6.28: Examples of signals from mid liner sensor position which show further burst-type activity, (a) engine E, (b) engine F.

A further AE event may arise from ring-pack/liner interaction just after TDC. This event was identified in Section 6.2.1 which detailed AE activity during the injection period on engine E, and was labelled as event E in Figure 6.2. It occurred in three of the four cylinders examined immediately after TDC and therefore may be attributable to the piston assembly changing direction and possibly impacting against the cylinder wall, i.e. piston slap. Disruption of the rings at around TDC may be compounded by the very high in-cylinder pressures and shockwaves resulting from the combustion process.

However, as is the case with the other events of unknown origin, there is no further evidence available to substantiate any suppositions regarding possible source mechanisms. Further work would be required in order to clarify the source, and significance, of these events.

6.4.2 Continuous-type AE activity

In addition to burst-type activity the signals from the liner sensor positions also contain a continuous AE component that varies in amplitude during the cycle. This is proposed to originate from continuous ring-pack/liner interaction and shall be investigated in greater detail for normal operation and over varied lubricating conditions in Chapter 7.

6.5 Cross cylinder propagation

Previous work on large, two-stroke engines has found cross-cylinder AE propagation to be minimal and this has somewhat eased analysis through isolation of AE events relating to the instrumented cylinder [82]. Furthermore, tests on engine E using simulated sources have quantified cylinder head to cylinder head attenuation as in the range 35 to 40 dB [6]. However, in this work, cross-cylinder propagation was believed responsible for the presence of some events in signals acquired from engine F. Figure 6.29 shows an example of RMS AE acquired from the mid liner position of cylinder 2 with the engine operating at 25 % of MCR on the propeller curve. Although the majority of the events in this signal can be attributed to the injection process, valve activity and ring-pack/scavenging port interaction there are still further low-amplitude events that would appear to bear little relation to the processes occurring in the monitored cylinder.

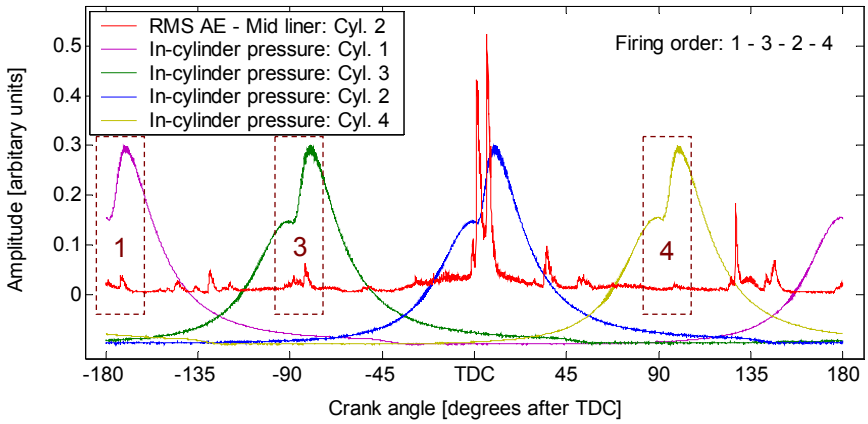

Figure 6.29: Engine F, mid liner signal showing AE events arising from cross-cylinder propagation.

Also shown in Figure 6.29 are in-cylinder pressure traces corresponding to the four cylinders of the engine. The occurrence of the injection process in each cylinder is signified by the sudden increase in pressure. A comparison of the AE signal for cylinder 2 with the in-cylinder traces of the other cylinders shows that there are low-amplitude AE events of similar structure that align with the injection processes in the adjacent cylinders 1 and 3. It is therefore a reasonable assumption that these events originate from the injection processes in these cylinders and that they are of sufficient source energy to overcome the cylinder to cylinder AE transmission losses. A similar comparison for the injection process of cylinder 4 supports this. In this case there are no corresponding events in the cylinder 2 AE signal and this can be explained since transmission losses would be greater as cylinder 4 is furthest from cylinder 2. The effects of cross-cylinder propagation are observed most at the mid liner sensor position as this location is closest to the neighbouring cylinders and the adjoining cylinder frame

Cross-cylinder propagation was not observed in signals acquired from engine E, due perhaps to a different cylinder frame construction and larger cylinder bores resulting in longer transmission paths.

6.6 Summary

This Chapter has been concerned with the interpretation of AE signals acquired from large, two-stroke engines. Through a combination of event mapping using knowledge of engine operation and source location via the use of sensor arrays source mechanisms for the majority of AE events generated in the upper cylinder area during normal operation have been identified. A summary of the major sources and characteristics of the resulting AE activity are presented in Table 6.1. For many of these events there was sufficient evidence to enable sources to be determined with a high degree of certainty. Conversely, for some events there was a lack of evidence to support assumptions regarding the source origins. In this case further work would be required with specific tests designed to elicit the information necessary to enable source location.

The findings of this Chapter are valuable in that they give an indication as to the aspects of engine operation which can be assessed through AE monitoring; these capabilities are discussed in greater detail in Chapter 9. Furthermore, this survey accounts for much

of the AE activity, which is beneficial when possible AE generation from sliding contact at the ring-pack/liner interface is investigated in the following Chapter.

Engine activity	AE characteristics
Fuel injection period	- High amplitude, burst-type events are generated from the series of impacts within the fuel valve that define the injection process. Further lower-amplitude AE activity is generated during the fuel delivery period. Naturally, these events are observed with greater amplitude at the injector and cylinder cover sensor positions. Evidence also suggests that for engine F some of these events are of sufficient strength to be represented in AE signals measured at adjacent cylinders.
Exhaust valve operation	- A significant feature of the cylinder cover and valve housing signals is a broad event arising from exhaust gas flow out of the cylinder as the exhaust valve opens. Characteristics of this event are related to the in-cylinder pressure at the point of opening. A further event appears to be generated at the fully open position. Closure of the valve is signified by a series of AE events. Again, all these events are best observed from locations close to the source, i.e. the valve housing and cylinder cover sensor positions.
Interaction between ring-pack and non-continuous features of the liner surface	- Burst-type events indicative of mechanical interaction were noted to result from the ring-pack passing over non-continuous features of the liner surface, i.e. the oil groove and scavenging ports. The amplitude of the event related to the oil groove was found to be highly variable, with the source thought to be ring clipping due to the relative orientation of rings and liner. The occurrence of scavenge port related events was found to be irregular, presumably due to the positional relationship between the scavenging ports and the ring ends. These events are principally observed in the liner signals.
Interaction between ring-pack and continuous liner surface	- The background AE in the liner signals is proposed to relate to source mechanisms associated with continuous ring-pack/liner interaction. This activity shall be investigated further in the following Chapter.

Table 6.1: Main sources and characteristics of AE generated within large, two-stroke, diesel engines.

Chapter 7

Two-stroke, crosshead, diesel engines: monitoring of sliding contact at the piston ring-pack and cylinder liner interface

7.1 Introduction

This Chapter investigates what information regarding the tribological behaviour at the ring-pack/liner interface is contained in the background continuous AE activity of signals acquired from large, two-stroke, diesel engines.

The basis for this investigation has been developed throughout this thesis. Similar analysis on signals acquired from small, four-stroke diesels, described in Chapter 5, revealed that they contained information relating to the ring-pack frictional behaviour. Exploratory experiments on a cylinder liner removed from engine E [142, 227] have also shown that AE events generated from Hsu-Nielsen sources anywhere on the internal surface are detectable from AE sensors located externally at the upper and mid liner sensor positions, albeit with varying source-sensor transmission properties dependant upon the respective source and sensor locations. Furthermore, a survey of the major AE sources under normal running conditions, detailed in Chapter 6, identified that burst-type AE activity originated from interaction between piston rings and non-continuous features of the liner surface. These observations support the belief that external AE measurements can provide an assessment of internal tribological conditions since if simulated and real impact-type sources were readily identifiable then it follows that other sources occurring at the ring-pack/liner interface, such as asperity contact or microseizure, may similarly be detectable.

This premise is evaluated in this Chapter through tests conducted on engine F, both over the engine operating range with normal lubricating conditions and with attempts made to degrade the ring-pack interfacial conditions through the removal of the lubricating oil supply. The signals acquired from these tests shall be investigated with a view to establishing; what changes occur in the continuous AE activity and which factors relating to engine operation determine these changes, what the source(s) of the continuous AE activity are, i.e. can it be attributable to source mechanisms active at the

ring-pack/liner interface, and what this means in terms of ring-pack monitoring capabilities.

The results and findings presented and discussed in this Chapter represent the most significant contribution to knowledge of all the work in this thesis.

7.2 Continuous AE activity generated during normal operation

The objective of this Section is to investigate continuous AE activity generated during normal running conditions. The variance of this activity will be evaluated against changes in engine operating parameters both during an engine cycle and over the engine operating range in order to assist in determining whether or not this activity relates to the ring-pack/liner interface. This is worthwhile not only to develop understanding of the AE source mechanism(s) but also to establish the baseline AE characteristics prior to testing with the removal of the ring-pack lubrication supply.

Examples of AE acquired during an engine cycle from sensors located on the liner were shown previously in Figures 6.17 and 6.18 for engines E and F respectively. These signals are a composite of transient, burst-type events and a continuous background component. The majority of the burst-type events have been attributed to ring-pack interaction with non-continuous parts of the liner surface as well as injector and exhaust valve operation. Other burst-type events have been observed and although there was insufficient evidence to confirm the source these were thought most likely to originate from impact-type interaction at the ring-pack interface.

The continuous background AE activity is a major component of the signals. As was the case for the small, four-stroke engines there are a number of possible AE source mechanisms. Several of these are associated with the ring-pack/liner interface including; asperity contact, blow-by, and sources related to full-film lubrication and oil transport. Further possible sources that are not directly related include exhaust valve leakage, bearing related sources (both main and crosshead bearings) and interfacial behaviour at the piston rod/stuffing box interface.

Examining signals corresponding to the upper liner positions in Figures 6.17 and 6.18 it can be seen that the background AE activity slowly fluctuates during the cycle, rising during the end of the compression stroke and falling during expansion. This feature is highly cyclically repeatable for signals acquired at steady-state conditions and has been observed consistently, although with varying attributes, in signals acquired from all cylinders examined of engines E and F. A comparison of the upper liner signal for engine F with the in-cylinder pressure trace in Figure 6.18 suggests that the amplitude of the background AE parallels the development of the in-cylinder pressure during the cycle. This initial link between in-cylinder pressure and AE activity around TDC shall be investigated further through tests over the operating range of engine F.

7.2.1 Variation over engine operating range

Tests over the engine operating range of engine F consisted of a number of loads on the propeller curve from 20 to 100 % of MCR (corresponding to engine speeds of 71.9 to 123 RPM, and power outputs of 1.4 to 7.1 MW) and three loads on the generator curve from 25 to 75 % of MCR (all at 123 RPM, and 1.8 to 5.3 MW) and are described by the in-cylinder pressure traces shown in Figures 7.1 and 7.2 respectively. The amplitude of these plots are shown in arbitrary units since calibration details were not available, although the relative variation of the peak compression and firing pressures with load are in line with that reported elsewhere [52].

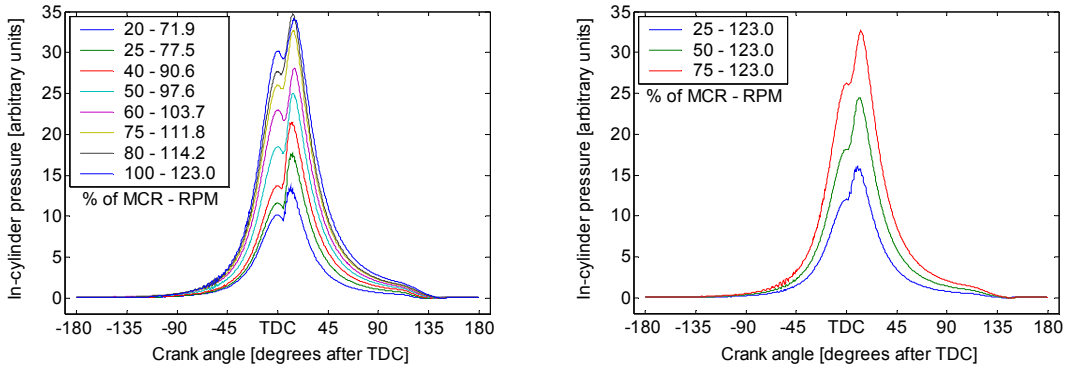

(a) *(b)*

Figure 7.1: Engine F, in-cylinder pressures from tests over engine operating range with normal lubricating conditions on (a) propeller curve, (b) generator curve.

The development of in-cylinder pressure with load is further described in Figure 7.2. For both operating modes, the area under the P-θ curve during the cycle, i.e. IMEP, is used as a qualitative measurement parameter.

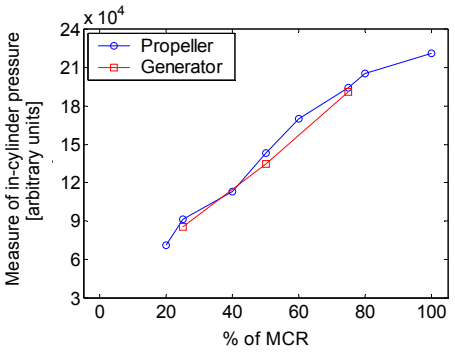

Figure 7.2: Measure of in-cylinder pressure versus load.

At each loading point the engine was run for a sufficient period of time to allow a dataset of over 400 cycles to be acquired using the slow-speed, 16-channel DAQ system with AE measurements made from the cylinder cover, mid liner and lower liner sensor positions. For each batch of data from each position a mean signal could be calculated and these are shown for both propeller and generator curve tests in Figures 7.3, 7.4 and 7.5 for the cylinder cover, mid liner and lower liner positions respectively. The lower liner signals shown in Figure 7.5 display significantly lower RMS AE levels due to the location of the sensor and the use of different instrumentation as was detailed in Figure 4.17. Nominally the same type of instrumentation was used in the measurement of the cylinder cover and mid liner AE signals, thus, barring differences in sensor sensitivity and coupling, the amplitudes of these two signals are comparable. The timings of the events for all three sensors are comparable.

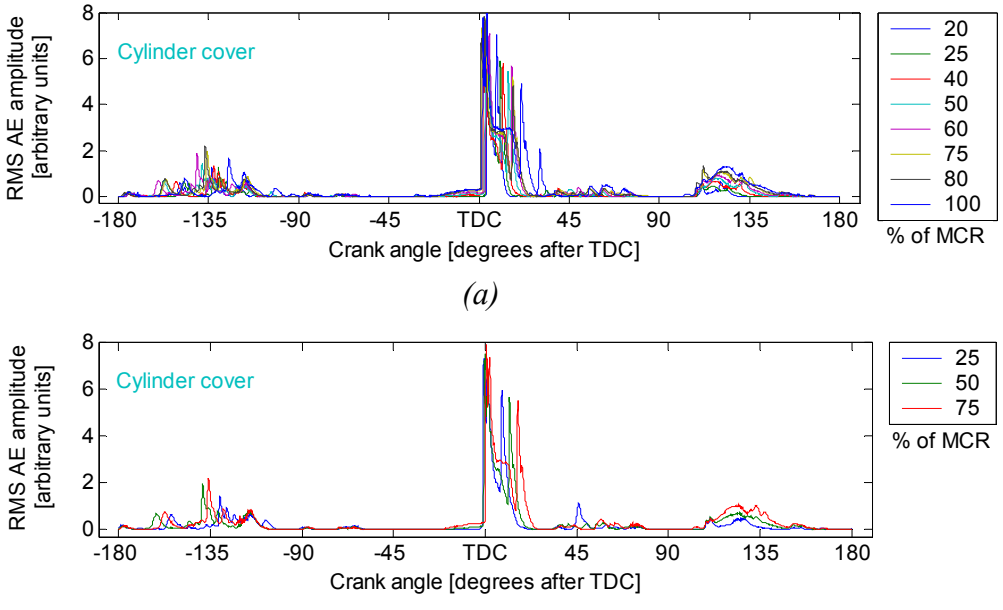

Figure 7.3: Engine F, cylinder cover, normal operating conditions, mean RMS AE signals at various loads on the (a) propeller curve, (b) generator curve.

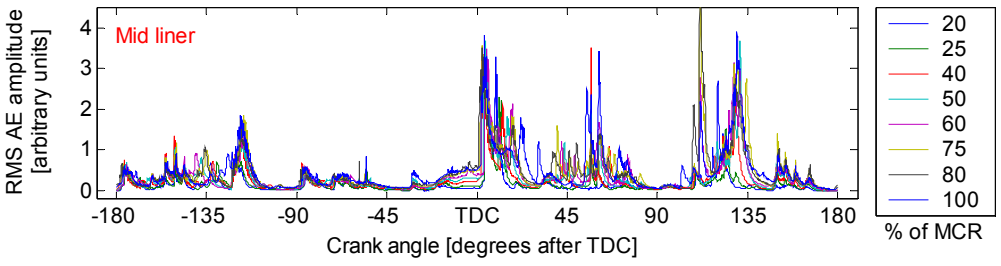

(a)

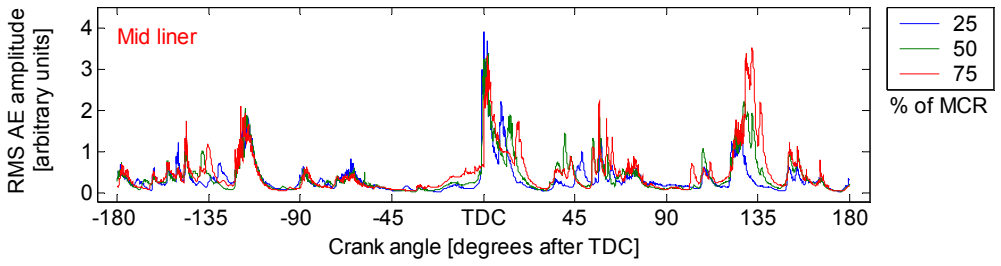

(b)

Figure 7.4: Engine F, mid liner, normal operating conditions, mean RMS AE signals at various loads on the (a) propeller curve, (b) generator curve.

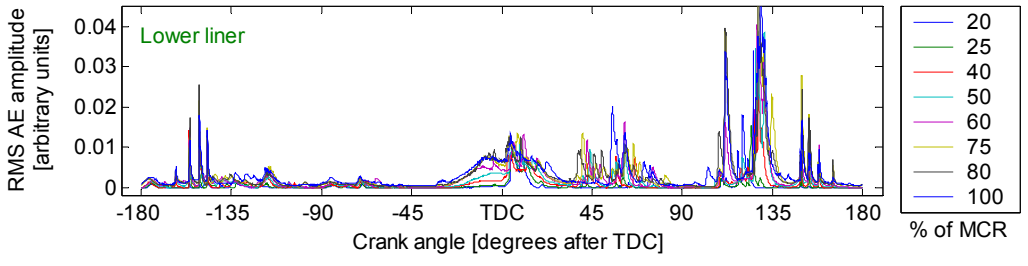

(a)

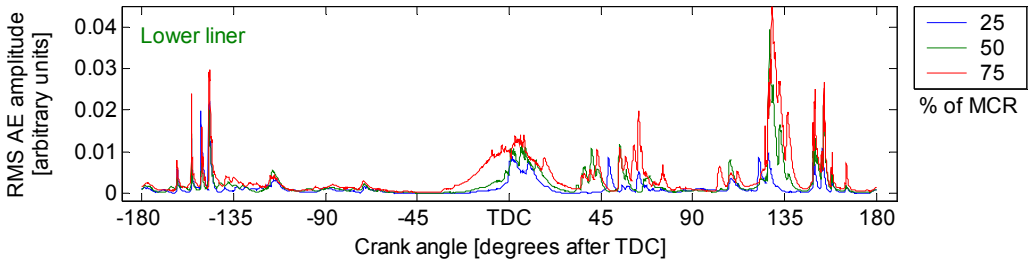

(b)

Figure 7.5: Engine F, lower liner, normal operating conditions, mean RMS AE signals at various loads on the (a) propeller curve, (b) generator curve.

With increasing load systematic changes in the signals can be observed. Many of these concern the events that arise due to injector and valve operation, and also ring-pack interaction with non-continuous parts of the liner surface. These events were described in greater detail in Chapter 6 including their variation with load and the rationale used in determining their respective sources.

The background continuous AE activity, however, displays little variation with load except for the area of the engine cycle around TDC. For clarity, windows of the signals from 40 degrees before to 40 degrees after TDC are shown enlarged in Figures 7.6, 7.7 and 7.8 for the cylinder cover, mid liner and lower liner positions. In each case, for both operating modes, the windows contain the background AE activity and also AE events relating to operation of the fuel injector. The injection events display the expected behaviour in that they indicate that injection duration increases with load. The influence of these events is greatest at the cylinder cover position, followed by the mid liner and then the lower liner position; which is simply a reflection of the distance of each position from the source and the corresponding attenuation of the events. The background activity for all sensor positions increases with load; this is particularly evident in the area prior to TDC where the injection sources are not active, although this is barely perceptible in Figures 7.6a and 7.6b which relate to the cylinder cover position due to the relative strength of the injection events. For the same reason, when the full amplitude of the signals is considered the variation of background AE is more appreciable at the lower liner position even though the amount of variance is greater at the mid liner position.

A further method to evaluate the variance of background AE with load is to compare the AE energy contained in the period of the cycle in which only the background AE source was active. In this case, the area 25 to 5 degrees before TDC was selected, the AE energy during this period for both operating modes is shown in Figures 7.6c, 7.7c and 7.8c for the cylinder cover, mid liner and lower liner sensor positions.

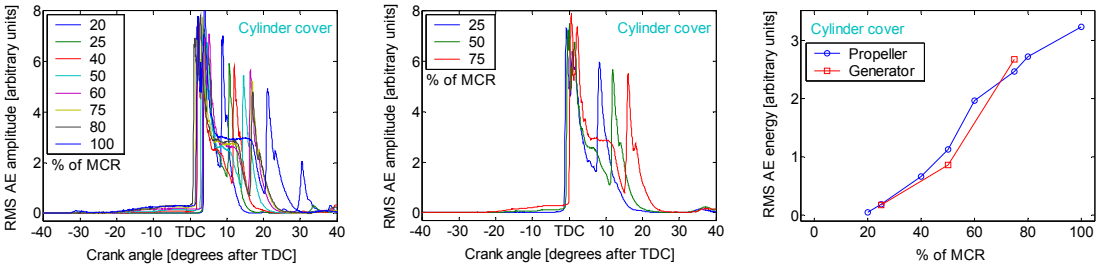

(a) *(b)* *(c)*

Figure 7.6: Engine F, cylinder cover, area of signal around TDC, (a) propeller curve, (b) generator curve, (c) AE energy during the period 25 to 5 degrees before TDC.

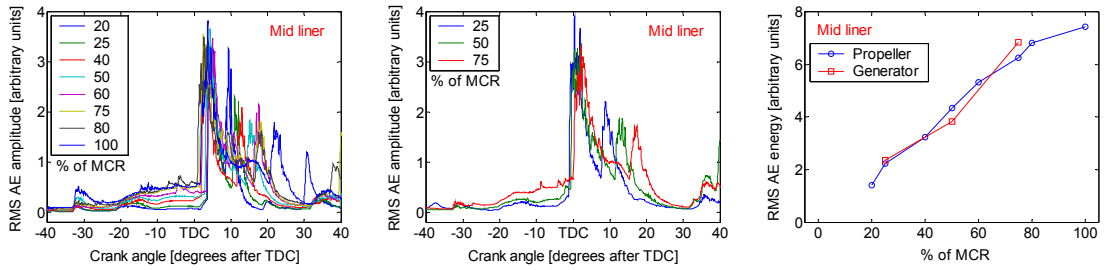

(a) *(b)* *(c)*

Figure 7.7: Engine F, mid liner, area of signal around TDC, (a) propeller curve, (b) generator curve, (c) AE energy during the period 25 to 5 degrees before TDC.

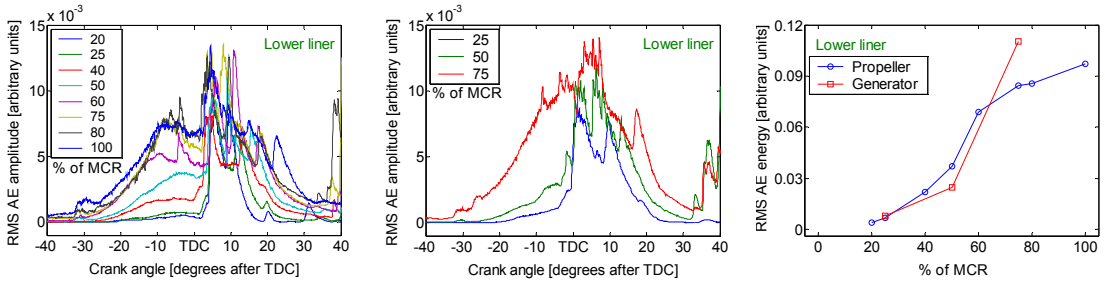

(a) *(b)* *(c)*

Figure 7.8: Engine F, lower liner, area of signal around TDC, (a) propeller curve, (b) generator curve, (c) AE energy during the period 25 to 5 degrees before TDC.

7.2.2 Discussion of results from normal operation

A systematic increase in the amount of continuous AE activity around TDC has been observed with load for tests conducted on both the propeller and generating operating curves. Evaluation of the increase in AE activity against the internal engine parameters which vary in response to increasing load may provide evidence that can indicate the source of the AE activity. For the propeller curve an increase in load entails an increase in engine speed and a proportional increase ($\propto n^2$) in torque output, whilst for the generator mode the engine speed is maintained constant, in this case at 123 RPM, and the torque output increases. In terms of the internal engine parameters the torque output can be directly related to the in-cylinder pressure and the engine speed dictates the piston sliding speed.

From analysis of the cyclic characteristics the background AE activity around TDC has been suggested to relate to the development of in-cylinder pressure. This hypothesis can be further examined in these tests over the engine operating range. The increase in

continuous AE activity around TDC with load for both operating modes, as quantified by the AE energies for each sensor position in Figures 7.6c, 7.7c and 7.8c, closely matches the increase of in-cylinder pressure with load shown in Figure 7.2. However, for the propeller curve, the increase in AE activity can also be attributed to engine speed as in this mode both parameters vary with load. Conversely, the increase in AE activity for the test on the generator curve can only be attributed to the increase of in-cylinder pressure.

Further substantiation of the relationship between in-cylinder pressure and continuous AE activity around TDC is offered in Figure 7.9 where the two parameters, AE energy contained in the windowed period from 25 to 5 degrees before TDC and the measure of in-cylinder pressure, are shown against each other in log-log format. Consistently for all three sensor positions the values from both the propeller and generator curve tests lie on an approximately linear relationship. This is significant as it suggests that the increase in AE activity for the propeller curve test is principally due to greater in-cylinder pressures and that the corresponding increase in engine speed, and thus piston speed, if it is a factor, is far less influential in the AE generation around TDC.

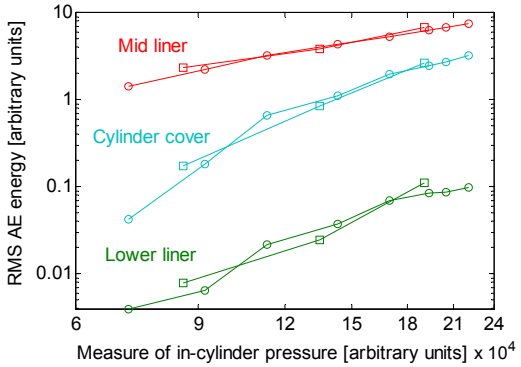

Figure 7.9: Correlation between in-cylinder pressure and background AE activity around TDC.

A relationship between in-cylinder pressure and continuous AE activity around TDC is consistent with several of the potential AE sources; valve leakage, asperity contact and blow-by.

Valve leakage is a known AE source which would be expected to generate greater amounts of AE with increasing in-cylinder pressure, moreover, in previous work on large, two-stroke engines background AE activity before and after TDC has been attributed to this source [82, 147]. However, for the AE activity under investigation in this Section there are a number of reasons which discount valve leakage as the source. Firstly, a comparison of the relative AE energy levels at the cylinder cover and mid liner sensor positions, Figure 7.9, shows that the background AE activity is stronger at the mid liner position, which suggests that the source is closer to the mid liner position.

Secondly, in the previous works [82, 147] leakage AE activity was evident in measurements at the exhaust valve housing only when sizeable damage was introduced to the exhaust valve; otherwise little AE activity was observed around TDC aside from injector related events. Further, it has to be assumed that for these tests on the dedicated research engine F the exhaust valve would be operating in a normal condition as damage would be identifiable from the frequent inspections. Thirdly, the background AE activity was observed consistently on each cylinder tested of both engines E and F thus indicating that it is a normal characteristic rather than a fault related feature.

A further observation which negates valve leakage as the source concerns signals acquired from the mid liner position. These typically show an increase in background AE in the period of approximately 40 to 55 degrees after TDC, as is demonstrated in Figures 6.17 and 6.18. This period of the engine cycle coincides with the passing of the ring-pack over the mid liner sensor position. Therefore, the implication is that during this period the background AE is attributable to a source at the moving ring-pack/liner interface and the variation of amplitude is due in part to the varying source-sensor attenuation as the ring-pack travels down the liner. A similar feature accompanies the ring-pack passing the mid liner sensor position on the piston upstroke although the amplitude is much reduced, presumably due to the lower in-cylinder pressures and therefore lower ring-pack/liner interaction forces.

Since the source of the AE is believed related to the ring-pack/liner interface then it may be possible to achieve a more precise identification of the source mechanism through comparison of the ring-pack behaviour with the characteristics of the continuous AE activity. However, in these tests there were no other measurement parameters acquired that would describe the actual ring-pack behaviour; therefore the comparison is limited to the expected, or typical, behaviour. This problem is compounded by the scarcity of published research which has considered ring-pack tribological behaviour of large, two-stroke engines on a detailed level. However, from information available [67, 81, 228, 229] it would appear that it operates in a similar manner to a compression ring of a small, four-stroke engine albeit with a more extensive boundary lubrication regime near TDC due to the slow speeds and long strokes [81]. Operational experiences and typical wear patterns are consistent with boundary conditions occurring around TDC [67, 81].

The expected ring-pack behaviour is further described by the modelled breakdown of friction forces during a cycle [228] shown in Figure 7.10. This indicates that hydrodynamic conditions are in place for the majority of the cycle but in the vicinity of TDC, with increasing in-cylinder pressure and liner temperature and decreasing sliding speed, friction due to asperity contact increases and becomes dominant. Since AE is known to be generated from asperity contact [170, 172, 216] this therefore represents a plausible explanation for the continuous AE generation around TDC. Asperity contact and boundary friction was also identified as the probable source of continuous AE in signals acquired from small, four-stroke engines discussed in Chapter 5. Further support can be garnered from the experimental evidence. The cyclic variation of friction force due to asperity contact indicated in Figure 7.10 corresponds well with the variation of the background AE activity. Additionally, with increasing load the friction force would be expected to increase due to increased loads applied to the rings through greater in-cylinder pressures, and this again is consistent with the variation of background AE activity with load.

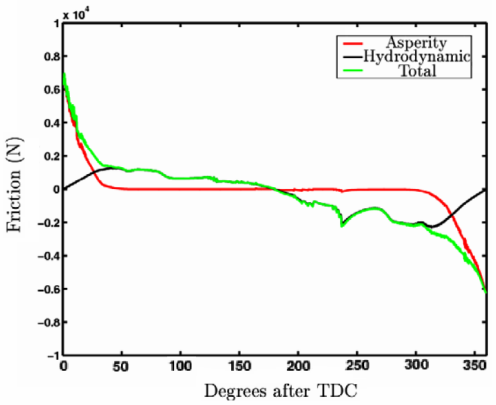

Figure 7.10: Modelled friction force for ring-pack of a large, two-stroke engine [228].

One observation that contradicts the concept that asperity contact is responsible for the continuous AE around TDC is that the engine speed, thus piston sliding speed, does not appear to be a significant factor in the AE generation over increasing load on the propeller curve. This is inconsistent with the body of previous work which has established that under mixed lubricating conditions both sliding speed and applied load are major factors in the amount of AE activity generated [172, 175, 182-184]. Piston sliding speed was also identified as a major factor in continuous AE generation from boundary friction within small, four-stroke engines, as discussed in Chapter 5, where a relationship was proposed between AE activity and frictional power loss. If this relationship were applicable also for the large engines then it may be anticipated that AE related to asperity contact would tend to zero at TDC as, regardless of the friction force, the frictional power loss is a function also of the piston speed.

A further possible source of the continuous AE around TDC is blow-by, i.e. the leakage of gases past the ring-pack [82]. In this case it does not necessarily mean gas leakage past the entire ring-pack as gas flow through the top ring gap into the second land (area of the piston between top and second rings), through the ring/liner contact area or circumferentially within the land areas may constitute an AE source. Blow-by is consistent with a source occurring at the ring-pack/liner interface and it can be assumed that some would occur, as even for an engine operating in a fault-free condition blow-by cannot be completely eliminated as long as the rings have gaps and are free to move in their grooves [64].

There is little published information available that would allow trends of normal blow-by flow-rates to be established over varying loads and speeds for large, two-stroke engines, however, predictions and measurements of normal flow-rates are available for small, four-stroke engines [65, 230]. Predictions for the mass flow-rate of gas past the top ring of a four-stroke diesel engine [65] showed a strong dependence to the development of in-cylinder pressure during the cycle. Given this relationship the blow-by flow-rate would then be expected to increase with load. Measurements of volumetric flow-rate per cycle [230], albeit on a spark ignition engine, confirmed that the amount of blow-by increased with engine load at constant speeds. The variation of the continuous AE activity around TDC, both during the cycle and with increasing load, is consistent with the characteristics of normal blow-by flow-rates.

A similar claim cannot be made regarding the observation that engine speed did not appear to be a significant factor in the continuous AE generation around TDC since, from the information available, the typical variation of normal blow-by levels with increasing engine speed could not be established. Predictions indicated that with increasing engine speed at constant load the blow-by mass flow-rate would increase [65]. However, measurements of volumetric flow-rate on the spark ignition engine [230] suggested otherwise, with the amount of blow-by per cycle observed to decrease with increasing engine speed at constant load. The explanation provided for this was that at increased engine speeds the time available for gases to flow through the ring-pack reduces.

To the author's best knowledge no prior work has considered the possibility of AE arising from blow-by; although it has been claimed that excessive blow-by can be

detected through monitoring of vibration and ultrasound activity [14]. In that example, the occurrence of excessive blow-by was signified by unexpectedly high energy vibration or ultrasonic activity coincident with high in-cylinder pressures. This is similar to the continuous AE activity with the exception that the AE feature appears to be a normal characteristic. This discrepancy can however be accounted for since in previous work AE monitoring has been found to be more sensitive to gas flows than vibration monitoring [82, 124, 125], and consequently it may be that AE monitoring is sensitive also to normal blow-by levels rather than just symptoms associated with faulty conditions.

One point of concern regarding the possibility of blow-by as the source is that a similar observation was not made consistently from AE signals acquired from the small, four-stroke engines investigated in Chapter 5. By the same principle, i.e. the rings have gaps and are free to move, some blow-by would be expected [64]; however, there was no significant continuous AE activity around TDC in all the work conducted on Engine B. A feature related to in-cylinder pressure was observed in the limited data acquired from the motored engine A. However, this appeared for only one cylinder out of the four, and considering the extent of AE propagation within the cylinder block of these small engines [152], it is therefore likely that this activity was fault related, perhaps due to excessive blow-by but equally as likely due to head gasket or valve leakage. The significance of the lack of blow-by related AE for the small engines may be tempered since the relative amounts of blow-by for each engine are unknown and it may be that normal blow-by flow-rates for the large engines are significantly greater than for the small, four-stroke engines.

The possibility that an aspect of the generation of hydrodynamic lubrication, i.e. oil shear, oil flows, etc., is directly responsible for continuous AE generation around TDC would appear unlikely since the existence of hydrodynamic lubrication would be expected to diminish close to TDC, as is typified in Figure 7.10. Furthermore, in previous work AE generation from interfaces where full-film lubrication is in place has been found to be minimal [170, 177].

Consideration of the lubrication characteristics of the overall ring-pack does though account for a significant difference between the signals acquired from the large, two-stroke and small, four-stroke engines. For the latter, at piston mid-strokes, continuous

AE activity was related to the influence of piston speed on ring-pack/liner boundary friction, whereas for the large, two-stroke diesels, at mid-strokes, there was little AE activity other than the anticipated events from valve operation and ring-pack interaction with non-continuous parts of the liner surface. However, this can be accounted for since the ring-pack composition, and thus operating characteristics, for the two types of engine are fundamentally different. The ring-pack of a two-stroke engine consists solely of compression rings, and therefore, unlike the four-stroke engine ring-pack, there is no oil-control ring. Consequently, at mid-strokes, with relatively high piston speeds and low ring loads, the entire ring-pack of the two-stroke engine will likely operate under full-film lubricating conditions [67, 229] and accordingly AE generation from asperity contact would be minimal.

In summary, the continuous AE activity around TDC has been attributed to an aspect of the ring-pack/liner interface although it is difficult to distinguish whether asperity contact or blow-by is the principle source mechanism. Arguments can be made to support each interpretation, based mainly on the observed relationship between AE activity and in-cylinder pressure, and there is insufficient evidence to discount either possibility. A major hindrance to the understanding of this AE activity is that the analysis is limited to comparisons with the expected ring-pack behaviour. A more definitive identification of the AE source could be achieved if other parameters were available that would describe the actual ring-pack behaviour in detail. Nevertheless, asperity contact and blow-by would appear to be the prime candidates and indeed it is perhaps likely that the AE activity around TDC is due to a combination of these sources (and possibly others). Little variation of continuous AE activity was observed with load at the piston mid-strokes and this was explained by the assumed predominance of full-film conditions for the entire ring-pack.

7.3 Variation of ring-pack lubricating condition

This Section presents and discusses results from the two destructive lubricant starvation tests conducted on engine F. The intention of these tests was to deteriorate ring-pack/liner interfacial conditions and to attempt to provoke scuffing through the removal of the lubricating oil supply to the instrumented cylinder during engine operation. The ability of AE monitoring to reveal changes in the internal conditions could then be

assessed with the premise being that if the expected deterioration can be detected then comparable changes occurring over a longer time-scale, i.e. the service life of a liner, would similarly be detectable.

However, in both tests the ring-pack interfacial conditions did not degrade to the point where scuffing was induced. Visual inspections were conducted at the end of each test in order to assess the incurred damage and no evidence of serious scuffing was found other than light scratches. This was true even for the second test in which cylinder 2 was operated without a direct supply of lubricating oil for 15 hours. In this case it was noted that although scuffing was not induced the wave cut surface profile was visibly worn down from the pre-test condition. For both tests, it was believed that the preservation of liner condition, or lack of scuffing, was likely due to the existence of an oil mist at the lower end of the liner originating from the other cylinders and available through the common air inlet and scavenging ports.

7.3.1 First lubricant starvation test

The structure of this test was described in Figure 4.16. To recap, it consisted of running the engine on the propeller curve at 25, 50 and 75 % of MCR, with the oil supply to cylinder 2 removed during the 25 % loading period and reconnected during the 75 % loading period. Over 200 cycles of data were acquired from the mid liner sensor position for each loading and oil supply condition. Figure 7.11 shows the mean signal for each batch of data.

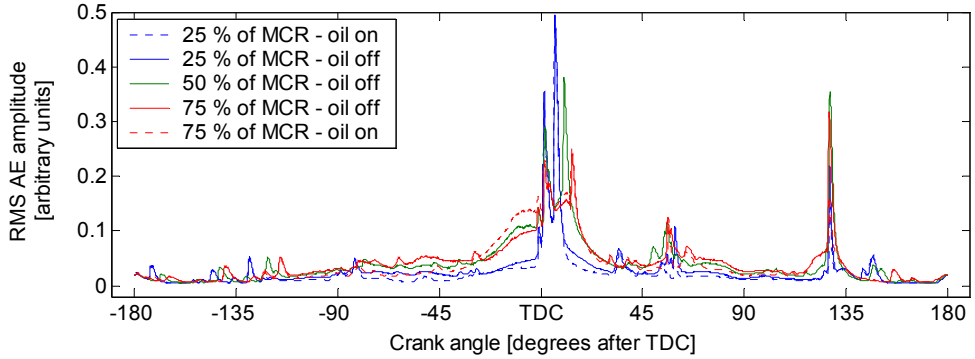

Figure 7.11: Engine F, mid liner, mean signal for each batch of data.

The continuous background AE activity has been suggested to arise from the tribological behaviour at the ring-pack/liner interface and it is evident that during this test this activity varied with both load and oil supply condition. For clarity,

comparisons of signals representative of the oil on and oil off conditions for 25 and 75 % of MCR are given in Figures 7.12 and 7.13 respectively, with the difference between the two signals highlighted in yellow. These plots do not contain the full amplitude of the burst-type events as the primary interest lies with the background activity.

In both cases the oil off signals displayed greater AE activity during the piston mid-stroke periods, i.e. from approximately 125 to 30 degrees before TDC and the corresponding period on the downstroke. However, there were differences in the angular period around TDC. For the 25 % of MCR case the oil off signal displayed greater activity whereas for the 75 % of MCR case the oil on signal showed greater activity during the period 30 degrees before TDC to TDC.

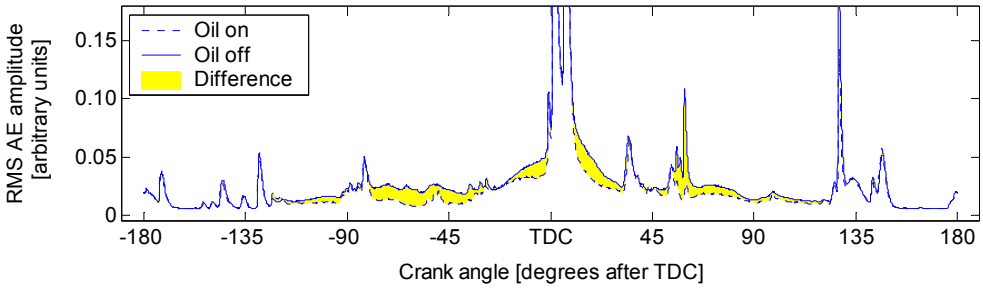

Figure 7.12: Engine F, mid liner, mean signals from oil on and oil off periods at 25 % of MCR.

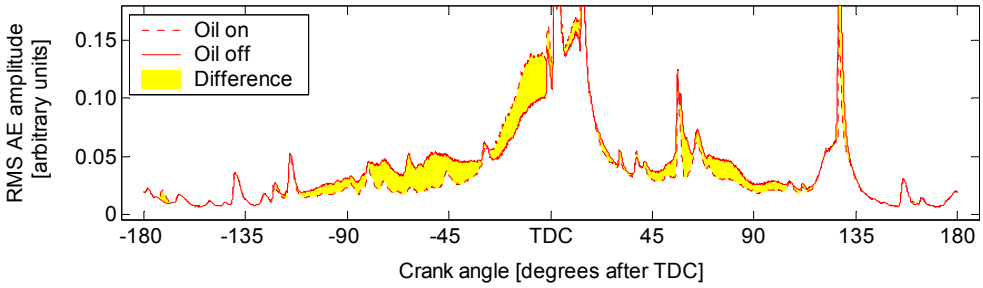

Figure 7.13: Engine F, mid liner, mean signals from oil on and oil off periods at 75 % of MCR.

A further method of examining variation in the AE activity during the course of the test is to calculate the AE energy of each individual cycle using Equation 3.2. The result of this is shown in Figure 7.14, the timing of the cylinder lubrication supply and loading condition changes are also indicated. It is clear that the cessation of the oil supply caused a small immediate increase in the overall cyclic AE activity. Conversely, when the oil supply was reconnected the cyclic AE activity immediately decreased, although this was followed by a progressive increase in overall AE activity till the end of the test.

Further variations in cyclic activity were evident during the test; a significant increase occurred when loading was raised from 25 to 50 % of MCR, although a similar step increase was not observed for the loading change from 50 to 75 %.

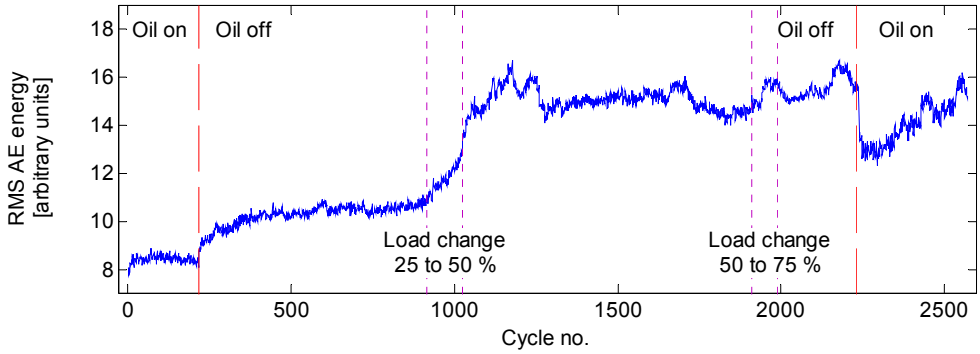

Figure 7.14: Engine F, first lubricant starvation test, variation of AE energy in whole cycle.

It can be of greater interest to examine the response of certain windowed areas of the data to the condition changes. Three windows were selected, as identified in Figure 7.15, each of which contained predominantly continuous AE activity thought to arise from the ring-pack/liner interface. The first is on the mid-stroke region of the compression stroke within the period 110 to 50 degrees before TDC, the second is the final part of the compression stroke from 30 before TDC to TDC, and the last is on the expansion stroke from 68 to 98 degrees after TDC.

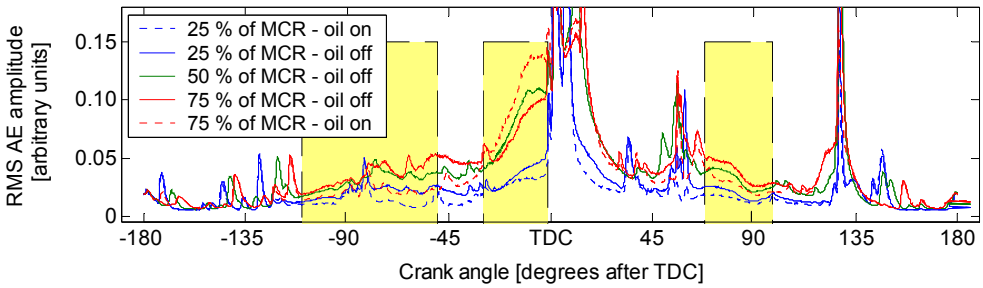

Figure 7.15: Engine F, mid liner, selected windows of cycle.

The AE energy contained within each window for each cycle of data during the test is shown in Figure 7.16. The plots relating to the mid-stroke regions on the compression, Figure 7.16a, and expansion, Figure 7.16c, strokes display similar responses to condition changes. Compared to the overall cyclic AE energy both windows show a greater relative response to changes in lubricating condition. They also display an increase in AE activity with each loading increase, although the response of the expansion window is greater for the 50 % to 75 % load change. A comparison of the two loading periods with normal oil supply conditions also shows that the 75 % period

generated greater activity. A further observation is that the energy in the final operating period, after the resupply of lubricating oil, remained relatively stable and did not display the progressive increase in activity that was evident in the whole cycle energy.

The windowed period relating to the end of the compression stroke, Figure 7.16b, displays a wholly different set of characteristics. During this period there appears to be only a small response to changes in the lubrication supply, the cessation of oil supply is accompanied by only a small increase in activity whilst the resupply of oil again shows only a minimal response. A relatively large increase in activity accompanies the load change from 25 to 50 %, however, during the 50 % loading period the AE energy drops with no immediately apparent explanation. From this point till the end of the test the AE rises progressively, being minimally influenced by the 50 to 75 % load change and the resupply of lubricating oil. It is this characteristic which is responsible for the increase in the overall cyclic AE energy towards the end of the test.

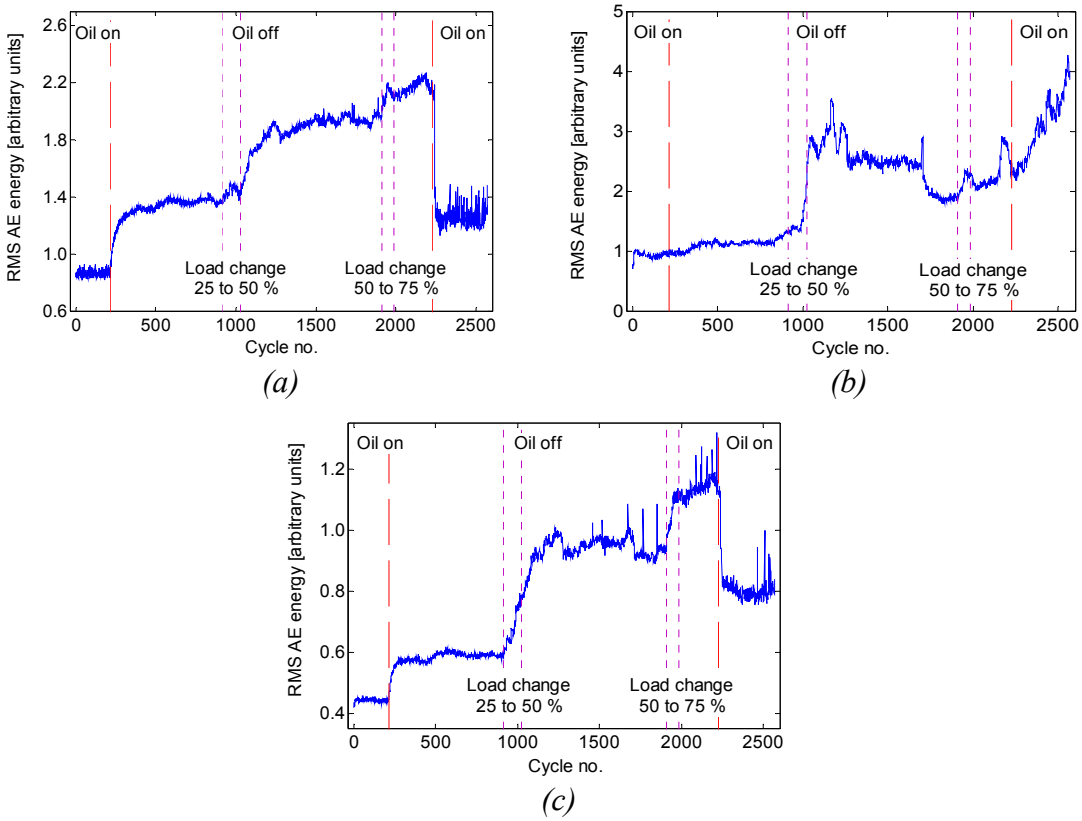

Figure 7.16: RMS AE energy during the test in the windowed period, (a) 110 to 50 degrees before TDC, (b) 30 degrees before TDC to TDC, (c) 68 to 98 degrees after TDC.

7.3.2 Second lubricant starvation test

A further test was conducted, several years after the initial lubricant starvation test, again on cylinder 2 of engine F, with a higher level of instrumentation and over a longer time period. In this case the cylinder was operated for 15 hours without a lubricating oil supply at various loads on the propeller curve as described previously in Figure 4.19. At each loading point the engine was run for a sufficient period of time to allow over 400 cycles of RMS AE data to be acquired from sensor positions on the liner using the slow-speed 16-channel NI DAQ system. Again, from each batch of data a mean RMS AE signal could be calculated.

Figure 7.17 shows mean signals acquired from the mid liner position at various points in time after the oil supply was turned off for (a) 25 %, (b) 50 %, (c) 75 % and (d) 100 % of MCR loading conditions, the full amplitude of the burst-type events is not shown as again the background AE is considered to be of primary interest. The time given for each signal is the time elapsed from the removal of the oil supply to the mid point of each batch of data. The last signal for the 100% of MCR loading conditions, Figure 7.17d, is the mean signal from the dataset acquired after the oil supply has been reconnected. Furthermore, for each plot, a mean AE signal representative of normal conditions for that particular loading condition is shown. These reference signals have been shown previously in the Section detailing AE activity over the normal operating range. Figure 7.18 shows similar plots with mean signals acquired from the lower liner sensor position.

In all the plots shown in Figs 7.17 and 7.18 there are features which develop over time after the oil supply was removed. This is particularly evident for the background activity at the mid-stroke areas which is observed to become more prominent with time, especially at the higher loads. A comparison of the signals between the two sensor positions shows that the changes in the signals appear to be more perceptible at the lower liner position. Again, this is due to the reduced influence of some of the burst-type events at the lower liner position.

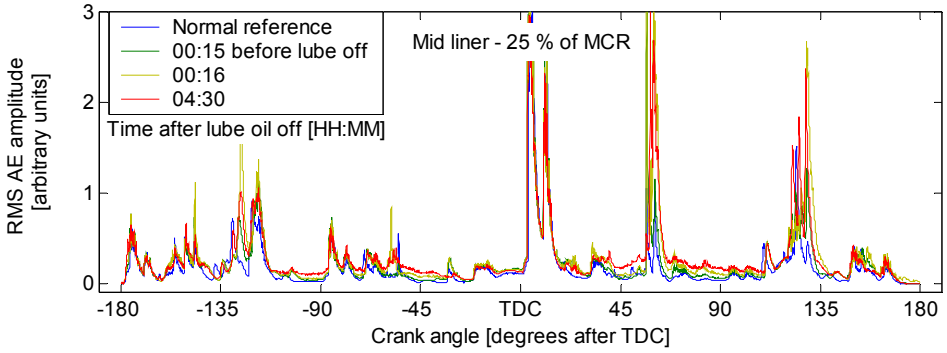

(a)

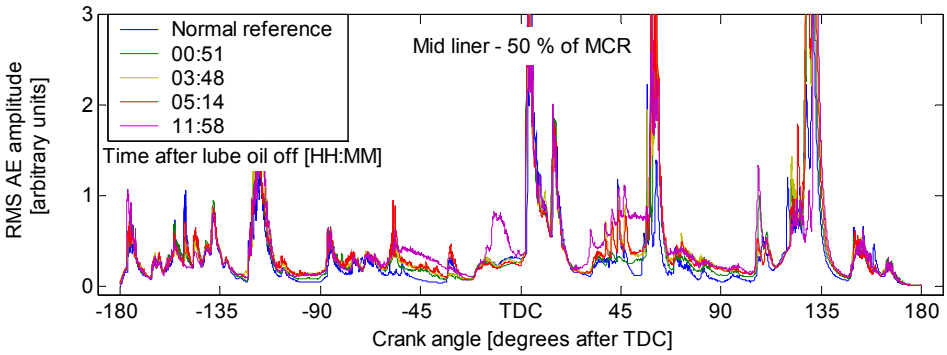

(b)

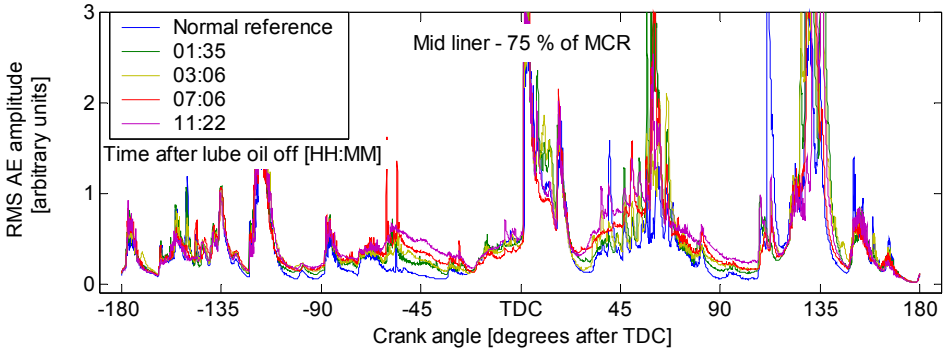

(c)

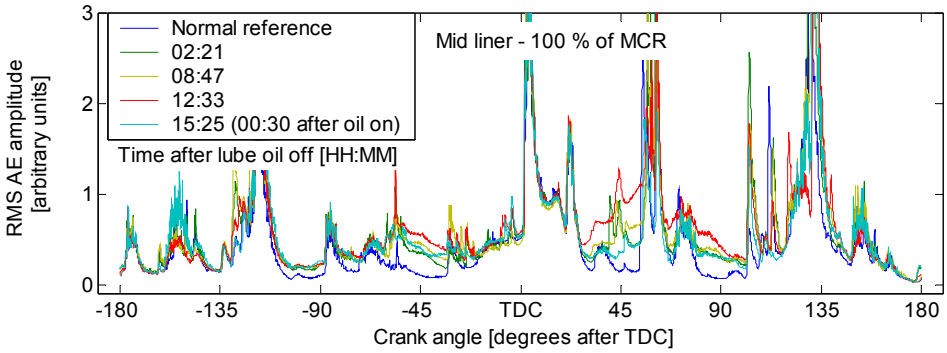

(d)

Figure 7.17: Engine F, mid liner sensor, mean RMS AE signals of over 400 cycles at various points in time after lubricating oil supply was removed for (a) 25 %, (b) 50 %, (c) 75% and (d) 100 % of MCR.

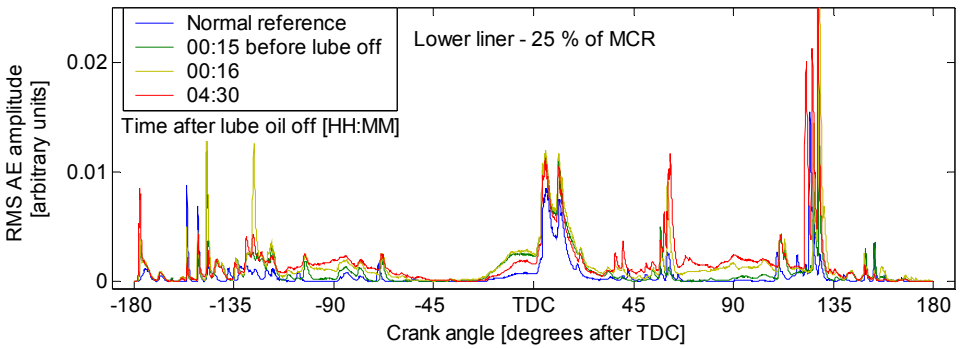

(a)

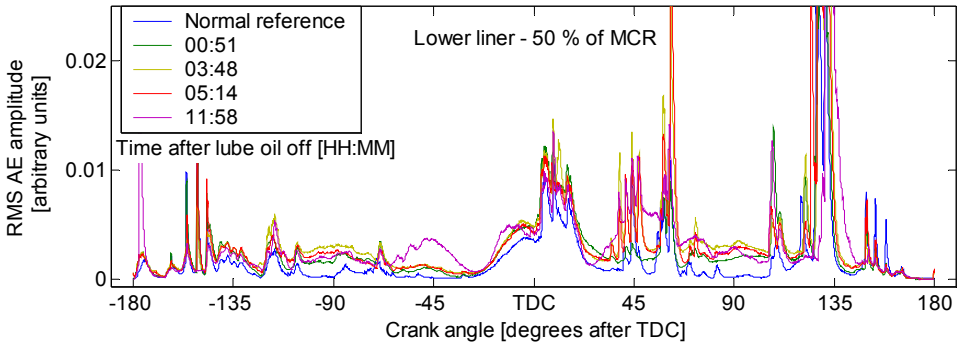

(b)

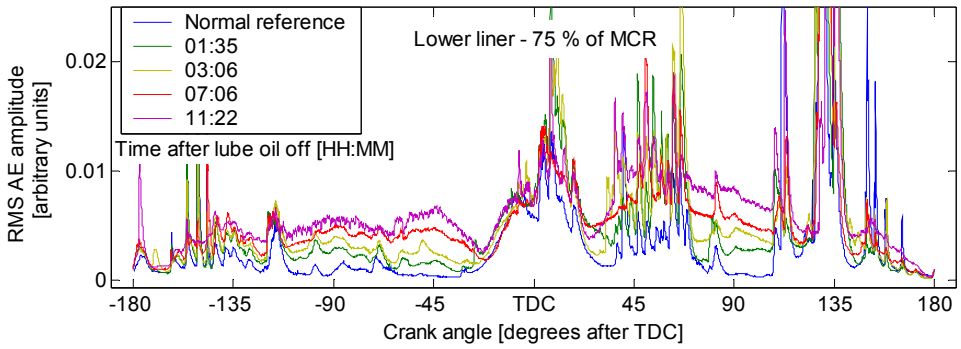

(c)

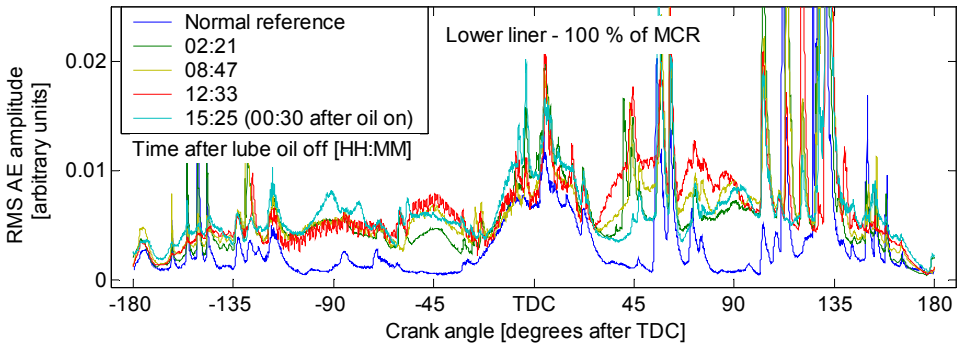

(d)

Figure 7.18: Engine F, lower liner sensor, mean RMS AE signals for over 400 cycles at various points in time after lubrication oil supply was removed for (a) 25 %, (b) 50 %, (c) 75% and (d) 100 % of MCR.

One point of concern is that the lubricant starvation test was not conducted immediately after the normal reference tests over the engine operating range. In between the two tests the engine was run for several days over different loads for purposes largely unrelated to this work. Over this period the conditions may have changed and therefore the signals shown for the normal reference tests may not be precisely indicative of the AE activity immediately prior to the lubricant starvation test. The effect of this can be evaluated through inspection of signals from the 25 % of MCR loading condition since for this case only data were available for the normal reference test and immediately prior to the removal of the oil supply. The relevant plots for mid and lower liner sensor positions are shown in Figures 7.17a and 7.18a, however, the amplitude of the background activity at 25 % of MCR is so low that comparison between the mean signals is difficult; therefore the lower liner plot is shown again in Figure 7.19 on an appropriate scale to emphasise the background activity. Further mean signals relating to the period immediately after the removal of the oil supply and several hours later are also shown.

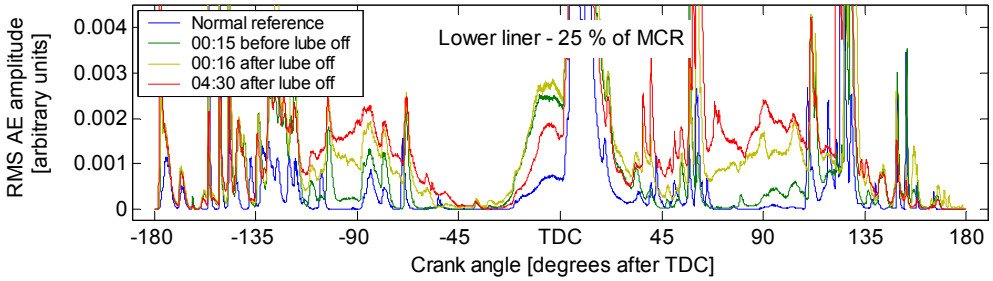

Figure 7.19: Engine F, lower liner sensor, exaggeration of background AE activity for 25 % of MCR loading condition.

From this it is clear that there are differences in the signals representing the normal reference test and the period immediately prior to the oil supply removal. The background activity for the latter was slightly greater at the piston mid-strokes and considerably greater for the area of the cycle just before TDC which has been identified previously as relating to ring-pack tribological behaviour governed by the in-cylinder pressure, i.e. asperity contact or blow-by. Since the external engine operating parameters were the same the differences in the signals can be considered as relating to changes in the engine condition that occurred between the two measurement times.

These differences represent only a small problem in terms of the overall analysis and interpretation of the results since it is also evident from Figure 7.19 that more substantial changes occurred after the oil supply was removed. A comparison of signals

representing immediately before and after the removal of oil supply shows that the mid-stroke activity increased considerably. The background activity in the area just before TDC, however, remained almost identical showing only a relatively small increase. Further changes can be observed after several hours of operation with no oil supply, the amount of continuous mid-stroke activity is greater still and the activity around TDC has reduced. A general observation covering the signals from all the loading conditions is that they all display changes between the first signal acquired after removal of the oil supply and the subsequent signals.

Similar to the analysis performed on data from the first lubricant starvation test the changes in the signals can be examined by calculating the AE energy generated during each cycle and during windows of the cycle. For the whole cycle AE a comparison of all data from each sensor position can be made, shown in Figure 7.20a for the mid liner position and in Figure 7.20b for the lower liner position. Each value represents the mean cyclic AE energy for a particular dataset and the error bars indicate the standard deviation of the cyclic AE energy over the dataset. The values given for zero hours are from the normal reference tests over the engine operating range. For the 25 % loading case values for both the normal reference test and the period immediately preceding the removal of the oil supply are given at zero hours, with the latter being of the greater value.

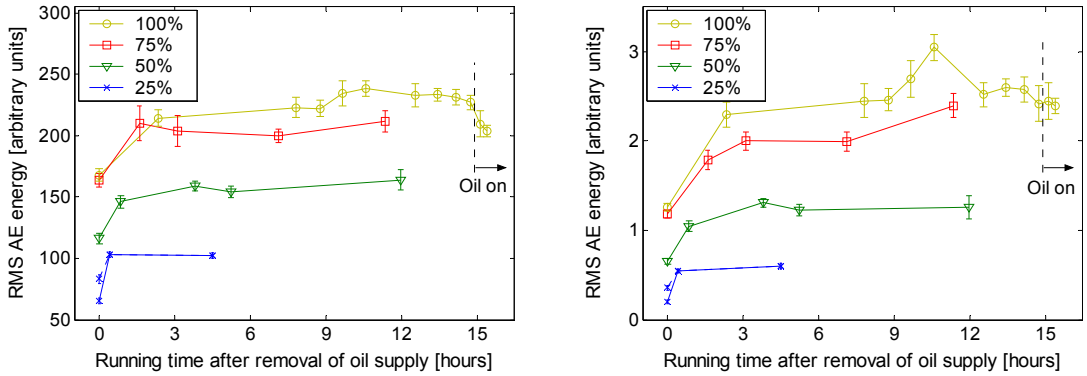

Figure 7.20: Engine F, lubricating oil off test 2, variation of RMS AE energy generated in a whole cycle from (a) mid liner, (b) lower liner.

The first observation is that the variation of AE energy per cycle is somewhat similar for both sensor positions and, as indicated previously from the plots of RMS AE signals at various times, the AE energy per cycle increases systematically with each increase in load.

Furthermore, for each load the AE activity for both sensor positions displayed a similar characteristic in that an immediate increase in activity was observed from the normal reference value to the first dataset after the oil supply was stopped. Although there may be some uncertainty regarding the values for the normal reference conditions it is considered that any discrepancy between this and the activity immediately prior to the lubricant starvation test would be relatively small and that there would still be an increase in activity for each load when the oil supply was removed. Indeed, this was the case for the 25 % of MCR values.

Closer examination of the cycle-by-cycle AE energy during the period of operation at 25 % of MCR when the oil supply was removed is provided in Figure 7.21. All three sensor positions displayed an increase in activity and, as expected considering the anticipated outcome of this condition change, this was more apparent from the liner sensor positions.

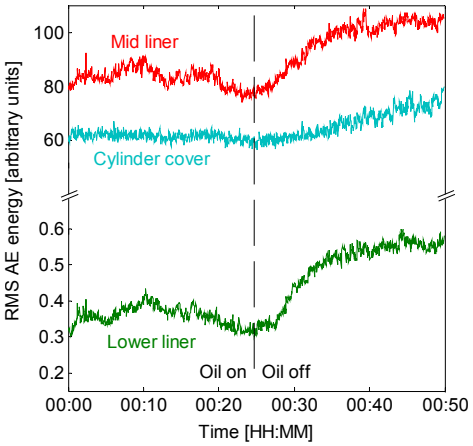

Figure 7.21: Variation of cyclic AE energy upon removal of oil supply.

Referring again to the development of AE energy during the test in Figure 7.20, after the initial increase due to the removal of oil supply, for all loads, the AE energy per cycle generally increased slowly with time. After the oil supply was reconnected time constraints limited the amount of engine running time and hence data were acquired from solely the 100 % of MCR loading condition. This showed that the cyclic AE energy at the mid liner position reduced by a small amount whilst the lower liner position displayed an even smaller reduction. The lack of data from the other loading conditions means that no broad conclusions can be made regarding this aspect of the test.

A cycle-by-cycle analysis of the operating period where the oil supply was reconnected is given in Figure 7.22; this covers the final three data points in the overall time-history plots given in Figure 7.20. Figure 7.22 shows that both the mid and lower liner activity reduced upon the resupply of oil. For the lower position the amount of this reduction appears to be within the general fluctuating range of the data and it is this characteristic which means that when this period is split up into three sections the activity in Figure 7.20 appears relatively stable.

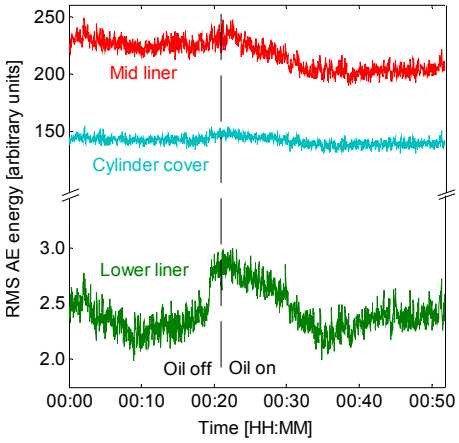

Figure 7.22: Variation of cyclic AE energy upon reconnection of oil supply.

Crank angle windows were selected in order to investigate how the AE activity in particular areas of the engine cycle changed with varying lubrication condition. Four windows were selected, as identified in Figure 7.23, three of these predominantly contained background continuous activity and the other, located just after TDC, contained background activity and events originating from the injection process. The AE energy in each window was calculated for each cycle of each dataset and the results of this are presented for each of the four windows in Figures 7.24 for the mid liner position and in Figure 7.25 for the lower liner position. Again, the values at zero hours correspond to the normal reference tests with the exception of the 25 % loading condition which also shows the value for the operating period immediately preceding the removal of the oil supply; in all cases this is greater than the normal reference value.

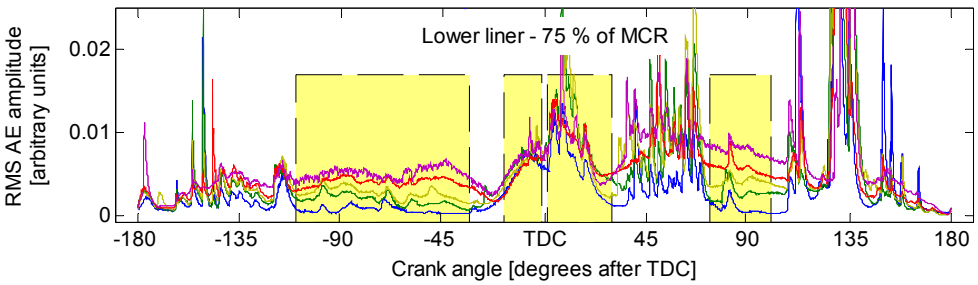

Figure 7.23: Engine F, lubricating oil off test 2, selected windows of cycle.

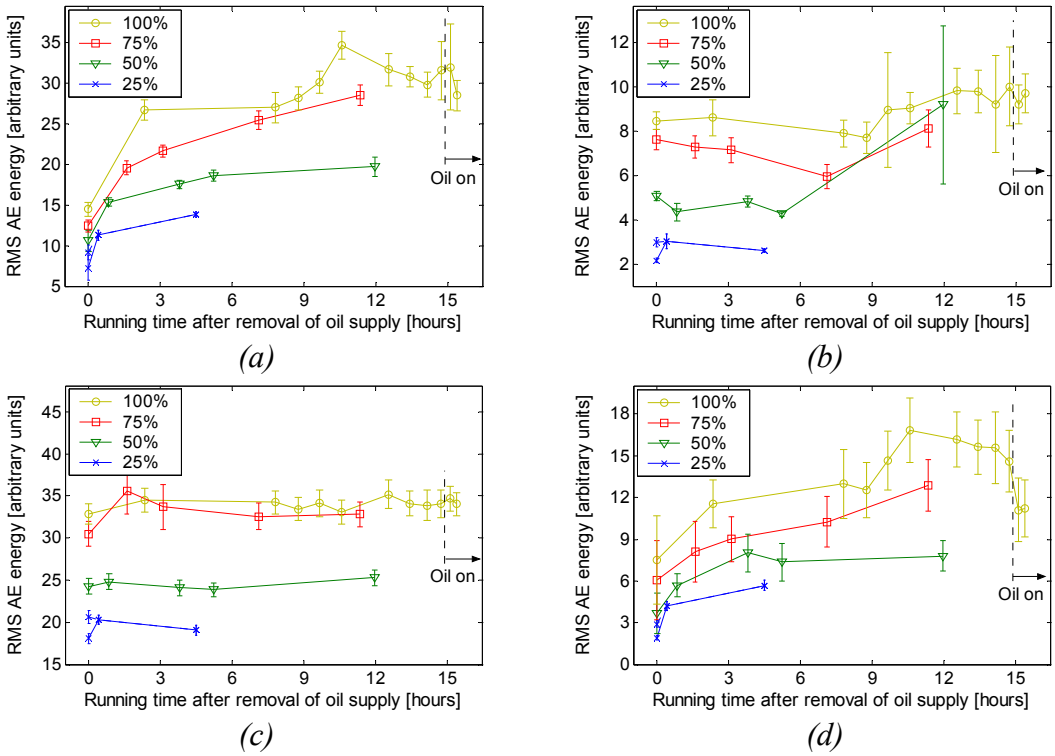

Figure 7.24: Engine F, mid liner, RMS AE energy during the test in the windowed period (a) 110 to 33 degrees before TDC, (b) 18 degrees before TDC to TDC, (c) TDC to 30 degrees after TDC, (d) 70 to 100 degrees after TDC.

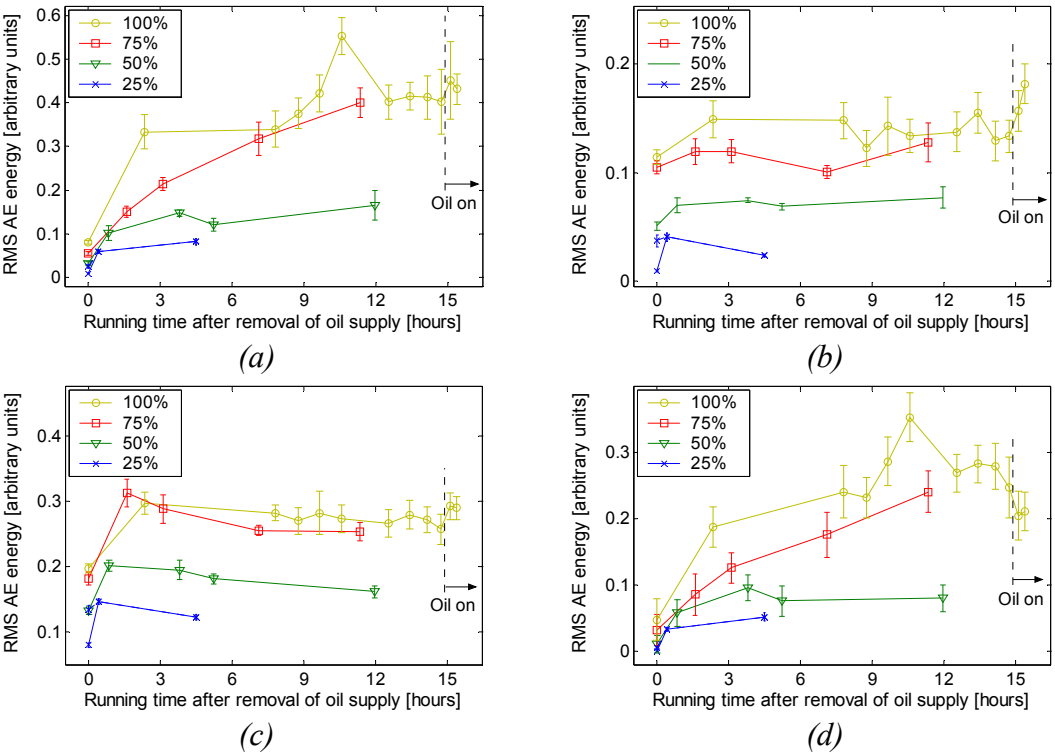

Figure 7.25: Engine F, lower liner, RMS AE energy during the test in the windowed period (a) 110 to 33 degrees before TDC, (b) 18 degrees before TDC to TDC, (c) TDC to 30 degrees after TDC, (d) 70 to 100 degrees after TDC.

There are a number of similarities in these results. Firstly, each window displayed a somewhat similar response at both sensor positions. Secondly, as was the case for the whole cycle energy the AE energy contained in each window increased with load. Thirdly, the findings were similar to the first lubricating oil off test in that the results from each windowed area vary depending upon where in the cycle the window is located.

The windows relating to the mid-stroke regions on the expansion and compression strokes produced similar results. The AE activity for each load showed an initial increase in activity after the oil supply was removed. This was true for the 25 % of MCR case regardless of whichever value was taken as the reference. Thereafter, particularly for the higher loads, the mid-stroke AE activity increased as the test progressed. The amount of this increase was much greater than for the cyclic AE energy shown previously in Figure 7.20.

The two windowed areas around TDC produced results that were similar to each other but different to the mid-stroke characteristics. It is clear that for the mid liner sensor position, Figures 7.24b and 7.24c, there was little significant variation in AE activity over the entire test, one exception being the last value for 50 % of MCR in Figure 7.24b. For the lower liner sensor position, Figure 7.25b and 7.25c, there was an initial increase in AE activity for all loads after the oil supply was removed but little change thereafter. However, a comparison of the values at zero hours for 25 % of MCR shows that the value for the period immediately prior to the oil supply removal was significantly greater than the normal reference value. Hence, for these windows, this brings the values for zero hours for the other loads into doubt and in actuality it may be that little or no change occurred upon the removal of the oil supply.

Each windowed area showed a different response to the resupply of lubricating oil. At both sensor positions the windowed area of the expansion stroke showed the greatest drop in activity. However, not all windows displayed a drop in AE activity. The window immediately prior to TDC for the lower sensor position, Figure 7.25b showed a sizeable increase in activity which was comparable to the response of the similar window during the first lubricant starvation test, Figure 7.16b. The other windows showed small fluctuations with AE activity marginally increasing or decreasing.

7.3.3 Discussion of results from lubricant starvation tests

Discussion and interpretation of the results from these tests can be separated based upon the two areas of the engine cycle which showed distinctly different results, these being the piston mid-stroke regions and the area around TDC. For both of these areas similar results were obtained from the two lubricant starvation tests which is indicative of good repeatability.

7.3.3.1 Piston mid-stroke regions

The strongest findings concern the continuous AE activity generated during the piston mid-stroke regions. From tests with normal lubricating conditions there was minimal continuous AE activity generated during the mid-stroke periods which was presumed due to the predominance of full-film lubricating conditions. For both tests where the lubricant supply was removed increased AE activity at the mid-stroke regions was observed. This was particularly apparent for the second test in which the cylinder was starved of a lubricant supply for a longer period of time; in this case the background AE activity became more prominent with time.

The changes in mid-stroke AE activity during the second lubricant starvation test are effectively summarised in Figures 7.26 and 7.27 for data acquired from the mid liner and lower liner sensor positions respectively. Selected values are shown over loads from 25 % to 100 % of MCR for three conditions; with normal oil supply, for the first dataset at each load after the oil supply was removed (up to 2:20 hours) and a significant period after the oil supply was removed (over 10 hours for the 50 %, 75 % and 100 % of MCR values and 4:30 hours for the 25 % of MCR value). Figure 7.26a consists of values extracted from Figure 7.24a, the compression stroke window from 110 to 33 degrees before TDC, and Figure 7.26b relates to Figure 7.24d, the expansion stroke window from 70 to 100 degrees after TDC. Similarly, for the lower liner position, Figure 7.27a corresponds to Figure 7.25a, the compression stroke window, and Figure 7.27b relates to Figure 7.25d, the expansion stroke window.

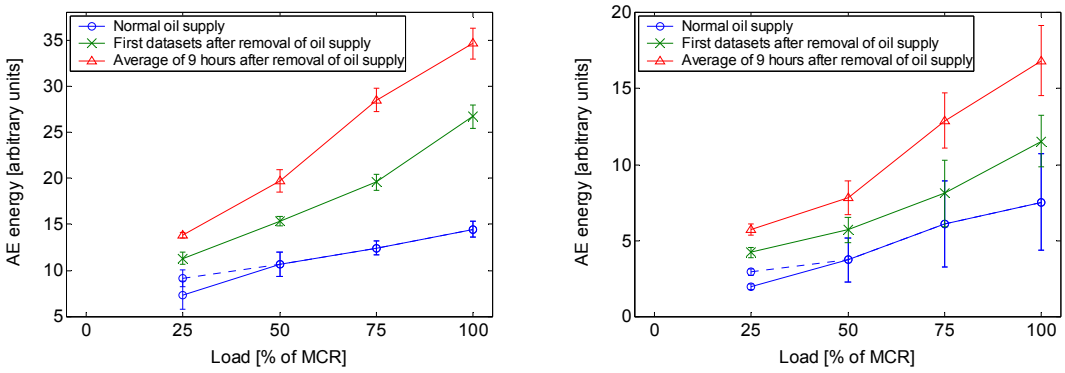

Figure 7.26: Engine F, mid liner, selected values from second lubricant starvation test, (a) compression mid-stroke window, (b) expansion mid-stroke window.

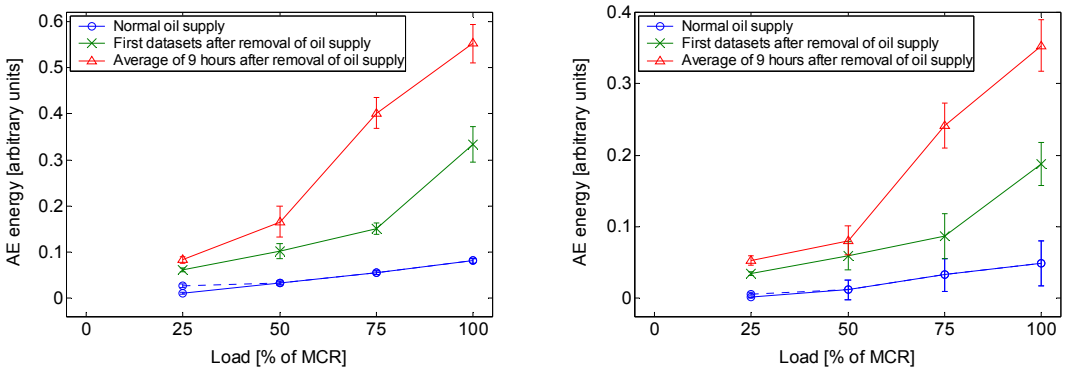

Figure 7.27: Engine F, lower liner, selected values from second lubricant starvation test, (a) compression mid-stroke window, (b) expansion mid-stroke window.

In all the plots in Figures 7.26 and 7.27 it is evident that under normal oil supply conditions the mid-stroke AE activity increased slightly with load. This was not perceptible beforehand from plots of the RMS AE signals in Figures 7.4 and 7.5 and it suggests that either full-film conditions were not in place for the entire ring-pack at mid-strokes and that there was a small element of asperity contact and boundary friction, or that blow-by was active at mid-strokes as well as around TDC albeit to a much lesser extent. After the oil supply was removed the amount of AE activity in each window and the gradients of the load-AE energy relationships increased progressively with time.

There remains the small possibility that the development of mid-stroke AE activity was due solely to the progression of engine running time rather than the combined effects of lubricant starvation and engine running time. However, this is discounted by the comparison shown in Figure 7.28 of signals acquired at the same operating conditions

approximately 35 engine running hours apart, i.e. a duration greater than the second lubricant starvation test. The signals correspond to datasets acquired at full load with normal oil supply during the reference tests on the propeller curve and from a period of operation between the reference tests and the second lubricant starvation test. It is clear from Figure 7.28 that there was little difference in continuous AE activity at mid-strokes over this time period, although AE activity around TDC increased. Testing on engine E over a time scale of several days also showed little variation in mid-stroke AE activity at constant operating conditions.

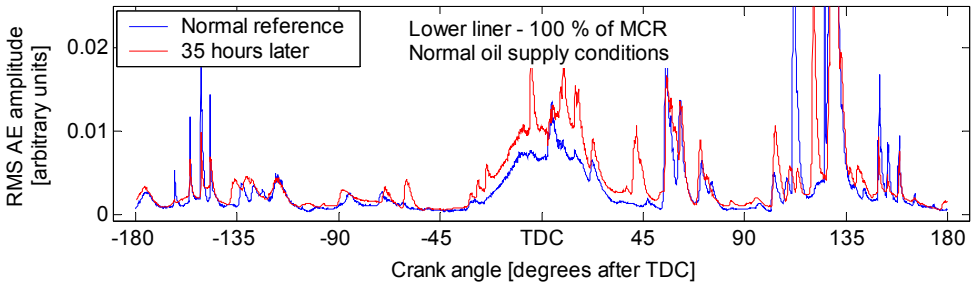

Figure 7.28: Engine F, lower liner, mean signals from normal reference test at 100 % of MCR and 35 hours running time later at the same operating conditions.

This therefore indicates that the starvation of lubricant, and consequent changes in tribological behaviour at the ring-pack/liner interface, was the underlying reason for the development of the mid-stroke AE activity. Further evidence is available to support this, for instance, changes in the oil supply condition were observed to have an immediate effect on the amount of AE activity, Figures 7.16a and 7.21. Regarding the AE sensor array, a comparison of relative AE energy levels at the mid liner and cylinder cover positions, Figures 7.21 and 7.22, is consistent with a source on the liner as it indicates that the mid liner signals contain the greatest energy.

The explanation for increased mid-stroke AE activity is straightforward. Large, two-stroke engines operate on a total-loss lubricating system, hence, there is a requirement for a continual supply of oil in order to replenish that lost from the liner through being scraped down or burned off during the combustion process. With no oil supply the availability of lubricant on the liner surface will gradually decrease over time and this will diminish the ability of the piston rings to generate hydrodynamic lubricating films. Therefore, as conditions deteriorate, an increasing amount of the ring load at piston mid-strokes would be supported by asperity contact and given that AE is known to be generated from asperity contact it would be expected that AE activity would increase in

relation to the increasing amounts of boundary friction incurred at the ring-pack/liner interface.

The experimental results closely match this anticipated behaviour, therefore implying that the ring-pack at mid-strokes was indeed operating under mixed or boundary lubricating conditions. It also indicates that AE relating to boundary friction at the ring-pack/liner interface can be detected at the external sensor positions, a fact not conclusively established through previous tests over the engine operating range. The post-test inspection of the liner further suggested the presence of boundary friction as the crests of the wave cut surface profile were found to have worn down.

Evidently, the principal factor in the mid-stroke AE generation is the lubrication regime in place at the ring-pack/liner interface. With boundary or mixed lubrication conditions in place it has been ascertained through work over a variety of applications [172, 183, 202] that there is a relationship between the amount of AE generated and the factors which govern the frequency and severity of asperity contacts and the corresponding boundary frictional losses. Two major factors are the relative sliding speed and the applied load. In terms of the ring-pack/liner interface these correspond to the piston sliding speed and the ring load, the latter being closely related to the in-cylinder pressure but also including a component relating to ring pre-tension.

Initial evidence that these two factors do influence mid-stroke AE generation can be obtained from Figures 7.26 and 7.27. In each plot relating to the windowed mid-stroke periods on the compression and expansion strokes the AE energy was observed to increase with load. Although this was true for the normal oil supply conditions the relationship became more apparent with time after the oil supply was removed and presumably the interfacial conditions deteriorated. A similar relationship between AE energy and load was observed for data from the windowed mid-stroke periods during the first lubricant starvation test shown in Figures 7.16a and 7.16c. However, given that both these tests were conducted on the propeller curve each increase in load constituted an increase in both engine speed, hence piston sliding speed, and in-cylinder pressure, i.e. ring load, and therefore the increase in AE activity cannot be attributed to a single factor and is more likely due to a combination of both factors.

Further understanding of the influence of these variables can be achieved from examination of the variation of background AE activity during a cycle. For instance, Figure 7.29 provides a comparison of the piston speed to the development of mid-stroke AE activity after the oil supply was removed for measurements from the lower sensor position at 75 % of MCR. It is clear that as the friction-related background AE developed over time it increasingly resembled the profile of the piston speed thereby offering further evidence that piston speed is an influential factor in the AE generation. This observation corresponds to the relationship identified previously in Chapter 5 between background AE activity and the influence of piston speed on frictional power loss at the ring-pack/liner interface of small, four-stroke engines.

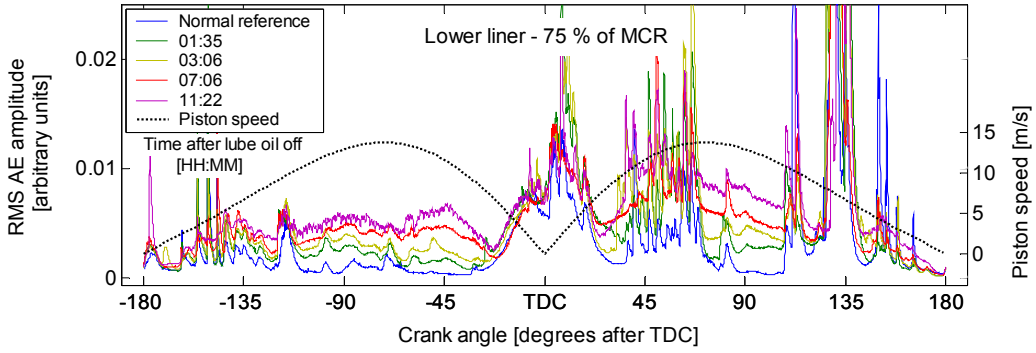

Figure 7.29: Engine F, lower liner, 75 % of MCR, comparison of mid-stroke AE activity at various times after lubricating oil supply turned off to piston speed.

In-cylinder pressure has previously been identified as influencing background AE generation in the vicinity of TDC through its effect on either asperity contact or blow-by. Evidence also suggests that it is a factor in AE generation at the mid-stroke regions when boundary lubrication conditions are in place. The background AE levels for each signal on the expansion stroke in Figure 7.29 are greater than the corresponding angular period on the compression stroke. This is considered to be due to the influence of in-cylinder pressure as it is greater on the expansion stroke and hence the piston rings are more highly loaded. This is consistent with a relationship between AE activity and frictional power loss.

The observations that sliding speed and in-cylinder pressure are factors in the mid-stroke AE generation further supports the belief that in these tests the ring-pack operated under mixed lubricating conditions after cessation of the oil supply. Conversely, this also strengthens the argument that prior to this, i.e. the tests with

normal lubricating conditions, the ring-pack operated with predominantly full-film lubrication at mid-strokes.

However, there has to exist a small element of doubt regarding these findings as interpretation of the changes in AE activity is limited only to a comparison with the expected ring-pack behaviour. The lack of any further measure of ring-pack behaviour means that there is no way of establishing the actual tribological conditions and therefore a more conclusive interpretation of the results cannot be achieved. Therein lies the root of the problem; there are few methods available that can reveal information about the internal conditions in running engines, and as described in Chapter 2, there are fewer still that are suitable for long-term condition monitoring. The positive aspect of this, in terms of the prospects of AE monitoring, is that there is a clear requirement for techniques which can offer insight into the ring-pack/liner interfacial conditions. Moreover, although it cannot be validated, the inference between mid-stroke AE activity and interfacial boundary friction would appear to be of sufficient robustness to justify the view that AE monitoring can provide valuable diagnostic information about mid-stroke conditions at the ring-pack/liner interface.

7.3.3.2 Region around TDC

Interpretation of the results concerning the continuous AE activity around TDC is less conclusive. This is primarily because the response of this AE activity to changes in the oil supply condition is different to that which may have been expected. Furthermore, the source mechanism of this activity under normal operating conditions has not been firmly established; tests over increasing load on the propeller and generator curves with normal lubricating conditions indicated that it was related to in-cylinder pressure with the source mechanism likely to be either asperity contact or blow-by.

Under normal operating conditions the ring-pack would be expected to function with mixed or boundary lubricating regimes in place at around TDC. With no oil supply the conditions around TDC would be anticipated to deteriorate, and consequently it may be expected that greater amounts of AE activity would be generated. However, the results for the first lubricant starvation test, Figure 7.16b, indicate that the amount of AE energy in the windowed period before TDC showed little response to changes in the oil

supply. Similar results were obtained for the second test, Figures 7.24b and 7.25b. The latter is summarised in Figure 7.30 which shows the relationship between load and AE energy at three conditions; with normal oil supply, just after removal of the oil supply and a significant time after removal of the oil supply, the values relate to the lower liner sensor position and the windowed period at the end of the compression stroke from 18 degrees before TDC to TDC. From Figure 7.30 it is observed that there was little variation in AE activity with time after the oil supply was removed. There is also an element of doubt as to whether any change occurred after the oil supply was removed as although the normal operation values lie below those which represent no oil supply the value representative of the period immediately prior to the removal of the oil supply at 25 % of MCR (shown via the dotted line) is similar to the other values at that load.

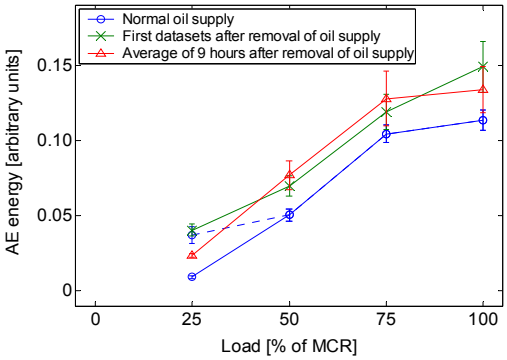

Figure 7.30: Engine F, selected values from second lubricant starvation test, lower liner, windowed period at end of compression stroke.

There are differing possible explanations for the lack of change in continuous AE activity around TDC. The first assumes that the source of this activity was asperity contact and that the removal of the oil supply brought about little or no change in the severity of lubrication conditions around TDC. Initially, this would seem unlikely since the evidence suggests that conditions deteriorated at around mid-stroke and therefore it follows that they would similarly deteriorate around TDC. However, it may be that if the lubrication condition prior to the removal of the oil supply were fully boundary lubrication then it may not deteriorate any further after removal of the oil supply. In these circumstances the tribological behaviour, in terms of asperity contact, would be influenced by the persistence of boundary layers on the surfaces due to the inclusion of friction modifying and anti-wear additives in the oil formulation.

The second explanation is based on the assumption that the primary source mechanism of the AE activity around TDC was blow-by. It may then be reasoned that the lack of change in this activity during these tests was because the removal of the oil supply had little effect on the sealing effectiveness of the piston rings. The likelihood of this account is perhaps questionable since the reduced oil availability on the liner surface

may well affect the ability of the piston rings to maintain an effective 'wet seal'. However, working on the basis that it is correct then it further suggests that the expected asperity contact around TDC would result in minimal AE generation. This is consistent with the premise that continuous AE activity resulting from asperity contact is related to the frictional power loss as this would tend to zero at TDC. It would also mean that the lubrication conditions at around TDC may deteriorate without generating significantly increased amounts of AE activity.

Again, there was no further information or measurement parameters acquired from the engine that would help to explain which source mechanism was responsible for the continuous AE generation around TDC. In order to resolve this issue further work would be required with either a greater level of instrumentation so to characterise the severity of blow-by and/or asperity contact during the cycle, or damage purposely inflicted to the ring-pack so as to establish the AE characteristics of blow-by. It is important that the source of this background AE activity be identified as it plays a key role in determining the capabilities of AE monitoring since it is in the area around TDC with high loads and high temperatures that the greatest frictional forces and wear rates would occur. It is also in this area that scuffing would be most likely to originate.

The ability to detect scuffing through AE monitoring cannot be evaluated from these tests since the conditions in cylinder 2 did not deteriorate to the extent whereby scuffing was initiated, even after 15 hours of operation with no direct supply of lubricant. There are some promising signs, deterioration in ring-pack frictional behaviour which is a precursor to scuffing, has been found to be detectable at the piston mid-strokes; however this observation was not replicated for the background AE activity around TDC where scuffing is most likely to originate. A further positive indication is that the severe material deformations that define scuffing have been found by other researchers [179-181] to result in a significant increase in AE activity, including work on a reciprocating set-up designed to replicate behaviour at the ring/liner interface [181].

7.4 Comparison with other cylinders of engine F

During the second lubricant starvation test some data were acquired from cylinders 3 and 4 of engine F, both of which were operating under normal conditions with a normal

supply of lubricating oil. Figure 7.31a shows the mean signals of 20 cycle datasets acquired from the mid liner positions on cylinders 3 and 4 with the engine operating at 100 % of MCR. In order to provide a comparison, signals from cylinder 2 operating at normal conditions and at two points in time after the oil supply was removed are shown in Figure 7.31b, again, each signal is the mean of 20 cycles and the engine was operating at 100 % of MCR. The signals for cylinder 2 display the response described previously whereby AE activity increased with time after the oil supply was removed, particularly at around the mid-stroke regions.

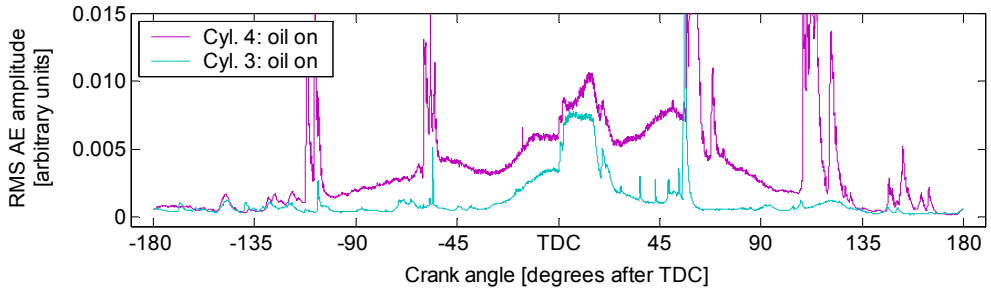

(a)

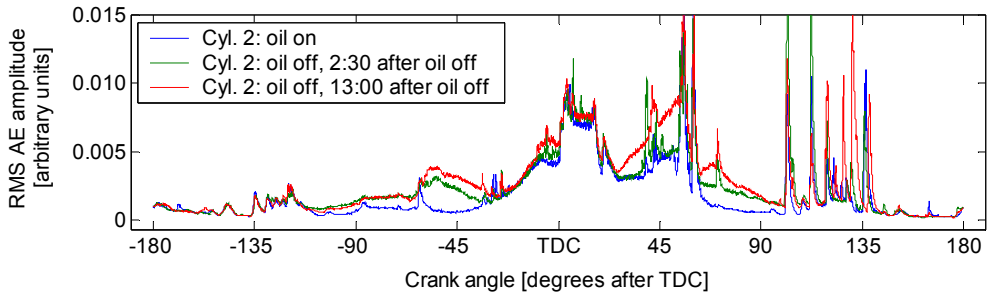

(b)

Figure 7.31: Engine F, mid liner, RMS AE signals at full load for (a) cylinders 3 and 4 operating with normal oil supply conditions, (b) cylinder 2 operating with normal and no oil supply conditions.

The signal for cylinder 3 in Figure 7.31a showed a similar structure although generally a lesser amplitude in the period 45 degrees before to 45 degrees after TDC when compared to the signal representing normal lubricating conditions for cylinder 2. Cylinder 4, however, despite a normal oil supply, displayed AE levels that were greater than the cylinder 2 signal after 13 hours of running with no oil supply. The background AE activity was consistently greater throughout the compression and expansion phases although during the scavenging period it displayed little or no increase, presumably due to the low in-cylinder pressures.

Cylinder 4 was visually inspected a month later. This revealed that the liner condition had deteriorated to such an extent that a cylinder overhaul and re-honing was required. The engine had seemingly been operating with this condition undetected despite the high-level of dedicated monitoring instrumentation employed. The amount of liner deterioration in the time between acquisition of the AE data and identification of the liner condition is not known. However, since engine F is used only intermittently as a research and development tool then the AE signal for cylinder 4 can be regarded as representative of poor, if not bad, operating conditions and it therefore contains a significant fault-related component.

Cylinder 3 showed no faults and hence the AE signal acquired can be regarded as indicative of good conditions. For the purposes of investigating fault related AE this activity can in this case be regarded as noise. A comparison of cylinders 3 and 4 therefore yields a signal to noise ratio of the fault related AE component, shown in Figure 7.32. Negating the peaks, which result from burst-type events, the ratios between poor and good running conditions in the regions of interest are between 10 and 15 and, as indicated from the results relating to the lubricant starvation tests, the greatest differences occur at around the piston mid-stroke regions.

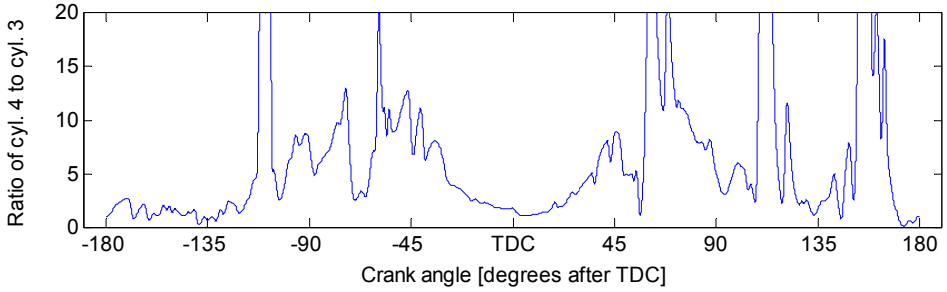

Figure 7.32: Engine F, mid liner, signal to noise ratio of poor to good condition.

7.5 Comparison to other work on AE monitoring of the ring-pack/liner interface

The techniques used in this work to identify changes in the signals, such as calculating the energy contained in windowed areas of the engine cycle, can be regarded as relatively basic when compared to other signal processing techniques. The use of more sophisticated techniques to detect change in the signals from the first lubricant starvation test has been investigated by Pontoppidan and Sigurdsson [8]. They applied ICA to effectively decompose the original RMS AE signals into four components.

Three of these corresponded to the three different loading conditions whilst the fourth related to the friction acting at the ring-pack/liner interface. This friction related component of the RMS AE signal is shown in Figure 7.33.

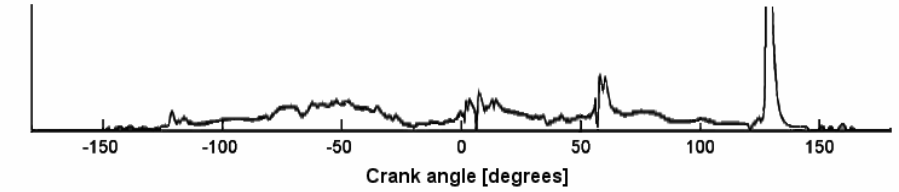

Figure 7.33: Friction related component of AE activity as determined through ICA, adapted from Pontoppidan and Sigurdsson [8].

It displays similar characteristics as to what has been determined in this Chapter to be friction related activity. It consists primarily of a background signal with the only major burst type event relating to the ring-pack passing the scavenging ports and possibly a further smaller burst type feature corresponding to interaction with the oil groove. The background signal contains the feature around TDC that has been attributed to either asperity contact or blow-by and is influenced by the in-cylinder pressure. It also contains the background activity at mid-stroke areas that has been correlated to the ring-pack lubricating conditions. Little was offered by way of interpretation of the physical meaning of this signal.

The ICA also returned a measure of the friction component's presence in each cycle of data acquired during the first lubricant starvation test. This was shown previously as source 1 in Figure 3.8b, and it indicated that the friction component appeared just after the oil supply was removed and increased throughout the test until the supply was restored. The development of this component bears a strong resemblance to the development of AE energy in the windowed mid-stroke areas such as was shown in Figure 7.16a. The close similarities regarding the identified friction signal and the changes in this signal during the test, arrived at independently using different signal processing techniques, implies to an extent that it is correct. It also suggests that in this case the basic analytical approach is equally as informative as the advanced processing techniques.

Noorul Haq and Tamizharasan [231] observed that RMS AE increased proportionally with ring wear from an investigation conducted on a very small, 3 hp, two-stroke engine using a modified ring so as to increase the wear rate. This relationship was attributed to

increasing amounts of asperity contact occurring over an increasing ring/liner contact area as wear occurred. Analysis of the AE activity was fairly basic and possible variation of AE activity during the engine cycle was not considered. Therefore, the use of this work to support interpretations made in this Chapter, other than the observation that AE occurs from asperity contact at the ring/liner interface, is limited.

To the authors best knowledge no further published work has investigated AE activity from ring-pack/liner interaction over varying tribological conditions. However, Sasaki *et al* [35] and Kimura *et al* [92] have analysed vibration data acquired during the running-in period of a two-stroke cylinder unit. One source of vibration activity was identified as contact between the ring-pack and the crests of the wave cut liner surface as the components conformed to each other. Similar to the finding in this Chapter the amplitude of the vibration activity was noted to be most prominent at the mid-stroke positions, furthermore, from STFT analysis a series of curves were observed that were proportional to piston speed, Figure 2.23. The fundamental frequency of these curves correlated well to the anticipated frequency if the rings were to interact with each crest of the wave cut liner profile. With increased running time the amplitude of this interaction feature decreased as the components conformed to each other. This observation may be regarded as similar, although in reverse, to that established for the mid-stroke AE activity in this Chapter as both are linked to the tribological behaviour at the ring-pack/liner interface.

Considering that the source of the mid-stroke background AE and the ring-pack/liner interaction feature in the STFT plots in Sasaki *et al* [35] and Kimura *et al* [92] were believed to be the same, i.e. asperity contact, it would be expected that this feature would also be present in STFT analysis of the AE signals. Since the frequency range of interest is below 5 kHz, i.e. several orders below the raw AE sampling frequency, there would be little gained from analysis of the raw AE. However, if the ring/liner profile source was present then the RMS AE signal may contain this information through lower-frequency modulation. STFT analysis of RMS AE data from the lower liner position at 75 % of MCR is shown in Figure 7.34, this data relates to approximately 11:30 hours after the oil supply was removed and the original RMS AE signal indicates that mixed lubrication conditions are in place at the piston mid-strokes.

The STFT analysis of the AE data appears to contain no trace of the piston speed feature that was clearly evident in analysis of the vibration signals [35]. It may be that vibration monitoring is more sensitive to this feature since the frequencies of interest are directly within its measurement range, rather than in possible modulation of the RMS AE signal. On the other hand, it may simply be that the lubricating conditions were not comparable with more severe interaction encountered during the running-in period in [35] than the lubricant starvation tests in this work.

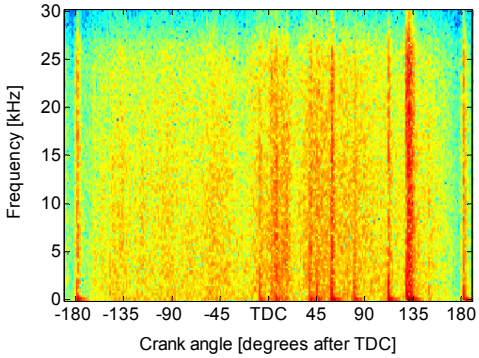

Figure 7.34: STFT analysis of RMS AE signal from lower liner position.

Other works which have considered vibration and ultrasound monitoring of large, two-stroke engines have claimed the ability to detect scuffing. Vibration spikes occurring symmetrically about TDC, Figure 2.21b, were believed to be indicators of scuffing [14], however, this related to measurements from a four-stroke engine. Work by Haller and Kelleher [33] showed that a poor cylinder condition prior to overhaul was signified by vibration activity at mid-strokes, Figure 2.22. Comparative measurements after overhaul no longer displayed this activity. This is entirely consistent with the findings discussed in this Chapter. The additional capability demonstrated for AE monitoring is the ability to identify changes in condition for much less severe conditions and probably much earlier in the degradation process.

7.6 Summary

This Chapter has investigated AE signals acquired from cylinder liners of a large, two-stroke engine during normal operation and with attempts made to deteriorate ring-pack/liner interfacial conditions in one cylinder through removal of the lubricant supply. The results showed that the continuous AE component in the signals varied differently in response to changes in load and lubricant supply in two areas of the engine cycle, the piston mid-stroke regions and the area around TDC.

Through consideration of the possible AE sources, observations from AE arrays and comparison with the anticipated ring-pack behaviour the changes in the AE activity

have been attributed to changes in the tribological behaviour at the ring-pack/liner interface. The development of continuous AE activity at the mid-stroke regions correlated well with the presumed changes in ring-pack frictional behaviour and, similarly to work on small, four-stroke engines described in Chapter 5, a relationship was identified between AE activity and frictional power loss due to boundary frictional contact. Examination of continuous AE activity around TDC did not produce such convincing results with the main shortcoming being that the source, or sources, of this activity could not be determined with any degree of confidence. Variance of this feature over normal operating conditions indicated that this activity was related to in-cylinder pressure with the source identified as either asperity contact or blow-by. The removal of the oil supply appeared to have minimal influence on this activity.

The ability to detect the occurrence of scuffing could not be evaluated, although further proof of the capability to provide diagnostic information was offered through comparison of signals acquired from cylinders known to be in a good and a poor condition. Signals from the cylinder in a poor condition displayed an appreciable increase in AE activity throughout most of the stroke, although the greatest differences were observed at the mid-stroke regions, which is consistent with observations made from the lubricant starvation tests.

The results presented and discussed in this Chapter indicate that AE signals acquired from cylinder liners contain qualitative diagnostic information regarding running conditions at the ring-pack/liner interface. The most useful feature identified was the AE energy contained within windowed areas of the signal at the piston mid-stroke areas. Furthermore, for this activity the relationship between load and AE energy was found to be sensitive to changes in running condition. Implications of the findings from this Chapter with respect to engine condition monitoring and management shall be discussed further in Chapter 9.

Chapter 8

Two-stroke, crosshead, diesel engines: monitoring of cylinder performance via measurements of AE and instantaneous crankshaft angular velocity

8.1 Introduction

This Chapter investigates the possibility of using AE signals acquired from the cylinder cover position of large, two-stroke diesels together with information about the rotational speed of the crankshaft to estimate the power generated by an engine and to provide diagnostic information regarding cylinder performance. As was discussed in Chapter 2 performance monitoring of specific cylinders and power balancing is best achieved from analysis of in-cylinder pressure traces. However, due to inherent difficulties with this technique, not least the requirement for intrusive measurements, other alternative techniques have been considered. Of particular interest are those which do not interfere with engine performance, and in addition to AE monitoring this includes analysis of the Instantaneous Crankshaft Angular Velocity (ICAV).

Both the AE activity generated during the fuel injection/combustion period and the fluctuations of ICAV during the engine cycle are expected to be indicative of engine power to some degree since the control action of an engine to varying load is to inject more (or less) fuel per cylinder and the effect of this is to produce more (or less) angular acceleration per cylinder. Moreover, a survey of AE generation with large, two-stroke diesels, Chapter 6, established that AE signals acquired at the cylinder cover position contain information regarding injector behaviour and possibly also combustion in the cylinder. For both engines E and F the relationship between AE and ICAV parameters is investigated to reveal whether a correlation exists. By these means, the diagnostic capabilities of AE monitoring are extended by reference to the relatively well-established (and somewhat more direct) technique of ICAV analysis. Some of the work in this Chapter has been reported previously by Douglas *et al* [232] and is given again here together with more recent results.

8.2 AE generated during fuel injection period

The characteristics of AE activity generated during the fuel injection process have been examined previously in Section 6.2. Through observations from sensor arrays and event mapping it was ascertained that the sequence of AE events reflects the mechanics of injector operation and that the events generated are of sufficient strength to propagate throughout the upper cylinder area. Signals acquired from an injector body contain rich information regarding the behaviour of the instrumented injector; however, the work in this Chapter considers signals acquired from the cylinder cover position since these contain contributions from the two injectors which supply each cylinder and therefore provide a better representation of overall injector performance.

During the injection process there are various AE sources which can contribute to the AE signal measured at the cylinder cover, including; impacts associated with the injector spindles, high-pressure discharge of fuel into chamber, fuel pressure build up prior to injection and fuel ignition and combustion. The timing and strength of these sources will relate to the fuel pressure profile, the condition of each injector and the consequent combustion performance. Since these are all major factors which influence cylinder performance the AE activity can therefore be regarded as an indicator of cylinder performance, and particularly as a representation of the fuel input to a cylinder.

8.2.1 Engine E

Due to the nature of the tests conducted on engine E the data available from the same cylinder over varying loads was limited to measurements acquired from cylinder 3. In total this consisted of 88 cycles of data acquired at approximately 6.2 MW and 104 cycles at approximately 8.4 MW on the generator curve (corresponding to 55 % and 75 % of MCR respectively) using PAC Micro80D sensors. Data were acquired from further cylinders but in each case this was at a single loading condition.

Figure 8.1a shows typical examples of the RMS AE signal acquired during the fuel injection period of cylinder 3 at the two loads. It was established previously in Section 6.2 that the two major peaks in the signals are the strongest events observed at the cylinder cover position and that they indicate the beginning and end of the injection period. On this basis the injection duration displays the expected increase with load. A

further parameter that can be extracted is the angular domain AE energy using Equation 3.2. In this case, the integral limits have been selected as 10 degrees before and 30 degrees after TDC in order to encompass all AE activity attributable to the main body of the injection process. Figure 8.1b shows the calculated AE energy during the injection period for each cycle of the dataset and from this it is observed that the AE energy increases with load. Through consideration of the RMS AE signals in Figure 8.1a it is clear that this is primarily due to the extended period of lower-amplitude AE activity between the injection start and end events. This activity has been attributed to high-pressure fuel flow within the injector body and nozzle areas and/or possibly fuel combustion. The other elements of the injection signals are almost identical although the amplitude, hence energy content, of the injection end event appears to decrease with load.

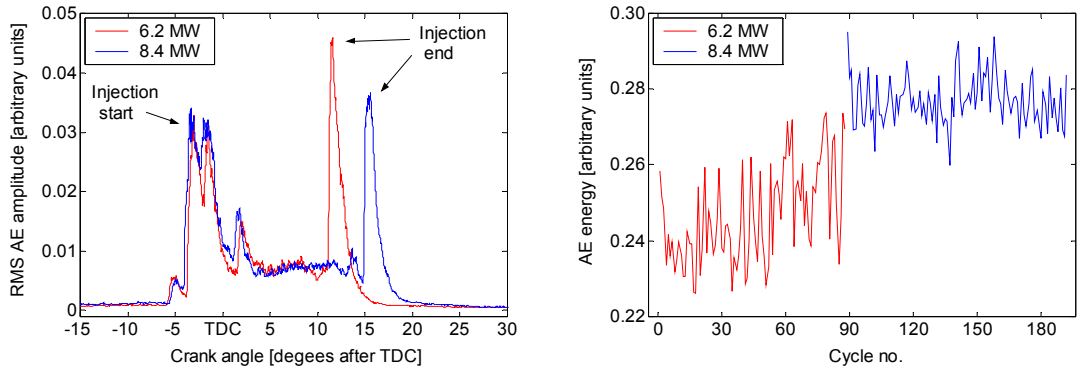

Figure 8.1: Engine E, (a) RMS AE signals from cylinder cover of cylinder 3 during fuel injection period for two loads, (b) AE energy during period 10 degrees before TDC to 30 degrees after TDC for each cycle of data acquired.

8.2.2 Engine F

The strongest events in AE signals acquired from the cylinder cover position of engine F are again related to the fuel injection process. Typical examples of signals acquired using PAC WD sensors located on cylinder 2 at three loads on the propeller curve, 1.7, 3.5 and 5.3 MW (corresponding to 25, 50 and 75 % of MCR), during the first lubricant starvation test were shown previously in Figure 6.13b. Similarly to engine E the start and end of the injection period can be identified and the injection duration increases with load. The amplitude of the injection end event also reduces slightly with load which is again consistent with observations from engine E.

The result of calculating the AE energy in the period 10 degrees before to 30 degrees after TDC for each cycle of the test is shown in Figure 8.2, the timing of the load and lubrication supply condition changes are also indicated. It is observed that AE energy increases with load and this can again be attributed to the extended duration of continuous AE activity presumed to relate to fuel delivery and/or combustion. The AE energy parameter shows no response to changes in the lubrication supply condition. This is as expected since it was established previously that the vast majority of AE activity at the cylinder cover position during the fuel injection period originates from injector related sources with only a very small contribution from sources that may be affected by changes in lubrication supply.

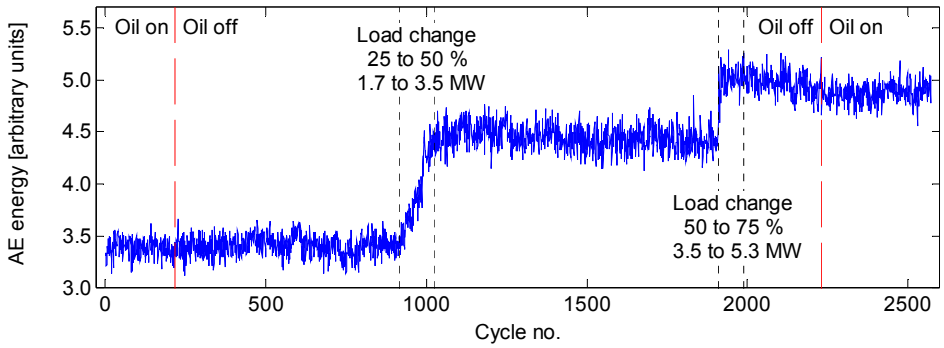

Figure 8.2: Engine F, AE energy during period 10 degrees before TDC to 30 degrees after TDC for each cycle of data acquired from the first lubricant starvation test.

.

8.3 Instantaneous crankshaft angular velocity

The ICAV waveform generally exhibits cyclic variations about the mean engine speed due to accelerations of the crankshaft caused by the compression and expansion strokes of each cylinder. Theory governing the physical mechanisms responsible for these fluctuations has been presented previously in Section 2.3.5.1. A decrease in angular velocity indicates the compression stroke of a cylinder since work is extracted in order to compress the air, conversely, an increase in angular velocity signifies the expansion stroke as the cylinder fires and the consequent forces accelerate the crankshaft via the piston and connecting rod assemblies. In addition to the torque resulting from the in-cylinder pressures, i.e. the indicated torque, T_i, there are further components which contribute to the instantaneous net torque, and thus crankshaft acceleration, including; inertial torque, frictional losses and the load torque.

The variation of indicated torque with load and the extent of the contribution from one cylinder are demonstrated in Figure 8.3. In-cylinder pressure traces measured from cylinder 2 of engine F at three loads on the propeller curve are shown in Figure 8.3a (the amplitudes are given in arbitrary units since calibration details were not available). Given this information, and with knowledge of the crank-slider geometry and the assumptions that the in-cylinder pressures relative to TDC of the remaining cylinders are identical, the crankshaft system is rigid and that the engine is operating in a steady-state condition, then the indicated torque can be calculated using Equation 2.3. The results for the three loads are shown qualitatively in Figure 8.3b.

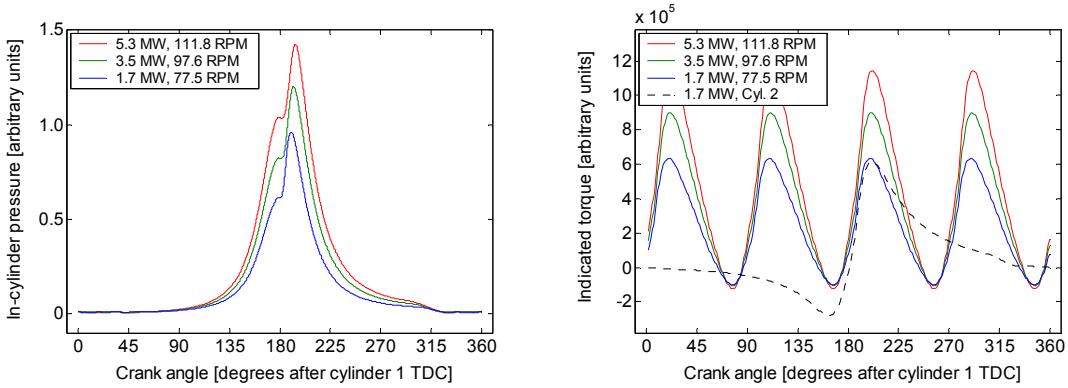

(a) *(b)*

Figure 8.3: Engine F, (a) measured in-cylinder pressures at three loads, (b) resulting indicated torques calculated using Equation 2.3.

Figure 8.3b also shows the contribution of cylinder 2 to the net indicated torque for the case of the 1.7 MW load. It can be observed that whilst the peak due to the expansion phase of cylinder 2 is responsible for the resulting peak in the net indicated torque the trough resulting from compression is offset to some extent by contributions from the other cylinders. It is also evident that the mean indicated torque and the magnitude of the fluctuations in the indicated torque waveform both increase with load. Considering the angular momentum balance in Equation 2.1, the magnitude of the crankshaft accelerations, and hence the ICAV fluctuations, will also increase with load. The fluctuations in the ICAV waveform are therefore directly related to the engine power output.

For this reason, analysis of ICAV waveforms has been used to provide information about the running condition of engines and to diagnose misfires in individual cylinders [15-17, 21-29], as was described in Section 2.3.5.2. For example, when the torque outputs of each cylinder are uniform it would be expected that the ICAV waveform

would exhibit a regular structure. An irregular waveform indicates that the cylinders are not performing equally and that, depending upon specifics of the irregularity, particular cylinder(s) may be operating in a poor or faulty condition. Evaluation of individual cylinder performance increases in complexity when two-stroke engines are considered, and also with increasing number of cylinders, since a greater proportion of each stroke will overlap between cylinders.

8.3.1 Engine E

For the engines considered in this Chapter the ICAV waveform is inferred simply from the shaft encoder signal. The accuracy of this waveform is dependant upon the number of pulses contained in this signal per revolution and the data sampling rate. For engine E the AE signals shown previously were acquired at 100 kHz. Some additional data were acquired at the raw AE sampling rate of 2.5 MHz. This allows a more accurate representation of the ICAV waveform to be established and also allows the effect of sampling frequency on the reproducibility of the waveform to be evaluated.

Figure 8.4a shows an example of the ICAV waveform during a cycle from engine E with load at 8.4 MW and a data sampling rate of 2.5 MHz. The signal consists of higher frequency content with some modulation at lower frequencies. This is demonstrated further by the spectrum of the waveform given in Figure 8.4b, the strongest component of the signal is at a frequency equivalent to 7 times the engine speed. Some of the higher frequency content can be attributed to the application of the engine and the effect of the load. In this case, engine E powered a generator consisting of 22 pairs of poles for 3-phase electricity production. This then accounts for the peak in the spectrum at 66 times the engine speed. Low-pass filtering the signal to remove this load-related noise produces the example ICAV waveform shown in Figure 8.4c. The location of TDC for cylinder 3, for which RMS AE data during the fuel injection has been presented, is also indicated.

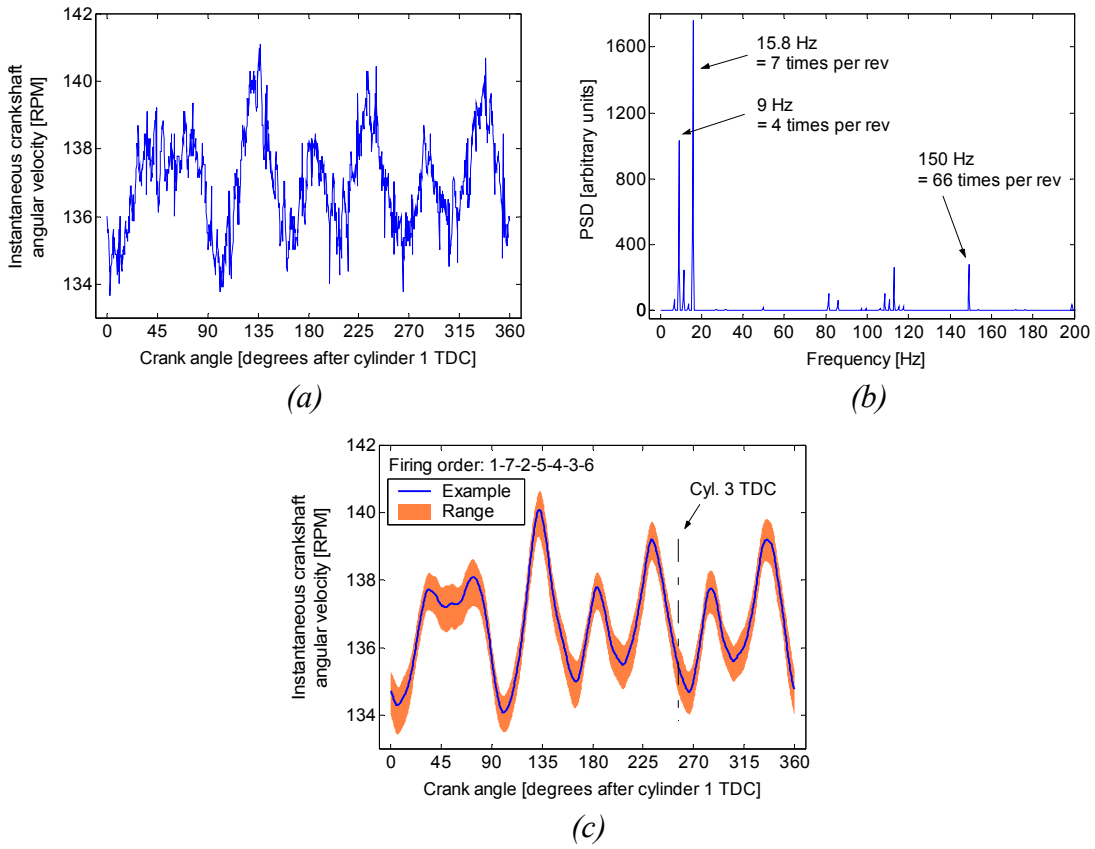

Figure 8.4: Engine E, (a) measured ICAV waveform, (b) corresponding frequency content, (c) low-pass filtered ICAV waveform.

It is clear that the ICAV waveform contains seven fluctuations during the cycle. These can be presumed to relate to the effects of compression and expansion in each of the seven cylinders of engine E. The irregular nature of the waveform indicates that the cylinders are not performing uniformly. In particular, the amount of ICAV reduction due to compression of cylinder 7 is significantly less than that caused by the other cylinders, which may be indicative of a compression fault.

A factor in the accuracy of the ICAV waveform is the sampling frequency. The use of a high sampling rate of 2.5 MHz for the waveforms shown in Figure 8.4 allows for a very accurate representation. However, the data considered in this Chapter were generally acquired at much lower rates; typically 100 kHz for engine E and 20 kHz for engine F, and this means that the angular velocity resolutions of the waveforms would be considerably lower. Nevertheless, when the signals are exposed to the same low-pass filtering the resulting filtered waveforms are very similar to that generated from the higher frequency data. This is demonstrated in Figure 8.4c through indication of the range of maximum and minimum ICAV observed from over 100 filtered waveforms

acquired at the lower sampling rate at the same operating conditions. The narrow range further suggests that under steady-state conditions the ICAV waveform is very consistent.

As described previously, the fluctuations of the ICAV waveform would be expected to increase with load. Figure 8.5 shows examples of low-passed ICAV signals at the two loads for which data are available from engine E. As anticipated, the amplitude of the fluctuations increases with load although the general form remains similar. Since engine E operated on the generator curve then with increasing load the engine speed, hence the contribution of the inertial forces to the ICAV waveform, remains constant, and therefore, the changes in the ICAV waveform can be attributed to the increased torque generated.

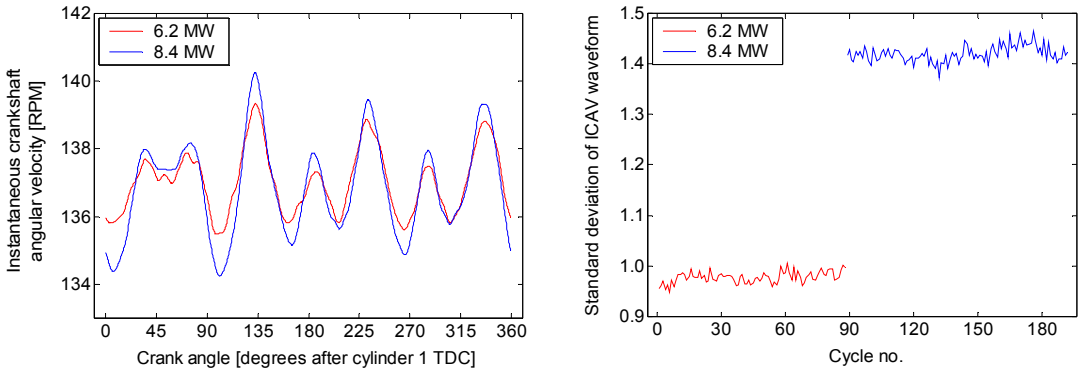

(a) *(b)*

Figure 8.5: Engine E, (a) low-pass filtered ICAV waveform at two loads, (b) standard deviation of the ICAV waveform per cycle.

Previous work has found the standard deviation of the ICAV waveform to be a sensitive diagnostic indicator [29]. This simple measure of distribution about the mean will include a load-related component and also distortion due to non-uniform operation of the cylinders. With reference to Equation 3.5 for this application n is the number of ICAV measurements per cycle, x_i is the i^{th} measurement and $\bar{x}$ is the mean angular velocity over the cycle. Figure 8.5b shows the standard deviation of the ICAV waveform for each cycle of the engine E dataset, from which it is evident that there is a significant increase with load.

8.3.2 Engine F

Figure 8.6a shows low-pass filtered ICAV waveforms at three loads during the first lubricant starvation test on engine F. For clarity each waveform is shown on a separate plot, although on the same scale. It is clear that each example contains four major fluctuations during the cycle which can again be presumed to relate to the four cylinders of the engine. The form of these fluctuations appears to be more regular than that observed from engine E which suggests that the cylinders of this engine operate more uniformly.

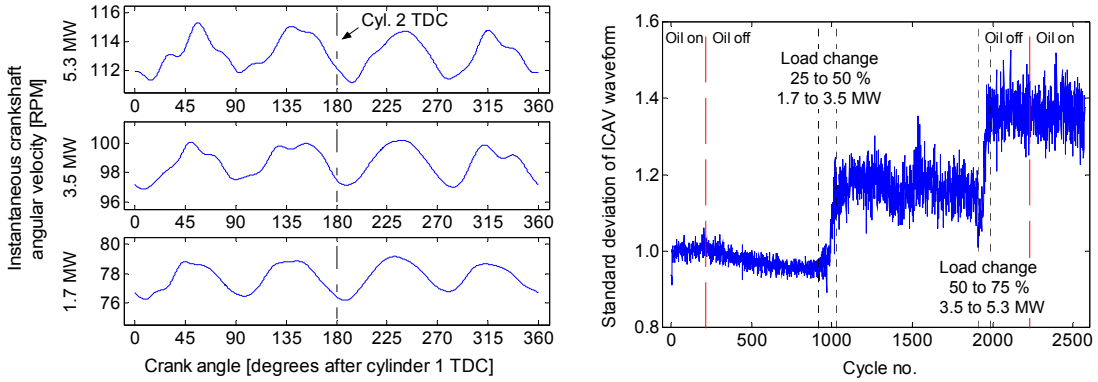

(a) *(b)*

Figure 8.6: Engine F, (a) low-pass filtered ICAV waveform, (b) standard deviation of the ICAV waveform per cycle during first lubricant starvation test.

The standard deviation of the ICAV waveform for each cycle of the test is shown in Figure 8.6b. Similarly to the observations from engine E this parameter increases with load. The scatter of the data also increases and this may be partly due to lower resolution of the ICAV measurements at higher speeds which is a simple matter of data sampling rate, a further factor is the increased speed itself.

During this test the lubrication supply was varied. There appears to be little response of the standard deviation parameter to these changes, although there may possibly be a small, gradual reduction after removal of the oil supply. It is to be expected that the lubrication supply condition would have little effect on the ICAV fluctuations as although the ring-pack frictional forces may increase they would still be small in relation to the forces exerted on the crankshaft.

8.4 Discussion and further data

It has been observed that for two, large, two-stroke engines the energy content of the AE activity during the fuel injection period and the magnitude of the ICAV fluctuations both increase with load. It follows, therefore, that both parameters can be used as non-intrusive indicators of the engine, or possibly even individual cylinder, power output.

However, it is not possible to directly compare the results from both engines as the amplitudes of the AE signals acquired from each engine are different. This is due to the instrumentation used in each test (different types of sensor), the dimensions of the actual engines tested (overall dimensions and resulting source-sensor transmission paths) and factors relevant to the source AE generation in each cylinder (injector type and control method, etc). Therefore, in order to allow initial comparison and to permit some more general conclusions the AE signals must be normalised. One method to achieve this is to divide each acquired RMS AE signal by the peak amplitude observed during the injection/combustion period. The AE energy can then be recalculated from the normalised signal and the amount is then dependent upon the duration of the overall injection event and the relative strengths of the AE signal components.

Figure 8.7 shows peak-normalised AE energy against standard deviation of the ICAV waveform for both engines, linear best-fit relationships for each dataset are also given. The various loading conditions are clearly grouped and hence it is observed that these two parameters could be used together to indicate power output. Moreover, a combination of parameters would likely yield a more reliable measure than consideration of a single parameter.

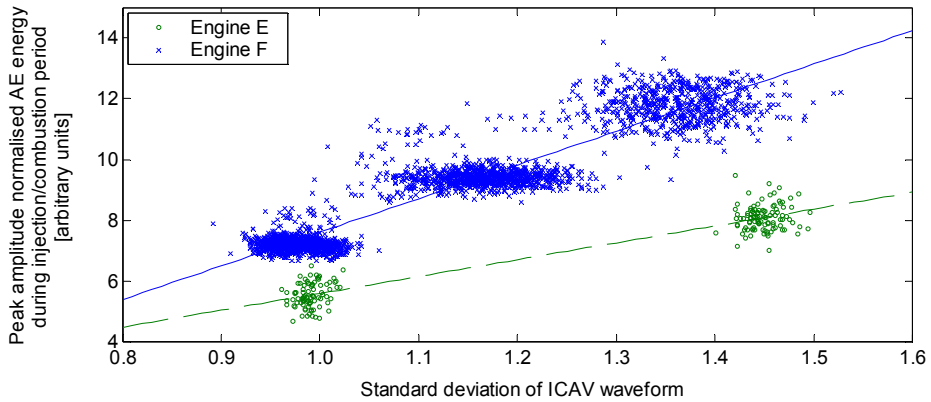

Figure 8.7: Peak amplitude normalised AE energy during fuel injection period against standard deviation of the ICAV waveform per cycle for both engines.

Comparing the relationships between AE energy and standard deviation, as represented by the best-fit lines, it is clear that the relationship for engine F displays a greater gradient than engine E, indicating that a given increase in AE energy, arising from longer fuel injection durations, produces a greater increase in ICAV fluctuation for engine E. There are a number of differences between the tests on each engine that could account for this. In addition to different AE instrumentation the two engines differ in design details, such as size, power output per cylinder and injector control method, and in condition details, such as degree of component wear. However, most significantly, each engine comprised of a different number of cylinders and in these tests the engines ran in different operating modes.

Furthermore, as indicated previously, the fluctuation of the ICAV waveform, quantified by the standard deviation, is related to the overall engine performance whereas the AE parameter relates to only the instrumented cylinder. The corresponding overall engine parameter, in terms of AE activity, would be the total AE energy generated during the injection/combustion periods of all the cylinders. This would require simultaneous acquisition of signals from all cylinders of the engine, which was not available in this work. Nevertheless, assuming that the changes in AE signals from the instrumented cylinders are representative of the overall performance of the engine then it is possible to indicate the likely total AE energy during the injection periods of all the cylinders through simply multiplying by the number of cylinders (engine E has seven and engine F has four). When this is done, as shown in Figure 8.8, the gradients of the best-fit lines through each dataset are very similar.

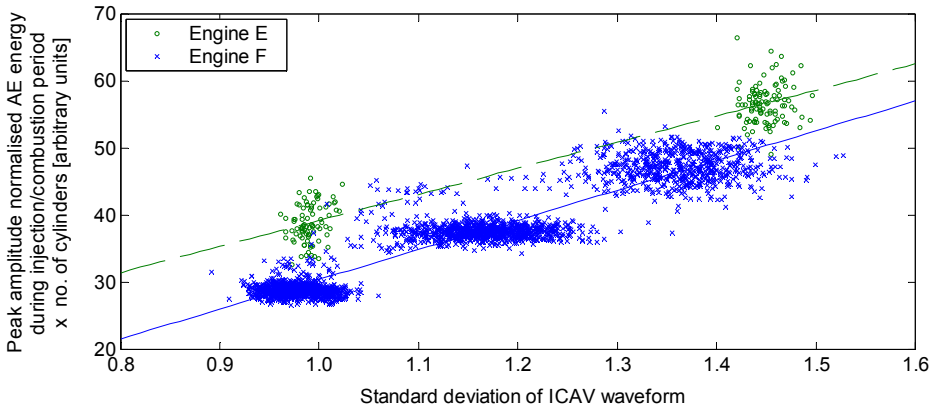

Figure 8.8: AE energy during fuel injection period versus standard deviation of the ICAV waveform taking into account the number of cylinders of each engine.

This implies that when overall engine performance is considered, and with engine E operating in generator mode and engine F in propeller mode, a given increase in AE energy results in a similar amount of change in ICAV fluctuation for both engines. Given the physical mechanisms responsible for these parameters the relationship may be interpreted as one which links cylinder input, as represented through the AE signals, to the resulting output, i.e. ICAV fluctuation. Although the currently available data are insufficient to investigate this fully, on this basis the characteristics of the relationship may provide a measure of the effectiveness of the input and consequently be indicative of engine performance and condition.

8.4.1 Further data for engine E

Additional datasets were available from other cylinder of engine E that would allow investigation of the range of the AE energy and ICAV parameters between cylinders. These ranged from measurements acquired from cylinder 2 at a load of approximately 6 MW to measurements from cylinders 4 and 6 at a load of approximately 9 MW. Figure 8.8 shows the outcome of applying the aforementioned analysis to these datasets with the results superimposed on the original data. Since measurements from each cylinder were limited to a single loading condition this data does not permit further examination of the AE energy-ICAV relationship over varying load, however, it does serve to indicate the amount of variation that can be expected between cylinders over a given load range.

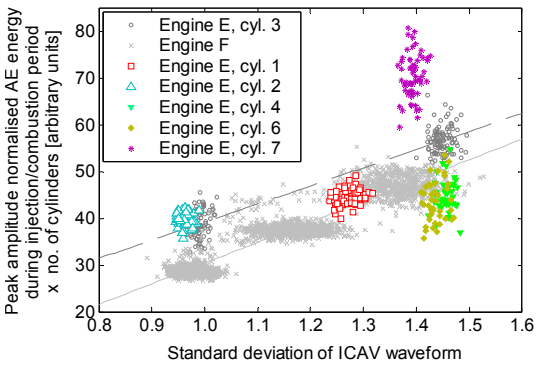

Figure 8.9: Engine E, comparison of data acquired from other cylinders.

It is observed that most of this data lies on a similar axis to that already found. A notable exception is the data from cylinder 7 which shows an increase in amplitude normalised AE energy compared to the other cylinders. This arises due to the structure of the AE signal and the normalising process. In this case the signal displayed lower amplitude burst-type activity and the effect of the normalising process is then to exaggerate the relative energy content of the continuous AE activity component. It is

interesting to note that this cylinder also displayed an irregular contribution to the ICAV waveform, as shown in Figure 8.4c.

8.4.2 Further data for engine F

8.4.2.1 Tests over engine operating range

A further difference between the tests on both engines was the operating mode, engine E ran on the generator curve whereas engine F operated in propeller mode. This dissimilarity could be investigated from further data acquired from cylinder 2 of engine F (several years after the original test) at various loads on the propeller and generator curves during normal operation. These tests functioned as the reference data for the second lubricant starvation test and were described in detail in Section 4.4.5, again, different instrumentation were used.

Figure 8.10a shows the AE energy during the fuel injection period calculated from the measured, i.e. unnormalised, RMS AE signals against standard deviation of the ICAV waveform for over 400 cycles at each load. Similar trends as the original data are displayed in that both parameters increase with load; furthermore, there is a clear difference in the relationship between AE energy and ICAV between the two operating modes. For equal power outputs it is observed that in generator mode the fuel injection AE energy is greater and the standard deviation of the ICAV waveform is less. The increase in AE energy can be explained by the increased fuel input per cycle required to maintain the engine at the greater speeds compared to the same power output in propeller mode. Similarly, the standard deviation of the ICAV waveform is less because for equal power outputs the torque produced in generator mode is lower and the effect of this, despite an increase in magnitude of the vertical inertial imbalance component with speed, is a smoother ICAV waveform.

A comparison between the normalised version of this data and the original data is given in Figure 8.10b. Again, the data are observed to lie on a similar axis to that found previously. There are, however, differences for nominally the same operating conditions. For equal power outputs the values of both the AE energy and standard deviation parameters are lower for the second propeller curve test and the gradient of

the AE energy-ICAV relationship is also slightly less. The principal factors likely to cause this variation are that there will be changes in engine condition between the two tests and also different instrumentation was used in acquisition of the AE signals.

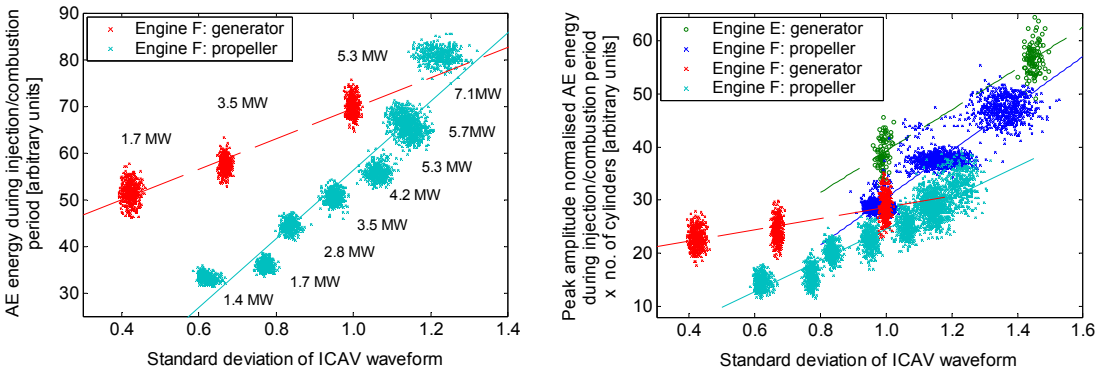

Figure 8.10: (a) Engine F, relationship between AE energy during fuel injection period and standard deviation of the ICAV waveform for propeller and generator operating modes, (b) normalised data compared with previous data.

8.4.2.2 Simulated misfire tests

Further tests were conducted on engine F with fuel injection to cylinder 2 completely disabled in order to simulate extreme misfire conditions. Although a fault of this severity would be unlikely to occur in reality the data from this test is still useful as it allows the response of the AE and ICAV parameters to engine unbalance to be evaluated. The dataset consisted of 300 cycles acquired at the cylinder cover position of cylinder 2 at two loads, 0.7 and 1.7 MW (corresponding to 10 and 25 % of MCR), under normal operating conditions and with no fuel injection in cylinder 2.

For each of these conditions examples of AE acquired during the fuel injection period have been shown previously in Figure 6.10. For both loads the misfire examples displayed little AE activity besides background levels and did not display the distinct events observed during normal operation. The AE energy during the fuel injection period for each cycle of the dataset is shown in Figure 8.11. Consistent with the results presented previously in this Chapter the AE energy increases with load for normal operation and, as expected considering the RMS AE signals shown in Figure 6.10, the AE energy is considerably lower when fuel injection is disabled.

Figure 8.12a shows typical ICAV waveforms from normal operation and with simulated misfire in cylinder 2 for the two loads. In both cases the normal operation waveform displays a regular structure indicating uniform operation. The misfire waveforms, however, have different characteristics; the signals have greater amplitudes and an irregular structure which is indicative of a poor engine balance. The standard deviations of the ICAV waveforms for each condition, shown in Figure 8.12b, reflect this with significantly greater values for the simulated misfire waveforms. This is consistent with other published works [21, 28] where a parameter describing non-uniformity of the ICAV waveform has been observed to increase when misfire conditions have been induced.

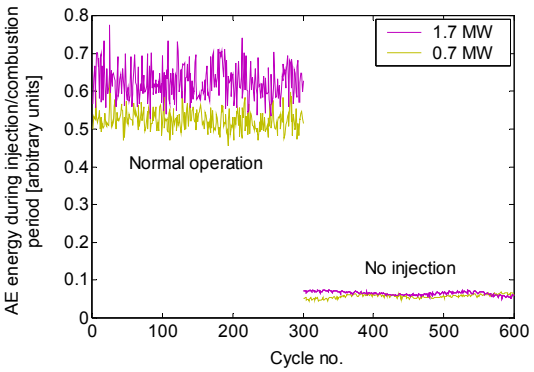

Figure 8.11: Engine F, AE energy during fuel injection period.

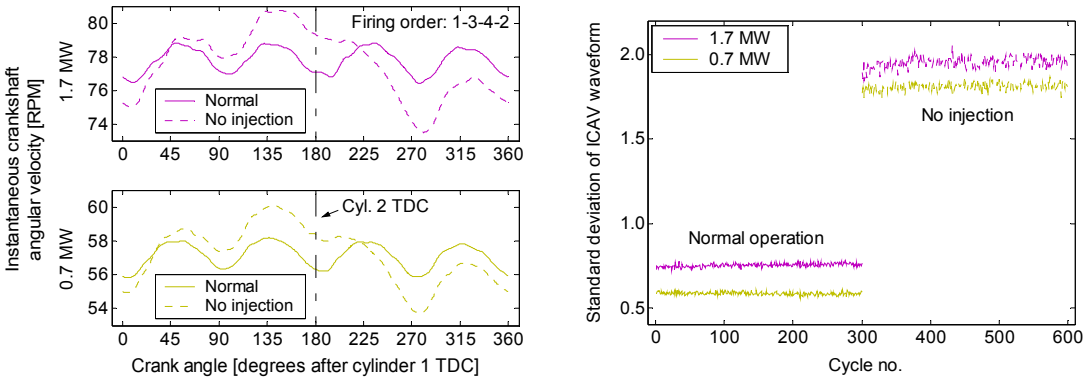

(a) *(b)*

Figure 8.12: Engine F, (a) example ICAV waveforms at each condition, (b) standard deviation of ICAV waveforms at each condition.

Both the injection period AE energy and standard deviation of the ICAV waveform are sensitive to abnormal engine operation. For the case of the AE parameter this is simply because the AE generating sources were purposely removed from the engine cycle and therefore this is not representative of faulty operation. Nevertheless, the amalgamated data (from unnormalised signals) is shown in Figure 8.13a. It is evident that the abnormal operation data deviates significantly from that relating to normal operation and also to the trends identified previously. The effect is also greater when the two parameters are considered together rather than singularly. For comparison, Figure 8.13b shows the normalised version of the data along with that shown previously in this

Chapter. Due to the normalisation process, and since the original signals contained only background levels, the AE energy for abnormal operation is considerably greater than for normal operation.

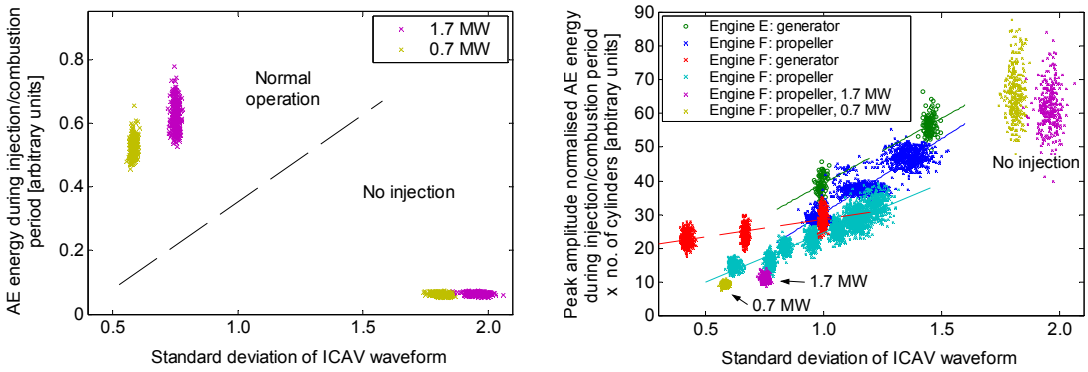

(a) *(b)*

Figure 8.13: (a) Engine F, unnormalised data from normal operation and simulated misfire tests, (b) normalised and compared with previous data.

A shortcoming with this analysis is that engine diagnosis via the standard deviation of the ICAV waveform is limited to only an assessment of the overall engine power balance. However, more detailed examination of the ICAV fluctuations during a cycle, i.e. comparison of the changes in ICAV resulting from compression and expansion in each cylinder, can provide an evaluation of individual cylinder performance [15, 22, 27]. Figure 8.14 shows ICAV waveforms during normal operation and with misfire simulated in cylinder 2 at 1.7 MW load with the effects of compression and expansion in cylinder 2 indicated. The corresponding amounts of ICAV change due to compression and expansion in each cylinder are quantified for both operating conditions in Table. 8.1, the percentage difference of each parameter upon disabling of fuel injection in cylinder 2 is also given.

From Table 8.1 it can be observed that for normal operation the amount of ICAV change due to compression and expansion in each cylinder is reasonably uniform, however, as expected, the values for the simulated misfire waveform are very different. The most obvious changes regarding the expansion parameters are that the amount of ICAV increase due to cylinder 2 reduces considerably whilst the other cylinders all increase. This reflects the lack of contribution from cylinder 2 as it effectively removes work from the system. As a consequence, the contributions from the other cylinders increase since to satisfy the load they have to generate increased power. For the compression strokes, the amount of ICAV reduction due to cylinder 4 compression

increases significantly which is simply a secondary effect of the lack of contribution from cylinder 2. These observations are consistent with the effects of underperforming cylinders on the ICAV waveform described by other authors for simulations [15] and experimental work [27].

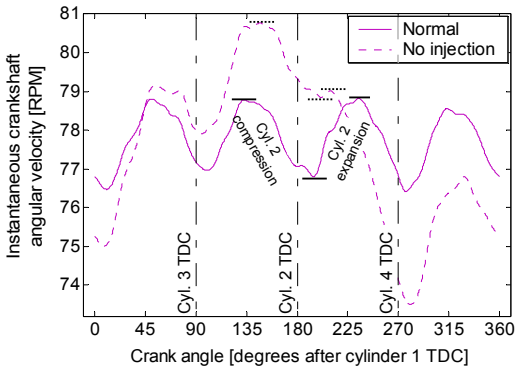

Figure 8.14: Engine F, ICAV waveforms for normal operation and simulated misfire conditions at 1.7 MW load with effects of compression and expansion in cylinder 2 indicated.

	Normal [RPM]		No injection [RPM]		Difference [%]	
Cylinder	Compression	Expansion	Compression	Expansion	Compression	Expansion
1	-2.09	2.33	-1.81	4.15	-13	+78
2	-1.99	2.02	-1.84	0.16	-8	-92
3	-1.84	1.82	-1.26	2.78	-32	+32
4	-2.41	2.16	-5.51	3.31	+129	+53

Table 8.1: Engine F, ICAV fluctuations due to compression and expansion of each cylinder, corresponding to waveforms shown in Figure 8.14.

Therefore, it would appear that breakdown of the ICAV waveform and extraction of parameters on a per cylinder basis yields more information than an overall non-uniformity parameter. This approach is also more attractive for the purposes of integrating ICAV and AE data since the AE signals are innately acquired on an individual cylinder basis.

8.5 Summary

This Chapter has investigated monitoring of engine motive output and balance through analysis of two non-intrusive parameters that are relatively easy to obtain. AE and shaft encoder signals were acquired from two, large, two-stroke, diesel engines over a range of power outputs and operating conditions. Although the engines differ in number of cylinders, control mechanism and mode of operation the observations from the two engines can be generalised in that AE activity is generated from operation of the fuel injectors and possibly combustion in the cylinders, and the ICAV waveforms (inferred from the shaft encoder signals) show the effects of compression and expansion in each

cylinder. Furthermore, the AE energy generated during the fuel injection period and the variation of the ICAV waveform, quantified by the standard deviation, both increase with power output.

By combining both power related parameters and accounting for the different number of cylinders of each engine, relationships emerged that could be used to infer power output and to aid assessment of overall engine balance. The physical mechanisms responsible for both parameters suggest that this relationship may be viewed as one which relates representations of engine input and output, and hence may be indicative of engine performance. Furthermore, the ICAV waveform can be dissected to provide information for each cylinder and, although the data available were insufficient to conclude unequivocally, it seems likely that when combined with AE energy on a per-cylinder basis this approach might be used to determine the effectiveness of individual cylinders and their contribution to overall power output.

Chapter 9

Conclusions and recommendations for future work

9.1 Overview

The primary motivation for the work in this thesis has been to address the growing requirement for a system that can monitor running conditions at the piston ring-pack and cylinder liner interface in large, two-stroke diesel engines. The possibility of achieving this through analysis of non-intrusive AE measurements has been investigated since prior work indicated a sound technical basis. AE monitoring has previously been found to be an effectual tool for examination of other engine processes [6, 122, 123, 137-150], furthermore, the friction and wear processes expected to occur at the ring-pack/liner interface are known AE generating sources [168-181] and finally, it has been shown that AE signals propagate from the internal liner surface to the external engine surfaces where measurements can be made [152, 227].

In this work a number of tests were conducted on large, two-stroke and small, four-stroke diesel engines where the effect on AE generation at the ring-pack/liner interface of parameters such as piston sliding speed, in-cylinder pressure and lubricating oil supply were evaluated in order to elucidate and understand the AE source mechanisms. Two further research objectives have been considered. For the large, two-stroke engines, a detailed survey of AE generation within the upper cylinder area was carried out in order to identify the various sources of AE and therefore determine the aspects of engine operation that can be monitored, this also functioned as a precursor to investigation of AE generation from the ring-pack/liner interface. A third objective was to investigate the use of AE measurements during the fuel injection period combined with information about crankshaft speed fluctuations to monitor overall engine performance and identify variations in individual cylinder performance.

Discussion and conclusions of results from the separate tests have been presented in each individual Chapter. The main results and conclusions from each are brought together in this Chapter to clarify what has been achieved. Overall conclusions regarding monitoring of the ring-pack/liner interface are then drawn and implications

for application towards engine monitoring and management are discussed. The Chapter closes with recommendations for future work.

9.2 Summary of main results and conclusions

Main findings from tests conducted on small, four-stroke, diesel engines:

- Testing on motored engines with measures taken to remove known AE sources revealed that relatively low-amplitude, continuous AE activity in signals acquired from the cylinder block was generated from the sliding ring-pack/liner interface. The amplitude of this activity was found to be related to piston speed.
- Similar observations were made from tests on a running engine. Tests over the engine operating range further showed that the AE activity at piston mid-strokes remained relatively constant when load was increased with engine speed held constant.
- This evidence was compared to both the expected ring-pack behaviour, determined from previous modelling and experimental work, and also prior work on AE monitoring of tribological processes. This indicated that the source of the mid-stroke activity was most likely asperity contact and boundary frictional losses at the oil-control ring/liner interface.

Main findings from a survey of AE generation within the upper cylinder areas of large, two-stroke diesels:

- Through a combination of source location via sensor arrays and event mapping using knowledge of engine operation source mechanisms for the majority of AE events generated during normal operation could be identified. This process is enhanced greatly when the AE signals are analysed in conjunction with parameters that describe the behaviour of the expected AE sources.
- Major AE events arise from the mechanical and fluid processes occurring during injector and valve activity. Although the identification of AE events originating from these sources is not new the body of evidence presented in this work is considered to be more substantial than that offered previously.
- A clear and precise indication of individual impacts within injectors can be gained from signals acquired from the injector and cylinder cover sensor positions. Other AE sources during the injection process are high-pressure fluid flow and possibly

- Gas flow during valve opening was found to generate a broad continuous event with an amplitude correlated to the in-cylinder pressure at the point of valve opening. Valve closure was signified by a series of AE events. These observations support previous work which has considered the viability of using this activity to monitor valve condition [82, 123, 146, 147].
- Burst-type AE events in signals acquired from the liners were identified as relating to the passing of the ring-pack over the oil groove and scavenging port features on the internal surface of the liner. The mechanical interaction generating these events may be a factor in ring breakage. Further burst-type events were observed in some cylinders and although the source of this activity could not be accurately determined they were also thought to originate at the ring-pack/liner interface.

Main findings from investigation of AE activity generated from sliding contact at the ring-pack/liner interface of large, two-stroke diesels:

- During normal operating conditions continuous AE activity was observed at around TDC in signals acquired from the liner surface. The amplitude of this activity paralleled the in-cylinder pressure; therefore it was attributed to the ring-pack/liner interface with the source believed to be asperity contact and/or blow-by. Unlike the smaller engines, there was little continuous AE activity observed at piston mid-strokes. This difference could be accounted for since the ring-pack of the large engines consisted entirely of compression rings.
- For two lubricant starvation tests an increase in mid-stroke continuous AE activity was observed after the oil supply was removed. The amount of AE activity increased with time and also varied during the cycle in relation to both piston speed and in-cylinder pressure. These observations correlated well with the expected changes in ring-pack behaviour upon removal of the oil supply, i.e. the breakdown of lubricating films with consequential increasing amounts of asperity contact. Therefore, similar to the small engines, this activity was believed related to the ring-pack frictional losses.
- Additional evidence of the ability to diagnose running condition was obtained from signals acquired from another cylinder liner a short time before an inspection deemed it should be removed from service. Even though this cylinder was receiving

a normal lubricant supply it showed greater levels of continuous AE generation than that observed previously for the cylinder starved of lubricant.

- For various practical reasons it was not possible to induced scuffing conditions in this work. Hence the response of the AE activity to scuffing and the full evolution of the signals during the development of scuffing could not be established.

Main findings from investigation of performance monitoring of large, two-stroke diesels via non-intrusive measurement of AE and ICAV:

- AE energy generated during the fuel injection period and the magnitude of the ICAV waveform fluctuations both increased with engine power output. The physical mechanisms responsible for these parameters suggest that they are representative of engine input and output.
- Evaluation of the two parameters against each other for two different engines produced relatively consistent relationships once the AE signals were normalised and the number of cylinders of each engine accounted for. These relationships may be indicative of engine performance and could therefore be used to infer power output and aid assessment of overall engine balance.
- Since the ICAV waveform displays the effects of combustion and expansion in each cylinder it can therefore be dissected to provide information about each process. It seems likely that when this information is combined with AE energy on a per-cylinder basis an assessment of individual cylinder performance may be made.

9.3 Overall conclusions regarding monitoring of ring-pack/liner interface and implications of findings with respect to engine condition monitoring and management

This work has established that continuous AE activity in signals acquired from the cylinder liners of large, two-stroke engines and the cylinder blocks of small, four-stroke engines is related to sliding contact at the ring-pack/liner interface. For the two different types of engine the evidence is consistent in that it indicates piston mid-stroke AE activity is related to the frictional power losses due to asperity contact. Continuous AE activity at around TDC was also attributed to the ring-pack/liner interface for the large engines although the source mechanism could not be precisely determined. One notable shortcoming is the lack of any further measure of ring-pack behaviour from

which to validate these deductions. Therefore, the correlation between AE activity and ring-pack frictional losses cannot be conclusively verified although the evidence strongly suggests it exists. This relationship also suggests tenuously that this AE activity is indicative of wear rate. Component wear would also be expected to be a factor since the condition and profile of rings are important elements that affect ring-pack frictional behaviour.

On this basis AE monitoring offers diagnostic information which may be exploited to offer monitoring of ring-pack condition and performance. The question is then how best to extract this information from the signals. The aim of the analytical methods used in this work has been mainly to characterise changes in the signals to aid understanding of the AE sources, nevertheless, it is possible that these methods could also be used as the basis of a monitoring system. For instance, for the tests conducted on engine F, the AE energy contained in windows of the signals where ring-pack friction was the predominant source clearly increased as running conditions deteriorated. Similarly, the gradient of the engine load verses AE energy relationship increased, Figures 7.26 and 7.27. These parameters could then be trended over time or evaluated against a predetermined knowledge archive in order to identify running condition.

However, since these diagnostic features are based on the measured AE amplitude the information they provide is inherently qualitative, that is the AE amplitude is a function not only of the intensity of source mechanism but also of the source-sensor transmission and the sensor response characteristics. This means that information obtained from one engine, by way of values indicative of certain running conditions, is only strictly applicable to engines of the same specification tested in conjunction with that particular instrumentation. This obviously presents a problem in terms of application over different engine types as each will possess different AE transmission characteristics and therefore require some form of recalibration of the knowledge archive.

Despite this problem the generic trends identified in the AE activity with changing conditions would be reproducible over different engine types and it is this information which is of value for a monitoring system. It is likely that other approaches to signal processing and feature extraction will be more efficient in extracting this information

and these may also achieve this in a manner more suitable for transferable application and integration into engine management systems.

A further concern for commercial application of AE monitoring may be the complexity and reliability of the AE measurement hardware. Experience gained from this project suggests that sensors of sufficient robustness for long-term application are available (Env sensors were installed on engine F for several thousand running hours with no obvious deterioration in sensor construction or response). Moreover, piezoelectric type sensors are already applied on the cylinder block of some engines to detect the occurrence of knock conditions. A further issue is the sophistication of DAQ hardware required as the high sampling rate necessary for raw AE acquisition may be excessive for incorporation within a mixed sensor array. However, the use of RMS AE reduces the sampling frequency to a more acceptable level and this work has shown that such measurements are an adequate base from which to evaluate ring-pack running condition.

Regardless of the issues that remain to be overcome the work in this thesis has shown that AE monitoring offers a unique insight into ring-pack behaviour and operating conditions. Furthermore, this diagnostic information can be obtained without the need for intrusive measurements or expensive engine modifications. It therefore represents a new and promising opportunity which may be of significant benefit to engine users, and one which complements existing monitoring systems. The potential benefits on offer are of greater consequence when it is considered that current methods to assess ring-pack running condition in production engines are limited to periodic inspections and oil analysis. In addition, AE measurements can be made on an on-line basis and are therefore available for potential integration into engine management systems. This means that as well as early diagnosis of problems the information may be used to adjust operating conditions so as to optimise operating costs or component lifetimes.

AE monitoring of ring-pack frictional behaviour further represents the transference and progression of findings from fundamental materials testing on laboratory test-rigs to the complexity of an industrial application. In doing so it broadens the scope of AE monitoring of tribological processes.

9.4 Recommendations for future work

The following recommendations are suggested for future research:

- Strengthening of findings from this work regarding AE generation from the ring-pack/liner interface. There are a number of tests that may be carried out on both engine types in order to validate or further support the findings. Of particular interest would be comparison of AE with simultaneous acquisition of parameters that allow the actual ring-pack behaviour to be established. Similarly, comparison to measures of wear during long-term testing would greatly enhance current understanding. Further evidence may also be gained from a series of tests which considers factors known to affect interfacial conditions such as; oil viscosity, particulate contamination, and component changes during the running-in period. Encouragingly, initial work which has examined AE activity during running-in of a reconditioned engine (not detailed in this thesis) has shown variation in the background AE activity as components bedded in. Regarding large, two-stroke diesels, further support for the proposed relationship between AE activity and ring-pack frictional losses may be obtained from tests with varying lubricant feed rates as evidence suggests a correlation to liner wear rates [67, 83]. A particularly informative test for the small, four-stroke engines would be motored teardown tests as the systematic removal of piston assembly components should allow confirmation of whether interaction at the oil-control ring/liner interface was responsible for the continuous AE activity.
- Experimentation on small, four-stroke diesels. Future research into the characteristics of AE sources would be simplified greatly if testing were conducted on a single-cylinder engine. This would eliminate the signal confusion and consequent analytical problems resulting from extensive cross-cylinder propagation. This would be particularly beneficial for further investigations into the low-level continuous activity arising from the ring-pack/liner interface.
- Induce scuffing conditions. In this work scuffing was not experienced, therefore, although AE monitoring has been shown sensitive to changes in lubrication condition, the ability to detect scuffing cannot be confirmed. In order to induce scuffing the cylinder should be starved of lubricant for a longer period of time and action should be taken to prevent an oil mist entering the cylinder via the scavenge

ports. If this fails to induce scuffing, water injection should be considered as a means to aid the removal of lubricating oil from the sliding surfaces.

- Instrumentation of a piston assembly. This would give greater insight into AE generation at the ring-pack/liner interface. Other transducers have been successfully installed within a piston assembly with cables extracted through various tubing arrangements [94, 96]. Therefore, as long as AE sensors can be selected to withstand the high temperatures then there is no practical reason why this cannot be achieved.
- Spatial reconstitution of AE arising from sliding contact at the ring-pack/liner interface. Previous work has shown the potential of using signal reconstitution to enhance the resolution of multi-source signals for events relating to injector and valve activity [154]. A similar technique applied to the ring-pack/liner source may improve the results by effectively separating this AE component from the original signal and reconstituting it as generated at the source. Implementation of this technique would require detailed knowledge of the AE propagation characteristics of the liner.
- Automatic source location of AE events. Develop automatic source location techniques using optimised sensor arrays and triangulation algorithms. Nivesrangsan *et al* [155] outlined methods to achieve this based upon time of flight or energy analysis. This may be valuable for pinpointing the source of burst-type events which could not be accurately identified but were believed to originate on the liner surfaces of the large, two-stroke engines.
- Improved understanding of AE activity from reciprocating sliding contact. A sizeable amount of work has considered AE monitoring of tribological behaviour in laboratory test-rigs; however, this has mostly involved constant speed set-ups with little consideration of reciprocating motion. Work which has investigated reciprocating motion has not acquired or analysed the AE activity in a manner that would allow the AE characteristics during a cycle to be established. Examination of reciprocating motion over varying lubricating conditions may substantiate the correlation between AE activity and frictional power loss. This belief is supported by recent exploratory work (in collaboration with the University of Leeds but unpublished) although further research is warranted.
- Clarification of injector behaviour through measurement of needle lift. This would provide greater information about the mechanical activities within the injector which may allow validation of observations made in this work. Testing of injectors of

various conditions on a calibration test-stand would further improve understanding of the potential for monitoring of injector deficiencies.

- Investigation of how the findings of this work can be applied towards engine monitoring and management. This will likely involve the development of signal processing techniques to improve the accuracy, efficiency and robustness of the analysis. These may also be more amenable to automation and integration with engine management systems. Particular application is foreseen as an element of a cylinder lubrication control system for the purpose of optimising oil dosage rates.
- Long-term testing. Long-term testing over a wider range of engines and correlation with engine performance and maintenance activities would allow a knowledge archive to be developed of the changes in AE activity during the service life of a liner and of the features which characterise various running conditions.

References

[1] Dunn, S. Condition monitoring in the 21st century [online]. *Plant maintenance Resource Center,* 2002, available at: http://www.plant-maintenance.com/articles/ConMon21stCentury.shtml.

[2] Bengtsson, M., Olsson, E., Funk, P. and Jackson, M. Technical design of condition based maintenance system – a case study using sound analysis and case-based reasoning. *Maintenance and Reliability Conference - Proc. of the 8th Congress, MARCON,* Knoxville, USA, 2-5 May, 2004.

[3] Wilson, K. Cylinder liner scuffing in 2-stroke low-speed engines as experienced by "users" WG members and others. *Proc. of 22nd Intl. Congress on Combustion Engines, CIMAC*, Copenhagen, Denmark, 19-21 May 1998, 2, pp. 303-310.

[4] Allen, R. W. and Yura, S. Developments in two-stroke engine cylinder lubrication. *Proc. of 6th Intl. Symposium on Marine Engineering, ISME,* Tokyo, Japan, 23-17 October 2000, 2, pp. 488-492.

[5] Reuben, R. L. Role of acoustic emission in industrial condition monitoring. *International Journal of COMADEM,* 1998, 1(4), pp. 35-46.

[6] Steel, J. A. and Reuben, R. L. Recent developments in monitoring of engines using acoustic emission. *The Journal of Strain Analysis for Engineering Design*, 2005, 40(1), pp. 45-57.

[7] Vallen, H. AE testing, fundamentals, equipment, applications [online]. *NDT.net,* 2002, 7(9), available at: http://www.ndt.net/article/az/ae_idx.htm.

[8] Pontoppidan, N. H. and Sigurdsson, S. Independent components in acoustic emission energy signals from large diesel engines. *Accepted for publication in International Journal of COMADEM*, 2006.

[9] Sigurdsson, S., Pontoppidan, N. H. and Larsen, J. Supervised and unsupervised condition monitoring of non-stationary acoustic emission signals. Proc. 18th *Intl. Congress on Condition Monitoring and Diagnostic Engineering Management, COMADEM,* Cranfield, UK, 31 August - 2 September 2005, pp. 535-541.

[10] Pedersen, P. S. and Grøne, O. The intelligent engine: prospects and experience from service. *Proc. of 6th Intl. Symposium on Marine Engineering, ISME,* Tokyo, Japan, 23-17 October 2000, 1, pp. 399-406.

[11] Marine Accident Investigation Branch, MAIB. Annual report 2005. Department for Transport.

[12] Japan Marine Accident Inquiry Agency, MAIA. Report on marine accidents. A message on prevention of marine accidents. July 2004.

[13] Martens, O. Experience with condition monitoring of slow speed engines. *Proc. of 12th Intl. Congress on Combustion Engines, CIMAC*, Tokyo, Japan, 22 May - 1 June 1977, vol. B, pp. 1403-1425.

[14] Long, B. R. and Boutin, K. D. Enhancing the process of diesel engine condition monitoring. *Proc. of the 18th Annual Fall Technical Conference of the ASME Internal Combustion Engine Division*, Fairborn, USA, 20-23 October 1996, 27(1), pp. 61-68.

[15] Yang, J., Pu, L., Wang, Z., Zhou, Y. and Yan, X. Fault detection in a diesel engine by analysing the instantaneous angular speed. *Mechanical Systems and Signal Processing,* 2001, 15(3), pp. 549-564.

[16] Gu, F., Jacob, P. J. and Ball, A. D. A RPF neural network model for cylinder pressure reconstruction in internal combustion engines. *IEEE Colloquium on Modelling and Signal Processing for Fault Diagnosis*, Leicester, UK, 18 September 1996, pp. 4/1-4/11.

[17] Gu, F., Jacob, P. J. and Ball, A. D. Non-parametric models in the monitoring of engine performance and condition. Part 2: non-intrusive estimation of diesel engine cylinder pressure and its use in fault detection. *Proc. of the IMechE Part D: Journal of Automotive Engineering*, 1999, 213(2), pp. 135-143.

[18] Fleming, W. J. Automotive torque measurement: a summary of seven different methods. *IEEE Transactions on Vehicular Technology*, 1982, VT-31(3), pp. 117-124.

[19] Li, Y., Gu, F., Harris, G., Ball, A., Bennett, N. and Travis, K. The measurement of instantaneous angular speed. *Mechanical Systems and Signal Processing*, 2005, 19(4), pp. 786-805.

[20] Azzoni, P. M., Minelli, G., Flora, R. and Serra, G. Indicated and load torque estimation using crankshaft angular velocity measurement. *SAE Intl. Congress and Exposition,* Detroit, USA, 1-4 March 1999, SAE Paper 1999-01-0543, pp. 87-93.

[21] Rizzoni, G. and Ribbens, W. B. Crankshaft position measurement for engine testing, control and diagnosis. *Proc. of 39th IEEE Vehicular Technology Conference*, San Francisco, USA, 1-3 May 1989, 1, pp. 423-436.

[22] Citron, S. J., O'Higgens, J. E. and Chen, L. Y. Cylinder by cylinder engine pressure and pressure torque waveform determination utilizing speed

fluctuations. *SAE Intl. Congress and Exposition,* Detroit, USA, 27 February - 3 March 1989, SAE Paper 890486, pp. 131-145.

[23] Lida, K, Akishino, K. and Kido, K. IMEP estimation from instantaneous crankshaft torque variation. February 1990, SAE Paper 900617.

[24] Brown, T. S. and Neill, W. S. Determination of engine cylinder pressures from crankshaft speed fluctuations. *SAE Intl. Congress and Exposition,* Detroit, USA, 22-26 February 1992, SAE Paper 920463, pp. 61-69.

[25] Mauer, G. and Watts, R. J. On-line cylinder diagnostics on combustion engines by noncontact torque and speed measurements. *SAE Intl. Congress & Exposition,* Detroit, USA, 27 February - 3 March, 1989, SP-771–Sensor and Actuators, SAE Paper 890485, pp. 123-130.

[26] Shimuza, T. Research for abnormal condition diagnosis on diesel engine. *Proc. of 6th Intl. Symposium on Marine Engineering, ISME*, Tokyo, Japan, 23-27 October 2000, 1, pp. 316-323.

[27] Tinaut, F. V., Melgar, A., Horillo, A. J., Fernández, L. and Montero, V. Faults detection in a reciprocating internal combustion engine from instantaneous engine speed. *Proc. of 22nd Intl. Congress on Combustion Engines, CIMAC*, Copenhagen, Denmark, 18-21 May 1998, 3, pp. 629-638.

[28] Mihelc, W. and Citron, S. J. An on-line engine roughness measurement technique. *SAE Intl. Congress & Exposition,* Detroit, USA, 27 February - 2 March, 1984, SP-567–Sensor and Actuators, SAE Paper 840136, pp. 9-18.

[29] Takats, M., Uhlir, I. and Lukas, N. Running roughness measurement-tools for development and diagnostic. *Proc. 23rd World Congress on Combustion Engine Technology for Ship Propulsion, Power Generation, Rail Traction, CIMAC,* Hamburg, Germany, 7-10 May 2001, 4, pp. 1340-1348.

[30] Taraza, D. Henein, N. A. and Bryzik, W. The frequency analysis of the crankshaft's speed variation: A reliable tool for diesel engine diagnosis. *Transactions of the ASME: Journal of Engineering for Gas Turbines and Power,* 2001, 123(2), pp. 428-432.

[31] Carmody, T. The measurement of vibration as a diagnostic tool. *Transactions of the Institute of Marine Engineers*, 1972, 94(6), pp. 147-157.

[32] Autar, R. K. An automated diagnostic expert system for diesel engines. *Transactions of the ASME: Journal of Engineering for Gas Turbines and Power,* 1996, 118(3), pp. 673-679.

[33] Haller, C. L. and Kelleher, E. P. Practical integrated maintenance and diagnostics for medium and slow speed diesel engines. *Proc. of IMarE Conference on Computers and Ships*, London, UK, 11-12 May 1999, 111(4 Part 1), pp. 103-128.

[34] Chandroth, G., Sharkey, A. J. C. and Sharkey, N. E. Cylinder pressures and vibration in internal combustion engine condition monitoring. *Proc. 12th Intl. Conference on Condition Monitoring and Diagnostic Engineering Management, COMADEM*, Sunderland, UK, 7-9 July 1999, pp. 141-151.

[35] Sasaki, S. Vibration monitoring for wear condition of cylinder liner and piston ring in marine diesel engine. *Proc. of 6th Intl. Symposium on Marine Engineering, ISME,* Tokyo, Japan, 23-17 October 2000, 2, pp. 556-561.

[36] Gu, F. and Ball, A. D. Diesel injector dynamic modeling and estimation of injection parameters from impact response. Part 2: prediction of injection parameters from monitored vibration. *Proc. of the IMechE Part D: Journal of Automobile Engineering*. 1996, 210(D4), pp. 303-312.

[37] Molinaro, F. and Castanié, F. Signal processing pattern classification techniques to improve knock detection in spark ignition engines. *Mechanical Systems and Signal Processing*, 1995, 9(1), pp. 51-62.

[38] Ghasemloonia, A. and Behzad, M. Engine knock detection by vibration monitoring. *Proc. 18th Intl. Congress on Condition Monitoring and Diagnostic Engineering Management, COMADEM*, Cranfield, UK, 31 August - 2 September 2005, pp. 153-163.

[39] Kitahara, T., Yanamoto, H., Otsubo, M. and Nakahara, D. Monitoring of abnormal vibration to prevent seizure of crosshead bearings. *Journal of the Japan Institution of Marine Engineering*, 2004, 39(5).

[40] Randall, R. B., Ren, Y. and Ngu, H. Diesel engine cylinder pressure reconstruction. *Proc. 21st Intl. Seminar of Modal Analysis (ISMA 23),* Leuven, Belgium, 18-20 September 1996, 2, pp. 847-856.

[41] Gao, Y. and Randall, R. B. Reconstruction of diesel engine cylinder pressure using a time domain smoothing technique. *Mechanical Systems and Signal Processing,* 1999, 13(5), pp. 709-722.

[42] Zurita, G., Ågren, A., Randall, R. B. and Gao, Y. Reconstruction of cylinder pressure time trace on a six-cylinder engine from acceleration measurements. *Proc. 23rd Intl. Seminar of Modal Analysis (ISMA 23),* Leuven, Belgium, 10-12 September 1998, 3, pp. 1387-1394.

[43] Albarbar, A., Gennish, R., Ali, M., Harris, G., Gu, F. and Ball, A. D. Diesel engine injector condition monitoring using air-borne acoustic measurement. *Proc. 18th Intl. Congress on Condition Monitoring and Diagnostic Engineering Management, COMADEM*, Cranfield, UK, 31 August - 2 September 2005, pp. 143-152.

[44] Gu, F., Li, W., Ball, A. D. and Leung, A. Y. T. The condition monitoring of diesel engines using acoustic measurements, part 1: acoustic characteristics of the engine and representation of the acoustic signals. *SAE 2000 World Congress, Noise & Vibration,* Detroit, USA, 6-9 March 2000, SAE Paper 2000-01-0730, pp. 51-57.

[45] Ball, A. D., Gu, F. and Li, W. The condition monitoring of diesel engines using acoustic measurements, part 2: fault detection and diagnosis. *SAE 2000 World Congress, Noise & Vibration,* Detroit, USA 6-9 March 2000, SAE Paper 2000-01-0368, pp. 57-64.

[46] Li, W., Gu, F., Ball, A. D., Leung, A. Y. T. and Phipps. A study of the noise from diesel engines using the independent component analysis. *Mechanical Systems and Signal Processing*, 2001, 15(6), pp. 1165-1184.

[47] Kimura, R., Nakai, N. and Kishimoto, T. Abnormal sound detection by neural network in the diesel engine. *Bulletin of the Marine Engineering Society in Japan*, 1998, 26(1), pp. 24-31.

[48] Kawai, T., Nonomura, M., Futamurai, M. and Ito, M. Estimation of valve clearance of engine by wavelet analysis. *Proc. 16th Intl. Conference on Condition Monitoring and Diagnostic Engineering Management, COMADEM*, Växjö, Sweden, 17-29 August 2003, pp. 759-766.

[49] Fog, T. L., Larsen, J. and Hansen, L. K. Training and evaluation of neural networks for multi-variate time series processing. *Proc. of IEEE Intl. Conference on Neural Networks, ICNN,* Perth, Australia, 27 November - 1 December 1995, 2, pp. 1194-1199.

[50] Chiavola, O. Combustion anomalies detection in SI engines from exhaust pressure signal processing. *Proc. of the IMechE Part A: Journal of Power and Energy*. 2003, 217(5), pp. 537-546.

[51] Gennish, R., Albarbar, A. Harris, G., Gu, F. and Ball, A. D. Diagnosis of diesel engine valve faults by using of exhaust manifold pressure signal. *Proc. 18th Intl. Congress on Condition Monitoring and Diagnostic Engineering Management, COMADEM*, Cranfield, UK, 31 August - 2 September 2005, pp. 297-305.

[52] Hountalas, D. T. and Kouremenos, A. D. Development and application of a fully automatic troubleshooting method for large marine diesel engines. *Applied Thermal Engineering*, 1999, 19(3), pp. 299-324.

[53] Warkman, D. C. BP's performance monitoring system for marine diesel engine. *Trans. of the Institute of Marine Engineers*, 1983, 95, paper no. 40, pp. 1-21.

[54] Takai, M. and Tsukahara, S. Performance and combustion analysis of high-speed diesel engine in fast ferry under normal service condition. *Proc. of 25th World Congress on Combustion Engine Technology, CIMAC*, Kyoto, Japan, 4-11 June 2004.

[55] Koike, N., Kumagai, Y. and Nakamura, K. Development of detection system for abnormal wear of engine bearings. *JSAE Review*, 1998, 19(1), pp. 27-32.

[56] Southwest Research Institute. Diagnosing engine problems with magnetorestrictive sensors [online]. available at: http://www.swri.edu/3pubs/brochure/d17/magneto/diagnos.htm.

[57] Kwun, H. Back in style: magnetostrictive sensors [online]. Southwest Research Institute, September 1991. available at: http://www.swri.edu/3pubs/brochure/d17/magneto/magneto.htm.

[58] Zhao, H. and Ma, T. Engine performance monitoring by means of spark plug. *Proc. of the IMechE Part D: Journal of Automotive Engineering*, 1995, 209(D2), pp. 143-146.

[59] Wickström, N., Taveniku, M., Linde, A., Larsson, M. and Svensson, B. Estimating pressure peaks position and air-fuel ration using the ionisation current and artificial neural networks. *Proc. of IEEE Conference on Intelligent Transportation Systems*, Boston, USA, 9-12 November 1998, pp. 972-977.

[60] Dowson, D., Ruddy, B. L. and Economou, P. N. The elastohydrodynamic lubrication of piston rings. *Proc. of the Royal Society of London*, 1983, A 386, pp. 409-430.

[61] Tung, S. C. and McMillan, M. L. Automotive tribology overview of current advances and challenges for the future. *Tribology International*, 2004, 37(7), pp. 517-536.

[62] Richardson, D. E. Review of power cylinder friction for diesel engines. *ASME: Journal of Engineering for Gas Turbines & Power, 2000*, 122(4), pp. 506-519.

[63] Priest, M. and Taylor, C. M. Automobile engine tribology – approaching the surface. *Wear*, 2000, 241(2), pp. 193-203.

[64] Andersson, P., Tamminen, J. and Sandström, C-E. Piston ring tribology. A literature survey. *Espoo 2002, VTT Tiedotteita – Research Notes 2178*, 2002, 105 p.

[65] Keribar, R., Dursunkaya, Z. and Flemming, M. F. An integrated model of ring pack performance. *Transactions of the ASME: Journal of Engineering for Gas Turbines and Power,* 1991, 113(3), pp. 382-389.

[66] Wilson, K., Dragsted, J. and Hansen, N. When knowledge is safety, and money – the use of an engine failure database. *Proc. of 6th Intl.Symposium on Marine Engineering, ISME,* Tokyo, Japan, 23-27 October 2000, 2, pp. 381-386.

[67] Golothan, D. W. A review of the causes of cylinder wear in marine diesel engines. *Transactions of the Institute of Marine Engineers*, 1977, 90(A: Part 3), pp. 137-163.

[68] Cook, S. J. Prevention of scuffing in 2-stroke crosshead marine diesel engines. *Proc. of 23rd World Congress on Combustion Engine Technology for Ship Propulsion, Power Generation and Rail Traction, CIMAC*, Hamburg, Germany, 7-10 May 2001, 4, pp. 1412-1417.

[69] IMechE. Memorandum on definitions, symbols and units. *Proc. of the IMechE Conference on Lubrication and Wear*, London, UK, 1-3 October 1957, pp. 4.

[70] Shuster, M. M., Stong, T., Deis, M. C. And Burke, D. C. Piston ring cylinder liner scuffing phenomenon: investigation, simulation and prevention. *Proc. of Conference*, Detroit, USA, 1-4 March 1999, SAE Paper 1999-01-1219.

[71] Rogers, M. D. Metallographic characterisation of transformation phases on scuffed cast-iron diesel engine components. *Tribology*, 1969, 2, pp. 123-127.

[72] Neale, M. J. Piston ring scuffing – a broad survey of problems and practice. *Proc. of the Institute of Mechanical Engineers*, 1970-71, 185(2/71), pp. 21-32.

[73] Schenk, C., Hengeveld, J. and Aabo, K. The role of temperature and pressure in wear processes in low speed diesel engines. *Proc. of 6th Intl. Symposium on Marine Engineering, ISME,* Tokyo, Japan, 23-17 Oct 2000, 2, pp. 562-569.

[74] Nakano, H. Piston ring scuffing as a limit in designing future diesel engines. *Proc. of 4th Intl. Symposium on Marine Engineering, ISME*, Kobe, Japan, 15-19 October 1990.

[75] Lauritsen, S., Dragsted, J. and Buchholz, B. Swirl injection lubrication – a new technology to obtain low cylinder oil consumption without sacrificing wear rates. *Proc. of 23rd World Congress on Combustion Engine Technology for Ship*

Propulsion, Power Generation and Rail Traction, CIMAC, Hamburg, Germany, 7-10 May 2001, 3, pp. 921-932.

[76] Tanaka, M. Improved cylinder lubricator. *Journal of the Japan Institution of Marine Engineering,* 2002, 37(2), 16 p.

[77] Jacobsen, S. Alpha adaptive cylinder – oil control alpha ACC. *The Greek CIMAC Association - Interaction between Engine Design, Cylinder Lube Oil Design, and Cylinder Condition*, Athens, Greece, 6 February 2003, 4 p.

[78] Maekawa, K., Akizuki, Y., Matsumoto, S., Motomura, O. and Ichimaru, K. Experimental estimation for behavior of cylinder oil on cylinder liner surface. *Bulletin of the Marine Engineering Society in Japan*, 2001, 29(1), 21-27.

[79] Tanaka, T., Mitake, S., Taguchi, S., Goto, T. And Knudsen, S. Development of spray-coated cylinder liner for diesel engine. *Proc. of 6th Intl. Symposium on Marine Engineering, ISME,* Tokyo, Japan, 23-27 October 2000, 2, pp. 550-555.

[80] Tanaka, M., Kitajima, Y., Endoh, Y., Watanabe, M. And Nagita, Y. Ceramic-metal composite coated piston ring and cylinder liner of marine low speed diesel engine. *Bulletin of the Marine Engineering Society in Japan*, 1993, 21(2), pp. 77-85.

[81] Stolarski, T. A., Zhou, Q., Smart, M., Green, D. and Allen, R. W. Temperature-friction characteristics of cylinder lubricants in large slow cross-head marine diesel engine under boundary lubrication conditions. *Proc. of 3rd World Tribology Conference*, Vienna, Austria, 3-7 September 2001, 4 p.

[82] Fog, T. L. Condition monitoring and fault diagnosis in marine diesel engines. *PhD Thesis, Danish Technical University*, August 1998.

[83] Grossmann, G. and Voss, A. Influence of the lub oil feed rate on the wear rate of liners of two stroke diesel engines. *Proc. of the 21st Intl. Congress on Combustion Engines, CIMAC*, Interlaken, Switzerland, 15 May 1995.

[84] Hatzigrigoris, S. Interaction between engine design, cylinder lub oil design and cylinder condition. *The Greek CIMAC Association - Interaction between Engine Design, Cylinder Lube Oil Design, and Cylinder Condition*, Athens, Greece, 6 February 2003.

[85] Saddler, K. P. Cylinder oil feed rate optimization – risk and reward. *The Greek CIMAC Association - Interaction between Engine Design, Cylinder Lube Oil Design, and Cylinder Condition*, Athens, Greece, 6 February 2003.

[86] Daniolos, S. Interaction between engine design, cylinder lub oil design and cylinder condition. *The Greek CIMAC Association - Interaction between Engine*

Design, Cylinder Lube Oil Design, and Cylinder Condition, Athens, Greece, 6 February 2003.

[87] Hashimoto, T., Baba, N, and Aoki, H. Monitoring of marine two stroke diesel cylinder lubricating condition by ferrography. *Proc. of 22nd Intl. Congress on Combustion Engines, CIMAC*, Copenhagen, Denmark, 19-21 May 1998, 4, pp. 901-911.

[88] Lim, K. C. Presentation. *The Greek CIMAC Association - Interaction between Engine Design, Cylinder Lube Oil Design, and Cylinder Condition*, Athens, Greece, 6 February 2003.

[89] Mitsutake, S., Ono'hk, S., Maekawa, K. and Inada, K. Evaluation method of lubrication by oil sampling from liner wall for marine diesel engine. *Bulletin of the Japan Society of Mechanical Engineers,* 1991, 19(1), pp. 1-9.

[90] Fagerland, H., Rothaug, K. and Tokle, P. Monitoring and diagnosing process deviations in marine diesel engine. *Transactions of the Institute of Marine Engineers,* 1978, 90(A), pp. 321-349.

[91] Jones, N. B. and Li, Y.-H. A review of condition monitoring and fault diagnosis for diesel engines. *Tribotest journal,* 2000, 6(3), pp. 267-291.

[92] Kimura, R., Terashima, W., Nakai, N., Yamada, T. and Takeda, S. Diagnostic method for 2-stroke cycle diesel engine by measurement of vibration on cylinder-jacket – observation of change in normal vibration pattern. *Bulletin of the Japan Society of Mechanical Engineers,* 1999, 27(2), pp. 57-64.

[93] Priest, M., Dowson, D. and Taylor, C. M. Predictive wear modeling of lubricated piston rings in a diesel engine. *Wear*, 1999, 231(1), pp. 89-101.

[94] Lee, P. M., Priest, M., Stark, M. S., Wilkinson, J. J., Lindsay Smith, J. R., Taylor, R. I. and Chung, S. Extraction and tribological investigation of top piston ring zone oil from a gasoline engine. *Proc. of the IMechE Part J: Journal of Engineering Tribology*, 2006, 220(2), pp. 171-180.

[95] Sherrington, I. and Smith, E. H. Experimental methods for measuring the oil-film thickness between the piston-rings and cylinder-wall of internal combustion engines. *Tribology International*, 1986, 18(6), pp. 313-320.

[96] Taylor, R. I. and Evans, P. G. In-situ piston measurements. *Proc. of the IMechE Part J: Journal of Engineering Tribology*, 2004, 218(3), pp. 185-200.

[97] Hamilton, G. M. and Moore, S. L. The lubrication of piston rings, first paper, measurement of the oil-film thickness between the piston rings and liner of a

small diesel engine. *Proc. of the Institute of Mechanical Engineers*, 1974, 188 (20/74), pp. 253-261.

[98] Ducu, D. O., Donahue, R. J. and Ghandhi, J. B. Design of capacitance probes for oil film thickness measurements between the piston ring and liner in internal combustion engines. *Transactions of the ASME: Journal of Engineering for Gas Turbines and Power,* 2001, 123(2), pp. 633-643.

[99] Furuhama, S., Takiguchi, M. and Tomizawa, K. Effect of piston and piston ring designs on the piston friction forces in diesel engines. SAE Paper 810977, 1981.

[100] Taylor, R. I., Kitahara, T., Saito, T. and Coy, R. C. Piston assembly friction and wear: the influence of lubricant viscometry. *Proc. of the Intl. Tribology Conference*, Yokohama, Japan, 29 October - 2 November 1995, 6 p.

[101] Cho, S., Choi, S. and Bae, C. The frictional modes of piston rings for a SI engine [in Korean with English summary]. SAE 2000-03-0094, pp. 114-120.

[102] Furuhama, S. A dynamic theory of piston-ring lubrication (1st report, calculation). *Bulletin of the JSME*, 1959, 2(7), pp. 423-428.

[103] Dowson, D., Economou, P. N., Ruddy, B. L., Strachan, P. J. and Baker, A. J. Piston ring lubrication: part II – theoretical analysis of a single ring and a complete ring pack. *Proc. of ASME Winter Annual Meeting. Energy Conservation Through Fluid Film Lubrication Technology: Frontiers in Research and Design,* 1979, pp. 23-52.

[104] Rhode, S. M. A mixed friction model for dynamically loaded contact with application for piston ring lubrication. *Proc. of 7th Leeds-Lyon Symposium on Tribology*, Leeds, UK, 9-12 September 1980, pp. 262-278.

[105] Ma, M.-T., Sherrington, I. Smith, E. H., and Grice, N. Development of a detailed model for piston-ring lubrication in IC engines with circular and non-circular cylinder bores. *Tribology International*, 1997, 30(11), pp. 779-788.

[106] Priest, M., Dowson, D. and Taylor, C. M. Theoretical modeling of cavitation in piston ring lubrication. *Proc. of the IMechE Part C: Journal of Mechanical Engineering Science*, 2000, 214(3), pp. 435-447.

[107] Ma, M.-T., Sherrington, I. and Smith, E. H. Analysis of lubrication and friction for a complete piston ring-pack with an improved oil availability model. Part 1: circumferentially uniform film. *Proc. of the IMechE Part J: Journal of Engineering Tribology*, 1997, 211(1), pp. 1-15.

[108] Seki, T., Nakayama, K., Yamada, T., Yoshida, A. and Takiguchi, M. A study on variation in oil film thickness of a piston ring package: variation of oil film thickness in piston sliding direction. *JSAE Review*, 2000, 21(3), pp. 315-320.

[109] Ruddy, B. L., Dowson, D. and Economou, P. N. A theoretical analysis of the twin-land type of oil control piston ring. *Journal of Mechanical Engineering Science*, 1981, 23(2), pp. 51-62.

[110] Pollock, A. A. Classical wave theory in practical AE testing. *Progress in Acoustic Emission III – Japanese Society of Non-Destructive Testing*, 1986, pp. 708-721.

[111] Brown, E. R., Reuben, R. L., Neill, G. D. and Steel, J. A. Acoustic emission source discrimination using a piezopolymer based sensor. *Materials Evaluation*, 1998, 57(5), pp. 515-520.

[112] Hsu, N. N., Simmons, J. A. and Hardy, S. C. An approach to acoustic emission signal analysis – theory and experiment. *Materials Evaluation*, 1977, 35(10), pp. 100-106.

[113] Hsu, N. N. and Breckenbridge, F. R. Characterisation and calibration of acoustic emission sensors. *Materials Evaluation*, 1981, 39(1), pp. 60-68.

[114] Beattie, A. G. and Jaramillo, R. A. The measurement of energy in acoustic emission. *Review of Scientific Instruments*, 1974, 45(3), pp. 352-357.

[115] Bagnoli, S., Capitani, R., Citti, P. Comparison of accelerometer and acoustic emission signals as diagnostic tools in assessing bearing damage. *Proc. of 2nd Intl. Conference on Condition Monitoring*, London, UK, 24-25th May 1988, 10, pp. 117-125.

[116] Welch, P. D. The use of fast fourier transform for the estimation of power spectra: a method based on time averaging over short, modified periodograms. *IEEE Transactions Audio Electroacoustics*, 1967, Vol. AU-15, pp. 70-73.

[117] Jeong, H. and Jang, Y. S. Wavelet analysis of plate wave propagation in composite laminates. *Composite Structures*, 2000, 49(4), pp. 443-450.

[118] Ding, Y, Reuben, R. L. and Steel, J. A. A new method for waveform analysis for estimating AE wave arrival times using wavelet decomposition. *NDT&E International,* 2004, 37(4), pp. 279-290.

[119] Hall, L. D. and Mba, D. Diagnosis of continuous rotor-stator rubbing in large scale turbine units using acoustic emissions. *Ultrasonics*, 2004, 41(9), pp. 765-773.

[120] Neill, G. D., Benzie, S., Gill, J. D., Sandford, P. M., Brown, E. R., Steel, J. A. and Reuben, R. L. The relative merits of acoustic emission and acceleration monitoring for the detection of bearing defects. *Proc. 11th Intl. Conference on Condition Monitoring and Diagnostic Engineering Management, COMADEM,* Launceston, Australia, 8-11 December 1998, pp. 651-661.

[121] Tandon, N. and Choudhury, A. A review of vibration and acoustic measurement methods for the detection of defects in rolling element bearings. *Tribology International*, 1999, 32(8), pp. 469-480.

[122] El-Ghamry, M. H., Brown, E. R., Ferguson, I., Gill, J. D., Reuben, R. L., Steel, J. A., Scaife, M. and Middleton, S. Gaseous air-fuel quality identification for a spark ignition gas engine using acoustic emission analysis. *Proc. 11th Intl. Conference on Condition Monitoring and Diagnostic Engineering Management, COMADEM,* Launceston, Australia, 8-11 December 1998, pp. 235-244.

[123] Fog, T. L., Brown, E. R., Hansen, H. S., Madsen, L. B., Sorensen, P., Hansen, E. R., Steel, J. A., Reuben, R. L. and Pedersen, P. S. Exhaust valve leakage detection in large marine diesel engines. *Proc. 11th Intl. Conference on Condition Monitoring and Diagnostic Engineering Management, COMADEM,* Launceston, Australia, 8-11 December 1998, pp. 269-278.

[124] Gill, J. D., Brown, E. R., Twite, M., Horner, G., Reuben, R. L. and Steel, J. A. Monitoring of a large reciprocating compressor. *Proc. 11th Intl. Conference on Condition Monitoring and Diagnostic Engineering Management, COMADEM,* Launceston, Australia, 8-11 December 1998, pp. 317-326.

[125] Sikorska, J. Z. and Hodkiewicz, M. Comparison of acoustic emission, vibration and dynamic pressure measurements for detecting change in flow conditions on a centrifugal pump. *Proc. 18th Intl. Congress on Condition Monitoring and Diagnostic Engineering Management, COMADEM*, Cranfield, UK, 31 August-2 September 2005, pp. 171-181.

[126] Singh, A., Houser, D. R. and Vijayakar, S. Early detection of gear pitting. *Proc. of 7th ASME Intl. Power Transmission and Gearing Conference,* San Diego, USA, 6-9 October 1996, 88, pp. 673–678.

[127] Siores, E. and Negro, A. A. Condition monitoring of a gearbox using acoustic emission testing. *Materials Evaluation*, 1997, 52(2), pp. 183-187.

[128] Tandon, N. and Mata, S. Detection of defects in gears by acoustic emission measurements. *Journal of Acoustic Emission*, 1999, 17(1-2), pp. 23-27.

[129] Cole, P. and Gautrey, S. Acoustic emission experience with AE monitoring of new vessels during initial proof test. *Proc. of 26th Conference on Acoustic Emission Testing, EWGAE*, Berlin, Germany, 15-17 September 2004, pp. 75-81.

[130] Rogers, L. M. Structural and engineering monitoring by acoustic emission methods – fundamentals and applications. *Report: Lloyd's Register: Technical Investigation Department*, 2001, 80 pages.

[131] Paulson, P. O. Continuous acoustic monitoring of suspension bridges and cable stays. *Structural Materials Technology III: An NDT Conference, Proc. of The Intl.Society for Optical Engineering, SPIE,* San Antonio, USA, 31 March-2 April 1998, 3400(26), pp. 205-213.

[132] Caneva, C., Pampallona, A. and Viskovic, S. Acoustic emission to assess the structural condition of bronze statues. Case of the "Nike" of Brescia. *Proc. of 26th Conference on Acoustic Emission Testing, EWGAE*, Berlin, Germany, 15-17 September 2004, pp. 567-574.

[133] Schwalbe, H-J., Bamfaste, G. and Franke, R. P. Non-destructive and non-invasive observation of friction and wear of human joints and of fracture initiation by acoustic emission. *Proc. of the IMechE, Part H; Journal of Engineering in Medicine*, 1999, 213(1), pp. 41-48.

[134] Rosner, S. and Kikuta, S. B. Ultrasound acoustic detection of cavitation events in water conducting elements of Norway spruce wood. *Proc. of 26th Conference on Acoustic Emission Testing, EWGAE*, Berlin, Germany, 15-17 September 2004, pp. 149-156.

[135] West, D., Venkatesan, G., Tewfik, A., Buckley, K., and Kaveh, M. Detection and modeling of acoustic emissions for fault diagnostics. *Proc. 8th IEEE Signal Processing Workshop on Statistical Signal and Array Processing, SSAP,* Corfu, Greece, 24-26 June 1996, pp. 303-306.

[136] Buckley, K., Venkatesan, G., West, D. and Kaveh, M. Detection and characterization of cracks for failure monitoring and diagnostics. *Proc. IEEE Intl. Conference on Acoustics, Speech and Signal Processing, ICASSP,* Atlanta, USA, 7-10 May 1996, pp. 2738-2741.

[137] Gill, J. D., Reuben, R. L., Scaife, M., Brown, E. R. and Steel, J. A. Detection of diesel engine faults using acoustic emission. *Proc. 2nd Intl. Conference: Planned Maintenance, Reliability and Quality,* Oxford, England, 2-3 April 1998, 1, pp. 57-61.

[138] Gill, J. D., Reuben, R. L., Steel, J. A., Scaife, M. W. and Asquith, J. A study of small HSDI diesel engine fuel injection equipment faults using acoustic emission. *Journal of Acoustic Emission*, 2000, 18, pp. 96-101.

[139] Berjger, A. An investigation of acoustic emission in fuel injection. *Proc. of 3rd European Conference of Young Research and Science Workers in Transport and Telecommunications, TRANSCOM,* Žilina, Slovakia, 29-30 June 1999, 7, pp. 135-138.

[140] Bialkowski, M. T., Pekdemir, T., Reuben, R. L., Brautsch, M., Towers, D. P. and Elsbett, G. Preliminary approach towards a CDI system modification operating on neat rapeseed oil. *31st Intl. Scientific Conference on Internal Combustion Engines, KONES*, Wroclaw, Poland, 4-7 September 2005, 12(1-2), 14 p.

[141] Godinez, V., Finlayson, R. D., Miller, R. K. and Carlos, M. F. AE characterization of cavitation and detonation in combustion engines. *Proc. of Acoustic Emission Working Group Meeting, AEWG-43*, Seattle, USA, 18-19 July 2000.

[142] Frances, A. K., Gill, J. D., Reuben, R. L. and Steel, J. A. Practical application of AE monitoring to diesel engines. *Proc. 17th Intl. Conference on Condition Monitoring and Diagnostic Engineering Management, COMADEM*, Cambridge, UK, 23-25 August 2004, pp. 325-333.

[143] Chandroth, G. O., Sharkey, A. J. C and Sharkey, N. E. Cylinder pressures and vibration in internal combustion engine condition monitoring. *Proc. 12th Intl. Congress on Condition Monitoring and Diagnostic Engineering Management, COMADEM,* Sunderland, UK, 7-9 July 1999, pp. 141-151.

[144] Sharkey, A. J. C., Chandroth, G. O. and Sharkey, N. E. Acoustic emission, cylinder pressure and vibration: a multisensor approach to robust fault diagnosis. *Proc. IEEE-INNS-ENNS Intl. Joint Conference on Neural Networks,* Como, Italy, 24-27 July 2000, 6, pp. 223-228.

[145] El-Ghamry, M., Steel, J. A., Reuben, R. L. and Fog, T. L. Indirect measurement of indicated power from diesel engines using acoustic emission. *Mechanical Systems and Signal Processing,* 2005, 19(4), pp. 751-765.

[146] Fog, T. L., Hansen, L. K., Larsen, J., Hansen, H. S., Madsen, L. B., Sørensen, P., Hansen, E. R. and Pedersen P. S. On condition monitoring of exhaust valves in marine diesel engines. *Proc. IEEE Workshop on Neural Networks for Signal Processing IX,* Piscataway, USA, 23-25 August 1999, pp. 554-563.

[147] Friis-Hansen, A. and Fog, T. L. Monitoring exhaust valve leaks and misfire in marine diesel engines. *Proc. 14th Intl. Conference on Condition Monitoring and Diagnostic Engineering Management, COMADEM,* Manchester, UK, 4-6 September 2001, pp. 641-648.

[148] El-Ghamry, M., Reuben, R. L. and Steel, J. A. The development of automated pattern recognition and statistical feature isolation techniques for the diagnosis of reciprocating machinery faults using acoustic emission. *Mechanical Systems and Signal Processing,* 2003, 17(4), pp. 805-823.

[149] Frances, A. K., Gill, J. D., Reuben, R. L. and Steel, J. A. Investigation into identification of faults in small HSDI diesel engine using acoustic emission. *Proc. of 26th Conference on Acoustic Emission Testing, EWGAE*, Berlin, Germany, 15-17 September 2004, pp. 357-369.

[150] Frances, A. K., Gill, J. D., Reuben, R. L. and Steel, J. A. A study of the variability of acoustic emission signals from a medium size marine diesel engine under service conditions. *Proc. 16th Intl. Congress on Condition Monitoring and Diagnostic Engineering Management, COMADEM,* Växjö, Sweden, 27-29 August 2003, pp. 503-512.

[151] Gill, J. D., Douglas, R. M., Neo, Y. D., Reuben, R. L. and Steel, J. A. Examination of plate valve behaviour in a small reciprocating compressor using acoustic emission. *Journal of Acoustic Emission,* 2000, 18, pp. 96-101.

[152] Nivesrangsan, P. Multi-source, multi-sensor approaches to diesel engine monitoring using acoustic emission. *PhD thesis*, Heriot-Watt University, Edinburgh, UK, December 2004.

[153] Nivesrangsan, P., Steel, J. A. and Reuben, R. L. AE mapping of engines for spatially located time series. *Mechanical Systems and Signal Processing*, 2005, 19(5), pp. 1034-1054.

[154] Nivesrangsan, P., Steel, J. A. and Reuben, R. L. Acoustic emission mapping of diesel engines for spatially located time series – Part II: Spatial reconstitution. *Mechanical Systems and Signal Processing*. 2007, 21(2), pp. 1084-1102.

[155] Nivesrangsan, P., Steel, J. A. and Reuben, R. L. Source location of acoustic emission in diesel engines. *Mechanical Systems and Signal Processing,* 2007, 21(2), 1103-1114.

[156] Pontoppidan, N. H. and Douglas, R. M. Event alignment, warping between running speeds. *Proc. 17th Intl. Conference on Condition Monitoring and*

Diagnostic Engineering Management, COMADEM, Cambridge, UK, 23-25 August 2004, pp. 621-628.

[157] Pontoppidan, N. H. and Larsen, J. Non-stationary condition monitoring through event alignment. *Proc. IEEE Workshop on Machine Learning for Signal Processing, MLSP*, São Luís, Brazil, 29 September - 1 October 2004, pp. 499-508.

[158] Pontoppidan, N. H. and Larsen, J. Unsupervised condition change detection in large diesel engines. *Proc. 2003 IEEE Workshop on Neural Networks for Signal Processing, NSSP*, Toulouse, France, 17-19 September 2003, pp. 565-574.

[159] Pontoppidan, N. H., Larsen, J. and Fog, T.L. Independent component analysis for detection of condition changes in large diesels. *Proc. 16th Intl. Conference on Condition Monitoring and Diagnostic Engineering Management, COMADEM*, Växjö, Sweden, 27-29 August 2003, pp. 493-502.

[160] Carlton, J. S. Techniques for ship and machinery failure investigation and performance assessment. *Greek CIMAC Association Seminar*, Athens, Greece, 3 April 2003.

[161] Grabec, P. and Leskovar, P. Acoustic emission of a cutting process. *Ultrasonics,* 1977, 15 (1), pp. 17–20.

[162] Iwata, K. and Moriwaki, T. Application of acoustic emission measurement to in-process sensing of tool wear. *Annals of CIRP 26*, 1977, 26(1-2), pp. 19-23.

[163] Dornfeld, D. A. and Kannatey-Asibu, E. Acoustic emission during orthogonal metal cutting. *International Journal of Mechanical Sciences*, 1980, 22(5), pp. 285–296.

[164] Saini, D. P. and Park, Y. J. A quantitative model of acoustic emissions in orthogonal cutting operations. *Journal of Materials Processing Technology*, 1996, 58(?), pp. 343-350.

[165] Carolan, T. A., Kidd, S. R., Hand, D. P., Wilcox, S. J., Wilkinson, P., Barton, J. S., Jones, J. D. C. and Reuben, R. L. Acoustic emission monitoring of tool wear during face milling of steels and aluminium alloys using a fibre optic sensor. 1. Energy analysis. *Proc. of the IMechE Part B*2: *Journal of Engineering Manufacture,* 1997, 211(4) pp. 299-309.

[166] Hwang, T. W., Whitenton, E. P., Hsu, N. N., Hsu, Blessing, G. V. and Evans, C. J. Acoustic emission monitoring of high speed grinding of silicon nitride. *Ultrasonics*, 2000, 38(1-8), pp. 614-619.

[167] Jayakumar, T., Mukhopadhyay, C. K., Venugopal, S., Mannan, S. L. and Raj, N. A review of the application of acoustic emission techniques for monitoring forming and grinding processes. *Journal of Materials Processing Technology*, 2005, 159(1), pp. 48-61.

[168] Belyi, V. A., Kholodilov, O. V. and Sviridyonok, A. I. Acoustic spectrometry as used for the evaluation of tribological systems. *Wear*, 1981, 69(3), pp. 309-319.

[169] McBride, S. L., Boness, R. J., Sobczyk, M. and Viner, M. R. Acoustic emission from lubricated and unlubricated rubbing surfaces. *Journal of Acoustic Emission,* 1989, 8(1-2), pp. 192-196.

[170] Boness, R. J., McBride, S. L. and Sobczyk, M. Wear studies using acoustic emission techniques. *Tribology International*, 1990, 23(5), pp. 291-295.

[171] Boness, R. J. and McBride, S. L. Adhesive and abrasive wear studies using acoustic emission. *Wear,* 1991, 149(1-2), pp. 41-53.

[172] Jiaa, C. L. and Dornfeld, D. A. Experimental studies of sliding friction and wear via acoustic emission signal analysis. *Wear*, 1990, 139(2), pp. 403-423.

[173] Hanchi, J. and Klamecki, B. E. Acoustic emission monitoring of the wear process. *Wear,* 1991, 145(1), pp. 1-27.

[174] Klamecki, B. E. and Hanchi, J. Wear process description based on acoustic emission. *Transactions of ASME: Journal of Tribology,* 1990, 112(3), pp. 469-476.

[175] Diei, E. N. Investigation of the milling process using acoustic emission signal analysis. *PhD thesis*, University of California, Berkeley, USA, 1985.

[176] Lingard, S. and Ng, K. K. An investigation of acoustic emission in sliding friction and wear of metals. *Wear*, 1989, 130(2), pp. 367-379.

[177] Lingard, S., Yu, C. W. and Yau, C.F. Sliding wear studies using acoustic emission. *Wear*, 1993, 162-164(1), pp. 597-604.

[178] Mechefske, C. K. Monitoring sliding wear using acoustic emission. *Proceedings of 14th Intl. Conference on Condition Monitoring and Diagnostic Engineering Management, COMADEM,* Manchester, UK, 4-6 September 2001, pp. 57-65.

[179] Boness, R. J. Measurements of wear and acoustic emission from fuel-wetted surfaces. Wear, 1993, 162-164(1), pp. 703-705.

[180] Price, E. D., Lees, A. W. and Friswell, M. I. Detection of severe sliding and pitting fatigue wear regimes through the use of broadband acoustic emission.

Proc. of the IMechE, Part J; Journal of Engineering Tribology, 2005, 219(2), pp. 85-98.

[181] Shuster, M., Combs, D., Karrip, K. and Burke, D. Piston ring cylinder liner scuffing phenomenon studies using acoustic emission technique. *Proc. of CEC/SAE Spring Fuels & Lubricants Meeting and Exposition,* Paris, France, 2000, pp. 901-913.

[182] Kita, T., Kogure, K., Mitsuya, Y. and Nakanishi, T. New method of detecting contact between floating-head and disk. *IEEE Transactions on Magnetics,* 1980, MAG-16(5), pp. 873-875.

[183] Khurshudov, A. G. and Talke, F. E. A study of subambient pressure tri-pad sliders using acoustic emission. *Transactions of ASME: Journal of Tribology*, 1998, 120(1), pp. 54-59.

[184] Ravikiran, A., Low, T. S. Estimation of lubricant thickness on a magnetic hard disk using acoustic emission. *Review of Scientific Instruments,* 2000, 71(4), pp. 1915-1916.

[185] Liew, T. Y. F., Chai, M. C., Weerasooriya, S. and Low, T. S. Head-disk interaction of proximity sliders studied by the acoustic emission probe, the dynamic height tester, and the laser Doppler vibrometer. *IEEE Transactions on Magnetics,* 1997, 33(5), pp. 3175-3177.

[186] Zhu, Y-L., Liu, B., Li, Y-H. and Leng, Q-F. Slider-disk interaction and its effect on the flying performance of slider. *IEEE Transactions on Magnetics*, 1999, 35(5), pp. 2403-2405.

[187] Benson, R. C., Chiang, C. and Talke, F. E. The dynamics of slider bearings during contacts between slider and disk. *IBM Journal of Research and Development*, 1989, 33(1), pp. 2-14.

[188] Ravikiran, A., Liew, T. and Low, T. S. Effect of disk acceleration on the generation of acoustic emission signal at the head-disk interface. *Journal of Applied Physics,* 1999, 85(8), pp. 5612-5614.

[189] Liu, Y., Jiaa, C. L. and Eltoukhy, A. Acoustic emission study of lubricant effect on proximity contact recording. *IEEE Transactions on Magnetics,* 1997, 33(5), pp. 3160-3162.

[190] Tanaka, H., Yonemura, S. and Tokisue, H. Slider dynamics during continuous contact with textured and smooth disks in ultra low flying height. *IEEE Transactions on Magnetics,* 2001, 37(2), pp. 906-911.

[191] Sharma, V., Talke, F. E. and Ng, Q. Tribological investigations of tri-pad sliders. *IEEE Transactions on Magnetics,* 1996, 32(5), pp. 3651-3653.

[192] Benson, R. C., Sundaram, R. and Talke, F. E. A study of the acoustic emission from slider/disk interface in a 5¼ inch hard disk drive. *STLE Special Publication 25: Tribology and Mechanics of Magnetic Storage System*, 1988, pp. 87-93.

[193] Xu, J., Tokisue, H. and Kawakubo, Y. Study on soft-particle intrusion in a head/disk interface of load/unload drives. *IEEE Transactions on Magnetics*, 2000, 36(5), pp. 2745-2747.

[194] Briggs, J. C., Chang, M-K. and Tse, M. K. High frequency slider vibrations during asperity impacts in rigid magnetic disk system. *Advanced Information Storage Systems*, 1992, 4, pp. 181-194.

[195] Matsuoka, K., Taniguchi, K. and Nakakita, M. In-situ wear monitoring of slider and disk using acoustic emission. *Transactions of ASME: Journal of Tribology,* 2001, 123(1), pp. 175-180.

[196] McMillan, T. C. and Talke, F. E. Identification of slider/disk contacts using the energy of the acoustic emission signal. *IEEE Transactions of Magnetics*, 1998, 34(4), pp. 1819-1821.

[197] O'Brien, K. and Harris, D. Head/disk interface contact detection using a refined acoustic emission technique. *ASME: Journal of Tribology,* 1996, 118(3), pp. 539-542.

[198] Ganapathi, S. K., Donovan, M. and Hsia, Y. T. Contact force measurements at the head/disk interface for contact recording heads in magnetic recording. *Proc. of the SPIE- The International Society for Optical Engineering*, 1996, 2604, pp. 236-243.

[199] Matsuoka, K., Forrest, D. and Tse, M. K. On-line wear monitoring using acoustic emission. *Wear*, 1993, 162-164(1), pp. 605-610.

[200] Matsuoka, K., Taniguchi, K. and Ueno, Y. Evaluation technique of head/tape contact using acoustic emission. *ASME: Journal of Tribology,* 1996, 120(2), pp. 259-265.

[201] Bhushan, B., Wu, Y. and Tambe, N. S. Sliding contact energy measurement using a calibrated acoustic emission transducer. *IEEE Transactions on Magnetics,* 2003, 39(2), pp. 881-887.

[202] Toutountzakis, T. and Mba, D. Observation of acoustic emission activity during gear defect diagnosis. *NDT and E International*, 2003, 36(7), pp. 471-477.

[203] Tan, C. K. and Mba, D. The source of acoustic emission during meshing of spur gears. *Proc. of 26th Conference on Acoustic Emission Testing, EWGAE*, Berlin, Germany, 15-17 September 2004, pp. 469-474.

[204] Tan, C. K. and Mba, D. Identification of the acoustic emission source during a comparative study on diagnosis of a spur gearbox. *Tribology International*, 2005, 38(5), pp. 469-480.

[205] Sentoku, H. AE in tooth surface failure process of spur gears. *Journal of Acoustic Emission*, 1998, 16(1-4), pp. S19-S24.

[206] Toutountzakis, T. Tan, C. K. and Mba, D. Application of acoustic emission to seeded gear fault detection. *NDT&E International*, 2005, 38(1), pp. 27-36.

[207] Miettinen, J. and Siekkinen, V. Acoustic emission in monitoring sliding contact behaviour. *Wear,* 1995, 181-183(2), pp. 897-900.

[208] Ferguson, I. G., Gill, J. D., Reuben, R. L., Steel, J. A., Brown, E. R. and Roosch, E. Condition monitoring of rotating seals using acoustic emission. *Proc. of the 23rd European Conference on Acoustic Emission testing, EWGAE,* Vienna, Austria, 6-8 May 1998, pp. 281-286.

[209] Douglas, R. M., Beugné, S., Jenkins, M. D., Frances, A. K., Steel, J. A., Reuben R. L. and Kew, P. A. Monitoring of gas turbine operating parameters using acoustic emission. *Proc. of 26th Conference on Acoustic Emission Testing, EWGAE*, Berlin, Germany, 15-17 September 2004, pp. 455-466.

[210] Sato, I. Rotating machinery diagnosis with acoustic emission techniques. *Electrical Engineering in Japan*, 1990, 100(2), pp. 115-127.

[211] Board, D. B. Stress wave analysis of turbine engine faults. *Proc. IEEE Aerospace Conference*, Big Sky, USA, 18-25 March 2000, 6, pp. 79-95.

[212] Hall, L. D. and Mba, D. Diagnosis of continuous rotor-stator rubbing in large scale turbine units using acoustic emissions. *Ultrasonics*, 2004, 41(9), pp. 765-783.

[213] Miettinen, J. The influence of the running parameters on the acoustic emission of grease lubricated rolling bearings, *Maintenance & Asset Management*, 2001, 16(2), pp. 7-11.

[214] Miettinen, J. and Andersson, P. Acoustic emission of rolling bearings lubricated with contaminated grease. *Tribology International*, 2000, 33(11), pp. 777-787.

[215] Miettinen, J., Andersson, P. and Wikström, V. Analysis of grease lubrication of rolling bearings using acoustic emission measurement. *Proc. of the IMechE Part J: Journal of Engineering Tribology*. 2001, 215(6), pp. 535-544.

[216] Dornfeld, D. and Handy, C. Slip detection using acoustic emission signal analysis. *Proc. of 1987 IEEE Intl. Conference on Robotics and Automation*, Raleigh, USA, 30 March - 3 April 1987, pp. 1868-1875.

[217] Tsimogiannis, A., Bollas, C., Chrissos, G. and Anastassopoulos, A. New sensor specification. EU Competitive and Sustainable Growth Programme, Project no. GRD2-2001-50014 (AE-WATT), Deliverable 1, October 2002.

[218] Nyquist, H. Certain topics in telegraph transmission theory. *AIEE Transactions,* 1928, 47. pp. 617-644.

[219] Lim, T., Nivesrangsan, P., Corney, J. R., Steel, J. A. and Reuben, R. L. Predicting AE attenuation within solids by geometric analysis. *Proc. of Intl. Conference on Shape Modelling and Applications*, SMI-05, 13-17 June 2005, MIT, USA, pp. 155-162.

[220] Oh, K. P., Li, C. H. and Goenka, P. K. Elastohydrodynamic lubrication of piston skirts. *Transactions of the ASME: Journal of Tribology*, 1987, 109(4), pp. 356 - 362.

[221] MAN B&W Diesel A/S. Instructions for 46-98 MC type engines, components and maintenance, Edition 8E, Plate 90910-83, pp. 326.

[222] MAN B&W Diesel A/S. Instructions for 46-98 MC type engines, components and maintenance, Edition 8E, Plate 90911-10, pp. 327.

[223] Heisler, H. Advanced engine technology. *Edward Arnold*, 1995, ISBN: 0 340 568224, pp. 518.

[224] MAN B&W Diesel A/S. Instructions for 46-98 MC type engines, components and maintenance, Edition 8E, Plate 90911, pp. 320.

[225] Lee, S. G., Park, J. H., Yoo, K. B., Lee, S. K. and Hong, S. Y. Evaluation of internal leak in valve using acoustic emission method. *Key Engineering Materials*, 2006, 326-328, pp. 661-664.

[226] Henshall, S. H. Medium and high speed diesel engines for marine use. *The Institute of Marine Engineers*, 1978, ISBN: 0 900976 77 2, pp. 159.

[227] Robertson, A. I. F., Douglas, R. M., Nivesrangsan, P., Brown, E. R., Steel, J. A. and Reuben, R. L. Source identification using acoustic emission on large bore cylinder liners. *Proc. of 26th Conference on Acoustic Emission Testing, EWGAE*, Berlin, Germany, 15-17 September 2004, pp. 773-781.

[228] I. P. Hercules. Hercules (High-efficiency Engine R&D on Combustion with Ultra Low Emissions for Ships), Task 9.2: Tribo-optimisation – Task Progress Highlights March 2005, Status and Progress [online], available at:

http://www.ip-hercules.com/article/english/17/index.html.

[229] Saburi, S., Saitoh, Y. and Yamada, T. Tribology between piston rings and cylinder liners of marine diesel engines. *IHI Engineering Review*, 2005, 38(1), pp. 11-18.

[230] Yilmaz, E. Sources and characteristics of oil consumption in a spark-ignition engine. *PhD thesis*, Massachusetts Institute of Technology, September 2003.

[231] Noorul Haq, A. and Tamizharasan, T. Ring wear monitoring in IC engines: an acoustic emission approach. *The International Journal of Advanced Manufacturing Technology*, 2007, 31(11-12), pp. 1148-1155.

[232] Douglas, R. M., Steel, J. A, Reuben, R. L. and Fog, T. L. On-line power estimation of large diesel engines using acoustic emission and instantaneous crankshaft angular velocity. *International Journal of Engine Research,* 2006, 7(5), pp. 399-410.